Targeting Sigma-2 Receptor and ZFP91 in Pancreatic Cancer

by

Maha Hanafi

A dissertation submitted in partial fulfillment
of the requirements for the degree of
Doctor of Philosophy
(Medicinal Chemistry)
in the University of Michigan
2021

Doctoral Committee:

Professor Nouri Neamati, Chair
Associate Professor Amanda L. Garner
Associate Professor Zaneta Nikolovska-Coleska
Research Associate Professor Andrew D. White

Maha Said Ahmed Abdeltawab Hanafi

mahasaid@umich.edu

ORCID iD: 0000-0002-5389-4656

Dedication

To the most important person in my life and my role model, my mother. Her constant

love, support, and encouragement makes everything possible.

.

Table of Contents

List of Tables

List of Figures

List of Abbreviations

ABCA1 – ATP-binding cassette transporter A1

ACAT1 – Acyl-CoA cholesterol acyl-transferase-1

Bru-seq – Bromouridine labeled RNA sequencing

CK1α – Casein Kinase 1α

CRBN – Cereblon

CX – Cycloheximide

DHCR7 – 7-Dehydrocholesterol reductase

DIC – Dicoumarol

DTG – 1,3 Di-o-tolylguanidine

ER – Endoplasmic reticulum

FC – Fold-change

FBS – Fetal bovine serum

GPCR – G-protein coupled receptor

GSEA – Gene set enrichment analysis

GSH – Glutathione

GSPT – G1 to S phase transition protein

HIF-1α – Hypoxia inducible factor 1 subunit alpha

HMCR – Hydroxymethylglutaryl-CoA reductase

HMOX1 – Heme oxygenase 1

IKZF1 – IKAROS family zinc finger 1

IKZF3 – IKAROS family zinc finger 3

IMiDs – Immunomodulatory drugs

INSIG – Insulin-induced gene

LDL – Low-density lipoprotein

LDLR – Low-density lipoprotein receptor

mPDAC – Metastatic pancreatic adenocarcinoma

MAC30 – Meningioma-associated protein 30

mTOR – Mammalian target of rapamycin

MTT – 3-(4,5-dimethylthiazol-2-yl)-2,5-diphenyltetrazolium bromide

MVK – Mevalonate kinase

NAC – N-acetyl cysteine

NF-κB – Nuclear factor kappa B

NP – Napabucasin

NPC1 – Niemann–Pick C1 protein

NQO1 – NAD(P)H quinone dehydrogenase 1

PCYT2 – Phosphorylethanolamine transferase

PDAC – Pancreatic ductal adenocarcinoma

PET - Positron emission tomography

PGRMC1 – Progesterone receptor membrane component 1

PROTAC – Proteolysis targeting chimera

ROS – Reactive oxygen species

SCAP – SREBP cleavage-activating protein

SCD – Stearoyl-CoA desaturase

SDR39U1 – Short chain dehydrogenase/reductase family 39U member 1

S2L – Sigma-2 ligand

S1R – Sigma-1 receptor

S2R – Sigma-2 receptor

SMAC – Second mitochondria-derived activator of caspase

SOAT1 – Sterol O-acyltransferase 1

SPR – Surface plasmon resonance

SREBP – Sterol regulatory element-binding protein

STAT3 – Signaling transducer and activator of transcription 3

TG – Triglycerides

TGF-β – Tumor transforming growth factor-β

TMEM97 – Transmembrane protein 97

VHL – Von hippel-lindau

ZBTB16 – Zinc finger and BTB domain containing 16

ZFP91 – Zinc finger protein 91 homolog

Abstract

Pancreatic cancer is one of the most aggressive malignancies with poor prognosis. The effectiveness of currently available conventional therapies is limited by chemoresistance and systemic toxicity. Thus, there is an urgent need to develop novel and effective anticancer agents by targeting critical pathways that drive tumorigenesis in pancreatic cancer. Pancreatic cancer cells rely on cholesterol for their growth. Cholesterol plays an important role in the cellular metabolism that is reprogrammed in cancer cells to meet the increased energy and biosynthetic demands associated with rapid tumor growth. Targeting cholesterol metabolism is an attractive strategy for inhibiting tumor growth. The sigma-2 receptor (S2R), also known as TMEM97, is an endoplasmic reticulum (ER) protein involved in the regulation of cellular cholesterol levels and is overexpressed in pancreatic cancer. Therefore, targeting S2R is a promising therapeutic approach for pancreatic cancer.

We synthesized a series of quinolinyl pyrazinamides showing cytotoxicity in pancreatic cancer cells and selected **JR235** for mechanistic studies. **JR235** kills the cancer cells through induction of ROS, autophagy, and cell cycle arrest. Bru-seq and proteomics analyses of **JR235**-treated cells showed the deregulation of genes and proteins involved in cholesterol/lipid biosynthesis and GPCR signaling. Screening of **JR235** for its binding affinity against a panel of GPCRs and membrane proteins revealed selectivity and nano-molar affinity to S2R. **JR235** binds to cellular S2R and a BODIPY-labeled derivative localizes in the ER. Furthermore, treatment with **JR235** results in accumulation of lipid droplets. TMEM97 knockdown resulted in only partial reduction in **JR235**'s cytotoxicity suggesting the involvement of additional targets. Importantly,

JR235 is synergistic with cholesterol and lipid biosynthesis inhibitors. This is the first in-depth study that uses bioinformatics analysis for the investigation of the mechanistic signature of sigma-2 ligands (S2Ls), like **JR235**, providing unprecedented insights into their role in cholesterol metabolism. In addition, our findings provide a strong rationale for the development of S2Ls as combination therapies with other anticancer agents including statins.

In the second part of the dissertation, we focused on validating the target of napabucasin, a reported signal transducer and transcription factor 3 (STAT3) inhibitor being evaluated in multiple clinical trials for the treatment of pancreatic cancer. To better elucidate its mechanism of action, we designed a napabucasin-based proteolysis targeting chimera (PROTAC), **XD2-149**, that resulted in inhibition of STAT3 signaling in pancreatic cancer cells without inducing proteasome-dependent degradation of STAT3. Proteomics analysis of **XD2-149** treated cells revealed the downregulation of the E3 ubiquitin-protein ligase ZFP91. **XD2-149** induces degradation of ZFP91 with DC_{50} values in the nanomolar range. The cytotoxicity of **XD2-149** was significantly, but not fully, reduced with ZFP91 knockdown providing evidence for its multi-targeted mechanism of action. The NQO1 inhibitor, dicoumarol rescued the cytotoxicity of **XD2-149** but not ZFP91 degradation suggesting that the NQO1-induced cell death is independent of ZFP91. Our findings provide a rationale for the development of ZFP91-targeted therapeutics for the treatment of pancreatic cancer.

In summary, this dissertation validates S2R and ZFP91 as important therapeutic targets in pancreatic cancer and provides new tool compounds to elucidate their role in tumor progression. Importantly, our work provides the foundation for the development of novel and promising S2L combination therapies for the treatment of pancreatic cancer.

CHAPTER I

Introduction[1]

Background

Pancreatic cancer remains one of the most aggressive malignancies that is challenging to treat.[1] Pancreatic cancer has a low five-year survival rate of approximately 9% and is projected to be the second leading cause of cancer mortalities in the United States by 2030.[2, 3] Late detection of pancreatic cancer due to the insidious symptoms and progress contributes to early metastasis and poor prognosis.[4] Traditional treatment modalities include surgery and chemotherapy. While surgery offers a potential for a cure, the majority of patients are diagnosed with metastatic disease and are not eligible for surgical resection.[5] Furthermore, almost 80% of the patients who undergo surgery will relapse.[5] Despite huge efforts to develop anticancer agents for the treatment of pancreatic cancer, a limited number of effective therapeutics are available.[5] Gemcitabine is the standard first-line treatment for pancreatic cancer, unfortunately, rapid chemoresistance challenges its effectiveness.[6] FOLFIRINOX (irinotecan, oxaliplatin, 5-fluorouracil, and leucovorin) is also one of the first-line treatments that offers the advantages of combination therapies including synergistic effects and improved prognosis.[7] Although treatment with FOLFIRINOX was associated with improved overall survival compared to gemcitabine, it offers limited benefits due to the increased adverse effects.[7] Thus, the regimen is only recommended for patients with good

---

[1] Sigma-2 receptor and TMEM97 are interchangeable terms.

performance status who can tolerate the treatment. The immunosuppressive microenvironment in pancreatic cancer also contributes to chemoresistance and reduced therapeutic effectiveness.[8] In conclusion, although conventional chemotherapeutics can improve patient survival, their success is limited by chemoresistance and systemic toxicity.

Targeted therapies have also been investigated as single agents or in combination with gemcitabine.[9] KRAS is an oncogenic protein that plays a role in cell division and differentiation and its mutation is the most common in pancreatic cancer.[10] Despite the huge efforts to develop KRAS inhibitors, no KRAS-targeted therapeutics are currently available. KRAS is often considered undruggable due to its complex signaling pathways.[10] The upstream epidermal growth factor receptor (EGFR) inhibitor, erlotinib combined with gemcitabine demonstrated statistically significant results over gemcitabine alone but was clinically of marginal benefit.[11] The high molecular heterogeneity of the disease and the tumor microenvironment contribute to the failure of targeted therapies in improving the outcome in pancreatic cancer patients.[12] Therefore, there is an urgent need to identify novel therapeutic approaches for the treatment of pancreatic cancer. In this dissertation, we shed the light on novel targets that can be intervened for the treatment of pancreatic cancer including the sigma-2 receptor that will be discussed in this chapter.

Sigma receptors have long been known for their role in neurological diseases and were initially identified as a subtype of opioid receptors.[13] Further studies revealed the distinction of opioid receptors from sigma receptors that were classified into two sub-types; sigma-1 and sigma-2.[14, 15] Cloning of sigma-1 receptor (S1R) revealed a transmembrane protein that was later elucidated by a crystal structure.[16, 17] S1R is a chaperone protein that plays a modulatory role in calcium signaling.[18] Sigma-2 receptor (S2R) is a regulator of cholesterol homeostasis.[19-21] While the crystal structure of S1R has been reported in the absence and presence of small-molecule

ligands, no crystal structure of the S2R is currently available. Although, homology models of S2R have been used for virtual screening,[22, 23] lack of co-crystal structures has hampered the design of highly selective ligands. However, in the absence of such co-crystal structures, there are currently several S2R ligands undergoing preclinical studies.[24-27]

Sigma-2 receptor (S2R) is an endoplasmic reticulum (ER) transmembrane protein with a molecular weight of 21.5 kDa.[15, 28] It is overexpressed in select tumor tissues and has been used as a biomarker for cell proliferation.[29, 30] Early studies demonstrated the involvement of S2R in cancer cell death through the activation of caspase-independent apoptotic pathways.[31] Initially, it was believed that the binding site of S2R was a part of the progesterone receptor membrane component 1 (PGRMC1).[32] However, it was proven later that PGRMC1 overexpression does not alter the ligand binding affinity to S2R suggesting they are two distinct proteins.[33-35] Importantly, the coding gene for the pharmacologically defined S2R was recently identified to be TMEM97.[19] This breakthrough will lead to a better understanding of the function and characteristics of S2R on the molecular level and will allow for a deeper investigation of its role in cancer. Select highlights on the discovery of S2R are presented in Figure I-1.

1976 — Discovery of Sigma Receptors as a Potential Target for CNS Diseases
1983 — Identification of Two Sub-types of Sigma Receptors (Sigma-1 & Sigma-2)
1995 — Sigma-2 Receptor is Overexpressed in Tumor Tissues – Sigma-2 Ligands are Cytotoxic
1996 — Cloning of Sigma-1 Receptor
2002 — Sigma-2 Receptor Activation Induces Apoptosis
2011 — Sigma-2 Receptor Proposed as Part of PGRMC1 Complex
2016 — Crystal Structure of Sigma-1 Receptor
2017 — TMEM97 is the Coding Gene for Sigma-2 Receptor

Figure I-1. Timeline highlighting milestones in the discovery of S2R.

TMEM97, also known as meningioma-associated protein 30 (MAC30) is implicated in cholesterol homeostasis and is proposed as a therapeutic target for the treatment of Niemann-Pick type C disease (NPC), a lysosomal storage disease that can lead to neurodegenerative disorders and early morbidity.[20] NPC disease arises from mutations in the cholesterol-transport regulatory protein, Niemann–Pick C1 protein (NPC1), that results in lysosomal cholesterol accumulation.[36] TMEM97 is a partner protein of NPC1 that modulates cholesterol levels by negatively regulating NPC1 (Figure I-2).[20] Moreover, TMEM97 was identified as a cholesterol-regulating gene involved in low-density lipoprotein (LDL) uptake.[37] Studies further demonstrated that TMEM97 forms a ternary complex with PGRMC1 and the LDL receptor (LDLR) that induces rapid LDL internalization resulting in increased cellular uptake of cholesterol (Figure I-2).[21] The involvement of TMEM97 in cholesterol uptake suggests its essential role in cholesterol metabolism and potential for therapeutic intervention in cancer.
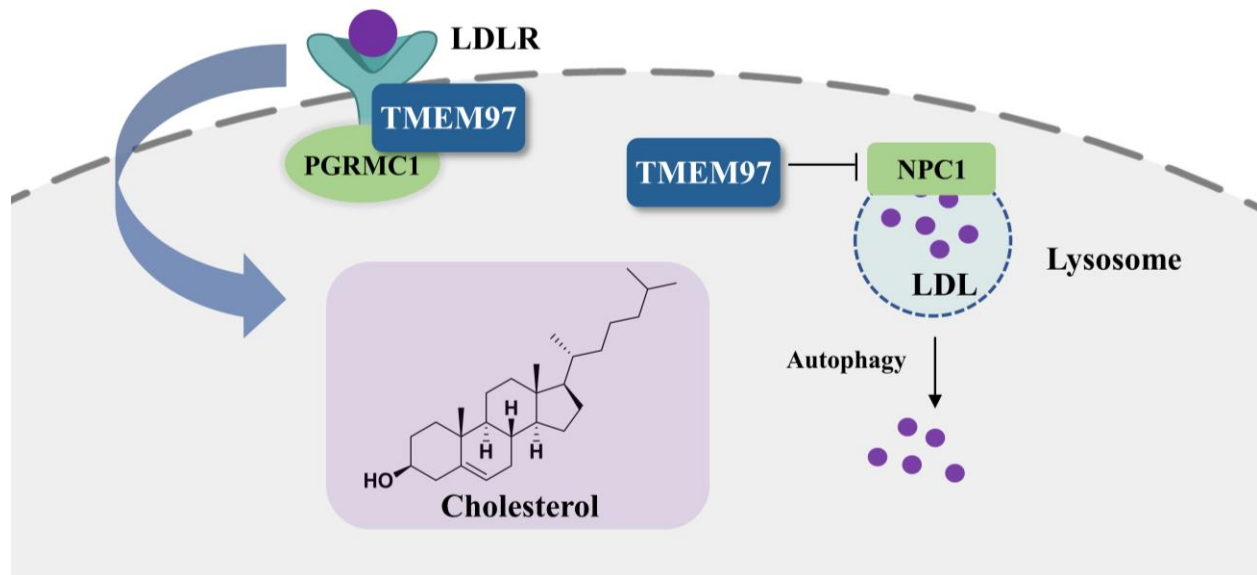
Figure I-2. Role of TMEM97 in the cells. TMEM97 plays two roles: 1) Forms a complex with PGRMC1 and LDLR to enhance LDL internalization. 2) TMEM97 is a negative regulator of the lysosomal membrane protein NPC1. Lysosomal degradation of LDL results in the release of free cholesterol.

Cholesterol is essential for cellular homeostasis and survival.[38] Cholesterol is a major lipid component of the cell membrane and it plays a key role in signaling pathways.[38-40] It is also a precursor to steroid hormones that control various cellular functions.[41] Cholesterol levels are tightly regulated in normal tissues by various mechanisms.[42] The sterol regulatory element-binding proteins (SREBP) regulate the transcription of genes involved in cholesterol metabolism and lipid biosynthesis by binding to the promoter regions of its target genes inside the nucleus.[43] While SREBP-1 activates genes involved in the fatty acid synthesis, SREBP-2 is the master regulator of cholesterol metabolism.[43] The transport and activation of SREBP is regulated by other proteins including SREBP-cleavage activating protein (SCAP) and insulin-induced gene (INSIG). Cholesterol depletion induces the binding of SCAP to SREBP for activation (Figure I-3).[42] Once the cholesterol levels exceed a certain limit, the INSIG protein binds to SCAP to prevent SREBP activation (Figure I-3).[42] A binding partner to INSIG and SCAP is the PGRMC1 that plays a regulatory role in SREBP activation.[44, 45] SREBP are also regulated by the mammalian target of rapamycin (mTOR) that can induce their activation.[46] The mTOR is a negative regulator of autophagy, a process that involves cholesterol transport to the lysosomes in the form of lipid droplets and its subsequent degradation resulting in the release of free cholesterol.[47] A key enzyme that regulates cholesterol levels is the hydroxymethylglutaryl-CoA reductase (HMGCR) that catalyzes the rate-limiting step in cholesterol biosynthesis (Figure I-4). HMGCR expression is regulated by SREBP-2 and is activated in response to low cholesterol levels (Figure I-3/4).[42] Cells can also acquire cholesterol from LDL through receptor-mediated endocytosis of the LDLR. Cholesterol export out of the cells is mediated by the ATP-binding cassette transporter A1 (ABCA1).[38] Cholesterol homeostasis is maintained by the balance between cholesterol uptake,

5

synthesis, and efflux (Figure I-4). Deregulation of any of these intricate mechanisms is associated

with diseases including cancer.[48]
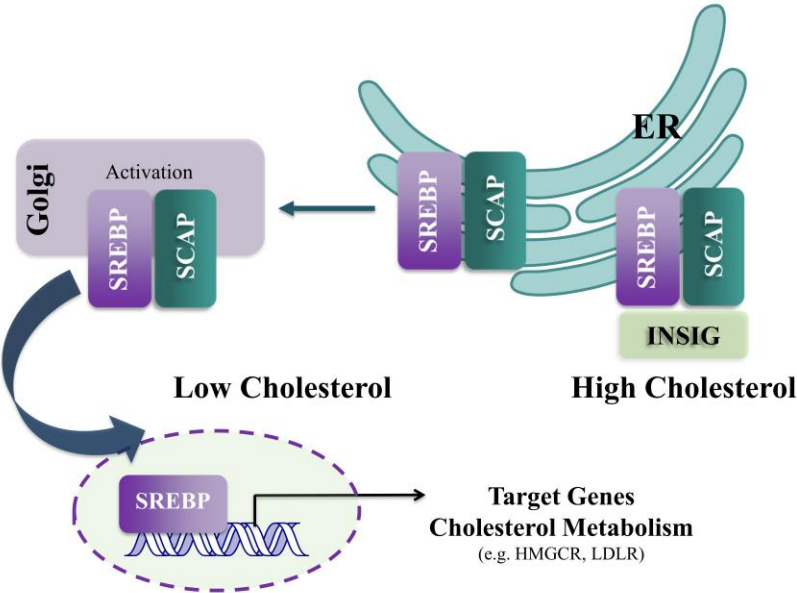
Figure I-3. Regulation of cholesterol metabolism by SREBP. At low cholesterol levels, SCAP escorts the SREBP to the Golgi where it is proteolytically cleaved to translocate to the nucleus and activate the transcription of target genes. At high cholesterol levels, the INSIG binds to the SCAP-SREBP complex causing its ER retention.
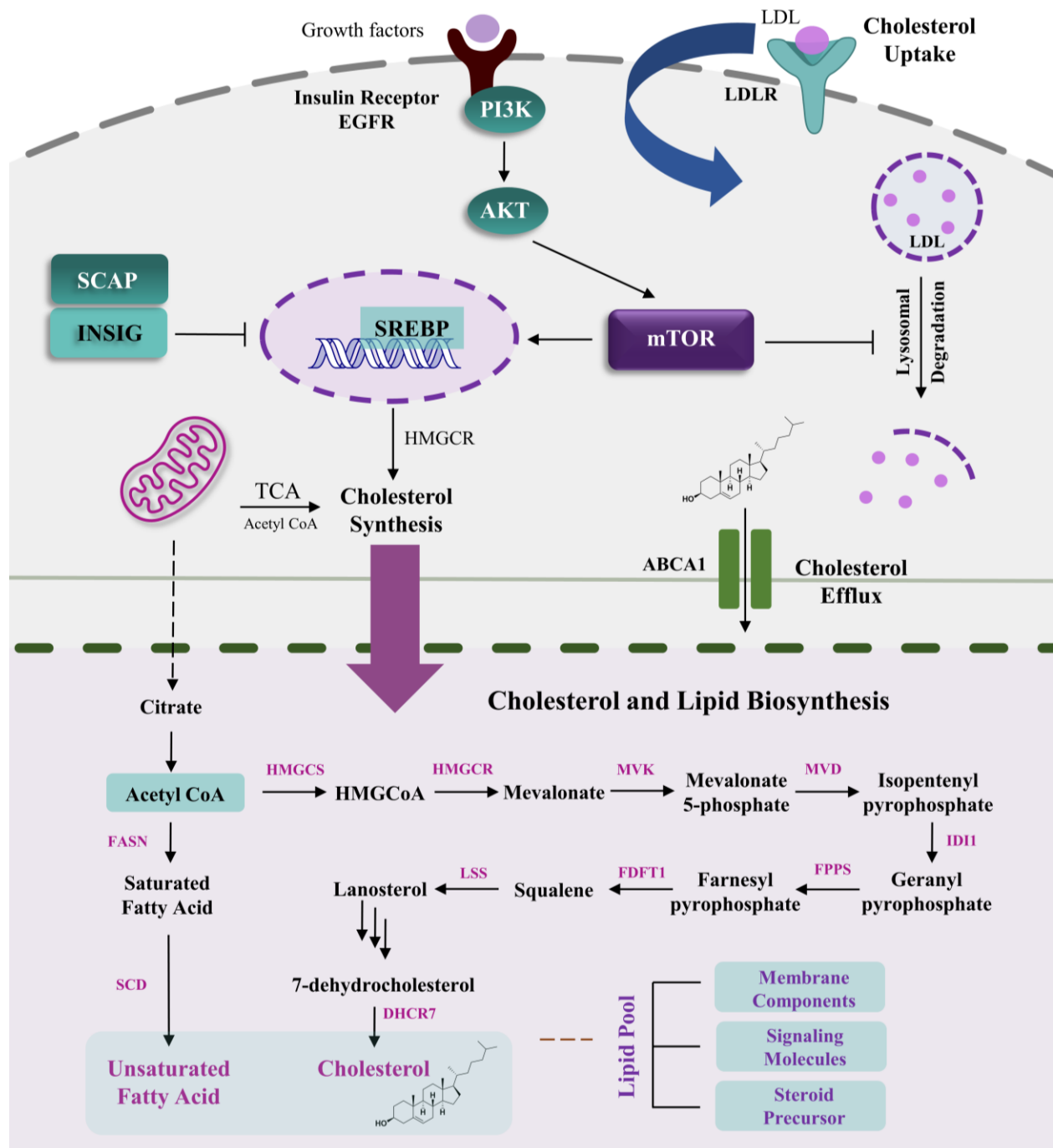
Figure I-4. Diagram highlighting cellular cholesterol homeostasis. The top diagram highlights the three main processes that contribute to cholesterol homeostasis (uptake, synthesis, and efflux) and important regulatory proteins. The PI3K/AKT pathway regulates SREBP through mTOR activation.[43, 49] PI3K: phosphatidylinositol 3-kinase; AKT: protein kinase B; SREBP: sterol regulatory element-binding protein; SCAP: SREBP cleavage-activating protein; INSIG: insulin-induced gene; ABCA1: ATP-binding cassette transporter. The bottom diagram highlights the cholesterol and lipid biosynthetic pathways. HMGCS: hydroxymethylglutaryl-CoA synthase; HMGCR: hydroxymethylglutaryl-CoA reductase; MVK: mevalonate kinase; MVD: diphosphomevalonate decarboxylase; IDI1: isopentenyl pyrophosphate isomerase 1; FPPS: farnesyl pyrophosphate synthase; FDFT: farnesyl-diphosphate farnesyltransferase 1; LSS: lanosterol synthase; DHCR7: 7-dehydrocholesterol reductase; FASN: fatty acid synthase; SCD: stearoyl-CoA desaturase.

7

Deregulation of cholesterol homeostasis is a signature of metabolic reprogramming, a hallmark of cancer.[50, 51] Cancer cells require high cholesterol levels for their increased metabolic needs and proliferation. Enhanced cholesterol synthesis and upregulation of the LDLR contribute to the increased cholesterol availability in cancer cells. The high energetic cost of *de novo* synthesis makes the uptake of exogenous cholesterol a more favored process for cells to acquire cholesterol.[52] Targeting cholesterol metabolism in cancer represents an attractive therapeutic strategy.[50, 53, 54] Importantly, previous studies demonstrated a correlation between cholesterol synthesis genes and patient survival.[48] Statins inhibit cholesterol synthesis by targeting the HMG-CoA reductase resulting in cancer cell starvation and death.[55] On the other hand, S2R is involved in enhancing the cholesterol uptake to increase its cellular availability with lower energy consumption. Thus, targeting S2R in cancer is a promising strategy for killing the cells through interference with cholesterol metabolism.

The Role of Sigma-2 Receptor in Cancer

S2R is involved in key cellular pathways important for cholesterol metabolism and can be exploited as an important therapeutic target for cancer. However, in-depth understanding of its role in tumor initiation and progression is currently lacking. No endogenous ligands for S2R have been identified, making it challenging to establish definitive pharmacological and physiological roles. S2R is overexpressed in select cancers including pancreatic, brain and breast cancers.[24, 30, 31, 56] Knockdown of TMEM97 reduces cell proliferation, migration, and invasion in several cancers validating its role in tumor growth.[57-60] Moreover, the overexpression of TMEM97 is associated with poor prognosis.[57, 61-64] The function of S2R in cancerous tissues is strongly related to cholesterol and calcium homeostasis as detailed below.

Cholesterol homeostasis. The cholesterol biosynthetic pathway is a major strategy for the manipulation of cancer cell metabolism. Early studies linked sigma receptors to cholesterol.[32, 65, 66] S1R in particular was suggested to be a mammalian homolog of the yeast sterol C_8-C_7 isomerase, an enzyme involved in sterol synthesis that has an identical topology and shares 30% identity.[65, 66] The study demonstrated the binding of the sigma ligand haloperidol, as well as, other sigma ligands with the yeast sterol C_8-C_7 isomerase.[66] Similarly, S2R has been linked to cholesterol long before the identification of its coding gene.[32] S2R was initially identified as the PGRMC1 demonstrated by the increased sigma-2 ligand (S2L) affinity with PGRMC1 overexpression as well as their colocalization.[32] PGRMC1 is a heme-binding protein that plays a regulatory role in cholesterol synthesis.[67-69] It binds to the SREBP regulatory proteins, INSIG and SCAP, however, the function of this interaction is not well explored.[44] PGRMC1 stimulates proliferation of cancer cells.[69-71] Although the S2R was later proven to be distinct from PGRMC1, S2Ls were found to be associated with PGRMC1 in the cells.[32] Accordingly, TMEM97 forms a complex with PGRMC1 and LDLR that facilitates LDL internalization.[21] This interaction provides a possible explanation to the previous postulation on the S2R's identity. TMEM97 knockout results in partial to complete loss in the binding of the S2Ls [^{3}H]1,3-di-*o*-tolylguanidine (DTG) and [1^{25}I]RHM-4 to S2R providing further support to the receptor's molecular identity.[21] More studies are now focused on understanding the exact role of S2R, its regulation and its targeting. For example, it was recently shown that bromodomain-containing protein 2 (BRD2) mediates epigenetic regulation of S2R under cholesterol deprived conditions.[72] BRD2 interacts with SREBP at the S2R promotor region to induce its expression.[72] These findings reveal a novel regulatory mechanism of the S2R and presents a potential strategy for S2R inhibition on the transcriptional level.

Calcium homeostasis. Calcium is involved in various cellular processes and plays an important role in cell growth, proliferation, and death.[73, 74] Calcium regulates the mitochondrial function and ATP production in cellular metabolism.[75] S2Ls induce calcium mobilization from the ER resulting in increased intracellular calcium levels that are accompanied by reduced metabolic activity, calcium-mediated apoptosis and cancer cell death.[76, 77] Activation of the ER calcium release channel, inositol 1,4,5-triphosphate receptor (IP$_3$R), is one mechanism by which S2Ls induce ER calcium efflux.[77, 78] S2R promotes the store-operated calcium entry (SOCE), a major route for calcium entry that is enhanced in cancerous tissues.[79] The SOCE requires the interaction of the sensory receptor, stromal interaction molecule (STIM), with the calcium channel protein 1 (ORAI1) to facilitate calcium entry (Figure I-5).[80] S2R interacts with STIM and its silencing reduces SOCE.[81] S2Ls that interfere with SOCE inhibit cell proliferation and cause apoptotic cell death.[81] However, not all S2Ls impair SOCE or cause calcium-induced cytotoxicity.[81, 82] The exact role of S2R in calcium homeostasis is yet to be established. The controversy over the cellular effects of various S2Ls on the intracellular calcium levels suggests different modes of action and requires further investigation.
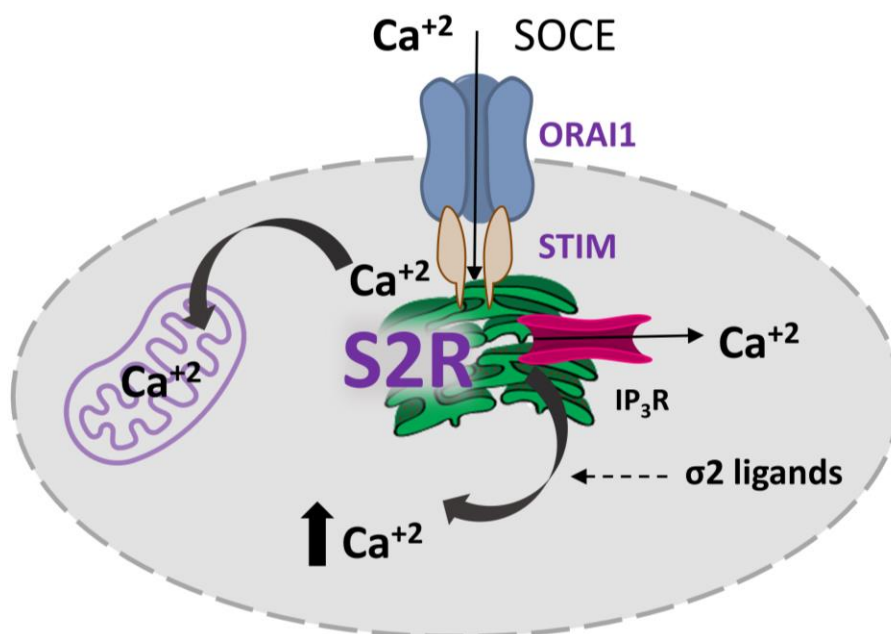
Figure I-5. Proposed role of S2R in calcium homeostasis: 1) Enhance SOCE by interacting with STIM. 2) Regulate IP$_3$R-mediated calcium release. The figure is adapted from Cantonero *et al*.[81]

S2R's regulatory role in cellular metabolism was also highlighted in a study demonstrating improved mitochondrial function in cells treated with the S2L, CM764.[83] Elevated ATP levels suggested CM764 induces glycolysis.[83] Further studies are required to establish the proposed role of S2R in glycolysis.

Collectively, S2R plays a role in the cancer cell metabolism by interfering with calcium and cholesterol levels. Calcium interferes with cholesterol homeostasis.[84] Reduced ER calcium levels enhance the nuclear SREBP activity.[84] While calcium deregulation has been reported to contribute to the cytotoxicity of S2Ls, there is no extensive research done on their effect on the metabolism of cholesterol and its involvement in cancer cell death. Further investigation is warranted to better elucidate the role of S2R in cancer and will determine if there is a correlation between the calcium- and cholesterol-mediated cellular effects. Interfering with cholesterol and calcium, two critical targets in cancer cell metabolism, is a promising strategy for cancer treatment.

Relevance of sigma-2 receptor in pancreatic cancer

Pancreatic cancer cells are highly dependent on cholesterol for growth.[85-90] Upregulation of LDLR is a metabolic signature in pancreatic cancer.[89] LDLR silencing results in reduced cell proliferation of the pancreatic cancer cells providing evidence of their dependence on cholesterol uptake for survival.[89, 90] In addition, LDLR knockdown sensitizes cancer cells to conventional therapies including gemcitabine.[89] Increased LDLR expression correlates with high relapse rate in patients with pancreatic ductal adenocarcinoma (PDAC).[89] Thus, interfering with the LDLR is an attractive therapeutic strategy for targeting cholesterol uptake in pancreatic cancer cells. Accumulation of cholesteryl ester is detected in pancreatic cancer cells.[86] Inhibition of the esterifying enzyme acyl-CoA cholesterol acyl-transferse-1 (ACAT1) increases the free cholesterol levels and ER stress resulting in tumor growth suppression which supports cholesterol esterification as a potential therapeutic strategy for pancreatic cancer.[86] Bioinformatics analysis of PDAC patient samples revealed the deregulation of genes relevant to cholesterol synthesis and further demonstrated its correlation with the PDAC subtype.[87, 88] It was demonstrated that cholesterol availability in p53 mutant pancreatic cancer cells is greater than the cellular demand.[85] This effect was attributed to sterol O-acyltransferase 1 (SOAT1), an abundant enzyme involved in cholesterol storage, where SOAT1 blockade was found to stall the tumor growth.[85] Overall, targeting cholesterol metabolism in pancreatic cancer represents a promising therapeutic strategy.

S2R is overexpressed in pancreatic cancer cell lines.[24] S2R plays a role in the cholesterol uptake by interacting with LDLR to facilitate its rapid internalization.[21] Thus, S2R represents a promising anticancer target that is involved in essential survival mechanisms acquired by the pancreatic cancer cells. Importantly, most preclinical studies on S2Ls were performed in murine pancreatic cancer models that displayed significant reduction in the tumor growth and improved

survival with no major toxicities (Table I-1). Several S2Ls were tested in combination with conventional chemotherapies like gemcitabine and paclitaxel.[25, 26] A superior reduction in tumor growth resulted from the combination treatment compared to either compound alone.[25, 26] This data not only supports the therapeutic potential of S2Ls in pancreatic cancer but also validates their use in combination therapies. Interference with cholesterol metabolism can contribute to the *in vivo* efficacy of S2Ls in pancreatic cancer.

Table I-1. Reported *in vivo* studies for S2Ls in pancreatic cancer.

S2L ID	Activity	Xenograft cell line	Year	References
WC26	- Reduced tumor growth - No acute toxicity - Improved overall survival.	PancO2	2007	[24]
SV119	- Single agent or combined with gemcitabine or paclitaxel: Reduced tumor growth and improved survival - No major toxicity	PancO2, BxPC-3	2009, 2010 2012	[25-27]
SW43	- Single agent or combined with gemcitabine: Reduced tumor growth and improved survival - No major toxicity	PancO2, BxPC-3	2010 2012	[26, 27]
Siramesine	- Single agent or combined with gemcitabine: Reduced tumor growth and improved survival - No major toxicity	PancO2	2010	[26]
PB28	- Reduced tumor growth	BxPC-3	2012	[27]

It is worth noting that a study investigating TMEM97 expression in pancreatic cancer demonstrated its variation among the analyzed samples where a large percentage displayed low TMEM97 levels suggesting a tumor suppressive role.[91] TMEM97 expression levels also varied among different pancreatic cancer cell lines. These findings should be followed up with TMEM97-silencing studies in different pancreatic cancer cell lines to determine its contribution to tumorigenesis. Nonetheless, the implication of TMEM97 in tumor progression has been verified in several cancers including gastric, brain and breast cancers where TMEM97 knockdown was associated with reduced cell viability and invasion.[57-59] Further in-depth studies on TMEM97's

role in pancreatic cancer is required to establish a correlation between its implication in tumor growth and the significant *in vivo* efficacy of S2Ls.

Commonly used Sigma Ligands

1,3 Di-*o*-tolylguanidine

DTG is a sigma ligand that displays neuroprotective properties and is considered the prototype compound for S2R studies.[92] TMEM97 knockout results in only partial reduction of [³H]DTG binding suggesting DTG has residual binding sites different from the identified S2R site.[21] These residual binding sites remain to be determined. Although DTG displays nonselective affinity to both sigma receptors, its radiolabeled form [³H]DTG has been the standard ligand in sigma-2 binding assays.

The radioligand binding assay is considered the primary assay for the identification of S2Ls. It is carried out on membrane fractions extracted from tissues with high S2R expression. The assay is based on the competition of potential ligands with the radioactive ligand [³H]DTG to its sigma-2 binding site.[93] The assay is performed in the presence of the selective S1R ligand pentazocine for masking of the S1R binding sites. Binding affinities (K_i) are calculated for identification of potential ligands.[93] The binding of DTG to multiple sites presents a challenge in the identification of selective S2Ls. Importantly, functional assays are needed to identify the mechanism of action of the binding ligand and whether it activates or blocks the receptor.

Haloperidol

Since the S2R was initially classified as an opioid receptor, interest was focused on neurological therapeutics like haloperidol.[94] Haloperidol is an antipsychotic drug that binds to various receptors including serotonin, dopamine and sigma receptors (Appendix Figure I-1).[95, 96]

Despite its high affinity to multiple receptors and lack of S2R/S1R selectivity, haloperidol is commonly used as a reference ligand in S2R studies.[24, 31, 35, 76] Haloperidol is cytotoxic to cancer cells through multiple mechanisms including apoptosis, oxidative toxicity and ferroptosis (Table I-2).[97-99] Studies have proven that haloperidol cytotoxicity is mediated by S2R where the presence of [³H]DTG reduces its apoptotic effect.[98] Haloperidol and other S2Ls were also found to potentiate the anticancer activity of other chemotherapeutics like doxorubicin in drug-resistant cells giving rise to the beneficial use of S2Ls in chemoresistance.[31] These findings support the potential role of S2R in cancer and validates its targeted therapeutics.

Reported Classes of Sigma-2 Ligands

Several reviews have discussed the structural features of various S2Ls.[100, 101] Early studies involved nonselective sigma ligands, but with increased evidence on the therapeutic potential of S2R, studies became more focused on developing selective ligands that are classified into five major classes (Figure I-6):
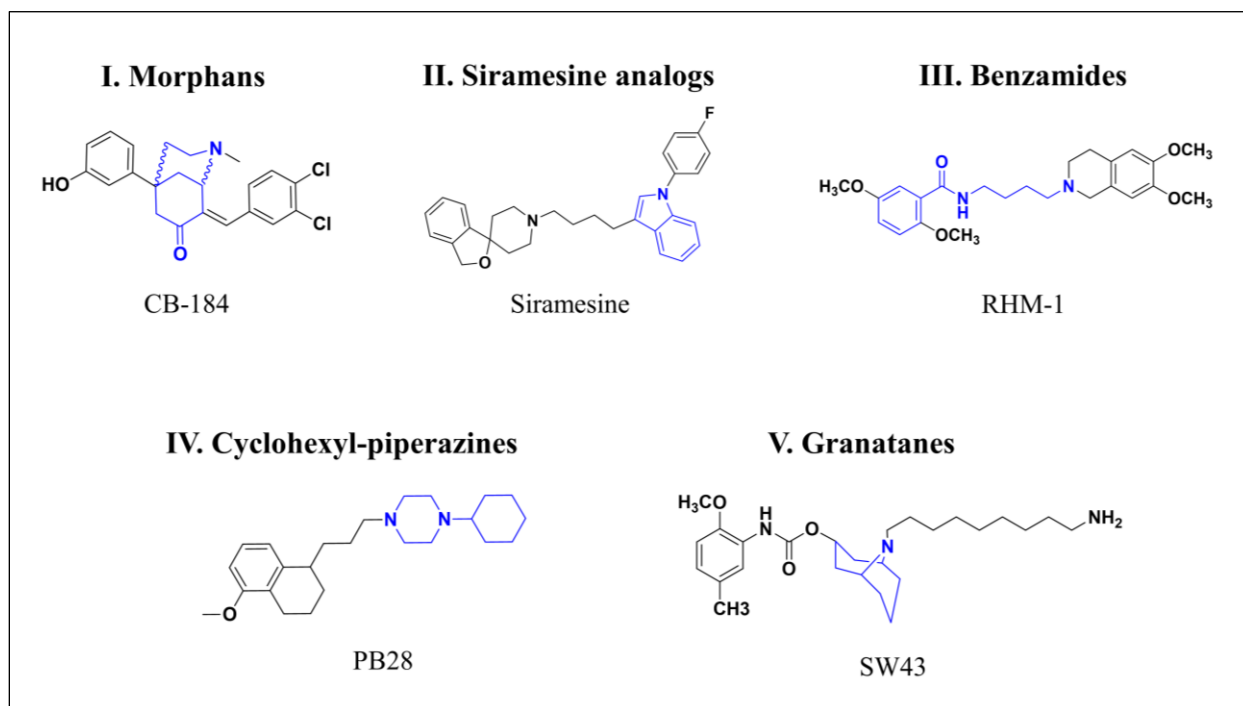
Figure I-6. Classes of reported S2Ls.

I. Morphans

The first attempt to develop selective S2Ls introduced the morphans that are characterized by having the opioid morphinan structure (Figure I-6).[102, 103] Unfortunately, these compounds had high affinity to the μ opioid receptor. Incorporation of a benzylidene moiety enhanced the S2R binding and reduced the μ receptor binding. CB-64D and CB-184 are examples of benzylidene morphan derivatives with nanomolar binding affinities and high S2R/S1R selectivity, >180-fold and >500-fold, respectively (Table I-3).[102] CB-64D and CB-184 induce S2R-mediated cytotoxicity that involves caspase-independent apoptosis and calcium deregulation.[31, 76] Although these compounds still possessed affinity for the μ opioid receptor, they were used in various S2R studies to investigate its role in cancer.[31, 76]

II. Siramesine

Siramesine is an indole-3-yl-alkyl-arylpiperazine derivative that emerged from the structural optimization of low efficacy serotonin 1A receptor (5-HT$_{1A}$) ligands (Figure I-6).[104] It displays a sub-nanomolar affinity to the S2R with 140-fold S2R/S1R receptor selectivity (Table I-3). Key structural features in siramesine included the 4-fluorophenyl group that contributes to reduced affinity to other receptors like dopamine and serotonin receptors while the butyl linker between the indole and the spiro-benzofuran-piperidine was optimal for a high S2R/S1R selectivity.[104] Siramesine is one of the most exploited S2Ls that was used in various studies involving the receptor's function and activity. Siramesine causes cell death *via* multiple mechanisms including apoptosis, reactive oxygen species (ROS), lysosomal destabilization, cell cycle arrest and autophagy.[26, 105, 106] Siramesine is a promising anticancer agent with *in vivo* efficacy in pancreatic cancer as a single agent or in combination with gemcitabine (Table I-1).[26] Extensive studies on siramesine provided insight into the potential of S2R as an anticancer target.

III. Benzamides

Benzamides are among the compounds that display the highest selectivity to the S2R. They were identified from optimized derivatives of dopamine antagonists that were found to possess affinity to S2R.[107] The structure of this class of compounds is comprised of a benzamide moiety usually separated by a 4-carbon linker from a nitrogen atom (Figure I-6). Synthetic derivatives that employed differently substituted benzamides led to the identification of two commonly used ligands RHM-4 and ISO-1 with high affinity and selectivity to the S2R (K_i = 11 nM and 7 nM, respectively) (Figure I-9).[108] The discovery of such selective compounds contributed to early S2R studies that utilized radiolabeled probes for the characterization of S2R and its imaging in cancer tissues (Figure I-9).[108] Another derivative that was widely exploited is RHM-1 with high selectivity to S2R over S1R by almost 300-fold (Table I-3). RHM-1 was tested for its activity in cancer cells but was found non-cytotoxic (Table I-3). The use of this class of compounds was mainly based on their association with the highly expressed S2R in tumor tissues for imaging and diagnostic purposes.

IV. Cyclohexyl-piperazines

This class of compounds comprises a *N*-cyclohexylpiperazine as a basic moiety (Figure I-6). Studies identified the lead compound PB28 that binds to both sigma receptors with high affinity (Table I-2). Attempts to optimize for less lipophilic ligands identified analogs that are more selective to the S2R, however, they displayed P-glycoprotein (P-gp) activity and lacked antiproliferative properties.[109] Furthermore, hydrophilic substitutions were found to reduce the S2R-mediated cytotoxicity suggesting a correlation between the lipophilicity and the antiproliferative activity.[110] F281, a close PB28 analog studied for its activity in the SK-N-SH neuroblastoma cells displayed greater cytotoxicity but lower sigma-2 affinity suggesting a

multitargeted mechanism (Table I-3).[77] PB28 displays cytotoxic properties against cancer cell lines *via* multiple mechanisms including apoptosis and mitochondrial ROS induction.[27, 111, 112] Affinity chromatography utilizing PB28 identified histone proteins suggesting they are a target that can contribute to its cytotoxicity.[113, 114] *In vivo* studies showed significant reduction of pancreatic tumor growth.[27] PB28 was also found beneficial with compounds that acquire drug resistance by enhancing the sensitivity to chemotherapeutic agents *via* P-gp modulation.[115] PB28 remains the lead of this class. It is a well investigated sigma ligand that is used as a reference compound in several studies despite its non-selectivity.

Another group of phenyl-piperazine derivatives optimized from the neuroprotective sigma receptor antagonist SN79, demonstrated various cellular effects with respect to their cytotoxicity.[83, 116, 117] While CM764 displayed cytoprotective properties in neuroblastoma cells, its analog CM572 is cytotoxic (Figure I-7).[83, 116, 118] CM572 was proposed to bind to S2R in an irreversible manner that contributes to cytotoxicity.[116] In addition, CM572 displayed a much greater S2R/S1R selectivity (> 600-fold) compared to CM794 (~ 25-fold) (Figure I-7).[83, 116] These findings suggest that the mode of binding to S2R has a great impact on the induced cellular effects.
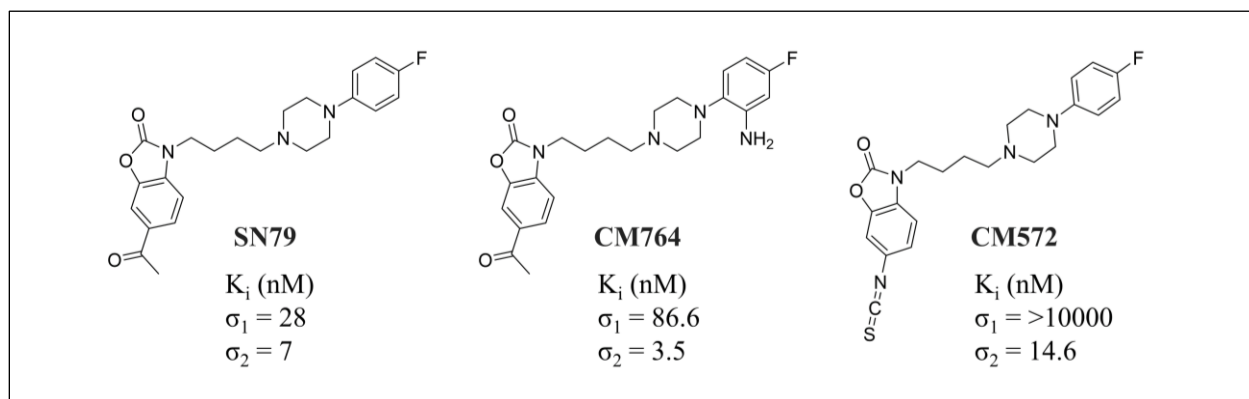
Figure I-7. Chemical structures of SN79 analogs.

V. Granatanes

Granatanes are considered the most promising class of S2Ls that advanced to preclinical studies. Structural optimization of serotonin receptor ligands introduced the granatane compounds with improved S2R binding.[119] Their structure comprises a granatane ring whose nitrogen can accommodate bulky substitutions and is optimal for S2R selectivity when it includes an additional nitrogen four or more carbon atoms apart (Figure I-6).[120] Three compounds from this class were the most exploited including SW43, WC26 and SV119 that display high S2R affinity (Table I-3). SV119 and SW43 include a *N*-aminoalkyl chain substitution with varying lengths and display >270-fold and >18-fold S2R/S1R selectivity, respectively, while WC26 includes a dimethylaminobenzyl moiety with >500-fold S2R/S1R selectivity (Table I-3).[119] The dansyl or 7-nitrobenzofurazane derivatives of this class are used as fluorescent probes for *in vitro* and *in vivo* imaging.[121] The preferential expression of S2R in tumor cells encouraged the design of SW43-drug conjugates to second mitochondria-derived activator of caspase (SMAC) mimetics for tumor-targeting drug delivery in ovarian cancer.[122, 123] SW43, WC26 and SV119 display *in vivo* efficacy in murine models of pancreatic cancer alone or in combination with gemcitabine (Table I-1). Treatment with WC26 resulted in reduced pancreatic tumor growth and improved survival rate, however, regrowth of tumors occurred but at a lower rate than the control group.[24] SV119 showed significant reduction of tumor growth when combined with gemcitabine or paclitaxel compared to SV119 alone.[25] *In vivo* studies investigating SV119, SW43, or siramesine in combination with gemcitabine displayed more prominent efficacy in pancreatic tumor reduction in the SW43 combination.[26] Further studies are needed to select a clinical candidate.

VI. Miscellaneous ligands

RC-106 is a nonselective sigma receptor ligand with a benzylpiperidine structure that displays antiproliferative properties in pancreatic cancer cell lines (Table I-2).[124, 125] The tropane analog RHM-138 displays high affinity and selectivity to the S2R and is widely used in the cancer-related studies of S2R due to its cytotoxic properties (Table I-3). In summary, several classes of S2Ls have been reported but only a limited number were tested for their *in vivo* efficacy. The selectivity and/or weak cytotoxicity are limitations to the development of S2Ls as anticancer agents.

Table I-2. Representative nonselective sigma ligands.
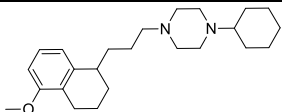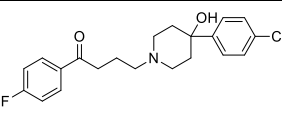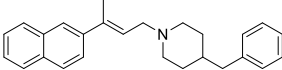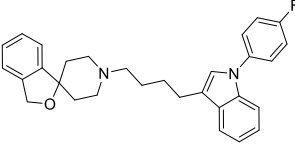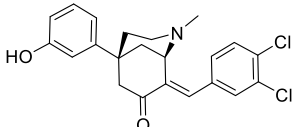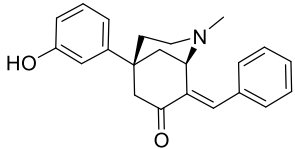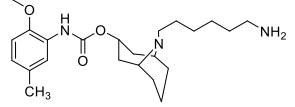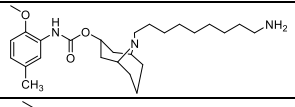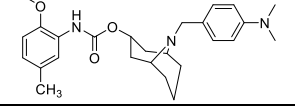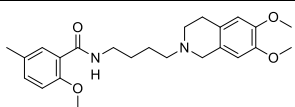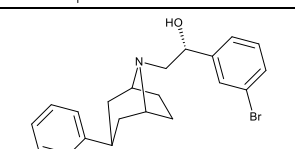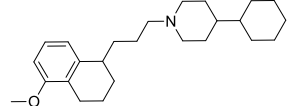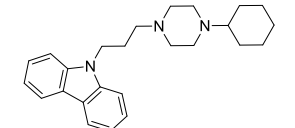
Name	Structure	S1R K_i (nM)	S2R K_i (nM)	Cytotoxicity (μM)	Reference
PB28		0.38	0.68	PancO2 (24 h) = 73 BxPC-3 (24 h) = 96 AsPC-1 (24 h) = 244 SK-N-SH (24 h) = 5.1	27, 110, 111
Haloperidol		2.3	6.5	K-562 (72 h) = 40 IMR-32 (72 h) = 24 A427 (96 h) = 9.6 MCF-7 (96 h) = 24.9 RT-4 (96 h) = 16 SK-N-SH (24 h) = 4.0	96, 111, 126, 127
RC-106		12	22	MDA-MB-231 (24 h) = 64.9 LNCaP (24 h) = 61.1 U87 (24 h) = 60.6 SUM159 (24 h) = 58.3 PC3 (24 h) = 50.6 CAPAN-2 (24 h) = 52.6 PaCa3 (24 h) = 49.8	124

Table I-3. Representative selective S2Ls.

Name	Structure	S1R K_i (nM)	S2R K_i (nM)	Cytotoxicity (μM)	Reference
Siramesine		17.0	0.12	HEK293A (21 h) = 10.7 MDA-MB-468 (21 h) = 8.2 HBL-100 (21 h) = 12.5 ME-180 (21 h) = 9.7 HeLa (21 h) = 10.7 NIH 3T3 (24 h) = 9.4 EMT-6 (48 h) = 5.3 MDA-MB-435 (48 h) = 9.3	104-106

Compound	Structure				
CB-184		7436	13.4	MCF-7 (48 h) = 4.3 SKBr3 (48 h) = 5.0 T47D (48 h) = 9.0	[31, 102]
CB-64D		3063	16.5	MCF-7 (48 h) = 36.3 SKBr3 (48 h) = 40.2 T47D (48 h) = 73.0	[31, 102]
SV119		1418.0	5.2	PancO2 (24 h) = 92 BxPC-3 (24 h) = 97 AsPC-1 (24 h) = 192 EMT-6 (24 h) = 16 MDA-MB-435 (24 h) = 36.7	[27, 106, 119]
SW43		134.3	7.07	PancO2 (24 h) = 26 BxPC-3 (24 h) = 56 AsPC-1 (24 h) = 65	[27, 119]
WC26		1436.0	2.6	EMT-6 (24 h) = 42.5 MDA-MB-435 (24 h) = 49.7	[106, 128]
RHM-1		3078.0	10.3	EMT-6 (24 h) = >200 MDA-MB-435 (24 h) = >200	[107, 129]
RHM-138		544.0	12.3	EMT-6 (24 h) = 32.5 MDA-MB-435 (24 h) = 26.7	[106, 129]
PB221		143	18.8	Panc02 (24 h) = 37 KP02 (24 h) = >100 KCKO (24 h) = 19 MIA PaCa-2 (24 h) = 50 BxPC-3 (24 h) = 100 AsPC-1 (24 h) = >100 Panc-1 (24 h) = >100	[112, 130]
F281		3450	12.6	SK-N-SH (24 h) = 0.1 LoVo (24 h) = 3.5 PancO2 (24 h) = 37 MIA PaCa-2 (24 h) = 29 BxPC-3 (24 h) = 42 KP02 (24 h) = 49 KCKO (24 h) = 62 AsPC-1 (24 h) = 98 PANC-1 (24 h) = >100	[77, 112, 131]

Predicted Pharmacophore for Sigma-2 Ligands

Structurally diverse compounds bind to the S2R. The lack of S2R co-crystal structures triggered studies to focus on the identification of the key pharmacophoric features required for binding. Early studies were more focused on the S1R for which several pharmacophore models

were reported.[132, 133] Further studies showed similarity in the pharmacophoric features for S1R and S2Rs. Essential features for binding included a proton donor site in most cases represented by a basic amine separated from a hydrophobic moiety by an alkyl chain linker. Abate *et al.* investigated the structure-affinity relationship of various classes of S2Ls and identified structural moieties that contribute to S2R selectivity and/or affinity.[110] A number of 3D pharmacophore models derived from different classes of S2Ls have also been proposed.[134-136] One model demonstrated that most features required for S1R binding are shared by S2R with a few changes including a shorter spacer length between the nitrogen and the secondary hydrophobic site (8.5 Å in S1R) (Figure I-8).[135] Such remarkable similarity presents a challenge in developing selective S2Ls. Another model agreed with the three key features reported including a primary hydrophobic site, a hydrogen bond donor region and a secondary hydrophobic region as outlined in Figure I-8.[134] Importantly, it was demonstrated that the S2R binding pocket includes ASP29 and ASP56 as key residues for recognition and binding of S2Ls.[19, 23] Recently, two S2R homology models were developed for virtual screening in an attempt to identify novel and selective S2Ls.[22, 23] One virtual screen identified a number of compounds with cytotoxic properties against cancer cell lines with high S2R expression.[23] The structural insight provided by these studies is beneficial in guiding the development of selective and potent S2Ls. However, a crystal structure will better assist in structure-based drug design and will help overcome the critical issue of nonspecific binding by identification of the key residues of interaction as well as structural similarities with other targets. It will also allow for the identification of different ligand binding modes that can contribute to various cellular effects.
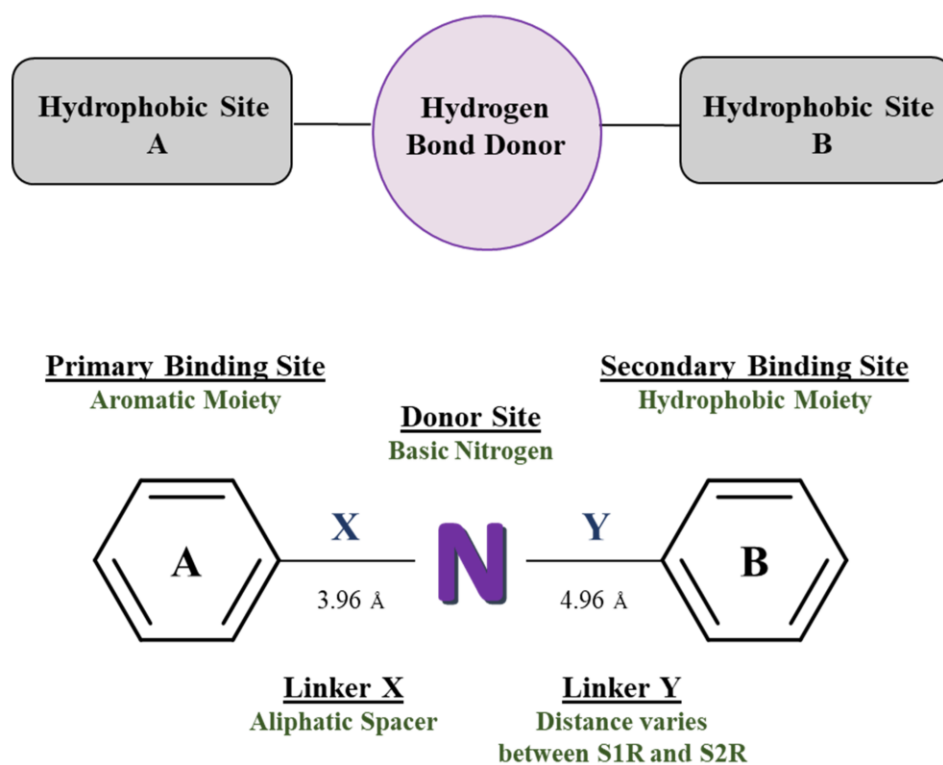
Figure I-8. Summary of the reported pharmacophoric features required for S2R binding. Features were adapted from Glennon's model for S1R that displays a longer distance for linker Y (6-10 Å).[137]

Sigma-2 Ligands as Imaging Tools

The unclear functional role of S2R and the lack of known endogenous ligands requires further understanding. Apart from the investigational use of S2Ls to study the receptor's function, they are primarily used as tumor imaging probes due to their high tissue localization.[138] The validation of S2R as a biomarker for tumor cell proliferation and the discovery of highly selective S2Ls led to the development of radiolabeled sigma-2 probes for *in vivo* tumor imaging and diagnostic purposes.[29, 139-142] [³H]DTG is one of the earliest ligands used to study the characteristics of S2R (Figure I-9).[143] Among the most widely used sigma-2 radioligands that were developed for imaging purposes are [¹⁸F]RHM-4 and [¹⁸F]ISO-1 (Figure I-9).[24, 108] Positron emission tomography (PET) images of mice administered with [¹⁸F]RHM-4 showed preferential binding to pancreatic cancer tissues versus normal tissues.[24] [¹⁸F]ISO-1 was used to assess the tumor

proliferative status and has entered clinical trials for tumor imaging studies by PET.[144-146] The preferential localization of S2Ls in pancreatic tumor tissues provides a promising strategy for selective targeting and killing of the cancer cells.

Fluorescently labeled S2Ls were also used not only for imaging purposes but also for their anticancer properties (Figure I-9). These compounds were used to further investigate the early postulation that PGRMC1 includes the S2R binding site which appeared to be controversial.[19, 32-34] F412 and NO1 are fluorescently labeled ligands that are highly selective for the S2R (Figure I-9) (Table II-3).[81] With the use of these ligands, it was shown that PGRMC1 and S2R are two distinct proteins.[33] The distribution of the compounds was studied by flow cytometry and confocal microscopy and it revealed that the S2R binding is independent of the PGRMC1 expression. Moreover, F412 and NO1 were displaced by S2Ls but not PGRMC1 inhibitors.[33]
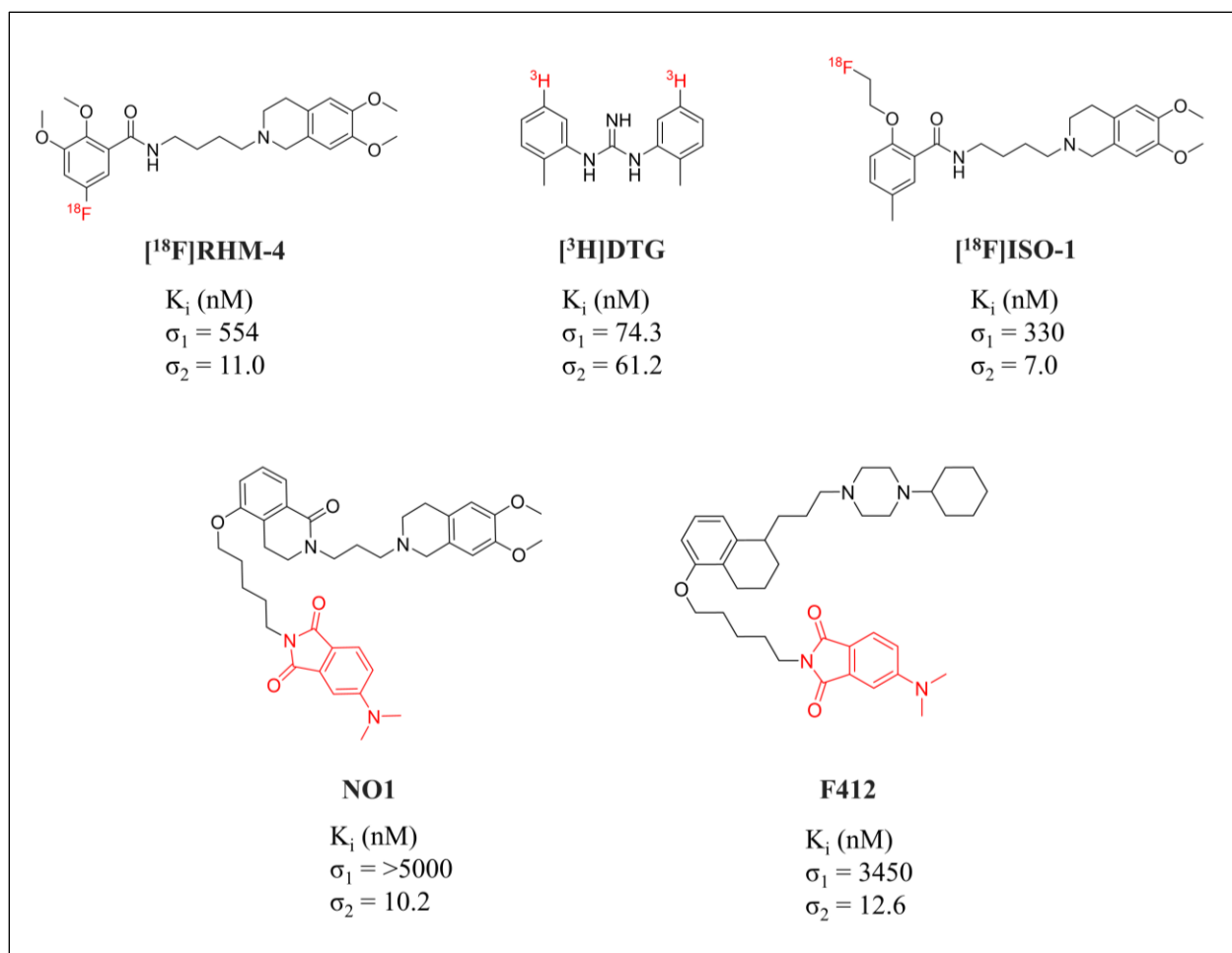
Figure I-9. Chemical structures of representative radiolabeled and fluorescent S2Ls.

Sigma-2 Ligands as Anticancer Agents

S2Ls have been reported to induce cancer cell death *via* multiple mechanisms.[106] Their cytotoxicity is more prominent in cells overexpressing TMEM97 providing evidence to the S2R-mediated cell death.[81] In early 1995, S2Ls were found to cause changes in the glioma cell morphology and subsequent cell death.[147] It was later reported that activation of the S2R induces apoptosis through novel caspase-independent pathways.[31] However, further studies proved the involvement of caspase-mediated pathways.[112] As the field emerged, several cell death mechanisms were reported for S2Ls including apoptosis, autophagy, ROS induction, and cell cycle arrest (Figure I-10).

Apoptosis. Apoptosis (programmed cell death) is an essential process for cellular homeostasis and its deregulation is implicated in cancer.[148] Most S2Ls are reported to induce cell death *via* caspase-dependent and/or -independent apoptosis. PB28 and its analogs exert their cytotoxicity in pancreatic cancer cells *via* caspase-3 activation that is blocked in the presence of the caspase inhibitor Z-DEVD-FMK.[112] Similarly, a significant increase in caspase-3 levels was demonstrated with SW43 and siramesine treatments but not SV119.[26] While caspase inhibition reduced the induced caspase-3 levels, the overall cytotoxicity of SW43 and siramesine was not affected.[26] Caspase-3 activation was also detected in breast cancer cell lines treated with WC-26, SV119 and RHM-138 where their cytotoxicity was partially rescued by caspase inhibition.[106] Interestingly, SV119 had a modest effect on the caspase-3 activation in pancreatic cancer cells compared to breast cancer cells. [26, 106] These results suggest that although caspase activation is associated with various S2Ls, it does not necessarily contribute to their cytotoxicity and might be cell line dependent. Variations in the expression of sigma-1 and sigma-2 receptors across different cell lines might contribute to the distinct cellular effects of the S2Ls. Moreover, selectivity of the ligands can be a contributing factor.

Some S2Ls induce caspase-independent apoptosis.[31, 105] Siramesine induces both caspase-dependent and -independent pathways.[26, 105] CB-64D and CB-184 induce caspase- and p53-independent apoptosis that was demonstrated by their consistent cytotoxicity irrespective of caspase inhibition or the p53 genotype.[31] It is unclear why S2Ls display distinct cellular effects. Further investigation is required to determine whether these variations are a result of different binding modes and/or different mechanisms of action.

S2R mediates cellular effects that interfere with calcium homeostasis, and its ligands can induce calcium-mediated apoptosis.[76, 77] Various mechanisms were proposed including reduced

SOCE by NO1 or opening of the IP$_3$R by F281.[77, 79] PB28 induces opposite effects by inhibiting the IP$_3$R and caffeine-sensitive calcium release.[82] It is worth noting that PB28 is also a S1R ligand hence, its cellular effects are not exclusive to S2R (Table I-2). Overall, deregulated calcium levels is a common cellular effect of S2Ls, that can impair the cancer cell metabolism and reduce cell survival. The lack of a functional assay that can identify agonists versus antagonists remains a challenge in establishing the function of S2R.

ROS Induction. The induction of ROS has been reported as a common mechanism of cell death with various S2Ls.[105, 112] Antioxidants like α-tocopherol blocked the caspase-3 activity and attenuated the cytotoxicity of PB28, SW43 and siramesine suggesting the involvement of ROS.[105, 112] Additionally, increased mitochondrial superoxide radicals were detected with PB28 treatment.[112] Siramesine induces oxidative stress and cell death that is prevented by lipophilic but not hydrophilic antioxidants suggesting siramesine induces lipid peroxidation.[105] It was also suggested that selective protection by lipophilic antioxidants is due to their incorporation into the lysosomal membrane to enhance its stability.[149] Lipid peroxidation is a sign of ferroptosis, a mechanism of cell death that involves iron and ROS.[150, 151] Haloperidol induces ferroptosis in cancer cells.[99] Reduced cholesterol uptake has been linked to ferroptosis.[152] It is worth investigating whether ferroptosis is a common mechanism of cell death with S2Ls especially now with the recently identified role of S2R in cholesterol metabolism.

Autophagy. Autophagy is a process that maintains cellular homeostasis by removal of misfolded proteins and damaged organelles including the lysosomes.[153] mTOR is an important regulator of autophagy and its activation promotes cell proliferation and survival.[154] Siramesine reduces the mTOR activity and induces autophagy.[149] Autophagosome accumulation observed with siramesine treatment is due to lysosomal malfunction.[149] Similarly, WC-26, SV119, and

RHM-138 increased the synthesis of autophagosome markers and reduced mTOR expression.[106] Studies demonstrated the subcellular localization of S2Ls in the lysosome.[155] Lysosomes play a role in cholesterol homeostasis and autophagy.[156, 157] S2L-mediated cell death involves lysosomal cathepsins.[27, 105, 149] Siramesine permeabilizes the lysosomal membrane resulting in the release of cathepsins that are involved in various cell death events.[149, 158] Similarly, SW43 and PB282 localize and accumulate in the lysosome to induce lysosomal destabilization that contributes to cell death.[27] Knockdown of protective lysosomal membrane glycoproteins enhanced the susceptibility of cancer cells to S2Ls.[27] Collectively, S2Ls can cause lysosomal destabilization and leakage of cathepsins that can induce autophagy and apoptosis, respectively.[86] Sterol-depleted cells showed TMEM97 lysosomal localization where it binds to the cholesterol transport-regulating protein NPC1.[159] This provides a possible explanation to the accumulation of S2Ls in the lysosomes..

Cell cycle regulation. WC-26, SV119, RHM-138, and siramesine showed a decrease in the Cyclin D1 expression and other cell cycle proteins suggesting S2Ls impair cell cycle progression at different phases.[106, 160] Indole-based compounds including siramesine demonstrated cell cycle arrest at the G1 phase.[160] Alterations in the cell cycle progression can result from impairment of various cellular processes including cholesterol biosynthesis.[161]

In summary, it is notable that the cellular effects induced by S2Ls are interconnected. S2R is a regulator of cholesterol homeostasis. Cholesterol is a central element for cellular homeostasis that has been linked to apoptosis, autophagy and lysosome integrity, ROS, lipid peroxidation and ferroptosis, and cell cycle.[86, 152, 156] Under starvation conditions, the cells induce lysosome-mediated lipophagy (autophagy of lipid droplets) to increase the availability of nutrients including cholesterol and meet its energy needs.[156] On the other hand, cholesterol accumulation can result in increased ROS levels and ER stress.[86] Further investigation can lead to the identification of critical

pathways that are mediated by S2R, possibly cholesterol-dependent, and establish its oncogenic role.
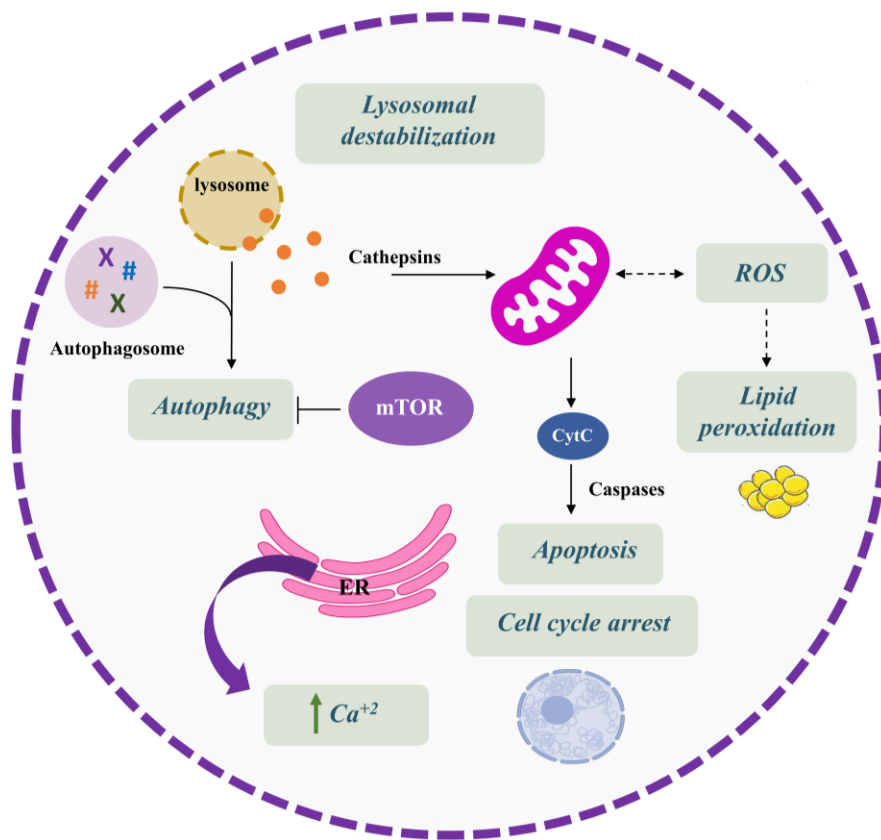
Figure I-10. Cell death mechanisms induced by S2Ls.

Despite many studies supporting the cytotoxicity of S2Ls in cancer cells, a recent study reported some challenging findings by demonstrating that their cytotoxicity is not mediated by TMEM97 or PGRMC1 in HeLa cells.[162] Knockout of TMEM97 and/or PGRMC1 did not affect the EC_{50} values of siramesine, SW43, or PB28.[162] The study demonstrated initial reduction in the internalization of the S2L SW120 with TMEM97 silencing that later became identical to the control.[162] These results require further confirmation. In this context, we have previously noted that there are high affinity S2Ls that displayed no cytotoxicity including RHM-1.[129] In-depth studies including various ligands and cancer cell lines are required to better understand the variations between the S2L affinity and its cytotoxicity.

Combination Strategies with Sigma-2 Ligands

With the increase in the number of research studies on S2R in cancer, *in vitro* therapeutic combinations have been examined and are summarized in Table I-4. S2Ls enhance the sensitivity of drug-resistant cells to conventional cancer therapies introducing a novel class of chemosensitizing agents. Importantly, *in vivo* combination studies (Table I-4) resulted in effective tumor regression and augmentation of the efficacy of chemotherapeutics like gemcitabine and paclitaxel providing evidence to S2Ls' preclinical success. Siramesine treatment was associated with increased autophagy that upon inhibition resulted in enhanced siramesine-mediated cell death suggesting beneficial combination studies with autophagy inhibitors.[149] Overall, these findings provide evidence to the potential of S2Ls in enhancing the tumor cell sensitivity to anticancer agents and introduces promising combinations that constitute a valuable approach for cancer treatment. With the identification of TMEM97 as the coding gene, we expect that combination studies with compounds targeting the cholesterol and lipid metabolism will be beneficial in killing the cancer cells.
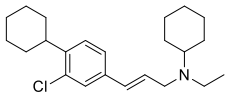
Table I-4. Examples of *in vitro* synergistic combinations of S2Ls.

Name	Combination Drug	Cancer Type	Reference
CB-184	Doxorubicin Actinomycin D	Breast	[31]
Haloperidol	Doxorubicin	Breast	[31]
SW43; SV119	Gemcitabine	Pancreatic	[26]
SW43; SV119	Olaparib; YUN3-6	Breast	[163]
Siramesine	Lapatinib	Breast	[164-166]
	Gemcitabine	Pancreatic	[26]

Clinical Trials on Sigma Receptor Modulators

So far, there are no clinically available anticancer sigma-2 targeting drugs. SR31747A was discovered in the 1990s and was identified to engage with the S2R. SR31747A binds with high affinity to four identified sites including SR31747A binding protein-1 (SRBP-1), SR31747A binding protein-2 (SRBP-2), S2R and human sterol isomerase (HSI).[167-169] Paul *et al.* suggested SR31747A works through allosteric modulation of sigma receptors since the compound inhibited the binding of other typical sigma ligands like DTG and pentazocine, but radiolabeling studies revealed binding sites distinct from the classical sigma receptor sites.[170] Interestingly, a study linked SR31747A's antiproliferative properties to cholesterol biosynthesis inhibition.[171] SR31747A displayed *in vivo* immunomodulatory and antiproliferative effects that led to its advance to clinical trials (Table I-5).[172, 173] However, there are no further updates on the clinical status of this compound since 2008.[174]

Table I-5. Sigma receptor modulator in clinical trials.

Name	Structure	Phase	Cancer Type	Reference
SR31747A		II NCT00174863	Prostate	[174]

Impact of TMEM97 on Patient Survival

The expression levels of TMEM97 in various cancers were obtained from the analysis of RNA sequencing data using GEPIA2.[175] Among the cancers with significantly overexpressed TMEM97 compared to the normal tissue were colon adenocarcinoma (COAD) and glioblastoma multiforme (GBM) (Figure I-11B). Data from patient samples demonstrated the involvement of TMEM97 in the progression and aggressiveness of colorectal cancer.[176] TMEM97 knockdown in glioma cells is associated with reduced cell proliferation.[57] Interestingly, the S2L PB221, demonstrated *in vivo* efficacy against brain tumors further supporting TMEM97's impact on tumor

growth.[177] Survival analysis of the TCGA patient samples comparing patients with low TMEM97 expression versus high expression was used to evaluate the contribution of TMEM97 to patient outcome (Figure I-A/C).[175] Poor prognosis was associated with several cancers including adrenocortical carcinoma (ACC), kidney renal papillary cell carcinoma (KIRP), acute myeloid leukemia (LAML), and sarcoma (SARC) (Figure I-11C). These cancer types are promising for further evaluation of the efficacy of S2Ls.
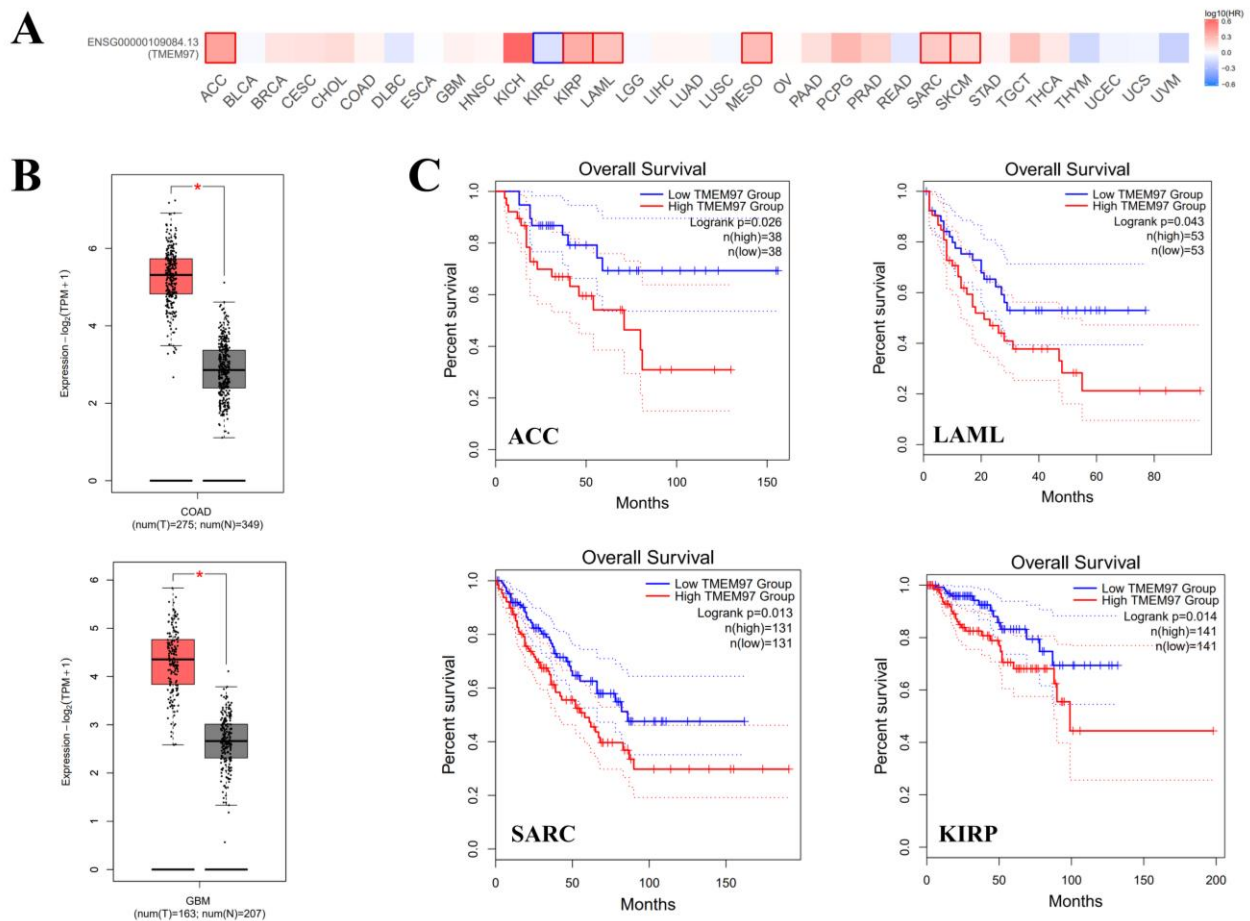
Figure I-11. High TMEM97 expression corelates with poor prognosis. (A) TMEM97 expression correlates with overall survival in several cancers. Red and blue blocks denote higher and lower risk, respectively, with an increase in the gene expression. Blocks with darkened outlines indicate statistical significance in prognostic analyses. (B) TMEM97 overexpression in colon adenocarcinoma (COAD) and glioblastoma multiforme (GBM) compared to normal tissues. (C) Survival analysis shows poor prognosis with high TMEM97 expression in adrenocortical carcinoma (ACC), kidney renal papillary cell carcinoma (KIRP), acute myeloid leukemia (LAML), and sarcoma (SARC). Samples were stratified into high and low expression populations using the 50th percentile.

Conclusion

In this chapter we highlight the role of S2R in cholesterol metabolism and its potential as a target for the treatment of pancreatic cancer. S2R plays a role in the regulation of intracellular cholesterol levels by enhancing the LDL uptake and increasing cholesterol availability in the cells. S2R is overexpressed in pancreatic cancer cells that rely on cholesterol for growth. Interfering with cholesterol metabolism is a promising strategy for cancer treatment, thus, targeting S2R represents an attractive therapeutic approach for pancreatic cancer. In-depth studies are still required to fully understand the exact role of S2R in cancer. The absence of a crystal structure and identified endogenous S2Ls makes it challenging to develop S2R-targeted molecules. Identification of the key pharmacophoric features for S2R binding will guide the design of selective ligands and eliminate nonspecific binding. Reported studies demonstrating the potential of S2R as an anticancer target are based on experimental observations from the use of synthetic tools. Importantly, S2Ls display promising *in vivo* antitumor activity against pancreatic cancer. The identification of the coding gene as TMEM97 will pave the way for more focused studies and functional characterization of the receptor. Studies involving S2Ls and their effect on the cholesterol metabolism still needs to be established and might unveil novel mechanisms. Combination studies of S2Ls with autophagy and cholesterol synthesis inhibitors are promising. Testing S2Ls in cancers that overexpress TMEM97 and correlate with poor prognosis might lead to the discovery of highly effective anticancer agents.

Appendix Figure I-1. Binding affinities of haloperidol. Graph was regenerated from previously reported data.
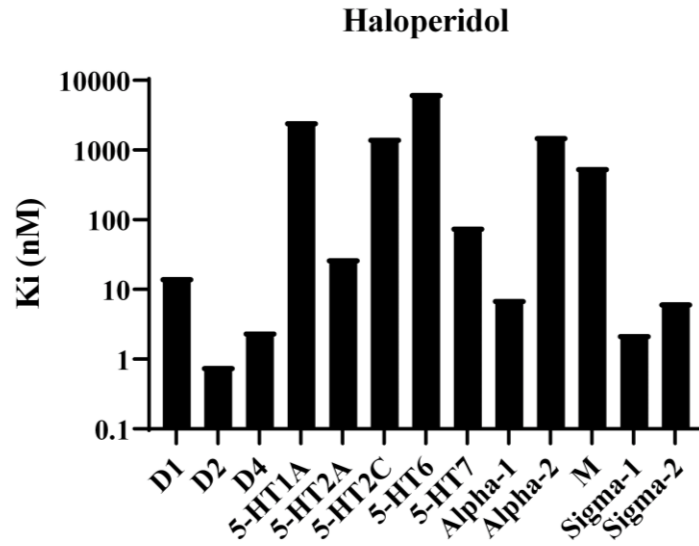
ID	D_1	D_2	D_4	$5\text{-}HT_{1A}$	$5\text{-}HT_{2A}$	$5\text{-}HT_{2C}$	$5\text{-}HT_6$	$5\text{-}HT_7$	α_1	α_2	M	σ_1	$\sigma2$	H_1
Haloperidol K_i (nM)[95, 96]	15	0.8	2.5	2600	28	1500	6600	80	7.3	1600	570	2.3	6.5	>730

References

1.   Zhu, H. Y.; Li, T.; Du, Y. Q.; Li, M., Pancreatic cancer: challenges and opportunities. *BMC Med* **2018,** *16*, 1-3.

2.   Rahib, L.; Smith, B. D.; Aizenberg, R.; Rosenzweig, A. B.; Fleshman, J. M.; Matrisian, L. M., Projecting cancer incidence and deaths to 2030: the unexpected burden of thyroid, liver, and pancreas cancers in the United States. *Cancer Res* **2014,** *74* (11), 2913-2921.

3.   Siegel, R. L.; Miller, K. D.; Jemal, A., Cancer statistics, 2020. *CA Cancer J Clin* **2020,** *70* (1), 7-30.

4.   Kikuyama, M.; Kamisawa, T.; Kuruma, S.; Chiba, K.; Kawaguchi, S.; Terada, S.; Satoh, T., Early diagnosis to improve the poor prognosis of pancreatic cancer. *Cancers (Basel)* **2018,** *10* (2), 48.

5.   Kleeff, J.; Korc, M.; Apte, M.; La Vecchia, C.; Johnson, C. D.; Biankin, A. V.; Neale, R. E.; Tempero, M.; Tuveson, D. A.; Hruban, R. H.; Neoptolemos, J. P., Pancreatic cancer. *Nat Rev Dis Primers* **2016,** *2*, 16022.

6.   Amrutkar, M.; Aasrum, M.; Verbeke, C. S.; Gladhaug, I. P., Secretion of fibronectin by human pancreatic stellate cells promotes chemoresistance to gemcitabine in pancreatic cancer cells. *BMC Cancer* **2019,** *19* (1), 1-16.

7.   Conroy, T.; Desseigne, F.; Ychou, M.; Bouche, O.; Guimbaud, R.; Becouarn, Y.; Adenis, A.; Raoul, J. L.; Gourgou-Bourgade, S.; de la Fouchardiere, C.; Bennouna, J.; Bachet, J. B.; Khemissa-Akouz, F.; Pere-Verge, D.; Delbaldo, C.; Assenat, E.; Chauffert, B.; Michel, P.; Montoto-Grillot, C.; Ducreux, M.; Groupe Tumeurs Digestives of, U.; Intergroup, P., FOLFIRINOX versus gemcitabine for metastatic pancreatic cancer. *N Engl J Med* **2011,** *364* (19), 1817-1825.

8.   Huang, X.; Ding, L.; Liu, X.; Tong, R.; Ding, J.; Qian, Z.; Cai, L.; Zhang, P.; Li, D., Regulation of tumor microenvironment for pancreatic cancer therapy. *Biomaterials* **2021,** *270*, 120680.

9.   Amanam, I.; Chung, V., Targeted Therapies for Pancreatic Cancer. *Cancers (Basel)* **2018,** *10* (2).

10.   Qian, Y.; Gong, Y.; Fan, Z.; Luo, G.; Huang, Q.; Deng, S.; Cheng, H.; Jin, K.; Ni, Q.; Yu, X.; Liu, C., Molecular alterations and targeted therapy in pancreatic ductal adenocarcinoma. *J Hematol Oncol* **2020,** *13* (1), 130.

11.   Moore, M. J.; Goldstein, D.; Hamm, J.; Figer, A.; Hecht, J. R.; Gallinger, S.; Au, H. J.; Murawa, P.; Walde, D.; Wolff, R. A.; Campos, D.; Lim, R.; Ding, K.; Clark, G.; Voskoglou-Nomikos, T.; Ptasynski, M.; Parulekar, W.; National Cancer Institute of Canada Clinical Trials, G., Erlotinib plus gemcitabine compared with gemcitabine alone in patients with advanced pancreatic cancer: a phase III trial of the National Cancer Institute of Canada Clinical Trials Group. *J Clin Oncol* **2007,** *25* (15), 1960-1966.

12.   Feig, C.; Gopinathan, A.; Neesse, A.; Chan, D. S.; Cook, N.; Tuveson, D. A., The pancreas cancer microenvironment. *Clin Cancer Res* **2012,** *18* (16), 4266-4276.

13.   Martin, W. R.; Eades, C. G.; Thompson, J. A.; Huppler, R. E.; Gilbert, P. E., The effects of morphine- and nalorphine- like drugs in the nondependent and morphine-dependent chronic spinal dog. *J Pharmacol Exp Ther* **1976,** *197* (3), 517-532.

14.   Vaupel, D. B., Naltrexone fails to antagonize the sigma effects of PCP and SKF 10,047 in the dog. *Eur J Pharmacol* **1983,** *92* (3-4), 269-274.

15.   Hellewell, S. B.; Bruce, A.; Feinstein, G.; Orringer, J.; Williams, W.; Bowen, W. D., Rat liver and kidney contain high densities of sigma 1 and sigma 2 receptors: characterization by ligand binding and photoaffinity labeling. *Eur J Pharmacol* **1994,** *268* (1), 9-18.

16.   Hanner, M.; Moebius, F. F.; Flandorfer, A.; Knaus, H. G.; Striessnig, J.; Kempner, E.; Glossmann, H., Purification, molecular cloning, and expression of the mammalian sigma1-binding site. *Proc Natl Acad Sci U S A* **1996,** *93* (15), 8072-8077.

17.   Schmidt, H. R.; Zheng, S.; Gurpinar, E.; Koehl, A.; Manglik, A.; Kruse, A. C., Crystal structure of the human sigma1 receptor. *Nature* **2016,** *532* (7600), 527-530.

18.   Hayashi, T.; Su, T. P., Sigma-1 receptor chaperones at the ER-Mitochondrion interface regulate Ca2+ signaling and cell survival. *Cell* **2007,** *131* (3), 596-610.

19.   Alon, A.; Schmidt, H. R.; Wood, M. D.; Sahn, J. J.; Martin, S. F.; Kruse, A. C., Identification of the gene that codes for the sigma(2) receptor. *Proc Natl Acad Sci USA* **2017,** *114* (27), 7160-7165.

20.   Ebrahimi-Fakhari, D.; Wahlster, L.; Bartz, F.; Werenbeck-Ueding, J.; Praggastis, M.; Zhang, J.; Joggerst-Thomalla, B.; Theiss, S.; Grimm, D.; Ory, D. S.; Runz, H., Reduction of TMEM97 increases NPC1 protein levels and restores cholesterol trafficking in Niemann-pick type C1 disease cells. *Hum Mol Genet* **2016,** *25* (16), 3588-3599.

21.   Riad, A.; Zeng, C. B.; Weng, C. C.; Winters, H.; Xu, K. Y.; Makvandi, M.; Metz, T.; Carlin, S.; Mach, R. H., Sigma-2 Receptor/TMEM97 and PGRMC-1 increase the rate of internalization of LDL by LDL receptor through the formation of a ternary complex. *Sci Rep* **2018,** *8* (1), 1-12.

22.   Alamri, M. A.; Afzal, O.; Alamri, M. A., Computational screening of natural and natural-like compounds to identify novel ligands for sigma-2 receptor. *SAR QSAR Environ Res* **2020,** *31* (11), 837-856.

23.   Floresta, G.; Amata, E.; Barbaraci, C.; Gentile, D.; Turnaturi, R.; Marrazzo, A.; Rescifina, A., A structure- and ligand-based virtual screening of a database of "small" marine natural products for the identification of "blue" sigma-2 receptor ligands. *Mar Drugs* **2018,** *16* (10), 384.

24.   Kashiwagi, H.; McDunn, J. E.; Simon, P. O.; Goedegebuure, P. S.; Xu, J.; Jones, L.; Chang, K.; Johnston, F.; Trinkaus, K.; Hotchkiss, R. S.; Mach, R. H.; Hawkins, W. G., Selective sigma-2 ligands preferentially bind to pancreatic adenocarcinomas: applications in diagnostic imaging and therapy. *Mol Cancer* **2007,** *6* (1), 1-12.

25.   Kashiwagi, H.; McDunn, J. E.; Simon, P. O., Jr.; Goedegebuure, P. S.; Vangveravong, S.; Chang, K.; Hotchkiss, R. S.; Mach, R. H.; Hawkins, W. G., Sigma-2 receptor ligands potentiate conventional chemotherapies and improve survival in models of pancreatic adenocarcinoma. *J Transl Med* **2009,** *7* (1), 1-8.

26.   Hornick, J. R.; Xu, J.; Vangveravong, S.; Tu, Z.; Mitchem, J. B.; Spitzer, D.; Goedegebuure, P.; Mach, R. H.; Hawkins, W. G., The novel sigma-2 receptor ligand SW43 stabilizes pancreas cancer progression in combination with gemcitabine. *Mol Cancer* **2010,** *9* (1), 1-11.

27.   Hornick, J. R.; Vangveravong, S.; Spitzer, D.; Abate, C.; Berardi, F.; Goedegebuure, P.; Mach, R. H.; Hawkins, W. G., Lysosomal membrane permeabilization is an early event in Sigma-2 receptor ligand mediated cell death in pancreatic cancer. *J Exp Clin Cancer Res* **2012,** *31* (1), 1-11.

28.   Hellewell, S. B.; Bowen, W. D., A sigma-like binding site in rat pheochromocytoma (PC12) cells: decreased affinity for (+)-benzomorphans and lower molecular weight suggest a different sigma receptor form from that of guinea pig brain. *Brain Res* **1990,** *527* (2), 244-253.

29.   Wheeler, K. T.; Wang, L. M.; Wallen, C. A.; Childers, S. R.; Cline, J. M.; Keng, P. C.; Mach, R. H., Sigma-2 receptors as a biomarker of proliferation in solid tumours. *Brit J Cancer* **2000,** *82* (6), 1223-1232.

30.   Vilner, B. J.; John, C. S.; Bowen, W. D., Sigma-1 and sigma-2 receptors are expressed in a wide variety of human and rodent tumor cell lines. *Cancer Res* **1995,** *55* (2), 408-413.

31.   Crawford, K. W.; Bowen, W. D., Sigma-2 receptor agonists activate a novel apoptotic pathway and potentiate antineoplastic drugs in breast tumor cell lines. *Cancer Res* **2002,** *62* (1), 313-322.

32.   Xu, J.; Zeng, C.; Chu, W.; Pan, F.; Rothfuss, J. M.; Zhang, F.; Tu, Z.; Zhou, D.; Zeng, D.; Vangveravong, S.; Johnston, F.; Spitzer, D.; Chang, K. C.; Hotchkiss, R. S.; Hawkins, W. G.; Wheeler, K. T.; Mach, R. H., Identification of the PGRMC1 protein complex as the putative sigma-2 receptor binding site. *Nat Commun* **2011,** *2* (1), 1-7.

33.   Pati, M. L.; Groza, D.; Riganti, C.; Kopecka, J.; Niso, M.; Berardi, F.; Hager, S.; Heffeter, P.; Hirai, M.; Tsugawa, H.; Kabe, Y.; Suematsu, M.; Abate, C., Sigma-2 receptor and progesterone receptor membrane component 1 (PGRMC1) are two different proteins: Proofs by fluorescent labeling and binding of sigma-2 receptor ligands to PGRMC1. *Pharmacol Res* **2017,** *117*, 67-74.

34.	Abate, C.; Niso, M.; Infantino, V.; Menga, A.; Berardi, F., Elements in support of the 'non-identity' of the PGRMC1 protein with the sigma2 receptor. *Eur J Pharmacol* **2015,** *758*, 16-23.

35.	Chu, U. B.; Mavlyutov, T. A.; Chu, M. L.; Yang, H.; Schulman, A.; Mesangeau, C.; McCurdy, C. R.; Guo, L. W.; Ruoho, A. E., The sigma-2 receptor and progesterone receptor membrane component 1 are different binding sites derived from independent genes. *EBioMedicine* **2015,** *2* (11), 1806-1813.

36.	Sturley, S. L.; Patterson, M. C.; Balch, W.; Liscum, L., The pathophysiology and mechanisms of NP-C disease. *Biochim Biophys Acta* **2004,** *1685* (1-3), 83-87.

37.	Bartz, F.; Kern, L.; Erz, D.; Zhu, M.; Gilbert, D.; Meinhof, T.; Wirkner, U.; Erfle, H.; Muckenthaler, M.; Pepperkok, R.; Runz, H., Identification of cholesterol-regulating genes by targeted RNAi screening. *Cell Metab* **2009,** *10* (1), 63-75.

38.	Ikonen, E., Cellular cholesterol trafficking and compartmentalization. *Nat Rev Mol Cell Biol* **2008,** *9* (2), 125-138.

39.	Chimento, A.; Casaburi, I.; Avena, P.; Trotta, F.; De Luca, A.; Rago, V.; Pezzi, V.; Sirianni, R., Cholesterol and Its metabolites in tumor growth: Therapeutic potential of statins in cancer treatment. *Front Endocrinol (Lausanne)* **2018,** *9*, 807.

40.	Incardona, J. P.; Eaton, S., Cholesterol in signal transduction. *Curr Opin Cell Biol* **2000,** *12* (2), 193-203.

41.	Payne, A. H.; Hales, D. B., Overview of steroidogenic enzymes in the pathway from cholesterol to active steroid hormones. *Endocr Rev* **2004,** *25* (6), 947-970.

42.	Luo, J.; Yang, H.; Song, B. L., Mechanisms and regulation of cholesterol homeostasis. *Nat Rev Mol Cell Biol* **2020,** *21* (4), 225-245.

43.	Walker, A. K.; Naar, A. M., SREBPs: regulators of cholesterol/lipids as therapeutic targets in metabolic disorders, cancers and viral diseases. *Clin Lipidol* **2012,** *7* (1), 27-36.

44.	Suchanek, M.; Radzikowska, A.; Thiele, C., Photo-leucine and photo-methionine allow identification of protein-protein interactions in living cells. *Nat Methods* **2005,** *2* (4), 261-267.

45.	Cai, H. L.; Tan, Q. Y.; Jiang, P.; Dang, R. L.; Xue, Y.; Tang, M. M.; Xu, P.; Deng, Y.; Li, H. D.; Yao, J. K., A potential mechanism underlying atypical antipsychotics-induced lipid disturbances. *Transl Psychiatry* **2015,** *5*, e661.

46.	Eid, W.; Dauner, K.; Courtney, K. C.; Gagnon, A.; Parks, R. J.; Sorisky, A.; Zha, X. H., mTORC1 activates SREBP-2 by suppressing cholesterol trafficking to lysosomes in mammalian cells. *Proc Natl Acad Sci USA* **2017,** *114* (30), 7999-8004.

47.   Ouimet, M.; Franklin, V.; Mak, E.; Liao, X.; Tabas, I.; Marcel, Y. L., Autophagy regulates cholesterol efflux from macrophage foam cells via lysosomal acid lipase. *Cell Metab* **2011,** *13* (6), 655-667.

48.   Kuzu, O. F.; Noory, M. A.; Robertson, G. P., The role of cholesterol in cancer. *Cancer Res* **2016,** *76* (8), 2063-2070.

49.   Gabitova, L.; Gorin, A.; Astsaturov, I., Molecular pathways: sterols and receptor signaling in cancer. *Clin Cancer Res* **2014,** *20* (1), 28-34.

50.   Faubert, B.; Solmonson, A.; DeBerardinis, R. J., Metabolic reprogramming and cancer progression. *Science* **2020,** *368* (6487).

51.   Huang, B. L.; Song, B. L.; Xu, C. Q., Cholesterol metabolism in cancer: mechanisms and therapeutic opportunities. *Nat Metab* **2020,** *2* (2), 132-141.

52.   Howe, V.; Sharpe, L. J.; Prabhu, A. V.; Brown, A. J., New insights into cellular cholesterol acquisition: promoter analysis of human HMGCR and SQLE, two key control enzymes in cholesterol synthesis. *Biochim Biophys Acta Mol Cell Biol Lipids* **2017,** *1862* (7), 647-657.

53.   Beloribi-Djefaflia, S.; Vasseur, S.; Guillaumond, F., Lipid metabolic reprogramming in cancer cells. *Oncogenesis* **2016,** *5*, e189.

54.   Gu, L.; Saha, S. T.; Thomas, J.; Kaur, M., Targeting cellular cholesterol for anticancer therapy. *FEBS J* **2019,** *286* (21), 4192-4208.

55.   Chan, K. K.; Oza, A. M.; Siu, L. L., The statins as anticancer agents. *Clin Cancer Res* **2003,** *9* (1), 10-19.

56.   Barg, J.; Thomas, G. E.; Bem, W. T.; Parnes, M. D.; Ho, A. M.; Belcheva, M. M.; McHale, R. J.; McLachlan, J. A.; Tolman, K. C.; Johnson, F. E.; et al., In vitro and in vivo expression of opioid and sigma receptors in rat C6 glioma and mouse N18TG2 neuroblastoma cells. *J Neurochem* **1994,** *63* (2), 570-574.

57.   Qiu, G.; Sun, W.; Zou, Y.; Cai, Z.; Wang, P.; Lin, X.; Huang, J.; Jiang, L.; Ding, X.; Hu, G., RNA interference against TMEM97 inhibits cell proliferation, migration, and invasion in glioma cells. *Tumour Biol* **2015,** *36* (10), 8231-8238.

58.   Qu, T.; Zhao, Y.; Chen, Y.; Jin, S.; Fang, Y.; Jin, X.; Sun, L.; Ma, Y., Down-regulated MAC30 expression inhibits breast cancer cell invasion and EMT by suppressing Wnt/beta-catenin and PI3K/Akt signaling pathways. *Int J Clin Exp Pathol* **2019,** *12* (5), 1888-1896.

59.   Xu, X. Y.; Zhang, L. J.; Yu, Y. Q.; Zhang, X. T.; Huang, W. J.; Nie, X. C.; Song, G. Q., Down-regulated MAC30 expression inhibits proliferation and mobility of human gastric cancer cells. *Cell Physiol Biochem* **2014,** *33* (5), 1359-1368.

60.   Ramalho-Carvalho, J.; Goncalves, C. S.; Graca, I.; Bidarra, D.; Pereira-Silva, E.; Salta, S.; Godinho, M. I.; Gomez, A.; Esteller, M.; Costa, B. M.; Henrique, R.; Jeronimo, C., A

multiplatform approach identifies miR-152-3p as a common epigenetically regulated onco-suppressor in prostate cancer targeting TMEM97. *Clin Epigenetics* **2018,** *10*, 40.

61.   Han, K. Y.; Gu, X.; Wang, H. R.; Liu, D.; Lv, F. Z.; Li, J. N., Overexpression of MAC30 is associated with poor clinical outcome in human non-small-cell lung cancer. *Tumour Biol* **2013,** *34* (2), 821-5.

62.   Ding, H.; Gui, X. H.; Lin, X. B.; Chen, R. H.; Cai, H. R.; Fen, Y.; Sheng, Y. L., Prognostic value of MAC30 expression in human pure squamous cell carcinomas of the lung. *Asian Pac J Cancer Prev* **2016,** *17* (5), 2705-2710.

63.   Xiao, M.; Li, H.; Yang, S.; Huang, Y.; Jia, S.; Wang, H.; Wang, J.; Li, Z., Expression of MAC30 protein is related to survival and clinicopathological variables in breast cancer. *J Surg Oncol* **2013,** *107* (5), 456-62.

64.   Yang, S.; Li, H.; Liu, Y.; Ning, X.; Meng, F.; Xiao, M.; Wang, D.; Lou, G.; Zhang, Y., Elevated expression of MAC30 predicts lymph node metastasis and unfavorable prognosis in patients with epithelial ovarian cancer. *Med Oncol* **2013,** *30* (1), 324.

65.   Moebius, F. F.; Striessnig, J.; Glossmann, H., The mysteries of sigma receptors: new family members reveal a role in cholesterol synthesis. *Trends Pharmacol Sci* **1997,** *18* (3), 67-70.

66.   Moebius, F. F.; Bermoser, K.; Reiter, R. J.; Hanner, M.; Glossmann, H., Yeast sterol C8-C7 isomerase: identification and characterization of a high-affinity binding site for enzyme inhibitors. *Biochemistry* **1996,** *35* (51), 16871-16878.

67.   Rohe, H. J.; Ahmed, I. S.; Twist, K. E.; Craven, R. J., PGRMC1 (progesterone receptor membrane component 1): a targetable protein with multiple functions in steroid signaling, P450 activation and drug binding. *Pharmacol Ther* **2009,** *121* (1), 14-19.

68.   Crudden, G.; Loesel, R.; Craven, R. J., Overexpression of the cytochrome p450 activator hpr6 (heme-1 domain protein/human progesterone receptor) in tumors. *Tumour Biol* **2005,** *26* (3), 142-146.

69.   Asperger, H.; Stamm, N.; Gierke, B.; Pawlak, M.; Hofmann, U.; Zanger, U. M.; Marton, A.; Katona, R. L.; Buhala, A.; Vizler, C.; Cieslik, J. P.; Ruckhaberle, E.; Niederacher, D.; Fehm, T.; Neubauer, H.; Ludescher, M., Progesterone receptor membrane component 1 regulates lipid homeostasis and drives oncogenic signaling resulting in breast cancer progression. *Breast Cancer Res* **2020,** *22* (1), 1-16.

70.   Neubauer, H.; Adam, G.; Seeger, H.; Mueck, A. O.; Solomayer, E.; Wallwiener, D.; Cahill, M. A.; Fehm, T., Membrane-initiated effects of progesterone on proliferation and activation of VEGF in breast cancer cells. *Climacteric* **2009,** *12* (3), 230-239.

71.   Ahmed, I. S.; Rohe, H. J.; Twist, K. E.; Mattingly, M. N.; Craven, R. J., Progesterone receptor membrane component 1 (Pgrmc1): a heme-1 domain protein that promotes tumorigenesis and is inhibited by a small molecule. *J Pharmacol Exp Ther* **2010,** *333* (2), 564-573.

72.   Shen, H.; Li, J.; Xie, X.; Yang, H.; Zhang, M.; Wang, B.; Kent, K. C.; Plutzky, J.; Guo, L. W., BRD2 regulation of sigma-2 receptor upon cholesterol deprivation. *Life Sci Alliance* **2021,** *4* (1).

73.   Humeau, J.; Bravo-San Pedro, J. M.; Vitale, I.; Nunez, L.; Villalobos, C.; Kroemer, G.; Senovilla, L., Calcium signaling and cell cycle: Progression or death. *Cell Calcium* **2018,** *70*, 3-15.

74.   Pinto, M. C.; Kihara, A. H.; Goulart, V. A.; Tonelli, F. M.; Gomes, K. N.; Ulrich, H.; Resende, R. R., Calcium signaling and cell proliferation. *Cell Signal* **2015,** *27* (11), 2139-2149.

75.   Bravo-Sagua, R.; Parra, V.; Lopez-Crisosto, C.; Diaz, P.; Quest, A. F.; Lavandero, S., Calcium transport and signaling in mitochondria. *Compr Physiol* **2017,** *7* (2), 623-634.

76.   Vilner, B. J.; Bowen, W. D., Modulation of cellular calcium by sigma-2 receptors: release from intracellular stores in human SK-N-SH neuroblastoma cells. *J Pharmacol Exp Ther* **2000,** *292* (3), 900-911.

77.   Cassano, G.; Gasparre, G.; Niso, M.; Contino, M.; Scalera, V.; Colabufo, N. A., F281, synthetic agonist of the sigma-2 receptor, induces Ca2+ efflux from the endoplasmic reticulum and mitochondria in SK-N-SH cells. *Cell Calcium* **2009,** *45* (4), 340-345.

78.   Foskett, J. K.; White, C.; Cheung, K. H.; Mak, D. O., Inositol trisphosphate receptor Ca2+ release channels. *Physiol Rev* **2007,** *87* (2), 593-658.

79.   Gui, L.; Wang, Z.; Han, J.; Ma, H.; Li, Z., High expression of Orai1 enhances cell proliferation and is associated with poor prognosis in human colorectal cancer. *Clin Lab* **2016,** *62* (9), 1689-1698.

80.   Abdullaev, I. F.; Bisaillon, J. M.; Potier, M.; Gonzalez, J. C.; Motiani, R. K.; Trebak, M., Stim1 and Orai1 mediate CRAC currents and store-operated calcium entry important for endothelial cell proliferation. *Circ Res* **2008,** *103* (11), 1289-1299.

81.   Cantonero, C.; Camello, P. J.; Abate, C.; Berardi, F.; Salido, G. M.; Rosado, J. A.; Redondo, P. C., NO1, a new sigma 2 receptor/TMEM97 fluorescent ligand, downregulates SOCE and promotes apoptosis in the triple negative breast cancer cell lines. *Cancers (Basel)* **2020,** *12* (2), 257.

82.   Cassano, G.; Gasparre, G.; Contino, M.; Niso, M.; Berardi, F.; Perrone, R.; Colabufo, N. A., The sigma-2 receptor agonist PB28 inhibits calcium release from the endoplasmic reticulum of SK-N-SH neuroblastoma cells. *Cell Calcium* **2006,** *40* (1), 23-28.

83.   Nicholson, H.; Mesangeau, C.; McCurdy, C. R.; Bowen, W. D., Sigma-2 receptors play a role in cellular metabolism: stimulation of glycolytic hallmarks by CM764 in human SK-N-SH neuroblastoma. *J Pharmacol Exp Ther* **2016,** *356* (2), 232-243.

84.   Wang, W. A.; Liu, W. X.; Durnaoglu, S.; Lee, S. K.; Lian, J.; Lehner, R.; Ahnn, J.; Agellon, L. B.; Michalak, M., Loss of calreticulin uncovers a critical role for calcium in regulating cellular lipid homeostasis. *Sci Rep* **2017,** *7* (1), 5941.

85.   Oni, T. E.; Biffi, G.; Baker, L. A.; Hao, Y.; Tonelli, C.; Somerville, T. D. D.; Deschenes, A.; Belleau, P.; Hwang, C. I.; Sanchez-Rivera, F. J.; Cox, H.; Brosnan, E.; Doshi, A.; Lumia, R. P.; Khaledi, K.; Park, Y.; Trotman, L. C.; Lowe, S. W.; Krasnitz, A.; Vakoc, C. R.; Tuveson, D. A., SOAT1 promotes mevalonate pathway dependency in pancreatic cancer. *J Exp Med* **2020,** *217* (9).

86.   Li, J.; Gu, D.; Lee, S. S.; Song, B.; Bandyopadhyay, S.; Chen, S.; Konieczny, S. F.; Ratliff, T. L.; Liu, X.; Xie, J.; Cheng, J. X., Abrogating cholesterol esterification suppresses growth and metastasis of pancreatic cancer. *Oncogene* **2016,** *35* (50), 6378-6388.

87.   Karasinska, J. M.; Topham, J. T.; Kalloger, S. E.; Jang, G. H.; Denroche, R. E.; Culibrk, L.; Williamson, L. M.; Wong, H. L.; Lee, M. K. C.; O'Kane, G. M.; Moore, R. A.; Mungall, A. J.; Moore, M. J.; Warren, C.; Metcalfe, A.; Notta, F.; Knox, J. J.; Gallinger, S.; Laskin, J.; Marra, M. A.; Jones, S. J. M.; Renouf, D. J.; Schaeffer, D. F., Altered gene expression along the glycolysis-cholesterol synthesis axis Is associated with outcome in pancreatic cancer. *Clin Cancer Res* **2020,** *26* (1), 135-146.

88.   Kugel, S.; Hingorani, S. R., Cholesterol biosynthesis influences subtype specificity and plasticity in pancreas cancer. *Cancer Cell* **2020,** *38* (4), 443-445.

89.   Guillaumond, F.; Bidaut, G.; Ouaissi, M.; Servais, S.; Gouirand, V.; Olivares, O.; Lac, S.; Borge, L.; Roques, J.; Gayet, O.; Pinault, M.; Guimaraes, C.; Nigri, J.; Loncle, C.; Lavaut, M. N.; Garcia, S.; Tailleux, A.; Staels, B.; Calvo, E.; Tomasini, R.; Iovanna, J. L.; Vasseur, S., Cholesterol uptake disruption, in association with chemotherapy, is a promising combined metabolic therapy for pancreatic adenocarcinoma. *Proc Natl Acad Sci U S A* **2015,** *112* (8), 2473-2478.

90.   Vasseur, S.; Guillaumond, F., LDL Receptor: An open route to feed pancreatic tumor cells. *Mol Cell Oncol* **2016,** *3* (1), e1033586.

91.   Kayed, H.; Kleeff, J.; Ding, J.; Hammer, J.; Giese, T.; Zentgraf, H.; Buchler, M. W.; Friess, H., Expression analysis of MAC30 in human pancreatic cancer and tumors of the gastrointestinal tract. *Histol Histopathol* **2004,** *19* (4), 1021-1031.

92.   Katnik, C.; Guerrero, W. R.; Pennypacker, K. R.; Herrera, Y.; Cuevas, J., Sigma-1 receptor activation prevents intracellular calcium dysregulation in cortical neurons during in vitro ischemia. *J Pharmacol Exp Ther* **2006,** *319* (3), 1355-1365.

93.   Chu, U. B.; Ruoho, A. E., Sigma receptor binding assays. *Curr Protoc Pharmacol* **2015,** *71* (1), 1-34.

94.   Quirion, R.; Bowen, W. D.; Itzhak, Y.; Junien, J. L.; Musacchio, J. M.; Rothman, R. B.; Su, T. P.; Tam, S. W.; Taylor, D. P., A proposal for the classification of sigma binding sites. *Trends Pharmacol Sci* **1992,** *13* (3), 85-86.

95.   Horacek, J., Novel antipsychotics and extrapyramidal side effects. Theory and reality. *Pharmacopsychiatry* **2000,** *33 Suppl 1*, 34-42.

96.   Hashimoto, K.; Ishiwata, K., Sigma receptor ligands: possible application as therapeutic drugs and as radiopharmaceuticals. *Curr Pharm Des* **2006,** *12* (30), 3857-3876.

97.   Post, A.; Holsboer, F.; Behl, C., Induction of NF-kappaB activity during haloperidol-induced oxidative toxicity in clonal hippocampal cells: suppression of NF-kappaB and neuroprotection by antioxidants. *J Neurosci* **1998,** *18* (20), 8236-8246.

98.   Wei, Z.; Mousseau, D. D.; Dai, Y.; Cao, X.; Li, X. M., Haloperidol induces apoptosis via the sigma2 receptor system and Bcl-XS. *Pharmacogenomics J* **2006,** *6* (4), 279-288.

99.   Bai, T.; Wang, S.; Zhao, Y.; Zhu, R.; Wang, W.; Sun, Y., Haloperidol, a sigma receptor 1 antagonist, promotes ferroptosis in hepatocellular carcinoma cells. *Biochem Biophys Res Commun* **2017,** *491* (4), 919-925.

100.   Narayanan, S.; Bhat, R.; Mesangeau, C.; Poupaert, J. H.; McCurdy, C. R., Early development of sigma-receptor ligands. *Future Med Chem* **2011,** *3* (1), 79-94.

101.   Abate, C.; Niso, M.; Berardi, F., Sigma-2 receptor: past, present and perspectives on multiple therapeutic exploitations. *Future Med Chem* **2018,** *10* (16), 1997-2018.

102.   Bowen, W. D.; Bertha, C. M.; Vilner, B. J.; Rice, K. C., CB-64D and CB-184: ligands with high sigma 2 receptor affinity and subtype selectivity. *Eur J Pharmacol* **1995,** *278* (3), 257-260.

103.   Bertha, C. M.; Mattson, M. V.; Flippen-Anderson, J. L.; Rothman, R. B.; Xu, H.; Cha, X. Y.; Becketts, K.; Rice, K. C., A marked change of receptor affinity of the 2-methyl-5-(3-hydroxyphenyl)morphans upon attachment of an (E)-8-benzylidene moiety: synthesis and evaluation of a new class of sigma receptor ligands. *J Med Chem* **1994,** *37* (19), 3163-3170.

104.   Perregaard, J.; Moltzen, E. K.; Meier, E.; Sanchez, C., Sigma ligands with subnanomolar affinity and preference for the sigma 2 binding site. 1. 3-(omega-aminoalkyl)-1H-indoles. *J Med Chem* **1995,** *38* (11), 1998-2008.

105.   Ostenfeld, M. S.; Fehrenbacher, N.; Hoyer-Hansen, M.; Thomsen, C.; Farkas, T.; Jaattela, M., Effective tumor cell death by sigma-2 receptor ligand siramesine involves lysosomal leakage and oxidative stress. *Cancer Res* **2005,** *65* (19), 8975-8983.

106.   Zeng, C.; Rothfuss, J.; Zhang, J.; Chu, W.; Vangveravong, S.; Tu, Z.; Pan, F.; Chang, K. C.; Hotchkiss, R.; Mach, R. H., Sigma-2 ligands induce tumour cell death by multiple signalling pathways. *Brit J Cancer* **2012,** *106* (4), 693-701.

107.   Mach, R. H.; Huang, Y.; Freeman, R. A.; Wu, L.; Vangveravong, S.; Luedtke, R. R., Conformationally-flexible benzamide analogues as dopamine D3 and sigma 2 receptor ligands. *Bioorg Med Chem Lett* **2004,** *14* (1), 195-202.

108.   Tu, Z.; Xu, J.; Jones, L. A.; Li, S.; Dumstorff, C.; Vangveravong, S.; Chen, D. L.; Wheeler, K. T.; Welch, M. J.; Mach, R. H., Fluorine-18-labeled benzamide analogues for imaging the sigma2 receptor status of solid tumors with positron emission tomography. *J Med Chem* **2007,** *50* (14), 3194-3204.

109.   Abate, C.; Niso, M.; Lacivita, E.; Mosier, P. D.; Toscano, A.; Perrone, R., Analogues of sigma receptor ligand 1-cyclohexyl-4-[3-(5-methoxy-1,2,3,4-tetrahydronaphthalen-1-yl)propyl]piperazine (PB28) with added polar functionality and reduced lipophilicity for potential use as positron emission tomography radiotracers. *J Med Chem* **2011,** *54* (4), 1022-1032.

110.   Abate, C.; Perrone, R.; Berardi, F., Classes of sigma2 (sigma2) receptor ligands: structure affinity relationship (SAfiR) studies and antiproliferative activity. *Curr Pharm Des* **2012,** *18* (7), 938-949.

111.   Colabufo, N. A.; Berardi, F.; Contino, M.; Niso, M.; Abate, C.; Perrone, R.; Tortorella, V., Antiproliferative and cytotoxic effects of some sigma2 agonists and sigma1 antagonists in tumour cell lines. *Naunyn Schmiedebergs Arch Pharmacol* **2004,** *370* (2), 106-113.

112.   Pati, M. L.; Hornick, J. R.; Niso, M.; Berardi, F.; Spitzer, D.; Abate, C.; Hawkins, W., Sigma-2 receptor agonist derivatives of 1-Cyclohexyl-4-[3-(5-methoxy-1,2,3,4-tetrahydronaphthalen-1-yl)propyl]piperazine (PB28) induce cell death via mitochondrial superoxide production and caspase activation in pancreatic cancer. *BMC Cancer* **2017,** *17* (1), 1-12.

113.   Colabufo, N. A.; Berardi, F.; Abate, C.; Contino, M.; Niso, M.; Perrone, R., Is the sigma2 receptor a histone binding protein? *J Med Chem* **2006,** *49* (14), 4153-4158.

114.   Abate, C.; Elenewski, J.; Niso, M.; Berardi, F.; Colabufo, N. A.; Azzariti, A.; Perrone, R.; Glennon, R. A., Interaction of the sigma(2) receptor ligand PB28 with the human nucleosome: computational and experimental probes of interaction with the H2A/H2B dimer. *ChemMedChem* **2010,** *5* (2), 268-273.

115.   Azzariti, A.; Colabufo, N. A.; Berardi, F.; Porcelli, L.; Niso, M.; Simone, G. M.; Perrone, R.; Paradiso, A., Cyclohexylpiperazine derivative PB28, a sigma2 agonist and sigma1 antagonist receptor, inhibits cell growth, modulates P-glycoprotein, and synergizes with anthracyclines in breast cancer. *Mol Cancer Ther* **2006,** *5* (7), 1807-1816.

116.   Nicholson, H. E.; Alsharif, W. F.; Comeau, A. B.; Mesangeau, C.; Intagliata, S.; Mottinelli, M.; McCurdy, C. R.; Bowen, W. D., Divergent cytotoxic and metabolically stimulative functions of sigma-2 receptors: Structure-activity relationships of 6-Acetyl-3-(4-(4-(4-fluorophenyl)piperazin-1-yl)butyl)benzo[d]oxazol-2(3H)-one (SN79) derivatives. *J Pharmacol Exp Ther* **2019,** *368* (2), 272-281.

117.   Kaushal, N.; Seminerio, M. J.; Robson, M. J.; McCurdy, C. R.; Matsumoto, R. R., Pharmacological evaluation of SN79, a sigma (sigma) receptor ligand, against methamphetamine-induced neurotoxicity in vivo. *Eur Neuropsychopharmacol* **2013,** *23* (8), 960-971.

118.   Nicholson, H.;   Comeau, A.;   Mesangeau, C.;   McCurdy, C. R.;   Bowen, W. D., Characterization of CM572, a Selective Irreversible Partial Agonist of the Sigma-2 Receptor with Antitumor Activity. *J Pharmacol Exp Ther* **2015,** *354* (2), 203-212.

119.   Vangveravong, S.;   Xu, J.;   Zeng, C.;   Mach, R. H., Synthesis of N-substituted 9-azabicyclo[3.3.1]nonan-3alpha-yl carbamate analogs as sigma2 receptor ligands. *Bioorg Med Chem* **2006,** *14* (20), 6988-6997.

120.   Mach, R. H.;   Wheeler, K. T., Development of molecular probes for imaging sigma-2 receptors in vitro and in vivo. *Cent Nerv Syst Agents Med Chem* **2009,** *9* (3), 230-245.

121.   Zeng, C.;   McDonald, E. S.;   Mach, R. H., Molecular probes for imaging the sigma-2 receptor: in vitro and in vivo imaging studies. *Handb Exp Pharmacol* **2017,** *244*, 309-330.

122.   Zeng, C.;   Vangveravong, S.;   McDunn, J. E.;   Hawkins, W. G.;   Mach, R. H., Sigma-2 receptor ligand as a novel method for delivering a SMAC mimetic drug for treating ovarian cancer. *Brit J Cancer* **2013,** *109* (9), 2368-2377.

123.   Garg, G.;   Vangveravong, S.;   Zeng, C.;   Collins, L.;   Hornick, M.;   Hashim, Y.;   Piwnica-Worms, D.;   Powell, M. A.;   Mutch, D. G.;   Mach, R. H.;   Hawkins, W. G.;   Spitzer, D., Conjugation to a SMAC mimetic potentiates sigma-2 ligand induced tumor cell death in ovarian cancer. *Mol Cancer* **2014,** *13* (1), 1-13.

124.   Rui, M.;   Rossi, D.;   Marra, A.;   Paolillo, M.;   Schinelli, S.;   Curti, D.;   Tesei, A.;   Cortesi, M.;   Zamagni, A.;   Laurini, E.;   Pricl, S.;   Schepmann, D.;   Wunsch, B.;   Urban, E.;   Pace, V.;   Collina, S., Synthesis and biological evaluation of new aryl-alkyl(alkenyl)-4-benzylpiperidines, novel Sigma Receptor (SR) modulators, as potential anticancer-agents. *Eur J Med Chem* **2016,** *124*, 649-665.

125.   Tesei, A.;   Cortesi, M.;   Pignatta, S.;   Arienti, C.;   Dondio, G. M.;   Bigogno, C.;   Malacrida, A.;   Miloso, M.;   Meregalli, C.;   Chiorazzi, A.;   Carozzi, V.;   Cavaletti, G.;   Rui, M.;   Marra, A.;   Rossi, D.;   Collina, S., Anti-tumor efficacy assessment of the sigma receptor pan modulator RC-106. A promising therapeutic tool for pancreatic cancer. *Front Pharmacol* **2019,** *10*, 490.

126.   Wiklund, E. D.;   Catts, V. S.;   Catts, S. V.;   Ng, T. F.;   Whitaker, N. J.;   Brown, A. J.;   Lutze-Mann, L. H., Cytotoxic effects of antipsychotic drugs implicate cholesterol homeostasis as a novel chemotherapeutic target. *Int J Cancer* **2010,** *126* (1), 28-40.

127.   Korpis, K.;   Weber, F.;   Wunsch, B.;   Bednarski, P. J., Cytotoxic activities of hydroxyethyl piperazine-based sigma receptor ligands on cancer cells alone and in combination with melphalan, PB28 and haloperidol. *Pharmazie* **2014,** *69* (12), 917-922.

128.   Chu, W.;   Xu, J.;   Zhou, D.;   Zhang, F.;   Jones, L. A.;   Wheeler, K. T.;   Mach, R. H., New N-substituted 9-azabicyclo[3.3.1]nonan-3alpha-yl phenylcarbamate analogs as sigma2 receptor ligands: synthesis, in vitro characterization, and evaluation as PET imaging and chemosensitization agents. *Bioorg Med Chem* **2009,** *17* (3), 1222-1231.

129.   Zeng, C.; Rothfuss, J. M.; Zhang, J.; Vangveravong, S.; Chu, W.; Li, S.; Tu, Z.; Xu, J.; Mach, R. H., Functional assays to define agonists and antagonists of the sigma-2 receptor. *Anal Biochem* **2014,** *448*, 68-74.

130.   Berardi, F.; Abate, C.; Ferorelli, S.; Uricchio, V.; Colabufo, N. A.; Niso, M.; Perrone, R., Exploring the importance of piperazine N-atoms for sigma(2) receptor affinity and activity in a   series   of   analogs   of   1-cyclohexyl-4-[3-(5-methoxy-1,2,3,4-tetrahydronaphthalen-1-yl)propyl]piperazine (PB28). *J Med Chem* **2009,** *52* (23), 7817-28.

131.   Ferorelli, S.; Abate, C.; Colabufo, N. A.; Niso, M.; Inglese, C.; Berardi, F.; Perrone, R., Design and evaluation of naphthol- and carbazole-containing fluorescent sigma ligands as potential probes for receptor binding studies. *J Med Chem* **2007,** *50* (19), 4648-4655.

132.   Ablordeppey, S. Y.; El-Ashmawy, M.; Fischer, J. B.; Glennon, R. A., A CoMFA investigation of sigma receptor binding affinity: Reexamination of a spurious sigma ligand. *European Journal of Medicinal Chemistry* **1998,** *33* (7), 625-633.

133.   Laggner, C.; Schieferer, C.; Fiechtner, B.; Poles, G.; Hoffmann, R. D.; Glossmann, H.; Langer, T.; Moebius, F. F., Discovery of high-affinity ligands of sigma1 receptor, ERG2, and emopamil binding protein by pharmacophore modeling and virtual screening. *J Med Chem* **2005,** *48* (15), 4754-4764.

134.   Cratteri, P.; Romanelli, M. N.; Cruciani, G.; Bonaccini, C.; Melani, F., GRIND-derived pharmacophore model for a series of alpha-tropanyl derivative ligands of the sigma-2 receptor. *J Comput Aided Mol Des* **2004,** *18* (5), 361-374.

135.   Laurini, E.; Zampieri, D.; Mamolo, M. G.; Vio, L.; Zanette, C.; Florio, C.; Posocco, P.; Fermeglia, M.; Pricl, S., A 3D-pharmacophore model for sigma2 receptors based on a series of substituted benzo[d]oxazol-2(3H)-one derivatives. *Bioorg Med Chem Lett* **2010,** *20* (9), 2954-2957.

136.   Abate, C.; Mosier, P. D.; Berardi, F.; Glennon, R. A., A structure-affinity and comparative molecular field analysis of sigma-2 (sig2) receptor ligands. *Cent Nerv Syst Agents Med Chem* **2009,** *9* (3), 246-257.

137.   Glennon, R. A.; Ablordeppey, S. Y.; Ismaiel, A. M.; el-Ashmawy, M. B.; Fischer, J. B.; Howie, K. B., Structural features important for sigma 1 receptor binding. *J Med Chem* **1994,** *37* (8), 1214-1219.

138.   Mach, R. H.; Zeng, C. B.; Hawkins, W. G., The sigma(2) receptor: A novel protein for the imaging and treatment of cancer. *J Med Chem* **2013,** *56* (18), 7137-7160.

139.   Xu, J.; Tu, Z.; Jones, L. A.; Vangveravong, S.; Wheeler, K. T.; Mach, R. H., [3H]N-[4-(3,4-dihydro-6,7-dimethoxyisoquinolin-2(1H)-yl)butyl]-2-methoxy-5-methyl benzamide: a novel sigma-2 receptor probe. *Eur J Pharmacol* **2005,** *525* (1-3), 8-17.

140.   Tu, Z.; Xu, J.; Jones, L. A.; Li, S.; Zeng, D.; Kung, M. P.; Kung, H. F.; Mach, R. H., Radiosynthesis and biological evaluation of a promising sigma(2)-receptor ligand radiolabeled

with fluorine-18 or iodine-125 as a PET/SPECT probe for imaging breast cancer. *Appl Radiat Isot* **2010,** *68* (12), 2268-2273.

141.   Weber, E.; Sonders, M.; Quarum, M.; Mclean, S.; Pou, S.; Keana, J. F. W., 1,3-Di(2-[5-H-3]tolyl)guanidine - a selective ligand that labels sigma-type receptors for psychotomimetic opiates and antipsychotic-drugs. *P Natl Acad Sci USA* **1986,** *83* (22), 8784-8788.

142.   Mach, R. H.; Smith, C. R.; al-Nabulsi, I.; Whirrett, B. R.; Childers, S. R.; Wheeler, K. T., Sigma 2 receptors as potential biomarkers of proliferation in breast cancer. *Cancer Res* **1997,** *57* (1), 156-161.

143.   Matsumoto, R. R.; Nguyen, L.; Kaushal, N.; Robson, M. J., Chapter nine - Sigma (σ) receptors as potential therapeutic targets to mitigate psychostimulant effects. In *Advances in Pharmacology*, Dwoskin, L. P., Ed. Academic Press: 2014; Vol. 69, pp 323-386.

144.   https://clinicaltrials.gov/ct2/show/NCT00968656. (accessed January 28, 2021).

145.   https://clinicaltrials.gov/ct2/show/NCT02284919. (accessed January 28, 2021).

146.   Dehdashti, F.; Laforest, R.; Gao, F.; Shoghi, K. I.; Aft, R. L.; Nussenbaum, B.; Kreisel, F. H.; Bartlett, N. L.; Cashen, A.; Wagner-Johnson, N.; Mach, R. H., Assessment of cellular proliferation in tumors by PET using 18F-ISO-1. *J Nucl Med* **2013,** *54* (3), 350-357.

147.   Vilner, B. J.; de Costa, B. R.; Bowen, W. D., Cytotoxic effects of sigma ligands: sigma receptor-mediated alterations in cellular morphology and viability. *J Neurosci* **1995,** *15* (1 Pt 1), 117-134.

148.   Lowe, S. W.; Lin, A. W., Apoptosis in cancer. *Carcinogenesis* **2000,** *21* (3), 485-495.

149.   Ostenfeld, M. S.; Hoyer-Hansen, M.; Bastholm, L.; Fehrenbacher, N.; Olsen, O. D.; Groth-Pedersen, L.; Puustinen, P.; Kirkegaard-Sorensen, T.; Nylandsted, J.; Farkas, T.; Jaattela, M., Anti-cancer agent siramesine is a lysosomotropic detergent that induces cytoprotective autophagosome accumulation. *Autophagy* **2008,** *4* (4), 487-499.

150.   Ursini, F.; Maiorino, M., Lipid peroxidation and ferroptosis: The role of GSH and GPx4. *Free Radic Biol Med* **2020,** *152*, 175-185.

151.   Yang, W. S.; Stockwell, B. R., Ferroptosis: Death by lipid peroxidation. *Trends Cell Biol* **2016,** *26* (3), 165-176.

152.   Rink, J. S.; Lin, A. Y.; McMahon, K. M.; Calvert, A. E.; Yang, S.; Taxter, T.; Moreira, J.; Chadburn, A.; Behdad, A.; Karmali, R.; Thaxton, C. S.; Gordon, L. I., Targeted reduction of cholesterol uptake in cholesterol-addicted lymphoma cells blocks turnover of oxidized lipids to cause ferroptosis. *J Biol Chem* **2020,** *296*, 100100.

153.   Mizushima, N.; Komatsu, M., Autophagy: renovation of cells and tissues. *Cell* **2011,** *147* (4), 728-741.

154.   Kim, Y. C.; Guan, K. L., mTOR: a pharmacologic target for autophagy regulation. *J Clin Invest* **2015,** *125* (1), 25-32.

155.   Zeng, C.; Vangveravong, S.; Xu, J.; Chang, K. C.; Hotchkiss, R. S.; Wheeler, K. T.; Shen, D.; Zhuang, Z. P.; Kung, H. F.; Mach, R. H., Subcellular localization of sigma-2 receptors in breast cancer cells using two-photon and confocal microscopy. *Cancer Res* **2007,** *67* (14), 6708-6716.

156.   Maan, M.; Peters, J. M.; Dutta, M.; Patterson, A. D., Lipid metabolism and lipophagy in cancer. *Biochem Biophys Res Commun* **2018,** *504* (3), 582-589.

157.   Meng, Y.; Heybrock, S.; Neculai, D.; Saftig, P., Cholesterol handling in lysosomes and beyond. *Trends Cell Biol* **2020,** *30* (6), 452-466.

158.   Kroemer, G.; Jaattela, M., Lysosomes and autophagy in cell death control. *Nat Rev Cancer* **2005,** *5* (11), 886-897.

159.   Bartz, F.; Kern, L.; Erz, D.; Zhu, M. G.; Gilbert, D.; Meinhof, T.; Wirkner, U.; Erfle, H.; Muckenthaler, M.; Pepperkok, R.; Runz, H., Identification of cholesterol-regulating genes by targeted RNAi screening. *Cell Metab* **2009,** *10* (1), 63-75.

160.   Xie, F.; Kniess, T.; Neuber, C.; Deuther-Conrad, W.; Mamat, C.; Lieberman, B. P.; Liu, B.; Mach, R. H.; Brust, P.; Steinbach, J.; Pietzsch, J.; Jia, H., Novel indole-based sigma-2 receptor ligands: synthesis, structure–affinity relationship and antiproliferative activity. *Medchemcomm* **2015,** *6* (6), 1093-1103.

161.   Singh, P.; Saxena, R.; Srinivas, G.; Pande, G.; Chattopadhyay, A., Cholesterol biosynthesis and homeostasis in regulation of the cell cycle. *PLoS One* **2013,** *8* (3), e58833.

162.   Zeng, C.; Weng, C. C.; Schneider, M. E., Jr.; Puentes, L.; Riad, A.; Xu, K.; Makvandi, M.; Jin, L.; Hawkins, W. G.; Mach, R. H., TMEM97 and PGRMC1 do not mediate sigma-2 ligand-induced cell death. *Cell Death Discov* **2019,** *5* (1), 1-12.

163.   McDonald, E. S.; Mankoff, J.; Makvandi, M.; Chu, W.; Chu, Y.; Mach, R. H.; Zeng, C., Sigma-2 ligands and PARP inhibitors synergistically trigger cell death in breast cancer cells. *Biochem Biophys Res Commun* **2017,** *486* (3), 788-795.

164.   Ma, S.; Henson, E. S.; Chen, Y.; Gibson, S. B., Ferroptosis is induced following siramesine and lapatinib treatment of breast cancer cells. *Cell Death Dis* **2016,** *7*, e2307.

165.   Ma, S.; Dielschneider, R. F.; Henson, E. S.; Xiao, W.; Choquette, T. R.; Blankstein, A. R.; Chen, Y.; Gibson, S. B., Ferroptosis and autophagy induced cell death occur independently after siramesine and lapatinib treatment in breast cancer cells. *PLoS One* **2017,** *12* (8), e0182921.

166.   Villalpando-Rodriguez, G. E.; Blankstein, A. R.; Konzelman, C.; Gibson, S. B., Lysosomal destabilizing drug siramesine and the dual tyrosine kinase inhibitor lapatinib induce a synergistic ferroptosis through reduced heme oxygenase-1 (HO-1) levels. *Oxid Med Cell Longev* **2019**.

167.   Jbilo, O.; Vidal, H.; Paul, R.; De Nys, N.; Bensaid, M.; Silve, S.; Carayon, P.; Davi, D.; Galiegue, S.; Bourrie, B.; Guillemot, J. C.; Ferrara, P.; Loison, G.; Maffrand, J. P.; Le Fur, G.; Casellas, P., Purification and characterization of the human SR 31747A-binding protein. A nuclear membrane protein related to yeast sterol isomerase. *J Biol Chem* **1997,** *272* (43), 27107-27115.

168.   Vidal, H.; Mondesert, G.; Galiegue, S.; Carriere, D.; Dupuy, P. H.; Carayon, P.; Combes, T.; Bribes, E.; Simony-Lafontaine, J.; Kramar, A.; Loison, G.; Casellas, P., Identification and pharmacological characterization of SRBP-2: a novel SR31747A-binding protein. *Cancer Res* **2003,** *63* (16), 4809-4818.

169.   Casellas, P.; Galiegue, S.; Bourrie, B.; Ferrini, J. B.; Jbilo, O.; Vidal, H., SR31747A: a peripheral sigma ligand with potent antitumor activities. *Anticancer Drugs* **2004,** *15* (2), 113-118.

170.   Paul, R.; Lavastre, S.; Floutard, D.; Floutard, R.; Canat, X.; Casellas, P.; Le Fur, G.; Breliere, J. C., Allosteric modulation of peripheral sigma binding sites by a new selective ligand: SR 31747. *J Neuroimmunol* **1994,** *52* (2), 183-192.

171.   Labit-Le Bouteiller, C.; Jamme, M. F.; David, M.; Silve, S.; Lanau, C.; Dhers, C.; Picard, C.; Rahier, A.; Taton, M.; Loison, G.; Caput, D.; Ferrara, P.; Lupker, J., Antiproliferative effects of SR31747A in animal cell lines are mediated by inhibition of cholesterol biosynthesis at the sterol isomerase step. *Eur J Biochem* **1998,** *256* (2), 342-349.

172.   Casellas, P.; Bourrie, B.; Canat, X.; Carayon, P.; Buisson, I.; Paul, R.; Breliere, J. C.; Le Fur, G., Immunopharmacological profile of SR 31747: in vitro and in vivo studies on humoral and cellular responses. *J Neuroimmunol* **1994,** *52* (2), 193-203.

173.   Berthois, Y.; Bourrie, B.; Galiegue, S.; Vidal, H.; Carayon, P.; Martin, P. M.; Casellas, P., SR31747A is a sigma receptor ligand exhibiting antitumoural activity both in vitro and in vivo. *Br J Cancer* **2003,** *88* (3), 438-446.

174.   https://clinicaltrials.gov/ct2/show/NCT00174863. (accessed January 24, 2021).

175.   Tang, Z.; Kang, B.; Li, C.; Chen, T.; Zhang, Z., GEPIA2: an enhanced web server for large-scale expression profiling and interactive analysis. *Nucleic Acids Res* **2019,** *47* (W1), W556-W560.

176.   Moparthi, S. B.; Arbman, G.; Wallin, A.; Kayed, H.; Kleeff, J.; Zentgraf, H.; Sun, X. F., Expression of MAC30 protein is related to survival and biological variables in primary and metastatic colorectal cancers. *Int J Oncol* **2007,** *30* (1), 91-95.

177.   Liu, C. C.; Yu, C. F.; Wang, S. C.; Li, H. Y.; Lin, C. M.; Wang, H. H.; Abate, C.; Chiang, C. S., Sigma-2 receptor/TMEM97 agonist PB221 as an alternative drug for brain tumor. *BMC Cancer* **2019,** *19* (1), 473.

CHAPTER II

Discovery of Sigma-2 Receptor as a Target for a Novel Class of Anticancer Agents that Deregulate Cholesterol Metabolism

Introduction

Cholesterol metabolism is strongly related to cancer initiation and progression.[1] Metabolic reprogramming is a common hallmark in cancer that involves adaptations to the increased cancer cell growth and proliferation.[2] Highly proliferating cancer cells tend to have increased cholesterol biosynthesis required for cell membrane biogenesis, providing energy and signaling.[3] In addition to the enhanced biosynthesis, cancer cells can obtain their cholesterol requirements through increasing the uptake of exogenous cholesterol.[1] Elevated cholesterol levels are associated with poor prognosis and increased aggressiveness of the disease.[4-6] Moreover, altered cholesterol and lipid metabolism contribute to drug resistance.[7-10] Thus, targeting cholesterol biosynthesis and metabolism to hinder tumor growth has garnered great interest as a potential therapeutic strategy for the treatment of various cancers.[11] Inhibitors of cholesterol biosynthesis like statins (hydroxymethylglutaryl-CoA reductase (HMGCR) inhibitors) have been tested in multiple clinical trials for pancreatic, esophageal, ovarian, and lung cancers that were associated with improved patient survival.[12-19]

Altered cholesterol homeostasis is a metabolic signature in pancreatic cancer.[20] Pancreatic cancer cells rely on cholesterol for proliferation and survival. Overexpression of the low-density lipoprotein receptor (LDLR) in pancreatic cancer results in increased cholesterol uptake and contributes to tumor progression. LDLR silencing reduces the proliferation of pancreatic cancer

cells and enhance their sensitivity to conventional chemotherapies.[20] Thus, targeting cholesterol metabolism in pancreatic cancer represents a promising therapeutic strategy.

Sigma-2 receptor (S2R)/TMEM97 is an ER transmembrane protein involved in cholesterol homeostasis.[21] Under sterol-depletion conditions, TMEM97 controls cholesterol levels by localizing to the lysosome and binding to Niemann–Pick C1 protein (NPC1), a lysosomal membrane protein that mediates intracellular cholesterol trafficking (Figure I-2).[22] It also forms a ternary complex with the LDLR and the progesterone receptor membrane component 1 (PGRMC1) for rapid internalization of the low-density lipoprotein (LDL) resulting in increased cholesterol uptake (Figure I-2).[23] S2R is overexpressed in several cancers and its overexpression is associated with poor prognosis.[24-31] S2R represents an attractive target for the treatment of pancreatic cancer for its critical role in cholesterol metabolism.

Sigma-2 ligands (S2Ls) are used for diagnostic imaging of tumors and have been studied as anticancer agents with *in vivo* efficacy in murine models of pancreatic cancer.[32-36] Currently, there are no S2Ls in clinical trials for the treatment of cancer. Additionally, there is no crystal structure available for S2R to facilitate structure-based drug design. The reported S2Ls share common structural features that led to a hypothetical binding pocket comprised of an amine binding site adjacent to at least one hydrophobic pocket.[37] Although both sigma-1 and sigma-2 receptors are linked to cancer, S2R is of particular interest as a promising anticancer target due to its higher expression in proliferative tumor cells compared to quiescent cells.[31] Therefore, S2Ls have the potential to be effectively exploited as anticancer therapeutics.

In this project, we report the discovery of a novel class of anticancer agents that target S2R and alter the cholesterol metabolism in pancreatic cancer cells. SAR studies led to the identification of the lead compound **JR235** that is cytotoxic to pancreatic cancer cells. Transcriptomics and

proteomics revealed upregulation of key genes involved in cholesterol and lipid biosynthesis and downregulation of genes involved in GPCR signaling. GPCR screening revealed selective binding of **JR235** to S2R with nanomolar affinity. **JR235** induces autophagy, reactive oxygen species (ROS), and cell cycle arrest in MIA PaCa-2 cells. In extensive mechanistic studies, we show that **JR235** binds to cellular S2R, produces lipid droplets, and a BODIPY-labeled derivative localizes in the ER. Importantly, **JR235** is synergistic with cholesterol and lipid biosynthesis inhibitors.

Results and Discussion

Design, synthesis, and structure-activity relationship

A previous phenotypic (cytotoxicity) screen of a library of 20,000 small molecules led to the identification of the hit scaffold (**QN523**) shared by a group of compounds that displayed cytotoxicity to cancer cells (Appendix Figure II-1). To explore the chemical space and further study the SAR of this scaffold, we designed a series of analogs to identify the structural features important for their cytotoxicity in the pancreatic cancer cell line MIA PaCa-2. We explored the SAR with respect to three key fragments: the quinoline moiety, the pyrazine ring and the core scaffold. Incorporation of fragments of interest led to the identification of **JR121** bearing a diethylamine pentane amine fragment attached to the pyrazine ring with $IC_{50} = 3.7 \pm 0.2$ µM (Appendix Figure II-1). **JR121** was used to first investigate the effect of substitutions in different positions on the quinoline moiety (Table II-1). The 6-methyl substitution in **JR235** was among one of the most potent analogs with IC_{50} value ~ 1 µM. Interestingly, the 7-methyl substitution was inactive (> 30 µM). To better understand of the conformation of the analogs with different positions of the methyl substitution, we performed energy minimization of the 3D structures (Appendix Figure II-2). The results showed a more linear conformation for the 7-methyl substituted analog that was different from the other derivatives. This provides a possible

explanation for the loss of activity and evidence of the importance of the orientation and spatial arrangement of the molecule. We obtained comparable cytotoxicity with the 6-F and 5-Cl substitutions in **JR2-298** and **JR157**, respectively.

Next, we proceeded with exploring tolerable substitutions on the pyrazine ring (Table II-2). While various substitutions were tolerated, the diethylamine pentane amine and the piperazine derivatives displayed the greatest cytotoxicity. On the other hand, the scaffold was found essential for activity. Changes applied to the quinoline ring, the pyrazine or the amide group mostly resulted in loss of activity (Table II-3). A summary of the SAR is shown in Figure II-1.

Table II-1. Cytotoxicity of analogs with quinoline substitutions in MIA PaCa-2 cells.
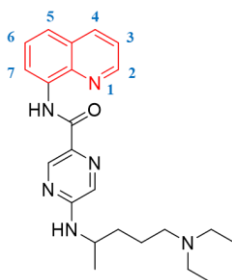
Position	6	5	3	2	7	4 - 4,7	2,5
	JR235	**JR135**	**JR2-120**	**JR236**	**JR240**		
IC$_{50}$ (µM)	1.3 ± 0.2	1.7 ± 0.7	2.3 ± 1.2	9.9 ± 1.1	> 30		
	JR251	**JR157**	**JR247**	**JR239**		**JR252**	
IC$_{50}$ (µM)	1.8 ± 0.2	1.2 ± 0.4	3.8 ± 0.9	4.9 ± 0.9		3.4 ± 0.9	
	JR194	**JR195**		**JR242**	**JR237**	**JR250**	**JR2-116**

IC$_{50}$ (µM)	2.3 ± 0.8	6.8 ± 2.0		1.9 ± 0.5	>30	6.6 ± 3.2	2.9 ± 0.9
	JR2-298	**JR184**					
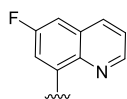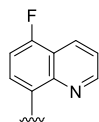
IC$_{50}$ (µM)	1.0 ± 0.4	3.1 ± 0.7

Miscellaneous

	JR191	**JR212**	**JR258**	**JR4-79**	**JR4-136**	**JR159**	**JR121**
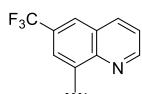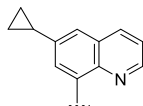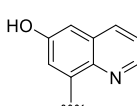
IC$_{50}$ (µM)	4.9 ± 1.9	3.0 ± 0.3	7.3, 9.9	1.6 ± 1.0	4.1 ± 0.7	8.3 ± 1.0	3.7 ± 0.2
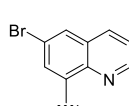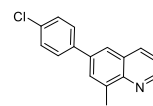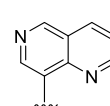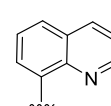
	JR2-118	**JR2-90**
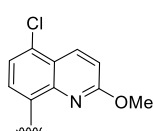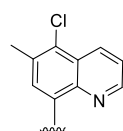
IC$_{50}$ (µM)	5.4 ± 1.6	3.2 ± 0.2

IC$_{50}$ values represent the mean ± SD of three independent experiments.

Table II-2. Cytotoxicity of analogs with pyrazine substitutions in MIA PaCa-2 cells.
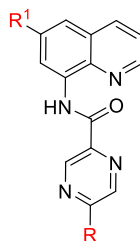
ID	R	R^1	IC$_{50}$ (µM)	ID	R	R^1	IC$_{50}$ (µM)
JR5-176A		F	3.7, 2.2	**JR2-52**		CH$_3$	1.7 ± 2.0
JR5-177A		F	2.4, 1.9	**JR4-188**		F	> 30
JR5-176B		F	2.4, 2.7	**JR4-189**		F	> 30
JR5-180		F	2.6, 2.0	**JR272**		CH$_3$	0.9 ± 0.2
JR2-259		CH$_3$	9.5 ± 0.9	**JR283**		CH$_3$	1.0 ± 0.7
JR4-69		F	21.4 ± 4.7	**JR3-8**		CH$_3$	1.2 ± 0.7

ID	Structure		IC$_{50}$	ID	Structure		IC$_{50}$
JR4-32	(structure) NH$_2$	CH$_3$	5.5, 8.5	**JR2-50**	(structure) O, NH	CH$_3$	6.5 ± 3.5
JR276	(structure) HN, NH	CH$_3$	15.6 ± 5.3	**JR4-76**	(structure) NH, N, S, O, O	F	> 30

IC$_{50}$ values represent the mean ± SD of three independent experiments. Values from two experiments are listed without averaging.

Table II-3. Cytotoxicity of analogs with changes in the core scaffold in MIA PaCa-2 cells.

ID	Structure	IC$_{50}$ (µM)	ID	Structure	IC$_{50}$ (µM)
PYRAZINE RING			AMIDE GROUP		
JR2-23	(structure)	>30	**JR2-157**	(structure)	17.6 ± 5.9
JR2-24	(structure)	>30	**JR4-174**	(structure)	>30
JR4-134	(structure)	>30	**JR4-165**	(structure)	>30
JR4-133	(structure) SO$_2$Me	13.2, 15.7	**JR5-55C**	(structure) CF$_3$	>30
JR4-140	(structure)	>30	**JR5-63B**	(structure)	>30
QUINOLINE RING					
JR4-162A	(structure)	>30	**JR4-162B**	(structure)	>30

I. Quinoline Moiety

R_1 substitution and its position:
- 6-position is optimal for activity
- 7-substitution results in loss of activity
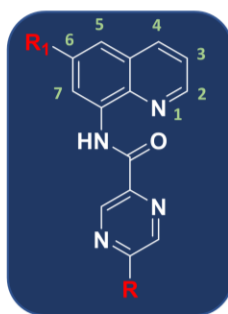
III. Core Scaffold

Amide group, pyrazine ring and quinoline moiety are essential for activity

II. Pyrazine Moiety

Various substitutions are tolerated

Figure II-1. Structure-activity relationship derived from the cytotoxicity of JR compounds in MIA PaCa-2 cells.

JR235 and JR272 are cytotoxic to cancer cells

SAR studies identified **JR235** and **JR272** with comparable IC_{50} values and improved potency over most of the compounds (Table II-1/2). The two compounds are analogs comprising counterparts of the core scaffold and were chosen as representative compounds for further mechanistic studies and better understanding of the activity of this class of compounds (Figure II-2A). We further tested **JR235** and **JR272** against a panel of cancer cell lines and the pancreatic cancer cell line MIA PaCa-2 was among the most sensitive and therefore was chosen for our experimental studies (Appendix Table II-1). **JR235** and **JR272** show significant cytotoxicity in the MTT assay with IC_{50} values, 1.3 and 0.9 µM, respectively and are over 4-fold more potent in inhibiting colony formation (Figure II-2B/C). The compounds were less potent in the normal cell line HFF-1 (> 8-fold) suggesting selective toxicity to cancer cells (Appendix Figure II-3).

Cytotoxicity of JR235 and JR272 in pancreatic cancer cells involves ROS

To investigate the mechanism of cell death, we combined **JR235** or **JR272** with known cell death inhibitors including: the apoptosis inhibitor, Z-VAD-FMK; the ROS scavenger, N-acetyl

cysteine (NAC); the autophagy inhibitor, chloroquine (CQ); and the ferroptosis inhibitor, deferoxamine (DFO). (Appendix Table II-2, Appendix Figure II-4C). Both **JR235** and **JR272** were significantly less cytotoxic in the presence of NAC suggesting a ROS-induced cell death (Figure II-2D/E, Appendix Figure II-4A/B). Reduced cytotoxicity of **JR235** was also observed in the presence of glutathione (GSH) (Appendix Figure II-4D). To validate this mechanism, we evaluated the effect of **JR235** and **JR272** on heme oxygenase 1 (HMOX1) protein levels. HMOX1 is an enzyme involved in heme catabolism and plays a role in cellular defense against oxidative stress by reducing ROS generation.[38] Treatment of MIA PaCa-2 cells with **JR235** or **JR272** resulted in a dose-dependent increase in HMOX1 levels after 24 h (Figure II-2F). This result is consistent with the antagonism we observed between the compound treatment and ROS scavengers suggesting ROS-mediated cell death.
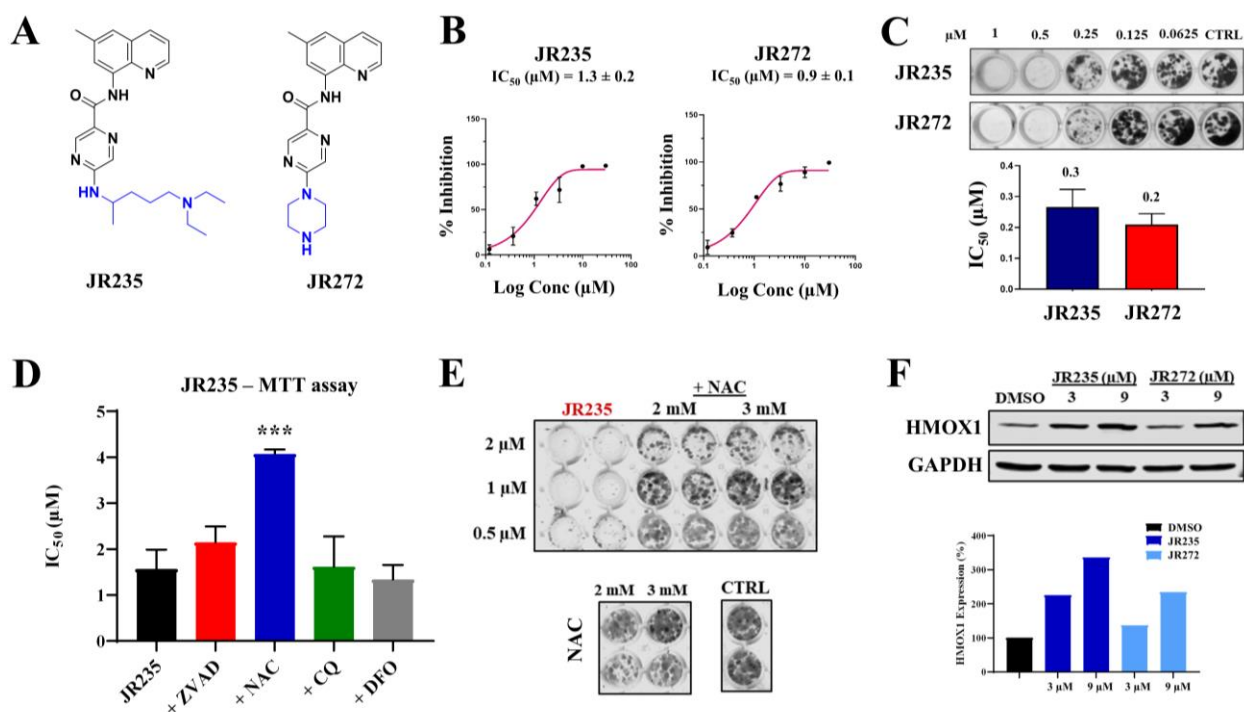
Figure II-2. **JR235** is cytotoxic to MIA PaCa-2 cells and induces ROS-mediated cell death. (A) Chemical structures of **JR235** and **JR272**. (B) Dose-response curves for **JR235** and **JR272** in the MTT assay. (C) Dose-response for **JR235** and **JR272** in the colony formation assay (CFA) with the IC_{50} values presented on top of the bars. (D) IC_{50} for **JR235** and its combination with different cell death mechanism inhibitors in MTT assay (apoptosis inhibitor, Z-VAD-FMK, 100 µM; ROS inhibitor, N-acetyl cysteine, 2 mM; autophagy inhibitor, chloroquine, 10 µM; ferroptosis inhibitor, deferoxamine, 2 µM). Cells were pretreated with the cell death inhibitors for 2 h prior to compound treatment. (E) Dose-response of **JR235** and its combination with NAC in the CFA. (F) **JR235**

and **JR272** result in a dose-dependent increase in HMOX1 levels. Quantification of the Western blot is from one experiment. The data are average of three biological replicates with the standard deviation represented as error bars. *** denotes $p < 0.001$.

JR235 and JR272 alter the cholesterol and lipid biosynthetic pathways

To further understand the mechanism of action of our compounds and gain insight into the altered tumorigenic pathways, we performed bromouridine labeled RNA sequencing (Bru-seq) of MIA PaCa-2 cells treated with **JR235** or **JR272**. The genes were ranked based on the $\log_2$ fold change ($\log_2$FC) to identify the top 25 downregulated and upregulated genes for each compound (Tables II-4 – II-7). A correlation of 0.798 between the $\log_2$ fold changes of **JR235** and **JR272** suggests they share a similar mechanism of action (Figure II-3A). Among the top 25 upregulated genes, seven were in common: INSIG1, DHCR7, SCD, SDR39U1, MVK, HIST1H3B and PCYT2 (Figure II-3B/C). Interestingly, almost all common genes are involved in cholesterol and lipid biosynthesis. Other genes involved in the cholesterol biosynthesis were among the top genes upregulated by **JR235** including HMGCS1, LSS, MVD, and FDFT1 (Table II-4).[39] This significant signature suggests our compounds are targeting cancer cell metabolism *via* alteration of cholesterol homeostasis.

While cholesterol levels are tightly regulated in normal cells, the deregulation and reprogramming of cholesterol metabolism is common in cancer cells and contributes to tumorigenesis.[1] The cholesterol biosynthetic pathway is highlighted in Chapter I, Figure I-4. The levels of several enzymes that are involved in the *de novo* synthesis of cholesterol were increased with **JR235** and **JR272** treatments including 7-dehydrocholesterol reductase (DHCR7), the enzyme that catalyzes the final step in the biosynthetic process converting 7-dehydrocholesterol (7DHC) to cholesterol.[40] DHCR7 inhibitors like tamoxifen are commonly used in breast cancer.[41] Another upregulated enzyme is mevalonate kinase (MVK) which phosphorylates mevalonate, an intermediate of cholesterol biosynthesis. Statins, a well-known class of cholesterol biosynthesis

inhibitors increase the expression of these genes through a feedback mechanism.[42] It was found that although cholesterol biosynthesis was potentiated in response to statin-treatment, plasma cholesterol levels decreased due to enhanced elimination resulting in cholesterol-lowering effects.[42] Thus, we postulated that the increased expression of the cholesterol biosynthesis genes caused by our treatments contributes to compensatory mechanisms that aim to increase the cellular cholesterol availability.

The expression of stearoyl-CoA desaturase (SCD), a key enzyme in fatty acid synthesis was also upregulated (Figure II-3C). SCD plays an important role in the *de novo* synthesis of fatty acids by converting saturated fatty acids into monounsaturated fatty acids which are essential components of cellular lipids and play a role in the regulation of the ER stress response.[43] SCD is highly expressed in several cancers and its expression correlates with cancer progression and poor prognosis.[44, 45] Other upregulated enzymes that are involved in the regulation of sterol/lipid metabolism include the short-chain dehydrogenase/reductase family 39U member 1 (SDR39U1) and phospholipid synthesis like phosphate cytidylyltransferase-2 (PCYT2) (Figure II-3B).[46, 47]

As previously discussed in Chapter I, SREBP-2 is the master regulator of cholesterol synthesis that regulates the transcription of biosynthetic enzymes as well as the LDLR.[48, 49] Insulin-induced gene 1 (INSIG1), a regulatory protein of SREBP was upregulated by our treatments further supporting their involvement in cholesterol metabolism. INSIG1 plays a role in the regulation of cholesterol homeostasis *via* feedback regulation of cholesterol synthesis.[50] In response to elevated cholesterol levels, it binds to SCAP and cause retention of the SCAP/SREBP complex in the ER resulting in reduced SREBP activity.[51]

Six genes from the top 25 downregulated genes are in common between **JR235** and **JR272** including GPR135, AKAP5, HRH4, FERMT1, CACNG8 and TXNRD3NB (Figure II-3B). Two

of these genes, G-protein coupled receptor 135 (GPR135) and histamine receptor H4 (HRH4) are GPCRs. A-kinase anchoring-protein 5 (AKAP5) is a key regulator of GPCR signaling and β-adrenergic signaling.[52, 53] The fermitin family member 1 (FERMT1) is another protein involved in the regulation of GPCR signaling through activation of integrin that plays a role in adhesion and cytoskeletal signaling.[54] Other proteins involved in GPCR signaling were among the top downregulated genes with **JR235** treatment including tensin 4 (TNS4), neurotensin receptor 1 (NTSR1) and MX dynamin like GTPase 2 (MX2). Cholesterol has been implicated in GPCR signaling and plays a role in modulating the function of GPCRs.[55-57] Cholesterol can alter the binding affinity of other ligands to their GPCR.[58, 59] These findings further support our hypothesis that **JR235** and **JR272** target cholesterol metabolism and GPCR pathways.
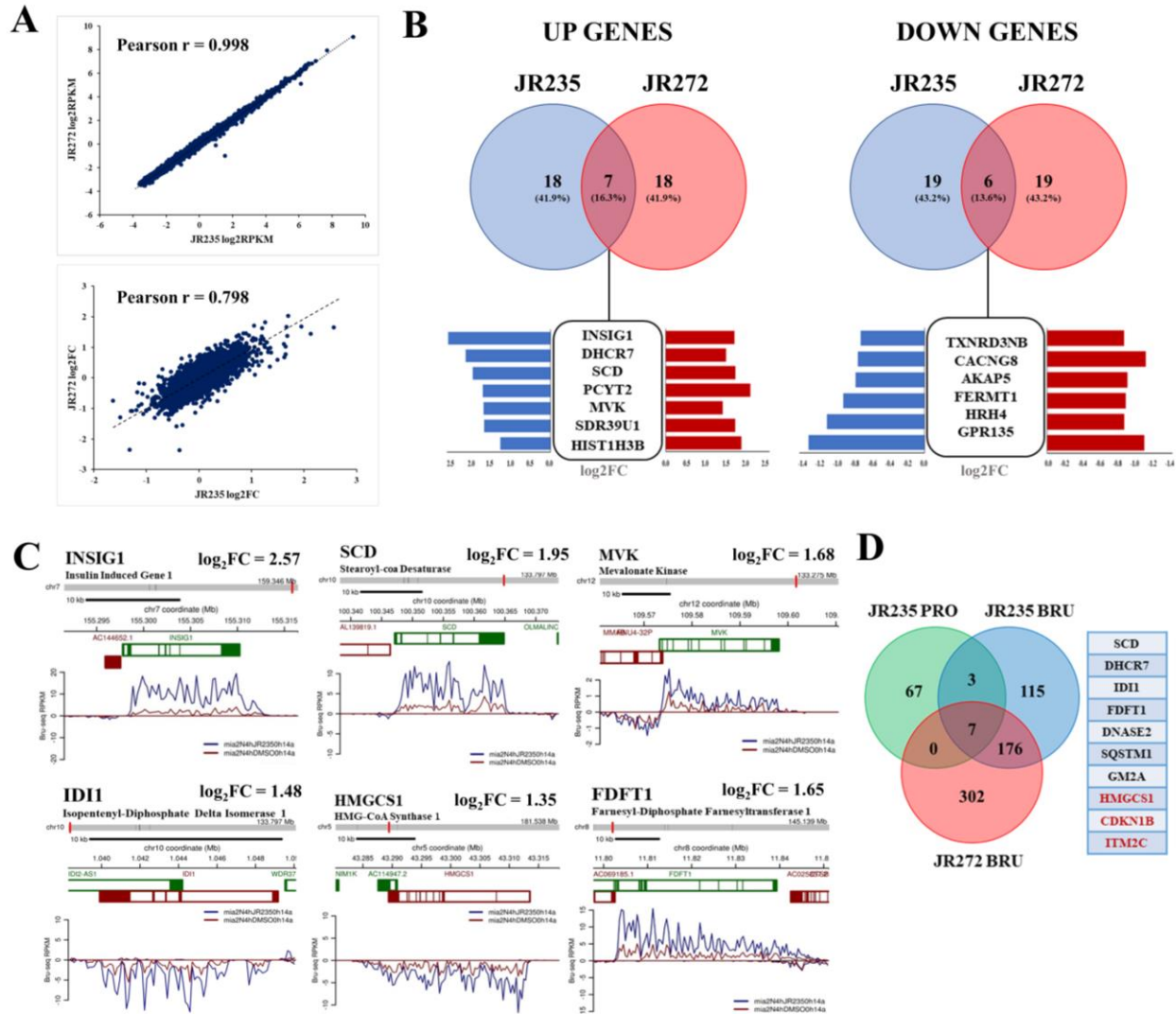
Figure II-3. **JR235** and **JR272** deregulate genes and proteins involved in cholesterol and lipid biosynthesis. (A) Pearson correlation between changes in expression of genes following **JR235** and **JR272** treatment from Bru-seq. (B) Venn diagram showing genes in common between the top 25 genes deregulated genes by **JR235** and **JR272** treatments. (C) Trace diagrams for the top genes involved in cholesterol/lipid biosynthesis deregulated by **JR235** treatment (blue) compared to the DMSO control (red). (D) Venn diagram showing upregulated genes and proteins in common between **JR235** and **JR272** treatments from Bru-seq and **JR235** treatment from proteomics. Proteins in red are common between the **JR235** Bru-seq and proteomics treatments but not **JR272** (HMGCS1: hydroxymethylglutaryl-CoA synthase 1; CDKN1B: cyclin-dependent kinase inhibitor 1B; ITM2C: integral membrane protein 2C). FC ≥ 1.5.

To identify the enriched pathways deregulated by **JR235** and **JR272** treatments, we performed gene set enrichment analysis (GSEA) (Appendix Tables II-3 – II-18). The two compounds shared ≥ 50% of the deregulated Hallmark gene sets (Appendix Figure II-5A). Upregulated Hallmark gene sets include cholesterol homeostasis and fatty acid metabolism confirming our previous analysis of the top common genes. Glycolysis and oxidative

phosphorylation (OXPHOS) were also upregulated (Figure II-4, Appendix Table II-3/II-11). High cholesterol levels regulate metabolic alterations through enhancing the 'Warburg' effect (aerobic glycolysis) to provide the necessary biomolecule precursors required by the highly proliferating cancer cells and protect against mitochondria-induced apoptosis.[60] Although cancer cells rely mainly on aerobic glycolysis, many cancers use OXPHOS to produce enough energy and meet the metabolic needs.[60, 61] Other **JR235** upregulated pathways include hypoxia, p53 pathway, TNF-α signaling *via* NF-κB and apoptosis. Downregulated gene sets include MYC targets, KRAS signaling and TGF-β signaling all of which play a role in cancer metabolism and have been linked to cholesterol.[62-66]

To explore our Bru-seq results at the protein level, we performed proteomics analysis of **JR235** treated MIA PaCa-2 cells. A Venn diagram between the **JR235** deregulated genes and proteins (FC ≥ 1.5) showed ten upregulated proteins in common (Figure II-3D). Inclusion of the upregulated genes from the **JR272** treatment identified seven proteins in common including DHCR7, SCD, IDI1, FDFT1, GM2A, DNASE2 and SQSTM1. Consistent with the Bru-seq data, the protein expression of the biosynthetic enzymes DHCR7 and SCD were upregulated. Other upregulated proteins that are involved in cholesterol biosynthesis include IDI1 and FDFT1. Upregulation of proteins involved in autophagy including sequestosome 1 (SQSTM1), a cargo protein that plays a role in autophagic degradation of aberrant proteins was also demonstrated.[67]

We performed STRING analysis for the top 25 upregulated and downregulated proteins to identify their functional enrichment (Appendix Figure II-5B). Upregulated proteins clustered into apolipoproteins and ribosomal proteins. Apolipoproteins are proteins associated with lipids and are responsible for their transport between the body organs for utilization in cellular processes.[68, 69] Downregulated proteins clustered into NADH dehydrogenases (ubiquinone) and mitochondrial

ribosomal proteins. Ubiquinone is an electron carrier that plays a role in mitochondrial electron transport and oxidative phosphorylation.[70] The functional signature from the proteomic analysis is consistent with the Bru-seq results confirming our compounds are targeting cancer metabolism and strongly suggests that the target in involved in cholesterol homeostasis.

We performed a similarity search for the **JR235** transcriptomic signature using the L1000FWD web-based tool that includes signatures induced by thousands of known drugs.[71] Among the top compounds with average matching profiles were compounds targeting the opioid and histamine receptors both of which are GPCR targets (Appendix Figure II-5C). In line with our previous data, **JR235** displayed a similar transcriptomic signature to the lipase inhibitor orlistat, as well as other cholesterol biosynthesis inhibitors (Appendix Figure II-5C).
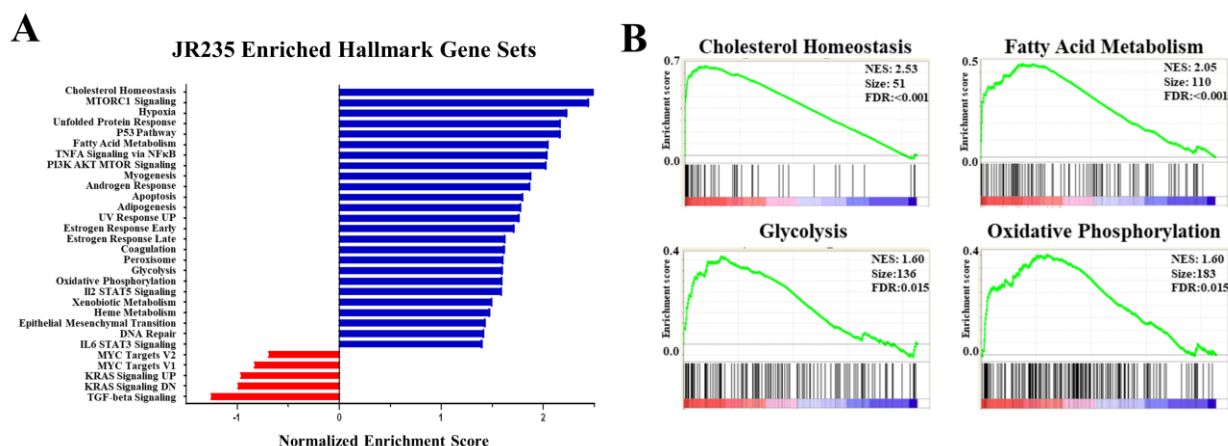
Figure II-4. **JR235** deregulates pathways involved in cholesterol and lipid homeostasis. (A) GSEA from Bru-seq showing the Hallmark gene sets deregulated by **JR235** treatment. (B) Enrichment plots for upregulated gene sets involved in cholesterol/lipid pathways. Plots were generated from GSEA using log_2FC of the genes.

Table II-4. Top 25 upregulated genes from the Bru-seq analysis of **JR235** treated MIA PaCa-2 cells.

No	Gene symbol	Gene name/function	Log_2FC
1	NEU1	Neuraminidase 1: Glycoproteins and glycolipids biosynthesis	2.68
2	INSIG1	Insulin Induced Gene 1	
		Cholesterol metabolism, lipogenesis, and glucose homeostasis regulation	2.57
3	DDIT4	DNA Damage Inducible Transcript 4	
		Cell growth, proliferation, and survival regulation	2.33
4	DHCR7	7-Dehydrocholesterol Reductase: Cholesterol biosynthesis	2.13
5	SCD	Stearoyl-CoA Desaturase: Fatty acid biosynthesis	1.95
6	LIPG	Lipase G, Endothelial Type	
		Lipoprotein metabolism and vascular biology	1.81
7	SLC2A6	Solute Carrier Family 2 Member 6/ GLUT9	
		Facilitative glucose transporter	1.74

8	PCYT2	Phosphate Cytidylyltransferase 2, Ethanolamine	
		Phospholipid biosynthesis	1.70
9	MVK	Mevalonate Kinase: Cholesterol biosynthesis	1.68
10	SDR39U1	Short Chain Dehydrogenase/Reductase Family 39U Member 1	
		Oxidoreductase	1.67
11	MSMO1	Methylsterol Monooxygenase 1: Cholesterol biosynthesis	1.65
12	FDFT1	Farnesyl-Diphosphate Farnesyltransferase 1	
		Cholesterol biosynthesis	1.65
13	CCNG2	Cyclin G2: Growth and cell cycle progression regulation	1.62
14	TBC1D17	TBC1 Domain Family Member 17	
		Autophagy regulation	1.62
15	IDI1	Isopentenyl-Diphosphate Delta Isomerase 1	
		Cholesterol biosynthesis	1.49
16	AVPI1	Arginine Vasopressin Induced 1: Cell cycle regulation	1.37
17	MVD	Mevalonate Diphosphate Decarboxylase	
		Cholesterol biosynthesis	1.36
18	HMGCS1	3-Hydroxy-3-Methylglutaryl-CoA Synthase 1	
		Cholesterol biosynthesis	1.35
19	DDIT3	DNA Damage Inducible Transcript 3: ER stress response	1.32
20	BHLHE40	Basic Helix-Loop-Helix Family Member E40	
		Circadian rhythm and cell differentiation	1.32
21	SH2D5	SH2 Domain Containing 5: Synaptic plasticity regulation	1.29
22	HIST1H3B	Histone Cluster 1 H3 Family Member B	
		Nucleosome assembly, chromatin organization and silencing	1.26
23	LSS	Lanosterol Synthase	
		Cholesterol biosynthesis	1.25
24	HIST1H1E	Histone Cluster 1 H1 Family Member E	
		Nucleosome assembly, gene transcription regulation	1.24
25	TUBA1A	Tubulin Alpha 1a: Cell cycle, mitosis	1.24

Table II-5.Top 25 downregulated genes from the Bru-seq analysis of **JR235** treated MIA PaCa-2 cells.

No	Gene symbol	Gene name/function	Log_2FC
1	GPR135	G Protein-Coupled Receptor 135	-1.30
		GPCR activity, β-arrestin recruitment	
2	SPDYA	Speedy/RINGO Cell Cycle Regulator Family Member A	-1.18
		Cell cycle regulation	
3	ABCA1	ATP Binding Cassette Subfamily A Member 1	-1.14
		Cholesterol transport (efflux)	
4	HRH4	Histamine Receptor H4: Allergy response	-1.09
5	NPR2	Natriuretic Peptide Receptor 2	-1.08
		Skeletal growth regulation (guanyl cyclase activity)	
6	TNS4	Tensin 4: Cell migration and signaling by GPCR	-1.05
7	SYCE2	Synaptonemal Complex Central Element Protein 2	-0.98
		Cell cycle regulation	
8	NOG	Noggin: Inactivates transforming growth factor-beta	-0.93
9	FERMT1	Fermitin Family Member 1	-0.91
		Cytoskeletal signaling and adhesion	
10	GPR75-ASB3	GPR75-ASB3 Protein	-0.89
		Paralog of ASB3 (class I MHC-mediated antigen processing and	
		presentation)	
11	NTSR1	Neurotensin Receptor 1	-0.89
		GPCR activity (downstream MAP kinase activation: antiapoptotic)	
12	ZDHHC11	Zinc Finger DHHC-Type Containing 11	-0.86
		Protein palmitoylation (lipid modification)	
13	AGAP6	ArfGAP With GTPase Domain, Ankyrin Repeat And PH Domain	-0.85

No	Gene name	Gene function	Log$_2$FC
		GTPase-activating protein	
14	TAS2R20	Taste 2 Receptor Member 20: GPCR signaling	-0.81
15	RFLNB	Refilin B	-0.79
		Cartilaginous skeletal elements formation	
16	MX2	MX Dynamin Like GTPase 2	-0.78
		GTPase activity (cell-cycle progression regulation)	
17	AKAP5	A-Kinase Anchoring Protein 5	-0.77
		Glutamate binding, GPCR signaling	
18	NEXN	Nexilin F-Actin Binding Protein: Cell adhesion and migration	-0.76
19	CACNG8	Calcium Voltage-Gated Channel Auxiliary Subunit Gamma 8	-0.75
		Glutamate binding, activation of AMPA receptors & synaptic plasticity	
20	NOXRED1	NADP Dependent Oxidoreductase Domain Containing 1	-0.73
		Reductase activity	
21	PTCH2	Patched 2	-0.72
		Tumor suppressor, Hedgehog receptor activity, ERK signaling	
22	TXNRD3NB	Thioredoxin Reductase 3 Neighbor	-0.72
23	TSPAN4	Tetraspanin 4	-0.68
		Integrin and antigen binding (cell development, growth, and motility)	
24	NPIPB11	Nuclear Pore Complex Interacting Protein Family Member B11	-0.67
25	CCND1	Cyclin D1: Cell cycle regulation, ERK signaling	-0.67

Table II-6. Top 25 upregulated genes from the Bru-seq analysis of **JR272** treated MIA PaCa-2 cells.

No	Gene name	Gene function	Log$_2$FC
1	PCYT2	Phosphate Cytidylyltransferase 2, Ethanolamine	2.03
		Phospholipid synthesis	
2	DBP	D-Box Binding PAR BZIP Transcription Factor	1.90
		Circadian rhythm regulation, DNA binding transcription factor activity	
3	HIST1H3B	Histone Cluster 1 H3 Family Member B	1.82
		Transcription regulation, DNA repair, DNA replication and chromosomal stability	
4	RNF26	Ring Finger Protein 26	1.71
		Protein ubiquitination, endosome organization	
5	DOLK	Dolichol Kinase: Oligosaccharide synthesis	1.70
6	SCD	Stearoyl-CoA Desaturase: Fatty acid biosynthesis	1.67
7	SDR39U1	Short Chain Dehydrogenase/Reductase Family 39U Member 1	1.67
8	INSIG1	Insulin Induced Gene 1	1.65
		Cholesterol metabolism, lipogenesis, and glucose homeostasis regulation	
9	HIST1H2BF	Histone Cluster 1 H2B Family Member F	1.63
		Replication-dependent, cell cycle regulation	
10	DDX28	DEAD-Box Helicase 28	1.46
		Translation initiation, nuclear and mitochondrial splicing, ribosome assembly	
11	HIST1H3C	Histone Cluster 1 H3 Family Member C: Cell cycle regulation	1.45
12	DHCR7	7-Dehydrocholesterol Reductase: Cholesterol biosynthesis	1.44
13	ORMDL3	ORMDL Sphingolipid Biosynthesis Regulator 3	1.39
		Sphingolipid synthesis (negative regulator)	
14	APRT	Adenine Phosphoribosyltransferase	1.39
		Pyrimidine metabolism	
15	MVK	Mevalonate Kinase: Cholesterol biosynthesis	1.37
16	HIST1H1D	Histone Cluster 1 H1 Family Member D	1.36
17	H2AFX	H2A Histone Family Member X: Cell cycle regulation	1.36
18	AC099811.2	GTP binding and histone acetyltransferase activity	1.35
19	COMMD5	COMM Domain Containing 5: Cell proliferation	1.31
20	POP7	POP7 Homolog, Ribonuclease P/MRP Subunit	1.30
		RNA transport, tRNA processing	

21	HIST1H3I	Histone Cluster 1 H3 Family Member I	1.28
22	ABHD14B	Abhydrolase Domain Containing 14B: Metabolism, CYP450	1.28
23	FASN	Fatty Acid Synthase	1.28
		Cholesterol biosynthesis, AMPK signaling	
24	ZC3H12A	Zinc Finger CCCH-Type Containing 12A	1.27
		Transcriptional activator, cardiomyocytes cell death	
25	UAP1L1	UDP-N-Acetylglucosamine Pyrophosphorylase 1 Like 1	1.26
		Amino sugar metabolism	

Table II-7. Top 25 downregulated genes from the Bru-seq analysis of **JR272** treated MIA PaCa-2 cells.

No	Gene name	Gene function	Log$_2$FC
1	ZNF816	Zinc Finger Protein 816: Transcriptional regulation	-1.58
2	IFT80	Intraflagellar Transport 80	-1.12
		Organelle biogenesis, intraflagellar transport	
3	CACNG8	Calcium Voltage-Gated Channel Auxiliary Subunit Gamma 8	-1.10
		Regulation of AMPA receptors channel gating, translation initiatoin	
4	GPR135	G Protein-Coupled Receptor 135	-1.08
		GPCR activity, regulatory interaction with metatoninR	
5	PTX3	Pentraxin 3: Innate immune system	-1.04
6	AC005726.2	RNA gene	-0.99
7	SLCO1B3	Solute Carrier Organic Anion Transporter Family	-0.96
		Taxane pathway, metabolism, bilirubin transport	
8	GRIN2C	Glutamate Ionotropic Receptor NMDA Type Subunit 2C	-0.95
		Memory, synaptic development	
9	TEX15	Testis Expressed 15, Meiosis And Synapsis Associated	-0.95
		Cell cycle	
10	CHML	CHM Like, Rab Escort Protein 2	-0.94
		Protein metabolism, GTPase activator activity	
11	SPTY2D1-AS1	SPTY2D1 Opposite Strand	-0.93
12	ZNF37A	Zinc Finger Protein 37A	-0.93
		DNA binding transcription factor activity	
13	PHLDB2	Pleckstrin Homology Like Domain Family B Member 2	-0.93
		Acetyl-choline receptor aggregation	
14	CCDC190	Coiled-Coil Domain Containing 190	-0.91
15	CD274	CD274 Molecule: Innate immune system	-0.90
16	AKAP5	A-Kinase Anchoring Protein 5	-0.90
		Activation of AMPA receptor, GPCR pathway	
17	GCNA	Germ Cell Nuclear Acidic Peptidase	-0.89
18	KLF10	Kruppel Like Factor 10	-0.88
		Transcriptional reprsessor (TGFB signaling)	
19	FERMT1	Fermitin Family Member 1	-0.88
		Cytoskeletal signaling and adhesion	
20	AC022335.1	Transporter activity	-0.86
21	HRH4	Histamine Receptor H4	-0.86
		GPCR, Akt signaling	
22	TXNRD3NB	Thioredoxin Reductase 3 Neighbor	-0.86
23	GCLM	Glutamate-Cysteine Ligase Modifier Subunit	-0.85
		Glutathione sunthesis, ferroptosis and metabolism	
24	CLEC2D	C-Type Lectin Domain Family 2 Member D	-0.84
		Innate immune system	
25	AC009690.1	Hydrolase activity	-0.83

Table II-8. Top 25 upregulated proteins from the proteomics analysis of **JR235** treated MIA PaCa-2 cells.

No	Protein name	Log$_2$FC	Exp. *q*-val

1	Serine/threonine-protein kinase PLK4	1.66	0.143
2	Protein FAM177A1	1.63	0.035
3	Dermcidin	1.3	0.001
4	Apolipoprotein B-100	1.1	<0.001
5	Acyl-CoA desaturase	1.1	<0.001
6	Iron-responsive element-binding protein 2	1.09	0.010
7	Apolipoprotein C-III	1.05	0.001
8	Filamin-C	1.02	<0.001
9	Phosphatidylserine synthase 1	0.96	0.025
10	Hydroxymethylglutaryl-CoA synthase, cytoplasmic	0.96	<0.001
11	E3 ubiquitin-protein ligase TRIM69	0.93	0.123
12	Apolipoprotein A-I	0.92	0.001
13	Kinesin-like protein KIF27	0.92	0.004
14	Mixed lineage kinase domain-like protein	0.9	0.001
15	Bleomycin hydrolase	0.88	0.037
16	Muellerian-inhibiting factor	0.87	0.119
17	60S ribosomal protein L37	0.85	<0.001
18	Copper-transporting ATPase 2	0.85	0.01
19	Putative ankyrin repeat domain-containing protein 31	0.84	0.123
20	40S ribosomal protein S8	0.83	<0.001
21	60S ribosomal protein L19	0.82	<0.001
22	GH3 domain-containing protein	0.8	0.015
23	40S ribosomal protein S26	0.78	<0.001
24	60S ribosomal protein L27a	0.78	<0.001
25	Protein PIMREG	0.77	0.114

Table II-9. Top 25 upregulated proteins from the proteomics analysis of **JR235** treated MIA PaCa-2 cells.

No	Protein name	Log$_2$FC	Exp. q-val
1	MBT domain-containing protein 1	-2.1	0.027
2	Elongation factor G, mitochondrial	-2.03	<0.001
3	Aldehyde dehydrogenase X	-1.85	<0.001
4	LanC-like protein 2	-1.61	0.001
5	28S ribosomal protein S18b, mitochondrial	-1.57	0.003
6	Transcription elongation factor 1 homolog	-1.46	0.003
7	DNA topoisomerase 2-alpha	-1.39	<0.001
8	FAST kinase domain-containing protein 5, mitochondrial	-1.39	0.002
9	Scaffold attachment factor B1	-1.32	<0.001
10	28S ribosomal protein S25, mitochondrial	-1.32	<0.001
11	28S ribosomal protein S16, mitochondrial	-1.31	0.006
12	Scaffold attachment factor B2	-1.3	<0.001
13	Constitutive coactivator of peroxisome proliferator-activated receptor gamma	-1.25	<0.001
14	28S ribosomal protein S22, mitochondrial	-1.21	<0.001
15	Keratin, type I cytoskeletal 20	-1.19	0.001
16	RNA-binding motif protein, X chromosome	-1.18	<0.001
17	28S ribosomal protein S17, mitochondrial	-1.15	0.002
18	Protein FAM83H	-1.12	0.001
19	Interleukin-36 beta	-1.12	<0.001
20	Histone H1.2	-1.11	0.150
21	NADH dehydrogenase [ubiquinone] iron-sulfur protein 4, mitochondrial	-1.1	0.001
22	NADH dehydrogenase [ubiquinone] 1 alpha subcomplex subunit 6	-1.08	0.004

23	Proliferation marker protein Ki-67	-1.08	<0.001
24	Nucleolar transcription factor 1	-1.05	<0.001
25	D-dopachrome decarboxylase	-1.04	<0.001

JR235 induces autophagy and results in accumulation of cytosolic lipid droplets

The mTOR signaling pathway and lysosome gene sets were upregulated after treatment with our compounds (Figure II-5A, Appendix Figure II-6). The mTOR pathway plays a role in promoting lipogenesis and is a negative regulator of autophagy. [72, 73] Cells respond to starvation *via* lysosome-mediated autophagy to clear defective organelles or aberrantly folded proteins and allow recycling of nutrients.[74] Cholesterol metabolism and autophagy play mutual regulatory roles in the cells.[73, 75] Compounds that target cholesterol synthesis like statins were also found to induce autophagy.[76, 77]

To determine whether our compounds acted through autophagy, we tested the effect of **JR235** and **JR272** on the expression of the autophagy biomarker LC3B using immunoblotting. Both compounds resulted in a dose-dependent increase in the LC3B protein levels suggesting the compounds induce autophagy (Figure II-5B).

Statins cause accumulation of cytosolic lipid droplets (LD) in pancreatic cancer cells, suggesting their role in lipid-mediated cell death.[78] LD are the storage sites of cholesteryl esters and triglycerides, and they play a role in lipid metabolism and regulation of free cholesterol levels.[78, 79] LD accumulation can result from increased lipid synthesis or uptake.[79] The similarity in the cellular effects between **JR235** and statins intrigued us to test its effect on the intracellular LD content using the Nile red stain. After a 24 h treatment in MIA PaCa-2 cells, we observed an increase in the intensity of the stained LD compared to the DMSO control suggesting that **JR235** results in accumulation of cytosolic lipids (Figure II-5C). This result supports the previously demonstrated upregulation of genes involved in cholesterol and lipid metabolism.
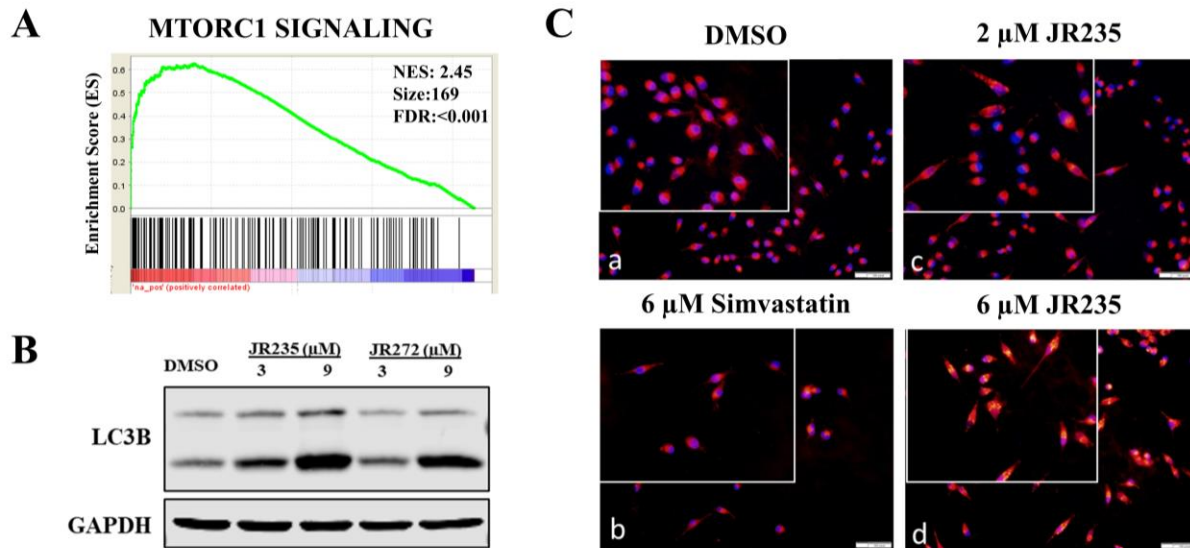
Figure II-5. **JR235** induces autophagy and causes lipid droplets accumulation. (A) Enrichment plot for the mTORC1 signaling gene set upregulated by **JR235** treatment in Bru-seq. (B) **JR235** and **JR272** result in a dose-dependent increase in LC3B protein levels. Immunoblotting was used to detect protein levels after a 24h-treatment at the indicated concentrations (C) **JR235** causes lipid droplet accumulation. MIA PaCa-2 cells were treated with **JR235** for 24 h and the lipid droplets were stained using Nile red (1 µg/ml). Data presented are from a single experiment.
.

JR235 causes cell cycle arrest

Several genes involved in the regulation of the cell cycle were downregulated with **JR235** treatment including Speedy/RINGO Cell Cycle Regulator Family Member A (SPDYA), Synaptonemal Complex Central Element Protein 2 (SYCE2), Cyclin D1 (CCND1) and MX2 (Table II-5). SPDYA is a cell cycle protein that activates cyclin-dependent kinases (CDKs) to promote cell proliferation.[80] CCND1 and MX2 are regulatory proteins required for the progression of the cells through the G1/S phase transition.[81, 82] SYCE2 plays a role in promoting DNA double-strand break repair by minimizing the binding of the heterochromatin protein 1 (HP1) to the trimethylated histone H3 lysine 9 (H3K9me3) resulting in H2AX phosphorylation and DNA repair.[83] In addition, HIST1H3B, a histone 3 family member that regulates cell cycle transitions[84] was found upregulated with our treatment suggesting **JR235** interferes with epigenetic modifications (Figure II-6A/B).

To confirm disruption in cell cycle, we treated MIA PaCa-2 cells with **JR235** for 72 h and observed a significant increase in the cell count in the S phase that appears to be dose-dependent suggesting **JR235** interferes with the cell cycle progression by inducing S phase arrest (Figure II-6C/D). Furthermore, treatment of MIA PaCa-2 cells with **JR235** resulted in a decrease in the Cyclin D1 protein levels at 24 h (Figure II-6E).
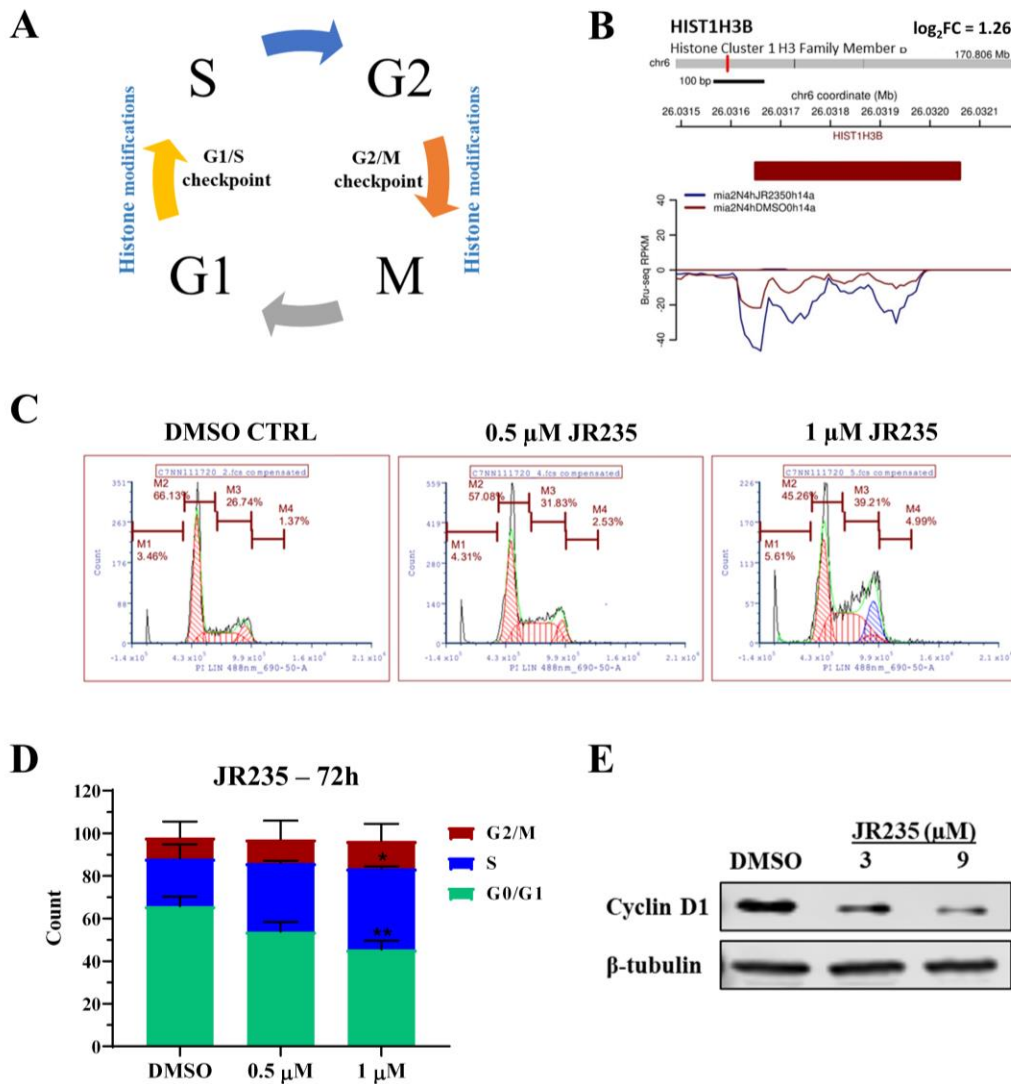
Figure II-6. **JR235** causes cell cycle arrest. (A) Schematic diagram showing cell cycle phases. (B) Trace diagram from Bru-seq showing the upregulation of HIST1H3B upon treatment with **JR235** (blue) compared to DMSO control (red). (C) **JR235** results in a dose-dependent arrest in S phase. Flow cytometric analysis was performed in MIA PaCa-2 cells after a 72 h-treatment with **JR235** at the indicated concentrations. (D) Quantification of different cell cycle phases after 72 h treatment with **JR235**. The data are an average of three biological replicates with the standard deviation represented as error bars. (E) **JR235** results in a decrease in Cyclin D1 levels. Immunoblotting was used to detect the protein levels in MIA PaCa-2 cells after 24 h treatment. Western blot result is from a single experiment.

JR235 binds to sigma-2 receptor with nanomolar affinity

Our bioinformatics analysis identified GPCR signaling as a mechanistic signature of our compounds. In an attempt to identify potential targets, we screened **JR235** and **JR272** in a panel of 50 GPCR radioligand binding assays through the National Institute of Mental Health Psychoactive Drug Screening Program (NIMH PDSP). Importantly, **JR235** displayed the highest affinity to S2R (K_i = 8 nM) while **JR272** displayed lower S2R affinity (K_i = 480 nM) (Figure II-7A/B, Appendix Figure II-7). **JR272** also binds to serotonin receptors 5HT3 (K_i = 164 nM) and 5HT2B (K_i = 332 nM). These results suggest that the structural fragment specific to **JR235** drives the binding and selectivity to S2R. Selectivity to S2R over S1R is a fundamental consideration in the design of S2Ls. While **JR235** displayed nanomolar affinity to S2R, it did not bind to S1R (K_i > 10 µM) (Figure II-7A). S2R is a protein that plays a regulatory role in cholesterol homeostasis and is implicated in cancer.[21-23] The identification of S2R as a potential target of our compounds further validates the interpretation of **JR235** and **JR272** transcriptomics/proteomics.

Haloperidol is an FDA-approved antipsychotic and a nonselective sigma ligand that is used as a positive control in the binding assay of S2R. **JR235** demonstrated superior selectivity to S2R compared to haloperidol (Figure II-7A, Appendix Figure I-1). Simultaneous treatment of MIA PaCa-2 cells with **JR235** and haloperidol in the CFA was synergistic at high concentrations (Appendix Figure II-8A). Interestingly however, pretreating the cells with haloperidol for 24 h followed by **JR235** resulted in antagonism and rescue of cell death suggesting they compete for the same target (Appendix Figure II-8B). However, these experiments must be repeated to confirm their significance in MIA PaCa-2 cells. It is also worth expanding these observations to other cancer cell lines with various S2R expression.

Transcriptomic profile of the independent analog JR274 poorly correlates to JR235

To better elucidate the importance of S2R/TMEM97 inhibition, we designed an independent analog, **JR274** that showed no binding to the S2R ($K_i > 10\ \mu M$) (Appendix Figure II-9A/B). Interestingly, the cytotoxicity of **JR274** was comparable to **JR235** suggesting there are differences in their mechanism of action. To further investigate this finding, we performed Bru-seq of **JR274** in MIA PaCa-2 cells and compared its transcriptomic profile to **JR235**. A poor correlation ($r = 0.354$) was found between the two treatments (Appendix Figure II-9C). Moreover, no genes were in common between the **JR235**, **JR272** and **JR274** top 25 deregulated genes suggesting that loss of binding results in gene signature variations (Appendix Figure II-9D) (Appendix Tables II-19/20). These results provide additional support to the contribution of S2R to the mechanism of action of our compounds.

JR235 engages cellular sigma-2 receptor

To determine whether our compound binds to S2R/TMEM97 in the cells, we tested **JR235** in the cellular thermal shift assay (CETSA). CETSA is used to test the thermal stability of the protein in presence of a ligand.[85] Treatment of MIA PaCa-2 cell lysate with **JR235** for 1 h resulted in TMEM97 stabilization demonstrated by a positive shift in the melting curve ($+ 3.5\ ^{\circ}C$) compared to the DMSO control (Figure II-7C). These results provide evidence to cellular binding and confirms S2R as the target.

JR5-151 localizes in the endoplasmic reticulum

S2R is an ER transmembrane protein therefore we sought to investigate colocalization using a BODIPY-conjugated derivative (**JR5-151**) of the analog, **JR272**. Immunofluorescence microscopy suggests **JR5-151** colocalizes with protein disulfide isomerase (PDI), a known ER resident protein (Figure II-7D), further supporting target engagement.
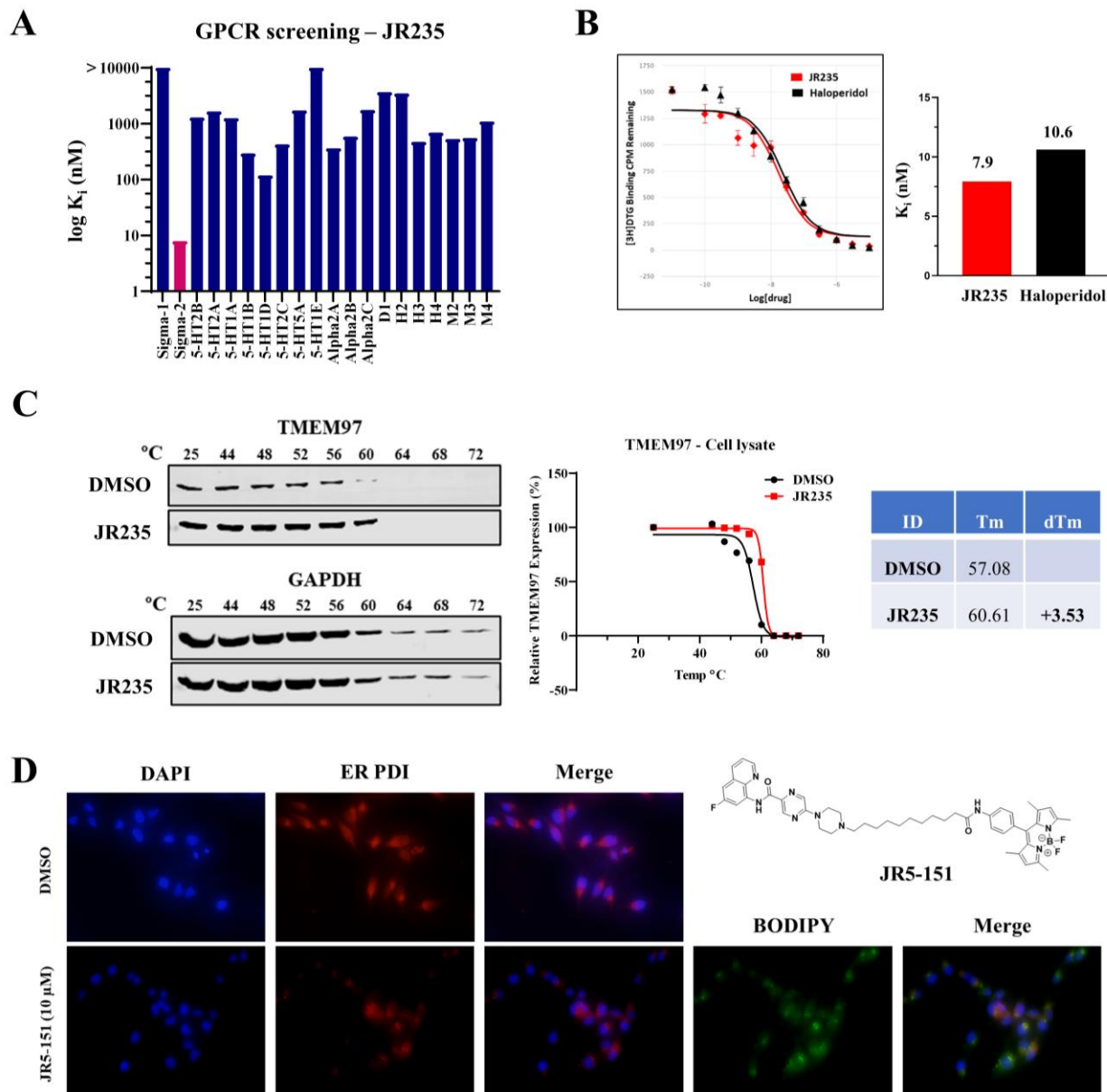
Figure II-7. **JR235** engages S2R *in vitro* and in cell lysates. (A) **JR235** shows the highest affinity to S2R among a panel of membrane proteins tested in a radioligand binding assay. (B) Dose-response curves for **JR235** binding to the S2R in the radioligand binding assay compared to haloperidol. (C) **JR235** stabilizes TMEM97 in MIA PaCa-2 cells. The cell lysate was treated with **JR235** (100 µM) for 1h and immunoblotting was used to detect TMEM97 protein levels. The result is from a single experiment. (D) BODIPY-labeled compound localizes in the endoplasmic reticulum. Immunofluorescence microscopy shows colocalization of **JR235** with PDI. MIA PaCa-2 cells were imaged after a 24h-treatment with 10 µM of **JR235**. Data presented is from a single experiment.

Cytotoxicity of JR235 is partially dependent on sigma-2 receptor

To examine the contribution of S2R to the cytotoxicity of our compounds, we performed

siRNA knockdown of TMEM97 and tested **JR235** and **JR272** in MTT. A significant reduction in

the cytotoxicity was demonstrated with **JR235** but not **JR272** (Figure II-8). It is worth noting that

JR235 is a highly selective ligand of S2R with K_i value of 8 nM while **JR272** has a binding affinity > 400 nM and non-selective binding to other receptors. The high affinity and selectivity of **JR235** possibly contributes to its dependence on S2R that is not demonstrated by **JR272**. Overall, these results suggest the involvement of S2R as well as other targets in the cytotoxicity of our compounds.
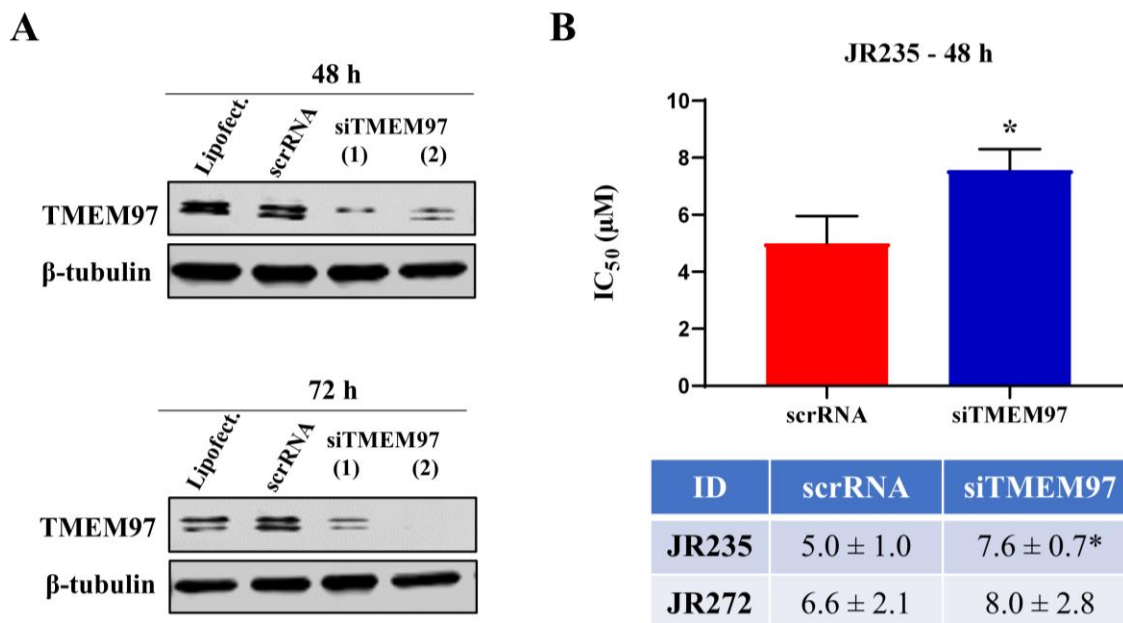
Figure II-8. **JR235** cytotoxicity is partially dependent on S2R/TMEM97. (A) TMEM97 knockdown in MIA PaCa-2 cells after 48 and 72 h transfection with the siRNAs: siTMEM97 (1) and siTMEM97 (2). (B) IC_{50} of **JR235** is significantly reduced with TMEM97 knockdown compared to the control scrambled siRNA. **JR272** shows no significant difference. Data were generated from three biological replicates and are presented as mean $\pm$ SD. * denotes $p < 0.05$.

JR235 and JR272 are synergistic with cholesterol and lipid synthesis inhibitors

In an attempt to identify drug synergy, we tested **JR235** and **JR272** in combination with HMGCR inhibitors (simvastatin; lovastatin) and SCD inhibitors (**MK-8245**; **A939572**). Remarkably, we observed synergy with all combinations (Figure II-9). The synergistic effect was more profound with the SCD1 inhibitor **A939572** which encouraged us to test the combination in a different cell line to validate its therapeutic potential in pancreatic cancer. Similar results were observed in Pan02 cells (Figure II-10). These promising results introduce novel potential

anticancer combination therapies that are effective in pancreatic cancer cells and is worth testing *in vivo*.
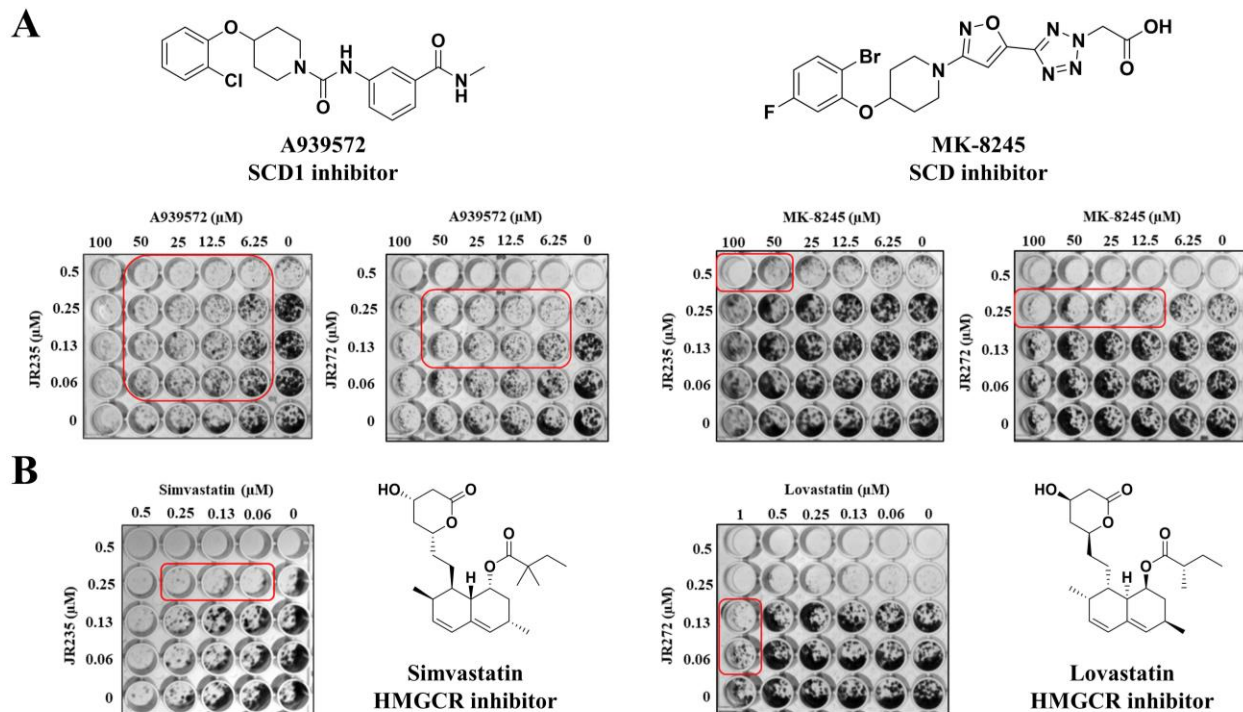
Figure II-9. **JR235** and **JR272** are synergistic with the FDA-approved cholesterol and lipid synthesis inhibitors in MIA PaCa-2 cells. (A) **JR235** and **JR272** are synergistic with the lipid synthesis inhibitor, **A939572**. (B) **JR235** and **JR272** are synergistic with simvastatin and lovastatin, respectively. MIA PaCa-2 cells were treated continuously with the compounds for 7 days. Data presented are from a single experiment.
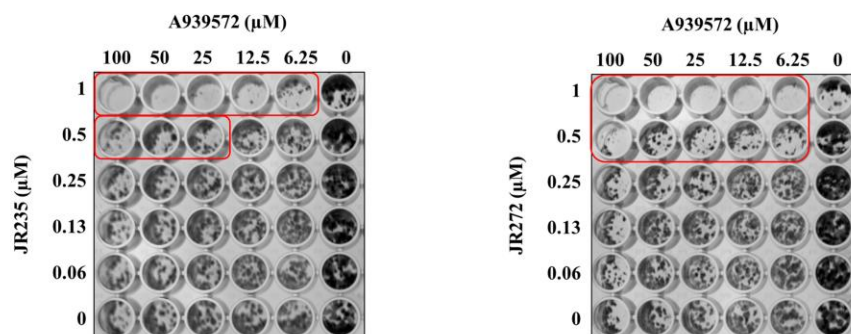
Figure II-10. **JR235** and **JR272** are synergistic with the SCD1 inhibitor **A939572** in Pan02 cells. Cells were treated continuously for 6 days. Data presented are from a single experiment.

Conclusions

SAR studies identified the lead compound **JR235** with a low micro-molar IC$_{50}$ value in MIA PaCa-2 cells. **JR235**'s cellular effects involve ROS, autophagy and cell cycle arrest. **JR235**

alters the cholesterol homeostasis demonstrated by an upregulation in the cholesterol metabolism genes and proteins and lipid droplet accumulation in the cells. **JR235** binds to the cholesterol regulatory protein, S2R with high affinity and selectivity and engages the cellular protein. S2R is implicated in cancer and its ligands have shown promising *in vivo* efficacy in pancreatic cancer. We showed that the cytotoxicity of **JR235** is only partially dependent on S2R suggesting the involvement of other targets. Further optimization is required to improve the S2R selectivity of the compound and eliminate nonspecific binding. Our study is the first to include in-depth bioinformatics analysis to investigate the mechanistic signature of S2Ls and demonstrate their role in cholesterol metabolism.

Experimental Section

Cell culture. The MIA PaCa-2 cell line was cultured in RPMI-1640 (ThermoFisher Scientific). U87, MDA-MB-231 and UM-UC-3 were maintained in DMEM (ThermoFisher Scientific) while WM115 was maintained in DMEM/F-12 (ThermoFisher Scientific) supplemented with 1% sodium pyruvate, 1% pen-strep and 1:5000 plasmocin. Other cell lines were cultured in RPMI-1640. All media were supplemented with 10% fetal bovine serum (Atlanta). The cells were grown as monolayer cultures at 37 ℃ in a humidified atmosphere of 5% CO_2 and tested for *Mycoplasma* contamination with the *Mycoplasma* detection kit, PlasmaTest (InvivoGen).

Cell survival assays. For the MTT assay, the experiment was carried out in a 96-well plate where cells (3000-7000 cells/well) were seeded and incubated overnight. The compounds or the vehicle (DMSO) were added to the cells the following day and incubated for 3 days. MTT solution (0.3 mg/ml) was added to the wells and plates were incubated for 3h at 37 ℃ after which MTT was discarded and cells were dissolved in DMSO. The absorbance of the formazan crystals was read by a microplate reader (Molecular Devices) at 570 nm and the data were analyzed using GraphPad

Prism 8 software. For the colony formation assay, cells (200-500 cells/well) were seeded in 96-well plates overnight and then treated with DMSO or the compound for 7-12 days until 80% confluency. After colonies were formed, the medium was removed and the cells were stained with 0.05% crystal violet, washed with water and imaged with iBRIGHT imaging system. The colonies were quantified using ImageJ. For combination studies, same procedures were followed, and compounds were added simultaneously unless otherwise noted.

Sigma receptor binding studies. Screening for a panel of GPCR receptors was performed through the NIMH PDSP. Briefly, sigma 2 receptors were obtained from rat PC12 cells and the binding affinity (K_i) was determined through competition binding assays using the radioligand [^{3}H]-DTG in the presence of (+)-pentazocine to block the S1R binding sites. K_i values are calculated from best-fit IC_{50} determinations and are the average of runs performed in triplicate. The assay protocol booklet can be accessed free of charge at: https://pdspdb.unc.edu/html/tutorials/UNC-CH%20Protocol%20Book.pdf.

Western blot analysis. MIA PaCa-2 cells were seeded (200,000 cells/well) in 6-well plates. Following treatment, cells were lysed at 4 ℃ *via* sonication with lysis buffer (25 mM tris(hydroxymethyl)aminomethane, 150 mM NaCl, 17 mM Triton X-100, 3.5 mM SDS, pH 7.4) supplemented with protease inhibitor and phosphatase inhibitor. The lysates were then spun at 12,000 rpm at 4 ℃ for 10 min and aliquots were collected for determining the protein concentration with the BCA assay (ThermoFischer Scientific). Samples were then prepared and loaded onto acrylamide (BioRad) gels followed by the transfer of the proteins onto PVDF membranes (EMD Millipore). The membranes were blocked for 1 h before incubation with the primary antibodies using StartingBlock blocking buffer (ThermoFischer Scientific). Membranes were then probed for LC3B (Cell Signaling, 1:1000), GAPDH (Cell Signaling, 1:4000), TMEM97 (NOVUS, 2 µg/ml),

Cyclin D1 (Cell Signaling, 1:1000), β-tubulin (Cell Signaling, 1:1000), or HMOX1 (Cell Signaling, 1:1000). Following overnight incubation with the primary antibodies at 4 ℃, the membranes were incubated with the secondary antibodies (anti-rabbit, Cell Signaling, 1:7500) for 1 h and imaged with the Odyssey imaging system (LI-COR Biosciences).

Cellular thermal shift assay. MIA PaCa-2 cells were collected and lysed in phosphate buffer (PBS pH 7.4, 300 mM NaCl, 0.2% NP-40) using freeze-thaw cycles with liquid nitrogen as described.[86] Lysates were centrifuged at 13,000 rpm for 10 min at 4 °C. Cleared lysate was incubated with 100 µM of **JR235** or DMSO for 1 h at room temperature. Each sample was then split into different tubes and treated with a gradient of temperatures between 44 and 72 °C at 4 °C intervals for 3 min. Samples were then transferred into Eppendorf tubes and spun down at 13,000 rpm for 20 min at 4 °C. Aliquots were collected and samples were prepared and loaded as previously described for Western blotting.

Nile red staining of lipid droplets. Nile red was prepared as 1 mg/ml in acetone. MIA PaCa-2 cells were seeded in chamber slides overnight. Next day, **JR235** (2 and 6 µM), simvastatin (6 µM), or DMSO were added to the cells. After 24 h, the cells were fixed in 4% formaldehyde and stained with Nile red (1 µg/ml) for 20 min then washed with PBS. ProLong Diamond with DAPI (Invitrogen) was used to prepare the slides for imaging using Olympus IX83 microscope using a 20x objective.

Protein identification and relative quantitation by TMT labeling and LC-Tandem MS. MIA PaCa-2 cells were treated with DMSO (control) or **JR235** (3 µM) for 24 h then collected and lysed in RIPA buffer (Pierce, #89900) at 4 ℃. The control and **JR235** treatments were carried out in duplicate. Protein samples were then collected, and the concentrations were determined using the

BCA assay (ThermoFisher Scientific). Samples (75 µg) were subjected to mass spectrometry at the Proteomics Core in the Department of Pathology at University of Michigan. Tandem mass tag (TMT) labeling was performed using the TMT 10plex™ isobaric labeling kit (ThermoFisher Scientific, #90110) according to the manufacturer's protocol with minor modifications. This involves reduction of the samples with DTT (1 h, 55 ℃) followed by alkylation with 2-chloroacetamide (30 min, RT). Proteins were precipitated using cold acetone overnight. Next, the proteins were pelleted and resuspended in TEAB to which trypsin (Promega, V5113) was added for digestion (overnight, 37 ℃). TMT reagents were reconstituted in anhydrous acetonitrile and the digested peptides were transferred to TMT reagent vials and incubated at RT for 1 h. The reaction was quenched with 5% hydroxylamine for 15 min then samples were combined and dried. Prior to MS analysis, two-dimensional separation of the sample was performed. For the first dimension, an offline fractionation of an aliquot of each sample into 10 fractions was performed following the manufacturer's protocol (Pierce, #84868). Fractions were then dried and reconstituted in loading buffer (0.1% formic acid and 2% acetonitrile). For quantitation, the MultiNotch-MS3 method was employed[87]. MS was performed on the Orbitrap Fusion Tribrid with ETD (Thermofisher) equipped with nano-LC system (Dionex RSLC-nano). Proteome discoverer (v2.1, ThermoFisher) was used for data analysis. MS2 spectra were searched against SwissProt human protein database. The abundance ratio data sets were transformed to $\log_2$FC values and the whole protein list was used for gene set enrichment analysis (GSEA v4.0.3).[88, 89]

Bromouridine labeled RNA sequencing. Nascent RNA-sequencing was performed as previously described.[90] Briefly, MIA PaCa-2 cells were treated with 5 µM of **JR235**, **JR272** or **JR274** for 4 h. Following treatment, bromouridine was added to the media to label the newly synthesized RNA during the last 30 min of treatment. Cell were then collected in TRIZOL and the total RNA was

collected from each sample. The bromouridine-labeled RNA was immunocaptured from total RNA, converted into cDNA libraries and deep sequenced at the University of Michigan sequencing core. Sequencing reads were mapped to the hg19 reference genome. Preranked gene lists were generated for each treatment through ranking of genes by their fold change in RNA synthesis levels compared to the DMSO control, and analyzed using GSEA (Broad Institute, MA).[88] The data were obtained from one experiment without biological replicates.

Cell cycle analysis. MIA PaCa-2 cells were treated with **JR235** or DMSO for 72 h then the cells were washed with cold PBS and fixed in 70% ethanol for 1 h at -20 °C. Next, the cells were spun down for 5 min at 4 °C, washed with PBS and resuspended in cold propidium iodide (PI) solution (40 mg/ml PI and 100 mg/ml RNAse in PBS) for 30 min in the dark at room temperature. Cells were analyzed for DNA content at the University of Michigan Flow Cytometry Core. The percentage of cells in different phases of the cell cycle was determined by flow cytometry (BD Bioscience).

Immunofluorescence microscopy. MIA PaCa-2 cells were seeded into chamber slides and incubated overnight. Next day, the cells were treated with the BODIPY-labeled compound **JR5-151** (10 µM) or DMSO (control) for 24h. The media was removed, and the cells were washed with DPBS. The cells were fixed with 4% formaldehyde (Electron Microscopy Sciences) for 40 min at 37 ºC then permeabilized with 0.1% Triton X-100 (Sigma-Aldrich) for 15 min at room temperature. Blocking proceeded using 5% FBS and 0.1% Tween 20 in DPBS for 1h. After blocking, antiPDI primary antibody (Cell Signaling) prepared in dilution buffer (0.1 g BSA, 30 µl Triton X-100, 10 ml DPBS) with ratio 1:200 was added and the cells were incubated overnight at 4 ºC. Next day, the cells were incubated with anti-rabbit secondary antibody (Alexa Fluor 594, Invitrogen) prepared in the dilution buffer for 1h at room temperature. ProLong Diamond with

DAPI (Invitrogen) was used to prepare the slides for imaging using Olympus IX83 microscope using a 20x objective.

siRNA knockdown studies. TMEM97 siRNA (hs.Ri.TMEM97.13.3, hs.Ri.TMEM97.13.4, Integrated DNA Technologies) or scrambled negative control siRNA (#51-01-19-09, Integrated DNA Technologies) with Lipofectamine iMAX transfection reagent (ThermoFisher Scientific) was added to MIA PaCa-2 cells in Opti-MEM medium (ThermoFisher Scientific) for 48 or 72 h after which the cells were harvested for immunoblotting. The siRNA transfection reagent complex was prepared following the manufacturer's instructions. Briefly, 30 pmol of siRNA in 150 µl of Opti-MEM medium were added to 9 µl of the lipofectamine reagent in 150 µl of Opti-MEM medium. After 5 min incubation at room temperature, the siRNA transfection complex was added to each well in a 6-well plate. For the MTT assay, 5 pmol of siRNA (hs.Ri.TMEM97.13.3) in 25 µl of Opti-MEM medium were added to 1.5 µl of the lipofectamine reagent in 25 µl of Opti-MEM medium. After 5 min incubation at room temperature, 10 µl of the siRNA transfection complex was added to each well in a 96-well plate. After 24 h transfection, **JR235** or **JR272** were added to the cells simultaneously with the siRNA transfection reagent complex for 48 h to determine their cytotoxicity.

Appendix

Hit Scaffold
QN523

JR121
MIA PaCa-2
$IC_{50}= 3.7 \pm 0.2 \ \mu M$
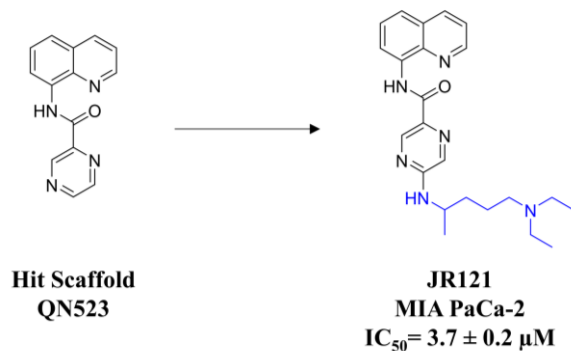
Appendix Figure II-1. Hit scaffold identified from the phenotypic screen and the **JR121** derivative.

JR236
2-methyl
$IC_{50} \ (\mu M)$: 9.9 ± 1.1

JR235
5-methyl
$IC_{50} \ (\mu M)$: 1.7 ± 0.7

JR235
6-methyl
$IC_{50} \ (\mu M)$: 1.3 ± 0.2

JR120
3-methyl
$IC_{50} \ (\mu M)$: 2.3 ± 1.2

JR240
7-methyl
$IC_{50} \ (\mu M)$: >30
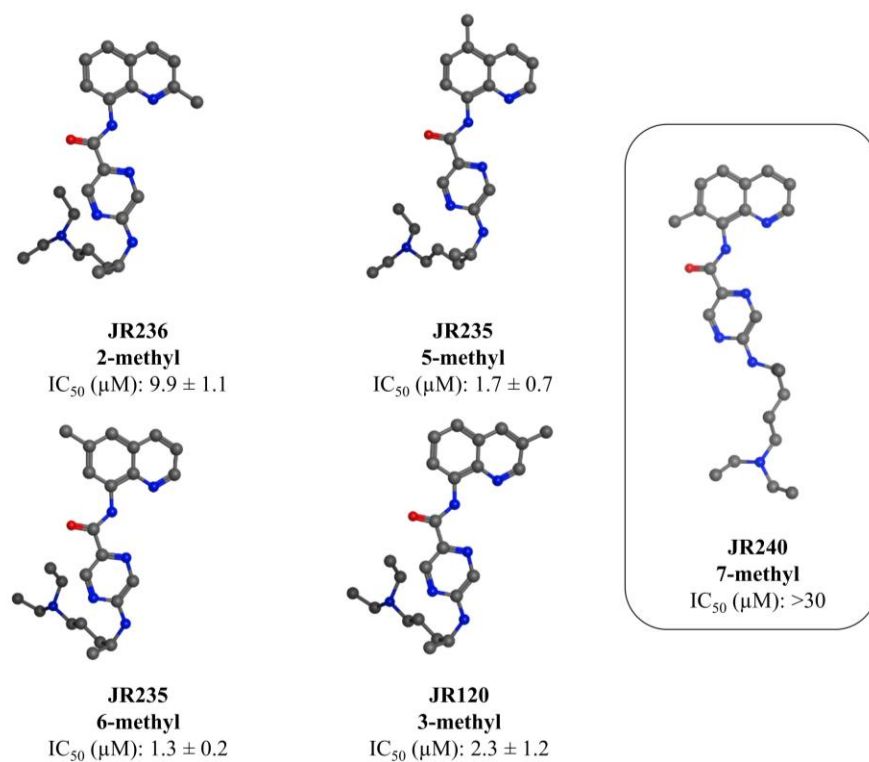
Appendix Figure II-2. Energy minimization for analogs with varying positions of quinoline methyl substitutions. Energy minimization and 3D protonation were conducted using MOE.[91]

82

MTT assay

ID	MIA PaCa-2	HFF-1
JR235	1.1, 1.3	4.8, 11.4
JR272	0.8, 0.9	9.7, 19.2
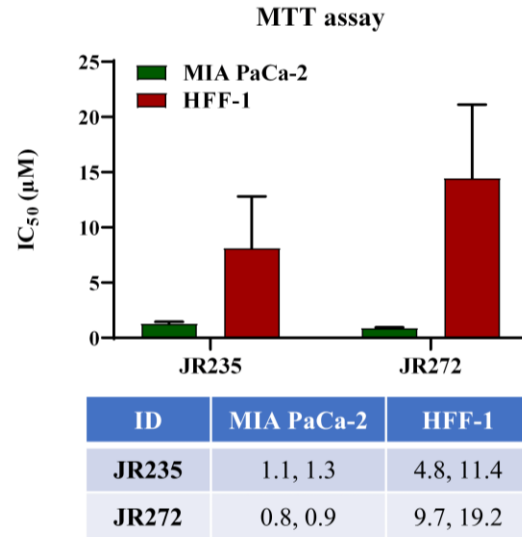
Appendix Figure II-3. **JR235** and **JR272** are less cytotoxic to normal tissue cells. MIA PaCa-2 or HFF-1 cells were treated with the compounds for 72 h in MTT assay. The values used for the bar graph are an average of two biological replicates with the standard deviation represented by error bars.
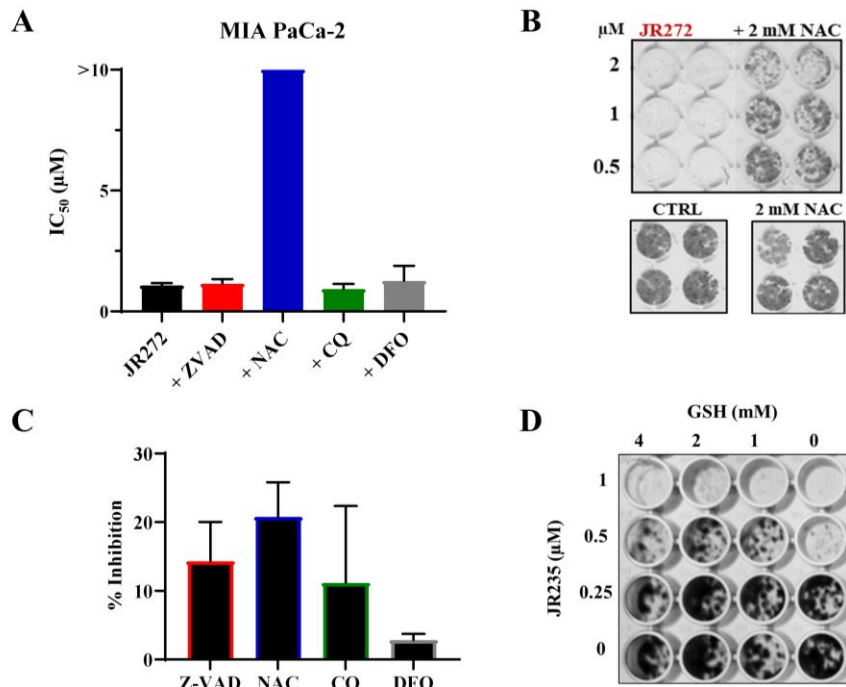
Appendix Figure II-4. Cytotoxicity of **JR235** and **JR272** is rescued by ROS inhibitors. (A) IC_{50} values for **JR272** when combined with cell death inhibitors. (B) Colony formation assay shows rescued **JR272**-induced cell death in presence of NAC. (C) Percent inhibition of different cell death inhibitors at the concentrations used in the combination studies in MTT assay: Z-VAD-FMK, 100 µM; NAC, 2 mM; CQ, 10 µM; DFO, 2 µM). MIA PaCa-2 cells were treated for 72h. (D) **JR235**-induced cell death is rescued in presence of glutathione in a colony formation assay after a 7-day treatment. Data presented in panels A and C were generated from three biological replicates and are presented as mean ± SD while data from panels B and D are from a single experiment.
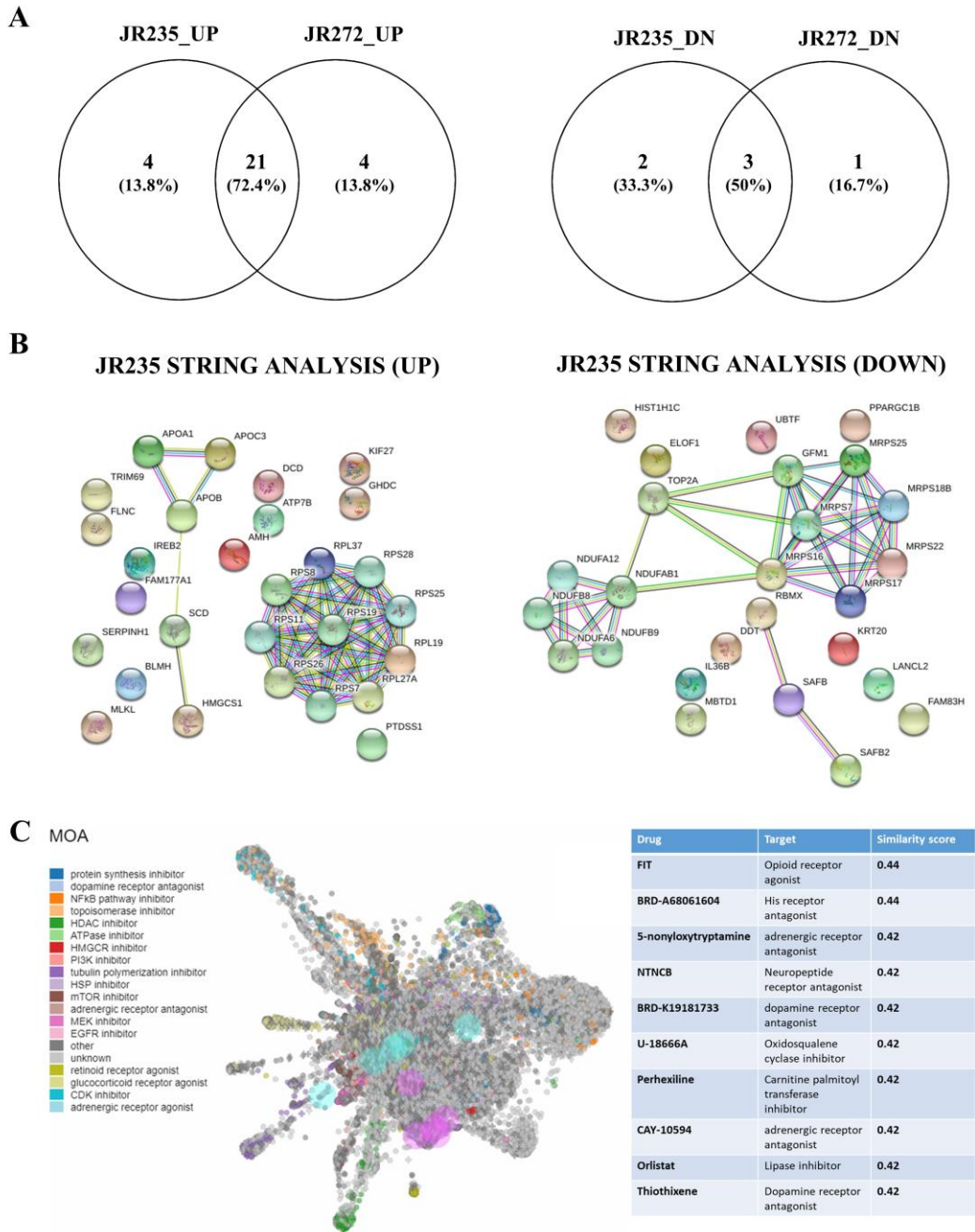
Appendix Figure II-5. **JR235** and **JR272** deregulate similar oncogenic pathways. (A) Venn diagram showing the deregulated Hallmark gene sets in common between **JR235** and **JR272**. Data were obtained from GSEA of the Bru-seq. (B) STRING analysis of **JR235** top 25 deregulated proteins from proteomics shows the upregulation of apolipoproteins and the downregulation of ubiquinone proteins. (C) Visualization of the drug-induced transcriptomic signatures similar to **JR235**. The top 25 up/down-regulated genes from Bru-seq were used to generate the firework display. The table includes the top 10 compounds with similar profiles.
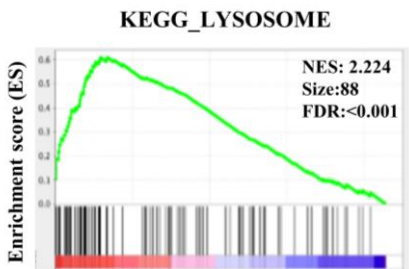
Appendix Figure II-6. Enrichment plot for the upregulated lysosome gene set from Bru-seq GSEA of **JR235** treated MIA PaCa-2 cells.
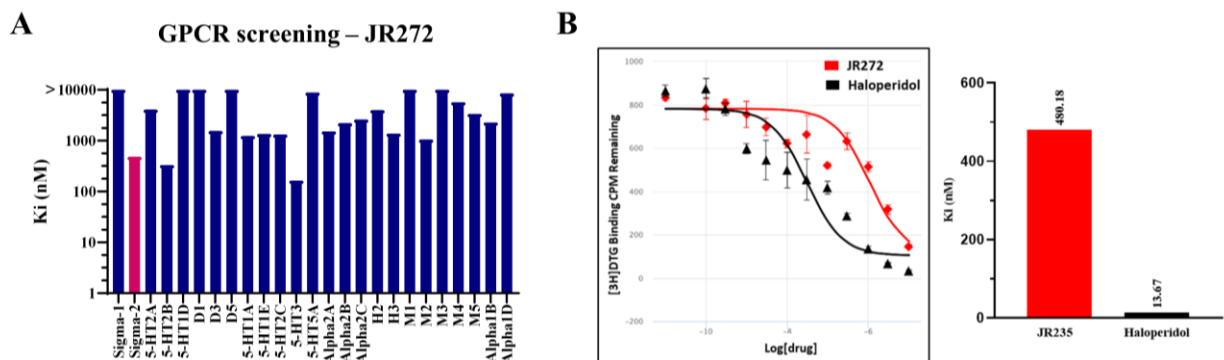
Appendix Figure II-7. **JR272** binds to S2R with lower affinity than haloperidol. (A) Binding affinity of **JR272** to a panel of GPCR/membrane proteins in the radiolabeling binding assay showing S2R one of the top three. (B) Dose-response binding curve for **JR272** with S2R compared to the positive control haloperidol.
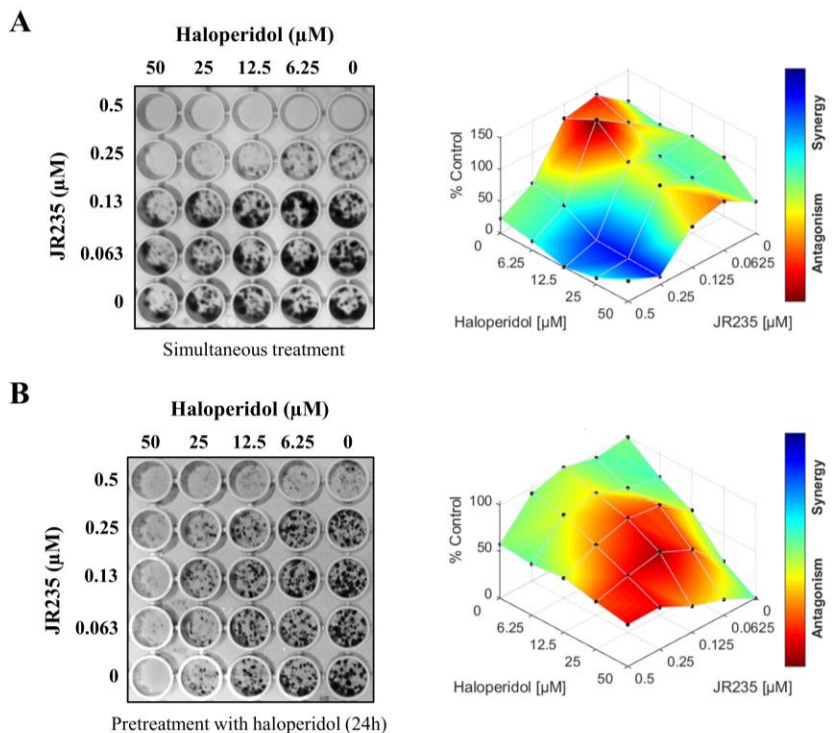
Appendix Figure II-8. **JR235** antagonizes haloperidol cytotoxicity in colony formation assay. (A) Simultaneous treatment of haloperidol and **JR235** shows synergy at high concentrations and antagonism at lower concentrations. (B) Pretreatment with haloperidol for 24h followed by **JR235** treatment results in antagonism. MIA PaCa-2 cells were treated with the compounds for 6-8 days. The results are from a single experiment. Synergy plots are generated using Combenefit software.[92]
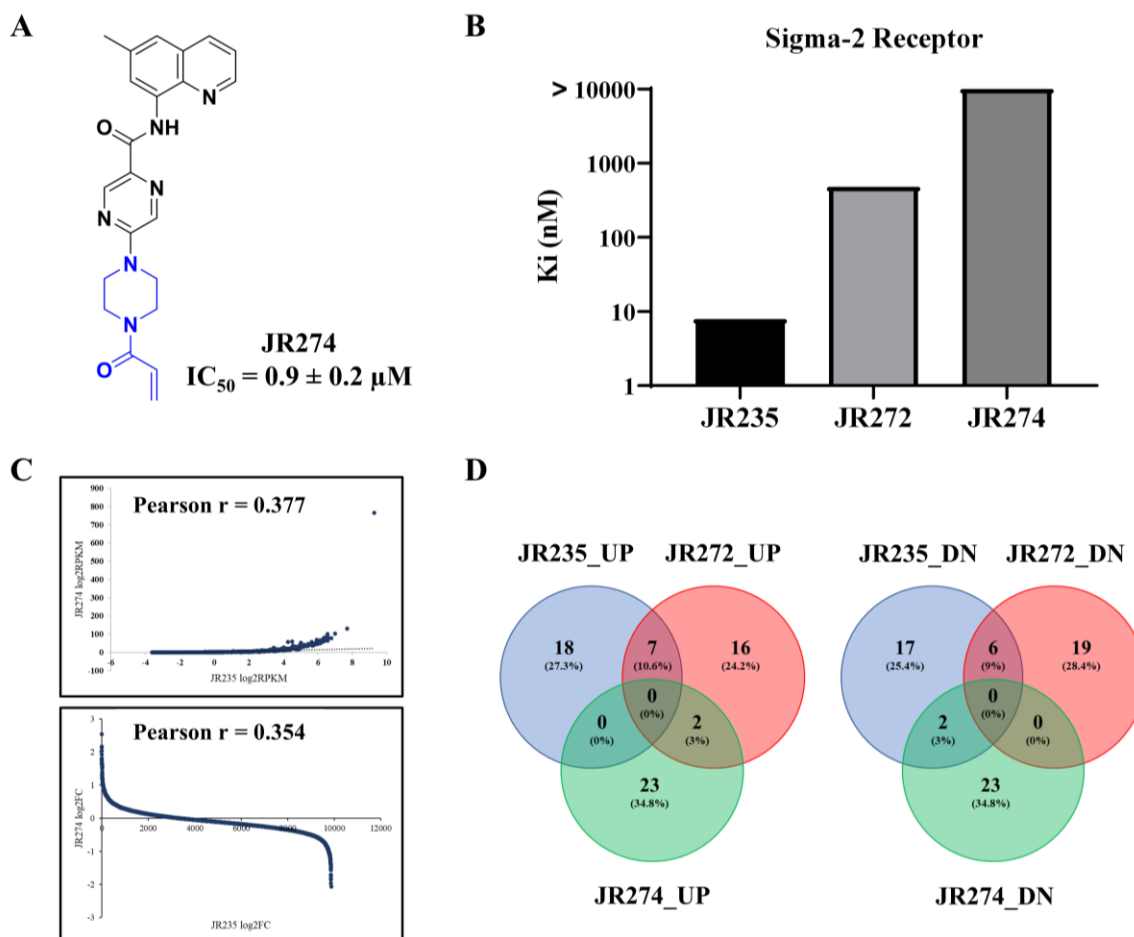
Appendix Figure II-9. The transcriptomic profile of the negative control **JR274** poorly correlates with **JR235**. (A) Chemical structure of **JR274** and its IC_{50} value from MTT assay in MIA PaCa-2 cells. (B) **JR274** does not bind to S2R as measured by the radioligand binding assay ($K_i > 10$ µM). (C) Pearson correlation between **JR235** and **JR274** deregulated genes. (D) Venn diagram showing no common genes between **JR235**, **JR272** and **JR274** treatments from Bru-seq in MIA PaCa-2 cells.
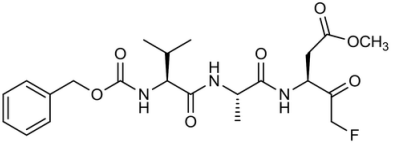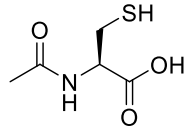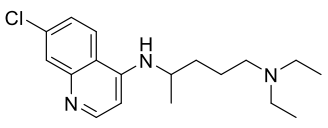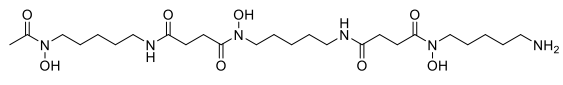
Appendix Table II-1. Cytotoxicity of JR compounds in a panel of cancer cell lines.

ID	JR235	JR272
MIA PaCa-2	1.3 ± 0.2	0.9 ± 0.1
PANC-1	8.4 ± 2.2	3.9 ± 0.5
BxPC-3	6.2; 8.1	3.9; 7.8
TFK-1	5.3; 5.8	4.8; 6.3
KYSE-70	5.2	4.2
KYSE-410	NT^a	14.8
HCT116	1.3 ± 0.5	1.2 ± 0.4
HUCCT1	1.6 ± 1.8	1.1 ± 1.3
SK-OV-3	17.1; 10.0	25.6 ± 1.3
OVCAR-8	10.4	8.2 ± 1.7
HEY	4.9	NT
UM-16	5.2	2.8

UM-UC-3	5.2	4.2
HL-60	2.4	3.0
WM115	3.8	4.4
U87	NT	25.2
MDA-MB-231	5.0; 8.4	5.6; 11.3

[a]Not tested.

Appendix Table II-2. Inhibitors of cell death mechanisms tested in combination with JR compounds.

Compound	Structure	Class	Mechanism of cell death
Z-VAD-FMK		Pan-caspase inhibitor	Apoptosis
N-acetyl cysteine		ROS scavenger	Reactive oxygen species
Chloroquine		Interference with lysosomal activity	Autophagy
Deferoxamine		Iron chelator	Ferroptosis

Appendix Table II-3. Top 25 upregulated Hallmark gene sets from the Bru-seq GSEA of **JR235** treated MIA PaCa-2 cells.

No	Gene set	NES	FDR q-val	Size
1	HALLMARK_CHOLESTEROL_HOMEOSTASIS	2.533	<0.001	51
2	HALLMARK_MTORC1_SIGNALING	2.450	<0.001	169
3	HALLMARK_HYPOXIA	2.235	<0.001	113
4	HALLMARK_UNFOLDED_PROTEIN_RESPONSE	2.173	<0.001	99
5	HALLMARK_P53_PATHWAY	2.171	<0.001	132
6	HALLMARK_FATTY_ACID_METABOLISM	2.054	<0.001	110
7	HALLMARK_TNFA_SIGNALING_VIA_NFKB	2.043	<0.001	120
8	HALLMARK_PI3K_AKT_MTOR_SIGNALING	2.033	<0.001	78
9	HALLMARK_MYOGENESIS	1.885	0.001	66
10	HALLMARK_ANDROGEN_RESPONSE	1.875	0.001	75
11	HALLMARK_APOPTOSIS	1.804	0.002	100
12	HALLMARK_ADIPOGENESIS	1.784	0.003	140
13	HALLMARK_UV_RESPONSE_UP	1.769	0.003	98
14	HALLMARK_ESTROGEN_RESPONSE_EARLY	1.719	0.005	106
15	HALLMARK_ESTROGEN_RESPONSE_LATE	1.631	0.013	99
16	HALLMARK_COAGULATION	1.624	0.014	39
17	HALLMARK_PEROXISOME	1.612	0.015	72
18	HALLMARK_GLYCOLYSIS	1.603	0.015	136
19	HALLMARK_OXIDATIVE_PHOSPHORYLATION	1.601	0.015	183
20	HALLMARK_IL2_STAT5_SIGNALING	1.597	0.015	102
21	HALLMARK_XENOBIOTIC_METABOLISM	1.503	0.033	102
22	HALLMARK_HEME_METABOLISM	1.480	0.039	128
23	HALLMARK_EPITHELIAL_MESENCHYMAL_TRANSITION	1.436	0.054	72

No	Gene set	NES	FDR q-val	Size
24	HALLMARK_DNA_REPAIR	1.422	0.059	120
25	HALLMARK_IL6_JAK_STAT3_SIGNALING	1.405	0.067	39

Appendix Table II-4. Top 25 upregulated KEGG gene sets from the Bru-seq GSEA of **JR235** treated MIA PaCa-2 cells.

No	Gene set	NES	FDR q-val	Size
1	KEGG_LYSOSOME	2.224	<0.001	88
2	KEGG_SYSTEMIC_LUPUS_ERYTHEMATOSUS	2.185	<0.001	40
3	KEGG_VIBRIO_CHOLERAE_INFECTION	1.841	0.030	39
4	KEGG_ADIPOCYTOKINE_SIGNALING_PATHWAY	1.770	0.059	43
5	KEGG_GLYCOLYSIS_GLUCONEOGENESIS	1.735	0.071	30
6	KEGG_PPAR_SIGNALING_PATHWAY	1.733	0.061	30
7	KEGG_MELANOGENESIS	1.713	0.067	42
8	KEGG_OXIDATIVE_PHOSPHORYLATION	1.705	0.064	89
9	KEGG_ACUTE_MYELOID_LEUKEMIA	1.701	0.058	43
10	KEGG_CITRATE_CYCLE_TCA_CYCLE	1.683	0.065	28
11	KEGG_INSULIN_SIGNALING_PATHWAY	1.663	0.073	93
12	KEGG_PORPHYRIN_AND_CHLOROPHYLL_ METABOLISM	1.657	0.073	20
13	KEGG_SNARE_INTERACTIONS_IN_VESICULAR_ TRANSPORT	1.642	0.079	32
14	KEGG_GLYCEROLIPID_METABOLISM	1.640	0.074	23
15	KEGG_MTOR_SIGNALING_PATHWAY	1.631	0.076	34
16	KEGG_PROSTATE_CANCER	1.564	0.132	64
17	KEGG_ENDOMETRIAL_CANCER	1.543	0.149	39
18	KEGG_VALINE_LEUCINE_AND_ISOLEUCINE_ DEGRADATION	1.536	0.148	36
19	KEGG_PARKINSONS_DISEASE	1.536	0.141	83
20	KEGG_FRUCTOSE_AND_MANNOSE_METABOLISM	1.529	0.141	21
21	KEGG_PYRUVATE_METABOLISM	1.529	0.135	25
22	KEGG_ANTIGEN_PROCESSING_AND_PRESENTATION	1.506	0.154	24
23	KEGG_FATTY_ACID_METABOLISM	1.505	0.149	28
24	KEGG_MAPK_SIGNALING_PATHWAY	1.504	0.143	129
25	KEGG_ALDOSTERONE_REGULATED_SODIUM_ REABSORPTION	1.480	0.165	18

Appendix Table II-5. Top 25 upregulated GO gene sets from the Bru-seq GSEA of **JR235** treated MIA PaCa-2 cells.

No	Gene set	NES	FDR q-val	Size
1	GO_STEROL_BIOSYNTHETIC_PROCESS	2.656	<0.001	30
2	GO_STEROID_BIOSYNTHETIC_PROCESS	2.632	<0.001	50
3	GO_STEROL_METABOLIC_PROCESS	2.604	<0.001	64
4	GO_ALCOHOL_BIOSYNTHETIC_PROCESS	2.531	<0.001	63
5	GO_STEROID_METABOLIC_PROCESS	2.432	<0.001	92
6	GO_DNA_PACKAGING_COMPLEX	2.422	<0.001	47
7	GO_ORGANIC_HYDROXY_COMPOUND_BIOSYNTHETIC_P ROCESS	2.372	<0.001	80
8	GO_RESPONSE_TO_TOPOLOGICALLY_INCORRECT_PROT EIN	2.337	<0.001	117
9	GO_CELLULAR_RESPONSE_TO_TOPOLOGICALLY_INCOR RECT_PROTEIN	2.333	<0.001	92
10	GO_IRE1_MEDIATED_UNFOLDED_PROTEIN_RESPONSE	2.300	<0.001	49
11	GO_PROTEIN_DNA_COMPLEX	2.288	<0.001	97
12	GO_SMALL_MOLECULE_BIOSYNTHETIC_PROCESS	2.227	<0.001	220
13	GO_NUCLEAR_NUCLEOSOME	2.218	<0.001	17
14	GO_CHROMATIN_ASSEMBLY_OR_DISASSEMBLY	2.165	<0.001	111

No	Gene set	NES	FDR q-val	Size
15	GO_DNA_PACKAGING	2.161	<0.001	120
16	GO_ER_NUCLEUS_SIGNALING_PATHWAY	2.156	<0.001	28
17	GO_REGULATION_OF_ENDOPLASMIC_RETICULUM_STRESS_INDUCED_INTRINSIC_APOPTOTIC_SIGNALING_PATHWAY	2.132	0.001	21
18	GO_ALCOHOL_METABOLIC_PROCESS	2.127	0.001	172
19	GO_ISOPRENOID_BIOSYNTHETIC_PROCESS	2.093	0.001	17
20	GO_CELLULAR_LIPID_CATABOLIC_PROCESS	2.080	0.001	81
21	GO_INTRINSIC_COMPONENT_OF_ENDOPLASMIC_RETICULUM_MEMBRANE	2.075	0.002	77
22	GO_RESPONSE_TO_ENDOPLASMIC_RETICULUM_STRESS	2.067	0.002	171
23	GO_LYSOSOMAL_LUMEN	2.060	0.002	43
24	GO_FATTY_ACID_BIOSYNTHETIC_PROCESS	2.043	0.003	45
25	GO_PROTEIN_DNA_COMPLEX_SUBUNIT_ORGANIZATION	2.041	0.003	157

Appendix Table II-6. Top 25 upregulated C2 gene sets from the Bru-seq GSEA of **JR235** treated MIA PaCa-2 cells.

No	Gene set	NES	FDR q-val	Size
1	PODAR_RESPONSE_TO_ADAPHOSTIN_UP	2.520	<0.001	100
2	LEONARD_HYPOXIA	2.480	<0.001	33
3	REACTOME_CHOLESTEROL_BIOSYNTHESIS	2.477	<0.001	19
4	SCHMIDT_POR_TARGETS_IN_LIMB_BUD_UP	2.469	<0.001	19
5	ENK_UV_RESPONSE_KERATINOCYTE_UP	2.464	<0.001	318
6	HORTON_SREBF_TARGETS	2.446	<0.001	19
7	DIRMEIER_LMP1_RESPONSE_EARLY	2.410	<0.001	37
8	HELLER_SILENCED_BY_METHYLATION_DN	2.396	<0.001	50
9	CUI_GLUCOSE_DEPRIVATION	2.383	<0.001	39
10	WILCOX_RESPONSE_TO_PROGESTERONE_UP	2.380	<0.001	104
11	REACTOME_RNA_POL_I_PROMOTER_OPENING	2.377	<0.001	26
12	CHANG_CORE_SERUM_RESPONSE_DN	2.370	<0.001	134
13	ZHANG_TLX_TARGETS_UP	2.353	<0.001	49
14	ZHANG_TLX_TARGETS_36HR_UP	2.339	<0.001	125
15	REACTOME_AMYLOIDS	2.309	<0.001	33
16	ADDYA_ERYTHROID_DIFFERENTIATION_BY_HEMIN	2.307	<0.001	45
17	DACOSTA_UV_RESPONSE_VIA_ERCC3_UP	2.301	<0.001	222
18	DAZARD_RESPONSE_TO_UV_NHEK_UP	2.291	<0.001	135
19	LE_EGR2_TARGETS_DN	2.287	<0.001	49
20	KAN_RESPONSE_TO_ARSENIC_TRIOXIDE	2.270	<0.001	63
21	QI_HYPOXIA	2.258	<0.001	84
22	BURTON_ADIPOGENESIS_10	2.254	<0.001	24
23	REACTOME_UNFOLDED_PROTEIN_RESPONSE	2.246	<0.001	66
24	GEORGANTAS_HSC_MARKERS	2.234	<0.001	32
25	AMIT_SERUM_RESPONSE_60_MCF10A	2.228	<0.001	34

Appendix Table II-7. Top 25 downregulated Hallmark gene sets from the Bru-seq GSEA of **JR235** treated MIA PaCa-2 cells.

No	Gene set	NES	FDR q-val	Size
1	HALLMARK_TGF_BETA_SIGNALING	-1.256	0.498	45
2	HALLMARK_KRAS_SIGNALING_DN	-0.992	1.000	32
3	HALLMARK_KRAS_SIGNALING_UP	-0.965	0.889	67
4	HALLMARK_MYC_TARGETS_V1	-0.831	1.000	192
5	HALLMARK_MYC_TARGETS_V2	-0.691	0.963	53

Appendix Table II-8. Downregulated KEGG gene sets from the Bru-seq GSEA of **JR235** treated MIA PaCa-2 cells.

No	Gene set	NES	FDR q-val	Size
1	KEGG_NEUROACTIVE_LIGAND_RECEPTOR_INTERACTION	-1.955	0.015	20
2	KEGG_TGF_BETA_SIGNALING_PATHWAY	-1.284	1.000	47
3	KEGG_PURINE_METABOLISM	-1.277	0.948	93
4	KEGG_CALCIUM_SIGNALING_PATHWAY	-1.264	0.756	51
5	KEGG_ABC_TRANSPORTERS	-1.220	0.762	18
6	KEGG_MISMATCH_REPAIR	-1.179	0.779	21
7	KEGG_PYRIMIDINE_METABOLISM	-1.109	0.924	75
8	KEGG_STARCH_AND_SUCROSE_METABOLISM	-1.006	1.000	17
9	KEGG_WNT_SIGNALING_PATHWAY	-0.992	1.000	82
10	KEGG_HEDGEHOG_SIGNALING_PATHWAY	-0.982	1.000	18
11	KEGG_DNA_REPLICATION	-0.912	1.000	34
12	KEGG_NUCLEOTIDE_EXCISION_REPAIR	-0.899	1.000	41
13	KEGG_AMYOTROPHIC_LATERAL_SCLEROSIS_ALS	-0.838	1.000	29
14	KEGG_AXON_GUIDANCE	-0.829	1.000	61
15	KEGG_HOMOLOGOUS_RECOMBINATION	-0.820	1.000	23
16	KEGG_CYTOSOLIC_DNA_SENSING_PATHWAY	-0.784	1.000	23
17	KEGG_PATHOGENIC_ESCHERICHIA_COLI_INFECTION	-0.782	1.000	36
18	KEGG_CELL_ADHESION_MOLECULES_CAMS	-0.738	1.000	20
19	KEGG_ALANINE_ASPARTATE_AND_GLUTAMATE_METABOLISM	-0.732	1.000	15
20	KEGG_RIG_I_LIKE_RECEPTOR_SIGNALING_PATHWAY	-0.724	1.000	36
21	KEGG_RNA_POLYMERASE	-0.669	1.000	23
22	KEGG_ECM_RECEPTOR_INTERACTION	-0.655	0.998	24
23	KEGG_ADHERENS_JUNCTION	-0.628	0.968	49

Appendix Table II-9. Downregulated GO gene sets from the Bru-seq GSEA of **JR235** treated MIA PaCa-2 cells.

No	Gene set	NES	FDR q-val	Size
1	GO_G_PROTEIN_COUPLED_RECEPTOR_ACTIVITY	-1.804	1.000	47
2	GO_NEGATIVE_REGULATION_OF_EPITHELIAL_CELL_DIFFERENTIATION	-1.799	0.948	17
3	GO_DENDRITIC_SHAFT	-1.746	1.000	20
4	GO_DNA_DEPENDENT_DNA_REPLICATION_MAINTENANCE_OF_FIDELITY	-1.697	1.000	18
5	GO_POTASSIUM_CHANNEL_COMPLEX	-1.693	0.962	22
6	GO_PHOSPHOLIPID_TRANSPORTER_ACTIVITY	-1.692	0.808	19
7	GO_HOMOPHILIC_CELL_ADHESION_VIA_PLASMA_MEMBRANE_ADHESION_MOLECULES	-1.691	0.702	15
8	GO_CELL_SURFACE_RECEPTOR_SIGNALING_PATHWAY_INVOLVED_IN_CELL_CELL_SIGNALING	-1.653	0.832	15
9	GO_RESPONSE_TO_X_RAY	-1.636	0.843	24
10	GO_BASAL_PART_OF_CELL	-1.629	0.796	21
11	GO_GLUTAMINE_METABOLIC_PROCESS	-1.616	0.801	15
12	GO_DNA_DOUBLE_STRAND_BREAK_PROCESSING	-1.613	0.750	16
13	GO_SOMITE_DEVELOPMENT	-1.594	0.796	33
14	GO_DNA_REPAIR_COMPLEX	-1.586	0.781	36
15	GO_REGULATION_OF_ACUTE_INFLAMMATORY_RESPONSE	-1.555	0.900	17
16	GO_RECOMBINATIONAL_REPAIR	-1.548	0.889	62
17	GO_MITOTIC_RECOMBINATION	-1.547	0.842	39
18	GO_DNA_DEPENDENT_ATPASE_ACTIVITY	-1.545	0.804	72
19	GO_DNA_HELICASE_ACTIVITY	-1.504	1.000	48
20	GO_CILIUM_ORGANIZATION	-1.502	0.964	110

No	Gene set	NES	FDR q-val	Size
21	GO_REGULATION_OF_MEMBRANE_LIPID_DISTRIBUTION	-1.498	0.937	16
22	GO_STRAND_DISPLACEMENT	-1.493	0.924	22
23	GO_RECIPROCAL_DNA_RECOMBINATION	-1.485	0.935	24
24	GO_SOMATIC_RECOMBINATION_OF_IMMUNOGLOBULIN_GENE_SEGMENTS	-1.483	0.906	18
25	GO_CYTOKINE_RECEPTOR_ACTIVITY	-1.467	0.962	19

Appendix Table II-10. Top 25 downregulated C2 gene sets from the Bru-seq GSEA of **JR235** treated MIA PaCa-2 cells.

No	Gene set	NES	FDR q-val	Size
1	DACOSTA_UV_RESPONSE_VIA_ERCC3_COMMON_DN	-2.348	0.001	418
2	ZHANG_TLX_TARGETS_36HR_DN	-2.309	0.001	173
3	HUTTMANN_B_CLL_POOR_SURVIVAL_DN	-2.076	0.026	30
4	HAMAI_APOPTOSIS_VIA_TRAIL_UP	-1.942	0.096	438
5	ZHANG_TLX_TARGETS_DN	-1.942	0.077	83
6	KEGG_NEUROACTIVE_LIGAND_RECEPTOR_INTERACTION	-1.898	0.109	20
7	ZHENG_FOXP3_TARGETS_IN_T_LYMPHOCYTE_DN	-1.893	0.097	19
8	DACOSTA_UV_RESPONSE_VIA_ERCC3_TTD_DN	-1.878	0.100	57
9	DAZARD_UV_RESPONSE_CLUSTER_G6	-1.855	0.111	118
10	BILD_CTNNB1_ONCOGENIC_SIGNATURE	-1.841	0.114	61
11	SENGUPTA_NASOPHARYNGEAL_CARCINOMA_WITH_LMP1_UP	-1.837	0.108	215
12	DOANE_BREAST_CANCER_CLASSES_DN	-1.830	0.105	23
13	REACTOME_ASSOCIATION_OF_TRIC_CCT_WITH_TARGET_PROTEINS_DURING_BIOSYNTHESIS	-1.804	0.125	23
14	SENGUPTA_NASOPHARYNGEAL_CARCINOMA_UP	-1.794	0.127	201
15	DACOSTA_UV_RESPONSE_VIA_ERCC3_XPCS_DN	-1.784	0.130	66
16	TCGA_GLIOBLASTOMA_COPY_NUMBER_DN	-1.738	0.181	23
17	MARTINEZ_RESPONSE_TO_TRABECTEDIN	-1.727	0.186	35
18	MILI_PSEUDOPODIA_HAPTOTAXIS_UP	-1.718	0.190	440
19	THUM_SYSTOLIC_HEART_FAILURE_DN	-1.673	0.260	150
20	HAN_JNK_SINGALING_DN	-1.665	0.265	15
21	LEE_TARGETS_OF_PTCH1_AND_SUFU_UP	-1.661	0.260	22
22	GUENTHER_GROWTH_SPHERICAL_VS_ADHERENT_DN	-1.656	0.258	20
23	GABRIELY_MIR21_TARGETS	-1.642	0.274	230
24	RAMALHO_STEMNESS_UP	-1.615	0.324	180
25	TURASHVILI_BREAST_LOBULAR_CARCINOMA_VS_DUCTAL_NORMAL_DN	-1.603	0.337	27

Appendix Table II-11. Top 25 upregulated Hallmark gene sets from the Bru-seq GSEA of **JR272** treated MIA PaCa-2 cells.

No	Gene set	NES	FDR q-val	Size
1	HALLMARK_CHOLESTEROL_HOMEOSTASIS	2.374	<0.001	50
2	HALLMARK_MYOGENESIS	2.098	<0.001	67
3	HALLMARK_P53_PATHWAY	1.986	<0.001	129
4	HALLMARK_HYPOXIA	1.984	<0.001	113
5	HALLMARK_MTORC1_SIGNALING	1.917	0.001	168
6	HALLMARK_UV_RESPONSE_UP	1.773	0.006	96
7	HALLMARK_UNFOLDED_PROTEIN_RESPONSE	1.739	0.009	96
8	HALLMARK_ADIPOGENESIS	1.653	0.023	141
9	HALLMARK_PI3K_AKT_MTOR_SIGNALING	1.634	0.025	78
10	HALLMARK_COAGULATION	1.628	0.024	40
11	HALLMARK_APOPTOSIS	1.615	0.025	101
12	HALLMARK_FATTY_ACID_METABOLISM	1.605	0.025	109

13	HALLMARK_OXIDATIVE_PHOSPHORYLATION	1.548	0.038	180
14	HALLMARK_HEME_METABOLISM	1.548	0.035	126
15	HALLMARK_WNT_BETA_CATENIN_SIGNALING	1.483	0.057	24
16	HALLMARK_PEROXISOME	1.483	0.054	72
17	HALLMARK_NOTCH_SIGNALING	1.473	0.055	22
18	HALLMARK_ESTROGEN_RESPONSE_EARLY	1.458	0.061	106
19	HALLMARK_APICAL_JUNCTION	1.422	0.076	90
20	HALLMARK_XENOBIOTIC_METABOLISM	1.415	0.077	101
21	HALLMARK_DNA_REPAIR	1.407	0.079	120
22	HALLMARK_ANDROGEN_RESPONSE	1.381	0.093	75
23	HALLMARK_GLYCOLYSIS	1.363	0.103	136
24	HALLMARK_ESTROGEN_RESPONSE_LATE	1.358	0.102	97
25	HALLMARK_BILE_ACID_METABOLISM	1.330	0.121	54

Appendix Table II-12. Top 25 upregulated KEGG gene sets from the Bru-seq GSEA of **JR272** treated MIA PaCa-2 cells.

No	Gene set	NES	FDR q-val	Size
1	KEGG_SYSTEMIC_LUPUS_ERYTHEMATOSUS	2.271	<0.001	39
2	KEGG_RIBOSOME	2.148	0.001	83
3	KEGG_LYSOSOME	1.958	0.008	87
4	KEGG_ACUTE_MYELOID_LEUKEMIA	1.872	0.022	43
5	KEGG_VEGF_SIGNALING_PATHWAY	1.705	0.114	37
6	KEGG_SNARE_INTERACTIONS_IN_VESICULAR_TRANSPORT	1.647	0.161	32
7	KEGG_PEROXISOME	1.643	0.145	57
8	KEGG_VIBRIO_CHOLERAE_INFECTION	1.626	0.149	39
9	KEGG_NON_SMALL_CELL_LUNG_CANCER	1.610	0.156	39
10	KEGG_PROGESTERONE_MEDIATED_OOCYTE_MATURATION	1.602	0.149	57
11	KEGG_PPAR_SIGNALING_PATHWAY	1.573	0.177	30
12	KEGG_GLYCOLYSIS_GLUCONEOGENESIS	1.563	0.174	31
13	KEGG_OXIDATIVE_PHOSPHORYLATION	1.544	0.189	90
14	KEGG_BIOSYNTHESIS_OF_UNSATURATED_FATTY_ACIDS	1.531	0.197	15
15	KEGG_PROSTATE_CANCER	1.527	0.188	65
16	KEGG_ADIPOCYTOKINE_SIGNALING_PATHWAY	1.493	0.229	41
17	KEGG_ENDOMETRIAL_CANCER	1.492	0.216	39
18	KEGG_LONG_TERM_DEPRESSION	1.491	0.205	29
19	KEGG_MTOR_SIGNALING_PATHWAY	1.469	0.229	34
20	KEGG_FC_EPSILON_RI_SIGNALING_PATHWAY	1.464	0.226	32
21	KEGG_PORPHYRIN_AND_CHLOROPHYLL_METABOLISM	1.448	0.240	20
22	KEGG_PARKINSONS_DISEASE	1.404	0.312	82
23	KEGG_INSULIN_SIGNALING_PATHWAY	1.403	0.301	93
24	KEGG_RENAL_CELL_CARCINOMA	1.392	0.307	47
25	KEGG_CARDIAC_MUSCLE_CONTRACTION	1.386	0.307	30

Appendix Table II-13. Top 25 upregulated GO gene sets from the Bru-seq GSEA of **JR272** treated MIA PaCa-2 cells.

No	Gene set	NES	FDR q-val	Size
1	GO_DNA_PACKAGING_COMPLEX	2.600	<0.001	46
2	GO_STEROL_METABOLIC_PROCESS	2.434	<0.001	64
3	GO_STEROL_BIOSYNTHETIC_PROCESS	2.428	<0.001	30
4	GO_PROTEIN_DNA_COMPLEX	2.251	0.001	95
5	GO_STEROID_BIOSYNTHETIC_PROCESS	2.176	0.002	49
6	GO_NEGATIVE_REGULATION_OF_RESPONSE_TO_OXIDATIVE_STRESS	2.162	0.003	18
7	GO_ALCOHOL_BIOSYNTHETIC_PROCESS	2.162	0.003	63

8	GO_STEROID_METABOLIC_PROCESS	2.100	0.007	91
9	GO_REGULATION_OF_STEROID_BIOSYNTHETIC_PROCESS	2.097	0.006	20
10	GO_NUCLEAR_NUCLEOSOME	2.088	0.006	17
11	GO_CYTOSOLIC_RIBOSOME	2.082	0.006	99
12	GO_CHROMATIN_SILENCING_AT_RDNA	2.078	0.006	19
13	GO_REGULATION_OF_STEROID_METABOLIC_PROCESS	2.031	0.013	31
14	GO_REGULATION_OF_ENDOPLASMIC_RETICULUM_STRESS_INDUCED_INTRINSIC_APOPTOTIC_SIGNALING_PATHWAY	2.024	0.014	21
15	GO_ALCOHOL_METABOLIC_PROCESS	2.022	0.013	173
16	GO_CELLULAR_RESPONSE_TO_TOPOLOGICALLY_INCORRECT_PROTEIN	2.013	0.015	91
17	GO_IRE1_MEDIATED_UNFOLDED_PROTEIN_RESPONSE	2.001	0.017	48
18	GO_INTRINSIC_COMPONENT_OF_ENDOPLASMIC_RETICULUM_MEMBRANE	2.000	0.017	77
19	GO_HEXOSE_METABOLIC_PROCESS	1.992	0.018	91
20	GO_STRUCTURAL_CONSTITUENT_OF_RIBOSOME	1.990	0.017	172
21	GO_CYTOSOLIC_LARGE_RIBOSOMAL_SUBUNIT	1.982	0.019	56
22	GO_DNA_PACKAGING	1.976	0.019	119
23	GO_RIBOSOMAL_SUBUNIT	1.976	0.019	140
24	GO_ORGANIC_HYDROXY_COMPOUND_BIOSYNTHETIC_PROCESS	1.959	0.022	81
25	GO_CHROMATIN_ASSEMBLY_OR_DISASSEMBLY	1.952	0.024	109

Appendix Table II-14. Top 25 upregulated C2 gene sets from the Bru-seq GSEA of **JR272** treated MIA PaCa-2 cells.

No	Gene set	NES	FDR q-val	Size
1	KIM_ALL_DISORDERS_DURATION_CORR_DN	2.457	<0.001	96
2	REACTOME_RNA_POL_I_PROMOTER_OPENING	2.411	<0.001	26
3	DAIRKEE_TERT_TARGETS_UP	2.400	<0.001	254
4	REACTOME_CHOLESTEROL_BIOSYNTHESIS	2.387	<0.001	19
5	REACTOME_AMYLOIDS	2.374	<0.001	33
6	NIKOLSKY_BREAST_CANCER_16Q24_AMPLICON	2.371	<0.001	35
7	RICKMAN_METASTASIS_DN	2.370	<0.001	138
8	LEONARD_HYPOXIA	2.369	<0.001	32
9	HORTON_SREBF_TARGETS	2.353	<0.001	19
10	ENK_UV_RESPONSE_KERATINOCYTE_UP	2.338	<0.001	314
11	BANDRES_RESPONSE_TO_CARMUSTIN_MGMT_48HR_DN	2.308	<0.001	64
12	SCHMIDT_POR_TARGETS_IN_LIMB_BUD_UP	2.303	<0.001	19
13	KEGG_SYSTEMIC_LUPUS_ERYTHEMATOSUS	2.294	<0.001	39
14	AMUNDSON_GAMMA_RADIATION_RESPONSE	2.280	<0.001	37
15	DACOSTA_UV_RESPONSE_VIA_ERCC3_UP	2.272	<0.001	216
16	REACTOME_RNA_POL_I_TRANSCRIPTION	2.250	<0.001	50
17	MARTENS_TRETINOIN_RESPONSE_UP	2.244	<0.001	96
18	DIRMEIER_LMP1_RESPONSE_EARLY	2.238	<0.001	36
19	CAMPS_COLON_CANCER_COPY_NUMBER_UP	2.238	<0.001	41
20	NIKOLSKY_BREAST_CANCER_16P13_AMPLICON	2.231	<0.001	28
21	QI_HYPOXIA	2.230	<0.001	81
22	FERREIRA_EWINGS_SARCOMA_UNSTABLE_VS_STABLE_DN	2.223	<0.001	49
23	REACTOME_PEPTIDE_CHAIN_ELONGATION	2.220	<0.001	81
24	DEBIASI_APOPTOSIS_BY_REOVIRUS_INFECTION_DN	2.211	<0.001	212
25	GINESTIER_BREAST_CANCER_ZNF217_AMPLIFIED_DN	2.203	<0.001	251

Appendix Table II-15. Downregulated Hallmark gene sets from the Bru-seq GSEA of **JR272** treated MIA PaCa-2 cells.

No	Gene set	NES	FDR *q*-val	Size
1	HALLMARK_KRAS_SIGNALING_UP	-1.382	0.160	67
2	HALLMARK_TGF_BETA_SIGNALING	-1.054	0.684	44
3	HALLMARK_PROTEIN_SECRETION	-1.015	0.562	90
4	HALLMARK_MYC_TARGETS_V1	-1.007	0.437	193

Appendix Table II-16. Top 25 downregulated KEGG gene sets from the Bru-seq GSEA of **JR272** treated MIA PaCa-2 cells.

No	Gene set	NES	FDR *q*-val	Size
1	KEGG_GLYCOSYLPHOSPHATIDYLINOSITOL_GPI_ANCHOR_BIOSYNTHESIS	-1.588	0.438	22
2	KEGG_MISMATCH_REPAIR	-1.309	1.000	21
3	KEGG_PROTEIN_EXPORT	-1.214	1.000	22
4	KEGG_PURINE_METABOLISM	-1.090	1.000	93
5	KEGG_NEUROACTIVE_LIGAND_RECEPTOR_INTERACTION	-1.080	1.000	21
6	KEGG_ALANINE_ASPARTATE_AND_GLUTAMATE_METABOLISM	-1.074	1.000	15
7	KEGG_ABC_TRANSPORTERS	-1.070	1.000	16
8	KEGG_JAK_STAT_SIGNALING_PATHWAY	-1.052	1.000	55
9	KEGG_NUCLEOTIDE_EXCISION_REPAIR	-1.048	1.000	41
10	KEGG_TGF_BETA_SIGNALING_PATHWAY	-0.991	1.000	46
11	KEGG_CALCIUM_SIGNALING_PATHWAY	-0.978	1.000	50
12	KEGG_CELL_CYCLE	-0.882	1.000	108
13	KEGG_PYRIMIDINE_METABOLISM	-0.876	1.000	75
14	KEGG_CELL_ADHESION_MOLECULES_CAMS	-0.866	1.000	20
15	KEGG_VIRAL_MYOCARDITIS	-0.861	1.000	22
16	KEGG_DNA_REPLICATION	-0.814	1.000	34
17	KEGG_STARCH_AND_SUCROSE_METABOLISM	-0.785	1.000	17
18	KEGG_DILATED_CARDIOMYOPATHY	-0.781	1.000	29
19	KEGG_WNT_SIGNALING_PATHWAY	-0.724	1.000	82
20	KEGG_PATHOGENIC_ESCHERICHIA_COLI_INFECTION	-0.698	1.000	35
21	KEGG_AMYOTROPHIC_LATERAL_SCLEROSIS_ALS	-0.684	1.000	29
22	KEGG_PROPANOATE_METABOLISM	-0.669	1.000	25
23	KEGG_CYTOSOLIC_DNA_SENSING_PATHWAY	-0.597	1.000	23
24	KEGG_HEDGEHOG_SIGNALING_PATHWAY	-0.590	1.000	19
25	KEGG_RNA_POLYMERASE	-0.431	0.999	23

Appendix Table II-17. Top 25 downregulated GO gene sets from the Bru-seq GSEA of **JR272** treated MIA PaCa-2 cells.

No	Gene set	NES	FDR *q*-val	Size
1	GO_KIDNEY_MORPHOGENESIS	-1.820	1.000	26
2	GO_NEGATIVE_REGULATION_OF_EPITHELIAL_CELL_PROLIFERATION	-1.746	1.000	57
3	GO_GLUTAMINE_METABOLIC_PROCESS	-1.707	1.000	15
4	GO_RESPONSE_TO_X_RAY	-1.645	1.000	24
5	GO_BASAL_PART_OF_CELL	-1.641	1.000	21
6	GO_DNA_REPLICATION_INITIATION	-1.636	1.000	26
7	GO_MITOTIC_RECOMBINATION	-1.634	1.000	39
8	GO_RECIPROCAL_DNA_RECOMBINATION	-1.628	1.000	24
9	GO_CILIUM_ORGANIZATION	-1.627	1.000	111
10	GO_HOMEOSTASIS_OF_NUMBER_OF_CELLS_WITHIN_A_TISSUE	-1.618	0.977	18
11	GO_PROTEIN_TRANSPORT_ALONG_MICROTUBULE	-1.610	0.941	22
12	GO_STRAND_DISPLACEMENT	-1.598	0.935	22

13	GO_NUCLEOCYTOPLASMIC_TRANSPORTER_ACTIVITY	-1.593	0.897	22
14	GO_GPI_ANCHOR_METABOLIC_PROCESS	-1.593	0.834	28
15	GO_DNA_DEPENDENT_DNA_REPLICATION_MAINTENANCE_OF _FIDELITY	-1.584	0.828	18
16	GO_DNA_DOUBLE_STRAND_BREAK_PROCESSING	-1.582	0.788	16
17	GO_ANCHORED_COMPONENT_OF_MEMBRANE	-1.574	0.788	15
18	GO_GLUTAMINE_FAMILY_AMINO_ACID_METABOLIC_PROCES S	-1.568	0.776	28
19	GO_DNA_DEPENDENT_ATPASE_ACTIVITY	-1.562	0.771	72
20	GO_MESONEPHRIC_TUBULE_MORPHOGENESIS	-1.555	0.766	18
21	GO_MALE_MEIOSIS	-1.550	0.760	15
22	GO_REGULATION_OF_RESPONSE_TO_INTERFERON_GAMMA	-1.545	0.749	17
23	GO_DNA_REPAIR_COMPLEX	-1.544	0.723	36
24	GO_DNA_DEPENDENT_DNA_REPLICATION	-1.540	0.710	83
25	GO_LYSOPHOSPHOLIPID_ACYLTRANSFERASE_ACTIVITY	-1.539	0.687	15

Appendix Table II-18. Top 25 downregulated C2 gene sets from the Bru-seq GSEA of **JR272** treated MIA PaCa-2 cells.

No	Gene set	NES	FDR q-val	Size
1	HAMAI_APOPTOSIS_VIA_TRAIL_UP	-2.848	<0.001	437
2	ZHANG_TLX_TARGETS_36HR_DN	-2.618	<0.001	173
3	SENGUPTA_NASOPHARYNGEAL_CARCINOMA _WITH_LMP1_UP	-2.612	<0.001	213
4	DACOSTA_UV_RESPONSE_VIA_ERCC3_COMMON _DN	-2.492	<0.001	418
5	GABRIELY_MIR21_TARGETS	-2.457	<0.001	229
6	SENGUPTA_NASOPHARYNGEAL_CARCINOMA_UP	-2.454	<0.001	200
7	MILI_PSEUDOPODIA_HAPTOTAXIS_UP	-2.372	<0.001	441
8	DACOSTA_UV_RESPONSE_VIA_ERCC3_XPCS_DN	-2.258	0.001	66
9	TAKEDA_TARGETS_OF_NUP98_HOXA9_FUSION _6HR_UP	-2.252	0.001	24
10	SHEN_SMARCA2_TARGETS_UP	-2.248	0.001	400
11	HUTTMANN_B_CLL_POOR_SURVIVAL_DN	-2.158	0.003	30
12	NIKOLSKY_BREAST_CANCER_8Q12_Q22 _AMPLICON	-2.099	0.007	64
13	DE_YY1_TARGETS_DN	-2.072	0.010	74
14	DAZARD_UV_RESPONSE_CLUSTER_G6	-2.065	0.010	118
15	BEGUM_TARGETS_OF_PAX3_FOXO1_FUSION_UP	-2.034	0.014	22
16	ZHANG_TLX_TARGETS_DN	-2.032	0.014	83
17	PYEON_CANCER_HEAD_AND_NECK_VS_CERVICAL _UP	-1.998	0.018	143
18	RIGGINS_TAMOXIFEN_RESISTANCE_DN	-1.996	0.017	125
19	TAKEDA_TARGETS_OF_NUP98_HOXA9_FUSION_3D _UP	-1.940	0.031	55
20	ZHENG_BOUND_BY_FOXP3	-1.929	0.034	285
21	YANG_BREAST_CANCER_ESR1_LASER_DN	-1.924	0.034	34
22	ZHANG_BREAST_CANCER_PROGENITORS_UP	-1.914	0.036	343
23	SCHLOSSER_MYC_TARGETS_AND_SERUM _RESPONSE_DN	-1.909	0.037	43
24	DOANE_BREAST_CANCER_CLASSES_DN	-1.907	0.036	23
25	ACEVEDO_LIVER_CANCER_WITH_H3K27ME3_UP	-1.897	0.038	71

Appendix Table II-19. Top 25 upregulated genes from the Bru-seq of **JR274** treated MIA PaCa-2 cells.

No	Gene name	Log$_2$FC	Gene function

No	Gene name	Log₂FC	Gene function
1	FSCN2	3.17	Fascin Actin-Bundling Protein 2, Retinal photoreceptor disk morphogenesis
2	CRIP2	3.08	Cysteine Rich Protein 2 Smooth muscle tissue differentiation
3	CTSD	2.96	Cathepsin D Peptidase (proteolytic activation of hormones and growth factors)
4	MRPL41	2.30	Mitochondrial Ribosomal Protein L41 Organelle biogenesis
5	ANKDD1A	2.17	Ankyrin Repeat And Death Domain Containing 1A
6	SCNN1D	2.15	Sodium Channel Epithelial 1 Delta Subunit *Sodium channel activity, activaton of cAMP-Dependent PKA*
7	GPX4	2.14	Glutathione Peroxidase 4: CYP450, ferroptosis
8	AIP	2.11	Aryl Hydrocarbon Receptor Interacting Protein Ligand-activated transcription factor, CYP450 and metabolism
9	MT1A	1.95	Metallothionein 1A Detoxification of heavy metals
10	HSPB1	1.93	Heat Shock Protein Family B (Small) Member 1 Chaperones, cell differentiaiotn, p38 MAPK and transcription P53 signaling
11	MRPS34	1.92	Mitochondrial Ribosomal Protein S34: Protein synthesis
12	ECH1	1.90	Enoyl-CoA Hydratase 1: Fatty acid biosynthesis
13	FKBP2	1.86	FK506 Binding Protein 2 Immunoregulation, protein folding
14	TCHH	1.84	Trichohyalin: Keratinization
15	D2HGDH	1.81	D-2-Hydroxyglutarate Dehydrogenase: TCA cycle
16	GRINA	1.79	Glutamate Ionotropic Receptor NMDA Type Subunit nNOS signaling
17	KCNK6	1.76	Potassium Two Pore Domain Channel Subfamily K Member 6 ABC transporters, cAMP-dependent PKA activation
18	SH3BGRL3	1.76	SH3 Domain Binding Glutamate Rich Protein Like 3 GTPase activator, protein disulfide oxidoreductase activity
19	RNF181	1.75	Ring Finger Protein 181 Protein metabolism and ubiquitination
20	APRT	1.75	Adenine Phosphoribosyltransferase: Pyrimidine metabolism
21	ABCA2	1.71	ATP Binding Cassette Subfamily A Member 2 Bile acid and glucose transport
22	ARL16	1.70	ADP Ribosylation Factor Like GTPase 16 Cellular antiviral response (inhibitory)
23	IGFBP6	1.69	Insulin Like Growth Factor Binding Protein 6 Myometrial relaxation and contraction, protein metabolism
24	HIST1H2BF	1.69	Histone Cluster 1 H2B Family Member F: Cell cycle
25	MT2A	1.68	Metallothionein 2A Detoxification of heavy metals

Appendix Table II-20. Top 25 downregulated genes from the Bru-seq of **JR274** treated MIA PaCa-2 cells.

No	Gene name	Log₂FC	Gene function
1	HIST1H3D	-2.06	Histone Cluster 1 H3 Family Member D: Cell cycle
2	ZIC5	-1.90	Zic Family Member 5 DNA binding transcription factor activity
3	DHFR2	-1.86	Dihydrofolate Reductase 2: Folate biosynthesis
4	AC073111.3	-1.73	Uncharacterized protein
5	SETMAR	-1.55	SET Domain And Mariner Transposase Fusion Gene DNA repair, PKMT methylate histone lysines
6	RPL41	-1.50	Ribosomal Protein L41: mRNA translation
7	TCTE3	-1.46	T-Complex-Associated-Testis-Expressed 3 Organelle biogenesis, motor activity

8	ZNF607	-1.44	Zinc Finger Protein 607
			DNA binding transcription factor activity, *Gene expression*
9	TLR5	-1.43	Toll Like Receptor 5
			Innate immune response
10	RRH	-1.42	Retinal Pigment Epithelium-Derived Rhodopsin Homolog
			GPCR signaling
11	TXNIP	-1.32	Thioredoxin Interacting Protein
			Regulator of cellular redox signaling
12	TEX14	-1.31	Testis Expressed 14, Intercellular Bridge Forming Factor
			Spermatogenesis
13	TMEM79	-1.30	Transmembrane Protein 79
			Epidermal integrity and skin barrier function
14	AGA	-1.30	Aspartylglucosaminidase
			Glycoprotein degradation, innate immune system
15	GSTO2	-1.29	Glutathione S-Transferase Omega 2: Drug metabolism
16	RPP40	-1.29	Ribonuclease P/MRP Subunit P40: rRNA processing
17	CYP2U1	-1.28	Cytochrome P450 Family 2 Subfamily U Member 1
			Drug metabolism, cholesterol and lipid synthesis
18	SNAI1	-1.28	Snail Family Transcriptional Repressor 1
			DNA binding and transcriptional repressor activity
19	GJA3	-1.28	Gap Junction Protein Alpha 3
			Vesicle-mediated transport
20	BBS10	-1.25	Bardet-Biedl Syndrome 10
			Chaperone, intracellular traficking
21	NOXRED1	-1.22	NADP Dependent Oxidoreductase Domain Containing 1
22	YY2	-1.22	YY2 Transcription Factor
			Development and differntiation
23	MANF	-1.21	Mesencephalic Astrocyte Derived Neurotrophic Factor
			ER stress, growth factor activity
24	PTCH2	-1.21	Patched 2
			Hedgehog pathway (tumor suppressor)
25	ZBTB8A	-1.17	Zinc Finger And BTB Domain Containing 8A
			Nucleic acid binding

Notes

References

1.	Huang, B. L.; Song, B. L.; Xu, C. Q., Cholesterol metabolism in cancer: mechanisms and therapeutic opportunities. *Nat Metab* **2020,** *2* (2), 132-141.

2.	Ward, P. S.; Thompson, C. B., Metabolic reprogramming: A cancer hallmark even warburg did not anticipate. *Cancer Cell* **2012,** *21* (3), 297-308.

3.	Ding, X.; Zhang, W. H.; Li, S.; Yang, H., The role of cholesterol metabolism in cancer. *Am J Cancer Res* **2019,** *9* (2), 219-227.

4.	Ehmsen, S.; Pedersen, M. H.; Wang, G. S.; Terp, M. G.; Arslanagic, A.; Hood, B. L.; Conrads, T. P.; Leth-Larsen, R.; Ditzel, H. J., Increased cholesterol biosynthesis is a key characteristic of breast cancer stem cells influencing patient outcome. *Cell Rep* **2019,** *27* (13), 3927-3938.

5.	Lee, H. J.; Yue, S. H.; Li, J. J.; Lee, S. Y.; Shao, T.; Song, B.; Cheng, L.; Masterson, T. A.; Liu, X. Q.; Ratliff, T. L.; Cheng, J. X., Cholesteryl ester accumulation induced by PTEN loss and PI3K/AKT activation underlies human prostate cancer aggressiveness. *Mol Cancer Ther* **2015,** *14* (7), 393-406.

6.	Kuzu, O. F.; Noory, M. A.; Robertson, G. P., The role of cholesterol in cancer. *Cancer Res* **2016,** *76* (8), 2063-2070.

7.	Greife, A.; Tukova, J.; Steinhoff, C.; Scott, S. D.; Schulz, W. A.; Hatina, J., Establishment and characterization of a bladder cancer cell line with enhanced doxorubicin resistance by mevalonate pathway activation. *Tumor Biol* **2015,** *36* (5), 3293-3300.

8.	Wu, Y. F.; Si, R. R.; Tang, H.; He, Z.; Zhu, H.; Wang, L. L.; Fan, Y. C.; Xia, S. H.; He, Z. L.; Wang, Q. M., Cholesterol reduces the sensitivity to platinum-based chemotherapy via upregulating ABCG2 in lung adenocarcinoma. *Biochem Bioph Res Co* **2015,** *457* (4), 614-620.

9.	Cotte, A. K.; Aires, V.; Fredon, M.; Limagne, E.; Derangere, V.; Thibaudin, M.; Humblin, E.; Scagliarini, A.; de Barros, J. P. P.; Hillon, P.; Ghiringhelli, F.; Delmas, D., Lysophosphatidylcholine acyltransferase 2-mediated lipid droplet production supports colorectal cancer chemoresistance. *Nat Commun* **2018,** *9* (1), 1-16.

10.	Kopecka, J.; Trouillas, P.; Gasparovic, A. C.; Gazzano, E.; Assaraf, Y. G.; Riganti, C., Phospholipids and cholesterol: Inducers of cancer multidrug resistance and therapeutic targets. *Drug Resist Update* **2020,** *49*, 100670.

11.	Gu, L.; Saha, S. T.; Thomas, J.; Kaur, M., Targeting cellular cholesterol for anticancer therapy. *FEBS J* **2019,** *286* (21), 4192-4208.

12.	Lacroix, O.; Couttenier, A.; Vaes, E.; Cardwell, C. R.; De Schutter, H.; Robert, A., Statin use after diagnosis is associated with an increased survival in esophageal cancer patients: a Belgian population-based study. *Cancer Causes Control* **2019,** *30* (4), 385-393.

13.   Nguyen, T.; Khan, A.; Liu, Y.; El-Serag, H. B.; Thrift, A. P., The association between statin use after diagnosis and mortality risk in patients with esophageal cancer: A retrospective cohort study of United States veterans. *Am J Gastroenterol* **2018,** *113* (9), 1310.

14.   Hassanabad, A. F., Current perspectives on statins as potential anti-cancer therapeutics: clinical outcomes and underlying molecular mechanisms. *Transl Lung Cancer R* **2019,** *8* (5), 692-699.

15.   Zhang, Y.; Liang, M.; Sun, C.; Qu, G.; Shi, T.; Min, M.; Wu, Y.; Sun, Y., Statin use and risk of pancreatic cancer: An updated meta-analysis of 26 Studies. *Pancreas* **2019,** *48* (2), 142-150.

16.   E, J. Y.; Lu, S. E.; Lin, Y.; Graber, J. M.; Rotter, D.; Zhang, L.; Petersen, G. M.; Demissie, K.; Lu-Yao, G.; Tan, X. L., Differential and Joint effects of metformin and statins on overall survival of elderly patients with pancreatic adenocarcinoma: A large population-based study. *Cancer Epidemiol Biomarkers Prev* **2017,** *26* (8), 1225-1232.

17.   Couttenier, A.; Lacroix, O.; Vaes, E.; Cardwell, C. R.; De Schutter, H.; Robert, A., Statin use is associated with improved survival in ovarian cancer: A retrospective population-based study. *PLoS One* **2017,** *12* (12), e0189233.

18.   Xia, D. K.; Hu, Z. G.; Tian, Y. F.; Zeng, F. J., Statin use and prognosis of lung cancer: a systematic review and meta-analysis of observational studies and randomized controlled trials. *Drug Des Devel Ther* **2019,** *13*, 405-422.

19.   Archibugi, L.; Arcidiacono, P. G.; Capurso, G., Statin use is associated to a reduced risk of pancreatic cancer: A meta-analysis. *Dig Liver Dis* **2019,** *51* (1), 28-37.

20.   Guillaumond, F.; Bidaut, G.; Ouaissi, M.; Servais, S.; Gouirand, V.; Olivares, O.; Lac, S.; Borge, L.; Roques, J.; Gayet, O.; Pinault, M.; Guimaraes, C.; Nigri, J.; Loncle, C.; Lavaut, M. N.; Garcia, S.; Tailleux, A.; Staels, B.; Calvo, E.; Tomasini, R.; Iovanna, J. L.; Vasseur, S., Cholesterol uptake disruption, in association with chemotherapy, is a promising combined metabolic therapy for pancreatic adenocarcinoma. *Proc Natl Acad Sci U S A* **2015,** *112* (8), 2473-2478.

21.   Bartz, F.; Kern, L.; Erz, D.; Zhu, M. G.; Gilbert, D.; Meinhof, T.; Wirkner, U.; Erfle, H.; Muckenthaler, M.; Pepperkok, R.; Runz, H., Identification of cholesterol-regulating genes by targeted RNAi screening. *Cell Metab* **2009,** *10* (1), 63-75.

22.   Ebrahimi-Fakhari, D.; Wahlster, L.; Bartz, F.; Werenbeck-Ueding, J.; Praggastis, M.; Zhang, J.; Joggerst-Thomalla, B.; Theiss, S.; Grimm, D.; Ory, D. S.; Runz, H., Reduction of TMEM97 increases NPC1 protein levels and restores cholesterol trafficking in Niemann-pick type C1 disease cells. *Hum Mol Genet* **2016,** *25* (16), 3588-3599.

23.   Riad, A.; Zeng, C. B.; Weng, C. C.; Winters, H.; Xu, K. Y.; Makvandi, M.; Metz, T.; Carlin, S.; Mach, R. H., Sigma-2 Receptor/TMEM97 and PGRMC-1 increase the rate of internalization of LDL by LDL receptor through the formation of a ternary complex. *Sci Rep* **2018,** *8* (1), 1-12.

24.   Wilcox, C. B.; Feddes, G. O.; Willett-Brozick, J. E.; Hsu, L. C.; DeLoia, J. A.; Baysal, B. E., Coordinate up-regulation of TMEM97 and cholesterol biosynthesis genes in normal ovarian surface epithelial cells treated with progesterone: implications for pathogenesis of ovarian cancer. *BMC Cancer* **2007,** *7* (1), 223.

25.   Yan, B. Y.; Wang, D. W.; Zhu, Z. L.; Yang, Y. H.; Wang, M. W.; Cui, D. S.; Zhang, H.; Sun, X. F., Overexpression of MAC30 in the cytoplasm of oral squamous cell carcinoma predicts nodal metastasis and poor differentiation. *Chemotherapy* **2010,** *56* (6), 424-8.

26.   Ding, H.; Gui, X. H.; Lin, X. B.; Chen, R. H.; Cai, H. R.; Fen, Y.; Sheng, Y. L., Prognostic value of MAC30 expression in human pure squamous cell carcinomas of the lung. *Asian Pac J Cancer Prev* **2016,** *17* (5), 2705-2710.

27.   Zhao, Z. R.; Zhang, L. J.; He, X. Q.; Zhang, Z. Y.; Zhang, F.; Li, F.; Pei, Y. B.; Hu, Y. M.; Wang, M. W.; Sun, X. F., Significance of mRNA and protein expression of MAC30 in progression of colorectal cancer. *Chemotherapy* **2011,** *57* (5), 394-401.

28.   Moebius, F. F.; Striessnig, J.; Glossmann, H., The mysteries of sigma receptors: new family members reveal a role in cholesterol synthesis. *Trends Pharmacol Sci* **1997,** *18* (3), 67-70.

29.   Ahmed, I. S. A.; Chamberlain, C.; Craven, R. J., S2R(Pgrmc1): the cytochrome-related sigma-2 receptor that regulates lipid and drug metabolism and hormone signaling. *Expert Opin Drug Met* **2012,** *8* (3), 361-370.

30.   Mach, R. H.; Smith, C. R.; al-Nabulsi, I.; Whirrett, B. R.; Childers, S. R.; Wheeler, K. T., Sigma 2 receptors as potential biomarkers of proliferation in breast cancer. *Cancer Res* **1997,** *57* (1), 156-161.

31.   Wheeler, K. T.; Wang, L. M.; Wallen, C. A.; Childers, S. R.; Cline, J. M.; Keng, P. C.; Mach, R. H., Sigma-2 receptors as a biomarker of proliferation in solid tumours. *Brit J Cancer* **2000,** *82* (6), 1223-1232.

32.   Mach, R. H.; Zeng, C. B.; Hawkins, W. G., The sigma(2) receptor: A novel protein for the imaging and treatment of cancer. *J Med Chem* **2013,** *56* (18), 7137-7160.

33.   Hornick, J. R.; Xu, J.; Vangveravong, S.; Tu, Z.; Mitchem, J. B.; Spitzer, D.; Goedegebuure, P.; Mach, R. H.; Hawkins, W. G., The novel sigma-2 receptor ligand SW43 stabilizes pancreas cancer progression in combination with gemcitabine. *Mol Cancer* **2010,** *9* (1), 1-11.

34.   Ostenfeld, M. S.; Fehrenbacher, N.; Hoyer-Hansen, M.; Thomsen, C.; Farkas, T.; Jaattela, M., Effective tumor cell death by sigma-2 receptor ligand siramesine involves lysosomal leakage and oxidative stress. *Cancer Res* **2005,** *65* (19), 8975-8983.

35.   Crawford, K. W.; Bowen, W. D., Sigma-2 receptor agonists activate a novel apoptotic pathway and potentiate antineoplastic drugs in breast tumor cell lines. *Cancer Res* **2002,** *62* (1), 313-322.

36.   Kashiwagi, H.; McDunn, J. E.; Simon, P. O.; Goedegebuure, P. S.; Xu, J.; Jones, L.; Chang, K.; Johnston, F.; Trinkaus, K.; Hotchkiss, R. S.; Mach, R. H.; Hawkins, W. G., Selective sigma-2 ligands preferentially bind to pancreatic adenocarcinomas: applications in diagnostic imaging and therapy. *Mol Cancer* **2007,** *6* (1), 1-12.

37.   Huang, Y. S.; Lu, H. L.; Zhang, L. J.; Wu, Z. W., Sigma-2 receptor ligands and their perspectives in cancer diagnosis and therapy. *Med Res Rev* **2014,** *34* (3), 532-566.

38.   Takahashi, T.; Morita, K.; Akagi, R.; Sassa, S., Heme oxygenase-1: a novel therapeutic target in oxidative tissue injuries. *Curr Med Chem* **2004,** *11* (12), 1545-1561.

39.   Cerqueira, N. M.; Oliveira, E. F.; Gesto, D. S.; Santos-Martins, D.; Moreira, C.; Moorthy, H. N.; Ramos, M. J.; Fernandes, P. A., Cholesterol Biosynthesis: A Mechanistic Overview. *Biochemistry* **2016,** *55* (39), 5483-5506.

40.   Moebius, F. F.; Fitzky, B. U.; Lee, J. N.; Paik, Y. K.; Glossman, H., Molecular cloning and expression of the human Delta 7-sterol reductase. *Proc Natl Acad Sci USA* **1998,** *95* (4), 1899-1902.

41.   Jordan, V. C., Tamoxifen: A most unlikely pioneering medicine. *Nat Rev Drug Discov* **2003,** *2* (3), 205-213.

42.   Schonewille, M.; de Boer, J. F.; Mele, L.; Wolters, H.; Bloks, V. W.; Wolters, J. C.; Kuivenhoven, J. A.; Tietge, U. J. F.; Brufau, G.; Groen, A. K., Statins increase hepatic cholesterol synthesis and stimulate fecal cholesterol elimination in mice. *J Lipid Res* **2016,** *57* (8), 1455-1464.

43.   Wei, Y. R.; Wang, D.; Topczewski, F.; Pagliassotti, M. J., Saturated fatty acids induce endoplasmic reticulum stress and apoptosis independently of ceramide in liver cells. *Am J Physiol-Endoc M* **2006,** *291* (2), E275-E281.

44.   Tracz-Gaszewska, Z.; Dobrzyn, P., Stearoyl-CoA desaturase 1 as a therapeutic target for the treatment of cancer. *Cancers* **2019,** *11* (7), 948.

45.   Pinkham, K.; Park, D. J.; Hashemiaghdam, A.; Kirov, A. B.; Adam, I.; Rosiak, K.; da Hora, C. C.; Teng, J.; Cheah, P. S.; Carvalho, L.; Ganguli-Indra, G.; Kelly, A.; Indra, A. K.; Badr, C. E., Stearoyl CoA desaturase is essential for regulation of endoplasmic reticulum homeostasis and tumor growth in glioblastoma cancer stem cells. *Stem Cell Rep* **2019,** *12* (4), 712-727.

46.   Persson, B.; Kallberg, Y.; Bray, J. E.; Bruford, E.; Dellaporta, S. L.; Favia, A. D.; Duarte, R. G.; Jornvall, H.; Kavanagh, K. L.; Kedishvili, N.; Kisiela, M.; Maser, E.; Mindnich, R.; Orchard, S.; Penning, T. M.; Thornton, J. M.; Adamski, J.; Oppermann, U., The SDR (short-chain dehydrogenase/reductase and related enzymes) nomenclature initiative. *Chem Biol Interact* **2009,** *178* (1-3), 94-8.

47.   Bakovic, M.; Fullerton, M. D.; Michel, V., Metabolic and molecular aspects of ethanolamine phospholipid biosynthesis: the role of CTP:phosphoethanolamine cytidylyltransferase (Pcyt2). *Biochem Cell Biol* **2007,** *85* (3), 283-300.

48.   Brown, M. S.; Goldstein, J. L., The SREBP pathway: Regulation of cholesterol metabolism by proteolysis of a membrane-bound transcription factor. *Cell* **1997,** *89* (3), 331-340.

49.   Attie, A. D.; Seidah, N. G., Dual regulation of the LDL receptor-some clarity and new questions. *Cell Metab* **2005,** *1* (5), 290-292.

50.   McFarlane, M. R.; Liang, G. S.; Engelking, L. J., Insig proteins mediate feedback inhibition of cholesterol synthesis in the intestine. *J Biol Chem* **2014,** *289* (4), 2148-2156.

51.   McPherson, R.; Gauthier, A., Molecular regulation of SREBP function: the Insig-SCAP connection and isoform-specific modulation of lipid synthesis. *Biochem Cell Biol* **2004,** *82* (1), 201-211.

52.   Li, X.; Nooh, M. M.; Bahouth, S. W., Role of AKAP79/150 protein in beta1-adrenergic receptor trafficking and signaling in mammalian cells. *J Biol Chem* **2013,** *288* (47), 33797-33812.

53.   Tao, J.; Malbon, C. C., G-protein-coupled receptor-associated A-kinase anchoring proteins AKAP5 and AKAP12: differential signaling to MAPK and GPCR recycling. *J Mol Signal* **2008,** *3* (1), 1-11.

54.   Pellinen, T.; Rantala, J. K.; Arjonen, A.; Mpindi, J. P.; Kallioniemi, O.; Ivaska, J., A functional genetic screen reveals new regulators of beta1-integrin activity. *J Cell Sci* **2012,** *125* (3), 649-661.

55.   Hanson, M. A.; Cherezov, V.; Griffith, M. T.; Roth, C. B.; Jaakola, V. P.; Chien, E. Y. T.; Velasquez, J.; Kuhn, P.; Stevens, R. C., A specific cholesterol binding site is established by the 2.8 angstrom structure of the human beta(2)-adrenergic receptor. *Structure* **2008,** *16* (6), 897-905.

56.   Paila, Y. D.; Tiwari, S.; Chattopadhyay, A., Are specific nonannular cholesterol binding sites present in G-protein coupled receptors? *Biochim Biophys Acta Biomembr* **2009,** *1788* (2), 295-302.

57.   Guixa-Gonzalez, R.; Albasanz, J. L.; Rodriguez-Espigares, I.; Pastor, M.; Sanz, F.; Marti-Solano, M.; Manna, M.; Martinez-Seara, H.; Hildebrand, P. W.; Martin, M.; Selent, J., Membrane cholesterol access into a G-protein-coupled receptor. *Nat Commun* **2017,** *8* (1), 1-12.

58.   Michal, P.; Rudajev, V.; El-Fakahany, E. E.; Dolezal, V., Membrane cholesterol content influences binding properties of muscarinic M2 receptors and differentially impacts activation of second messenger pathways. *Eur J Pharmacol* **2009,** *606* (1-3), 50-60.

59.   Bari, M.; Paradisi, A.; Pasquariello, N.; Maccarrone, M., Cholesterol-dependent modulation of type 1 cannabinoid receptors in nerve cells. *J Neurosci Res* **2005,** *81* (2), 275-83.

60.   Ribas, V.; Garcia-Ruiz, C.; Fernandez-Checa, J. C., Mitochondria, cholesterol and cancer cell metabolism. *Clin Transl Med* **2016,** *5* (1), 1-24.

61.   Nayak, A. P.; Kapur, A.; Barroilhet, L.; Patankar, M. S., Oxidative phosphorylation: A target for novel therapeutic strategies against ovarian cancer. *Cancers* **2018,** *10* (9), 337.

62.   Takwi, A. A. L.; Li, Y.; Buscaglia, L. E. B.; Zhang, J. W.; Choudhury, S.; Park, A. K.; Liu, M. F.; Young, K. H.; Park, W. Y.; Martin, R. C. G.; Li, Y., A statin-regulated microRNA represses human c-Myc expression and function. *Embo Mol Med* **2012,** *4* (9), 896-909.

63.   Stine, Z. E.; Walton, Z. E.; Altman, B. J.; Hsieh, A. L.; Dang, C. V., MYC, Metabolism, and Cancer. *Cancer Discov* **2015,** *5* (10), 1024-1039.

64.   Gouw, A. M.; Eberlin, L. S.; Margulis, K.; Sullivan, D. K.; Toal, G. G.; Tong, L.; Zare, R. N.; Felsher, D. W., Oncogene KRAS activates fatty acid synthase, resulting in specific ERK and lipid signatures associated with lung adenocarcinoma. *Proc Natl Acad Sci USA* **2017,** *114* (17), 4300-4305.

65.   Chen, C. L.; Huang, S. S.; Huang, J. S., Cholesterol modulates cellular TGF-beta responsiveness by altering TGF-beta binding to TGF-beta receptors. *J Cell Physiol* **2008,** *215* (1), 223-233.

66.   Soukupova, J.; Malfettone, A.; Hyrossova, P.; Hernandez-Alvarez, M. I.; Penuelas-Haro, I.; Bertran, E.; Junza, A.; Capellades, J.; Giannelli, G.; Yanes, O.; Zorzano, A.; Perales, J. C.; Fabregat, I., Role of the Transforming Growth Factor-beta in regulating hepatocellular carcinoma oxidative metabolism. *Sci Rep* **2017,** *7* (1), 1-15.

67.   Islam, M. A.; Sooro, M. A.; Zhang, P. H., Autophagic regulation of p62 is critical for cancer therapy. *Int J Mol Sci* **2018,** *19* (5), 1405.

68.   Ribalta, J.; Vallve, J. C.; Girona, J.; Masana, L., Apolipoprotein and apolipoprotein receptor genes, blood lipids and disease. *Curr Opin Clin Nutr Metab Care* **2003,** *6* (2), 177-87.

69.   Kastelein, J. J.; van der Steeg, W. A.; Holme, I.; Gaffney, M.; Cater, N. B.; Barter, P.; Deedwania, P.; Olsson, A. G.; Boekholdt, S. M.; Demicco, D. A.; Szarek, M.; LaRosa, J. C.; Pedersen, T. R.; Grundy, S. M.; Group, T. N. T. S.; Group, I. S., Lipids, apolipoproteins, and their ratios in relation to cardiovascular events with statin treatment. *Circulation* **2008,** *117* (23), 3002-9.

70.   Zhao, R. Z.; Jiang, S.; Zhang, L.; Yu, Z. B., Mitochondrial electron transport chain, ROS generation and uncoupling (Review). *Int J Mol Med* **2019,** *44* (1), 3-15.

71.   Wang, Z.; Lachmann, A.; Keenan, A. B.; Ma'ayan, A., L1000FWD: fireworks visualization of drug-induced transcriptomic signatures. *Bioinformatics* **2018,** *34* (12), 2150-2152.

72.   Wang, B. T.; Ducker, G. S.; Barczak, A. J.; Barbeau, R.; Erle, D. J.; Shokat, K. M., The mammalian target of rapamycin regulates cholesterol biosynthetic gene expression and exhibits a rapamycin-resistant transcriptional profile. *Proc Natl Acad Sci USA* **2011,** *108* (37), 15201-15206.

73.   Eid, W.; Dauner, K.; Courtney, K. C.; Gagnon, A.; Parks, R. J.; Sorisky, A.; Zha, X. H., mTORC1 activates SREBP-2 by suppressing cholesterol trafficking to lysosomes in mammalian cells. *Proc Natl Acad Sci USA* **2017,** *114* (30), 7999-8004.

74.   Ben-Sahra, I.; Manning, B. D., mTORC1 signaling and the metabolic control of cell growth. *Curr Opin Cell Biol* **2017,** *45*, 72-82.

75.   Lim, S. C.; Parajuli, K. R.; Duong, H. Q.; Choi, J. E.; Han, S. I., Cholesterol induces autophagic and apoptotic death in gastric carcinoma cells. *Int J Oncol* **2014,** *44* (3), 805-811.

76.   Parikh, A.; Childress, C.; Deitrick, K.; Lin, Q. O.; Rukstalis, D.; Yang, W. N., Statin-induced autophagy by inhibition of geranylgeranyl biosynthesis in prostate cancer PC3 cells. *Prostate* **2010,** *70* (9), 971-981.

77.   Toepfer, N.; Childress, C.; Parikh, A.; Rukstalis, D.; Yang, W. N., Atorvastatin induces autophagy in prostate cancer PC3 cells through activation of LC3 transcription. *Cancer Biol Ther* **2011,** *12* (8), 691-699.

78.   Gbelcova, H.; Sveda, M.; Laubertova, L.; Varga, I.; Vitek, L.; Kolar, M.; Strnad, H.; Zelenka, J.; Bohmer, D.; Ruml, T., The effect of simvastatin on lipid droplets accumulation in human embryonic kidney cells and pancreatic cancer cells. *Lipids Health Dis* **2013,** *12* (1), 126.

79.   Cruz, A. L. S.; Barreto, E. A.; Fazolini, N. P. B.; Viola, J. P. B.; Bozza, P. T., Lipid droplets: platforms with multiple functions in cancer hallmarks. *Cell Death Dis* **2020,** *11* (2), 105.

80.   Porter, L. A.; Dellinger, R. W.; Tynan, J. A.; Barnes, E. A.; Kong, M.; Lenormand, J. L.; Donoghue, D. J., Human Speedy: A novel cell cycle regulator that enhances proliferation through activation of Cdk2. *J Cell Biol* **2002,** *157* (3), 357-366.

81.   Musgrove, E. A.; Caldon, C. E.; Barraclough, J.; Stone, A.; Sutherland, R. L., Cyclin D as a therapeutic target in cancer. *Nat Rev Cancer* **2011,** *11* (8), 558-572.

82.   Juraleviciute, M.; Pozniak, J.; Nsengimana, J.; Harland, M.; Randerson-Moor, J.; Wernhoff, P.; Bassarova, A.; Oy, G. F.; Troen, G.; Florenes, V. A.; Bishop, D. T.; Herlyn, M.; Newton-Bishop, J.; Slipicevic, A., MX 2 is a novel regulator of cell cycle in melanoma cells. *Pigm Cell Melanoma R* **2020,** *33* (3), 446-457.

83.   Hosoya, N.; Ono, M.; Miyagawa, K., Somatic role of SYCE2: an insulator that dissociates HP1 alpha from H3K9me3 and potentiates DNA repair. *Life Sci Alliance* **2018,** *1* (3).

84.   Li, X., Epigenetics and cell cycle regulation in cystogenesis. *Cell Signal* **2020,** *68*, 109509.

85.   Martinez, N. J.; Asawa, R. R.; Cyr, M. G.; Zakharov, A.; Urban, D. J.; Roth, J. S.; Wallgren, E.; Klumpp-Thomas, C.; Coussens, N. P.; Rai, G.; Yang, S. M.; Hall, M. D.; Marugan, J. J.; Simeonov, A.; Henderson, M. J., A widely-applicable high-throughput cellular thermal shift assay (CETSA) using split Nano Luciferase. *Sci Rep* **2018,** *8* (1), 1-16.

86.   Kawatkar, A.; Schefter, M.; Hermansson, N. O.; Snijder, A.; Dekker, N.; Brown, D. G.; Lundback, T.; Zhang, A. X.; Castaldi, M. P., CETSA beyond soluble targets: A broad application to multipass transmembrane proteins. *ACS Chem Biol* **2019,** *14* (9), 1913-1920.

87.   McAlister, G. C.; Nusinow, D. P.; Jedrychowski, M. P.; Wuhr, M.; Huttlin, E. L.; Erickson, B. K.; Rad, R.; Haas, W.; Gygi, S. P., MultiNotch MS3 enables accurate, sensitive, and multiplexed detection of differential expression across cancer cell line proteomes. *Anal Chem* **2014,** *86* (14), 7150-7158.

88.   Subramanian, A.; Tamayo, P.; Mootha, V. K.; Mukherjee, S.; Ebert, B. L.; Gillette, M. A.; Paulovich, A.; Pomeroy, S. L.; Golub, T. R.; Lander, E. S.; Mesirov, J. P., Gene set enrichment analysis: A knowledge-based approach for interpreting genome-wide expression profiles. *Proc Natl Acad Sci USA* **2005,** *102* (43), 15545-15550.

89.   Mootha, V. K.; Lindgren, C. M.; Eriksson, K. F.; Subramanian, A.; Sihag, S.; Lehar, J.; Puigserver, P.; Carlsson, E.; Ridderstrale, M.; Laurila, E.; Houstis, N.; Daly, M. J.; Patterson, N.; Mesirov, J. P.; Golub, T. R.; Tamayo, P.; Spiegelman, B.; Lander, E. S.; Hirschhorn, J. N.; Altshuler, D.; Groop, L. C., PGC-1alpha-responsive genes involved in oxidative phosphorylation are coordinately downregulated in human diabetes. *Nat Genet* **2003,** *34* (3), 267-273.

90.   Paulsen, M. T.; Veloso, A.; Prasad, J.; Bedi, K.; Ljungman, E. A.; Magnuson, B.; Wilson, T. E.; Ljungman, M., Use of Bru-Seq and BruChase-Seq for genome-wide assessment of the synthesis and stability of RNA. *Methods* **2014,** *67* (1), 45-54.

91.   Chemical Computing Group Inc. "Molecular operating environment (MOE)". **2016**.

92.   Di Veroli, G. Y.; Fornari, C.; Wang, D.; Mollard, S.; Bramhall, J. L.; Richards, F. M.; Jodrell, D. I., Combenefit: an interactive platform for the analysis and visualization of drug combinations. *Bioinformatics* **2016,** *32* (18), 2866-8.

CHAPTER III

Discovery of a Napabucasin PROTAC as an Effective Degrader of ZFP91

Introduction

Naphthoquinone 2-acetylbenzo[f][1]benzofuran-4,9-dione (NPQ) was first discovered in 1982 as a plant-derived compound with anticancer activity.[1] In 1998, NPQ was reported to have antipsoriatic, antibacterial and antifungal activities.[2] Despite the promising preliminary data on NPQ, there was no interest in its development for almost a decade until 2009 when it was re-discovered by Boston Biomedical, Inc. and given the name napabucasin, also known as BBI608. Napabucasin was dubbed as the first-in-class cancer stemness inhibitor through inhibition of the signal transducer and transcription factor 3 (STAT3) signaling pathway.[3, 4] Significant efforts were directed towards the development of napabucasin that resulted in clinical trials in several cancers as a single agent and in combination with chemotherapy (Appendix Table III-1). Napabucasin was also formulated in polymeric vesicles that resulted in a decrease in the pancreatic cancer cell viability by 70%.[5] Promising data from clinical trials accelerated the designation of napabucasin to orphan drug status for gastric/gastroesohphageal and pancreatic cancer in 2016 (Figure III-1A).[6]

Pancreatic cancer is a devastating disease and is one of the leading causes of cancer-related deaths worldwide, therefore novel therapies are highly sought after.[7] *In vivo* studies have shown that napabucasin is capable of blocking cancer metastasis and its relapse in pancreatic and colon cancers through inhibition of cancer stemness.[3] Combination with nab-paclitaxel and gemcitabine in a Phase I/II clinical trial showed that napabucasin is well tolerated and displays activity against

metastatic pancreatic adenocarcinoma (mPDAC).[8] However, a Phase III study investigating the efficacy of napabucasin when given with the standard-of-care chemotherapy in patients with mPDAC was discontinued due to futility.[9, 10]

Several analogs of napabucasin were synthesized to improve its efficacy and/or physicochemical properties. Introducing a (piperidinyl)ethylamino-substitution enhanced the activity 10-fold and resulted in improved solubility.[11] Another compound (LD-19) that possesses a methyl piperazine group displayed enhanced *in vitro* cytotoxicity in liver cancer cells and improved water solubility.[12] However, none of the optimized analogs have been advanced to in-depth pre-clinical studies. While napabucasin is facing a lack of success in the clinic, there is still considerable interests in understanding its mechanism of action since it is reported as a STAT3 inhibitor.

STAT3 is a transcription factor that is implicated in the majority of human cancers and is associated with poor prognosis.[13, 14] The constitutive activation of STAT3 in cancer cells is highly advantageous for proliferative and metastatic phenotypes. This master regulatory role allows for selective cancer cell killing, making it an attractive target for cancer treatment.[15] Over the past 30 years, significant efforts were directed towards understanding the biological function of STAT3 and developing an effective inhibitor capable of blocking STAT3 activity. However, very few compounds including napabucasin made it to clinical trials. Most of these studies displayed insufficient efficacy and/or intolerable side effects.[16, 17]

Although napabucasin has been reported as a STAT3 inhibitor, its exact mechanism of action is not clearly understood. Napabucasin has been claimed to directly bind STAT3 by preventing its proteolytic degradation.[18] Furthermore, a series of napabucasin analogs were reported to bind to STAT3 using surface plasmon resonance (SPR) analysis with a K_D of 110 nM

for the most potent analog.[11] It is claimed that napabucasin inhibits STAT3 by binding to its SH2 domain and preventing its dimerization and subsequent activation but there is no crystallographic evidence to support that claim.[11, 12, 18] Napabucasin is also reported to act on multiple other oncogenic pathways including WNT/ß-catenin pathway that is constitutively activated in tumor tissues.[19] Napabucasin is a substrate for NAD(P)H: quinone oxidoreductase 1 (NQO1), and its activity is dependent on NQO1 levels.[20] This enzyme catalyzes the reduction of a quinone to hydroquinone resulting in the generation of reactive oxygen species (ROS), DNA alkylation and subsequent cancer cell death.[21] This suggests that part of napabucasin's mechanism of action could be a result of ROS induction and/or DNA alkylation.[22] Recently, our lab showed that napabucasin induces ROS, has similar transcriptomic signature as H_2O_2, and induces cancer cell death *via* necroptosis.[23] Napabucasin was also reported to act through inhibition of protein synthesis *via* regulating the eukaryotic initiation factor 4E **(**Figure III-1B**).**[24]

In an attempt to better understand napabucasin's mechanism of action and its connection to STAT3, we designed a series of novel napabucasin-derived proteolysis targeting chimeras (PROTACs) and assessed their cytotoxicity in pancreatic cancer cell lines. PROTACs are heterobifunctional molecules that simultaneously bind an E3 ligase and a target protein, driving target protein ubiquitination by the E3 ligase complex leading to recognition and degradation by the 26S proteasome.[25-27] The first-in-class STAT3 degrader, SD-36, was recently reported by applying a cereblon (CRBN)-based PROTAC targeting the SH2 domain of STAT3.[28, 29] SD-36 degraded STAT3 with nanomolar DC_{50} values in leukemia and lymphoma cell lines and elicited complete tumor regression within two weeks.[29] This study validates the use of PROTACs in effective and selective targeting of STAT3. As napabucasin is also reported to target the SH2 domain of STAT3, we hypothesized that napabucasin-based PROTACs would be a novel and

effective strategy to degrade STAT3. Herein, we describe the synthesis and evaluation of a series of napabucasin-PROTACs with cellular potency in pancreatic cancer cell lines. Proteomics and mechanistic studies did not reveal proteasome-dependent degradation of STAT3. Instead, we observed a significant degradation of ZFP91 with the napabucasin-PROTAC, **XD2-149 (3-6d)** (Figure III-2). Our study provides further insight into the mechanism of action of napabucasin and for the first time, linking napabucasin to the potential oncogenic protein ZFP91.
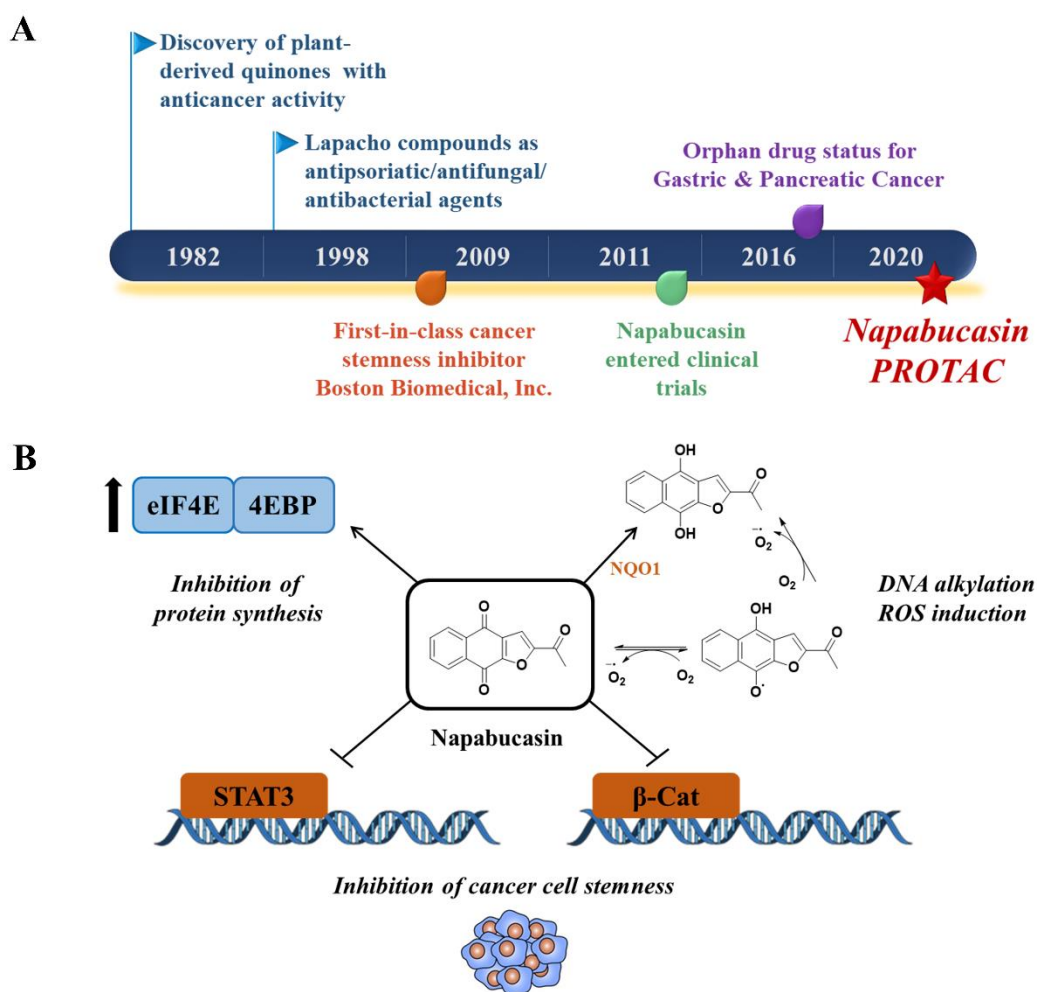
Figure III-1. (A) Discovery timeline of napabucasin highlighting select milestones. (B) Reported mechanisms of action for napabucasin.
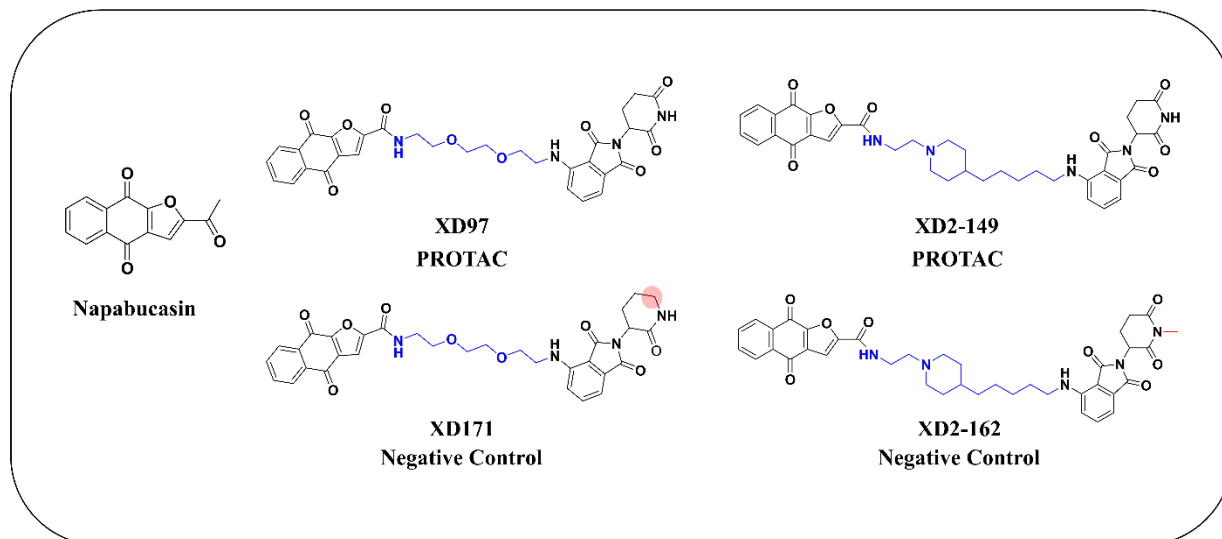
Figure III-2. Chemical structures of napabucasin, the designed PROTACs, and their respective negative controls.

Results and Discussion

Design of PROTACs using napabucasin as the targeting warhead

In order to develop an effective PROTAC that can bind to and degrade the potential target of napabucasin, we designed a series of compounds applying three major optimization approaches. The design followed a systematic strategy that included the optimization of the linker length/composition, the position of the linker attachment to napabucasin and the choice of the E3 ligase ligand. It is critical to adjust for the distance between the two partner proteins to allow for efficient binding and degradation. CRBN and Von Hippel Lindau (VHL) E3 ligases have been successfully employed in the design of the PROTACs for degrading different proteins.[29-33] CRBN E3 ligase ligands are composed of the low molecular weight immunomodulatory drugs (IMiDs) including pomalidomide, thalidomide and lenalidomide that makes them ideal for the design of PROTACs with good physicochemical properties.[34] Therefore, we focused our studies on the design of CRBN-based PROTACs with exploration of the effect of VHL E3 ligase ligand. Pomalidomide has a high cellular stability compared to lenalidomide and thalidomide[35, 36] so, we initially designed pomalidomide-based compounds for studying the choice of the optimal linker.

The synthesized compounds were evaluated for their cytotoxicity and protein degradation in the two pancreatic cancer cell lines, BxPC-3 and MIA PaCa-2. We used BxPC-3 to guide our structure-activity relationship studies (SAR) due to the improved activity of the compounds in immunoblotting experiments, in addition to, its higher expression and activation of STAT3 (Figure III-3).[37]
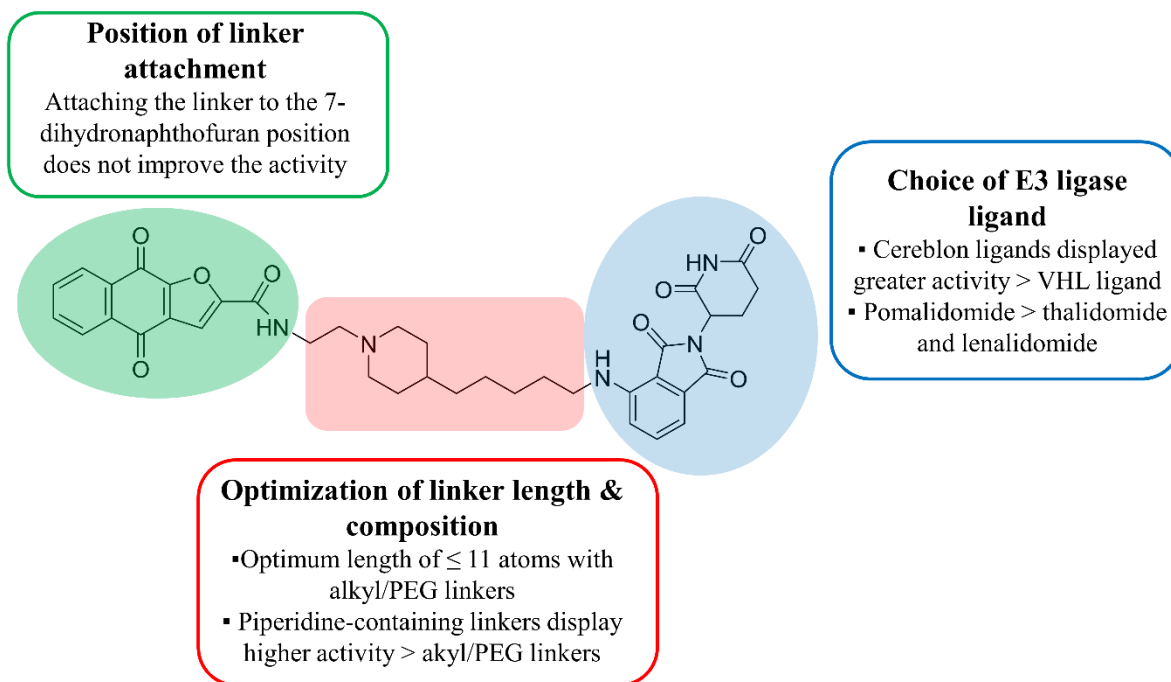
Figure III-3. Summary for PROTAC optimization including linker length and composition, point of linker attachment to napabucasin, and the choice of the E3 ligase ligand.

In order to obtain the optimum PROTAC, it is important to consider the stability of the ternary complex in which the linker plays an important role. With pomalidomide as the CRBN handle and napabucasin as the targeting warhead, we designed a series of PROTACs applying various linker lengths and compositions. We synthesized compounds with alkyl and PEG linkers of different lengths (2 – 20 atoms) and evaluated their cytotoxicity (Table III-1). Compound **2-5a** with the 2-atom spacer displayed low micromolar cytotoxicity while compounds with linkers ranging between 3 and 11 atoms were 2-fold less potent than **2-5a**. Increasing the linker length > 11 atoms in **2-5c** and **2-5j** resulted in decreased cytotoxicity. Our results show that the optimal

linker length for the cytotoxicity of compounds is ≤ 11 atoms and that there is no significant difference between the hydrophobic and hydrophilic linkers.

XD97 (2-5g) reduces STAT3 expression in a proteasome-independent manner

We tested a selection of the compounds in a panel of cell lines outside of pancreatic cancer to determine if there is a specific cell line in which the compounds are selective **(**Appendix Tables III-2/3**)**. **2-5 g (XD97)** with an IC_{50} of ~ 0.3 μM in OVCAR-3 cells was the most cytotoxic. To determine whether the cytotoxicity of these compounds is STAT3-dependent, we used a pair of OVCAR-3 wildtype (WT) and STAT3 knockout (KO) cell lines (Appendix Table III-3).[38] Overall, the compounds were more potent in the WT cell line, among which **XD97** displayed high selectivity over the STAT3 KO cell line (> 6-fold). These data suggest that STAT3 is involved in the mechanism of cell death. Since the cytotoxicity was STAT3-dependent, we tested whether the napabucasin PROTAC **XD97** degraded STAT3. **XD97** at different concentrations and times caused near complete depletion of STAT3 after 12 h while decrease in pSTAT3 levels was observed after 6 h **(**Appendix Figure III-1B**)**.

To investigate if the degradation of STAT3 was proteasome-dependent, we employed three approaches: treatment in the presence of a proteasome inhibitor, competition with the E3 ligase ligand, and synthesis of a negative control incapable of binding CRBN. Upon treatment with the proteasome inhibitor MG132, we observed no blockade of the **XD97**-induced decrease in STAT3 expression concluding this decrease is not dependent on the proteasome **(**Appendix Figure III-1C**)**. In fact, MG132 enhanced the activity of **XD97** resulting in a more prominent reduction in STAT3 protein levels. Similarly, competition experiments in the presence of pomalidomide did not antagonize the effect of **XD97** indicating it is not a substrate of CRBN **(**Appendix Figure III-1D**)**. We synthesized **10-5 (XD171)** as a negative control by replacing the glutarimide ring in

pomalidomide by a δ-lactam ring that abrogates its binding to CRBN (Appendix Figure III-1A).[39] **XD171** displayed comparable activity to **XD97** (Appendix Figure III-1E). Among the STAT family members, STAT1 has a high structural similarity to STAT3.[40] Surprisingly, we observed a decrease in STAT1 levels that is even more prominent than that observed with STAT3 at the same concentrations of **XD97 (**Appendix Figure III-1B**)**. Taken together, the mechanism of action of **XD97** is independent of the proteasome and the observed effects are possibly due to inhibitory activity or changes on the transcriptional level. We also conclude that the activity of **XD97** is not specific to STAT3.

We further tested **XD97** for its effect on STAT3 expression in the pancreatic cancer cell line BxPC-3 to determine if it possessed a different mechanism of action and possibly act as a degrader. Similar to OVCAR-3, **XD97** reduced the STAT3 level after 12 h but the effect in BxPC-3 was observed at a lower concentration (DC_{50} = 7.8 μM) despite of the greater cytotoxicity of **XD97** in OVCAR-3 (IC_{50} of ∼ 0.2 and 4.3 μM in OVCAR-3 and BxPC-3, respectively) **(**Appendix Figure III-2A/B**)**. This encouraged us to test **XD97** in combination with the proteasome inhibitor bortezomib. Unfortunately, bortezomib did not block the activity of **XD97** thereby proving its STAT3 inhibitory activity is independent of the proteasome-mediated degradation **(**Appendix Figure III-2C**)**. Interestingly, we observed reduced STAT3 expression with napabucasin (DC_{50} = 2.1 μM) that was not observed in OVCAR-3 at the same time-point (Appendix Figure III-2B). Moreover, napabucasin and **XD97** both reduced NQO1 levels **(**Appendix Figure III-2D**)**. It is possible that napabucasin has multiple targets or acts through interfering with the transcription/translation of target proteins.

Although PROTACs have the advantage of selectively degrading the target protein, recruitment of other neo-substrates can be a challenge. The surface of CRBN can change upon

binding of IMiDs like pomalidomide and allow recruitment of other proteins such as the translation termination factor GSPT1 which has been previously reported as an off target substrate for CRBN-targeted PROTACs.[41, 42] This change in the surface structure leads to creation of hotspots that cause the PROTAC molecule to act as a 'molecular glue' and bind non-specific proteins.[43] The protein level of GSPT1 was not affected by **XD97** or napabucasin treatments **(**Appendix Figure III-2D**).** This provides evidence that napabucasin does not non-specifically cause degradation of proteins and that its effect is mechanism-based.

Optimization of napabucasin-based PROTACs

Moving forward with the linker optimization, we synthesized compounds with cyclized linkers using piperidine. The piperidine linkers displayed improved activity over the alkly/PEG linkers (Table III-1). Piperidine groups have been previously incorporated into PROTACs to improve water solubility.[44] **3-6c** and **3-6d (XD2-149)** showed comparable potency with $IC_{50} < 1$ µM in BxPC-3. Compound **3-6a** with a piperazine ring resulted in significant loss of activity (Table III-1). Our data shows that piperidine-containing linkers display the best cytotoxicity and are superior to napabucasin suggesting these compounds might act as effective degraders. Therefore, **XD2-149** was selected as a representative PROTAC for further mechanistic studies.

The small molecule **1-6** is a previously reported analog of napabucasin that displayed greater cytotoxicity (>10-fold) and was used to investigate the effect of the position of linker attachment (Appendix Table III-4).[11] Attaching the linker to the 7-dihydronaptho[2,3-b]furan position in **13-11** did not result in improved cytotoxicity (Appendix Table III-5). Changing the position of the linker attachment to the E3 ligase ligand from position 4 of the isoindoline-1,3-dione ring to position 5 (**12-5**) reduced the cytotoxicity as compared to **XD97** (Appendix Table III-5).

115

To examine the CRBN ligand portion, another set of compounds was designed using thalidomide as the CRBN E3 ligase ligand employing various linkers (Table III-1). Amide-containing linkers displayed a significant decrease in activity with $IC_{50} > 10$ µM except for **6-6b** with a linker that extends to > 13 atoms contributing to its enhanced activity. Compound **5-5b** with a 9-atom PEG linker had an $IC_{50} \sim 8$ µM while **5-5a** with a 4-atom alkyl linker was almost 2-fold more potent. Two other compounds with alkyl and PEG linkers conjugated to lenalidomide showed moderate cytotoxicity (IC_{50} range 6-14 µM) (Table III-1).

Our synthetic efforts extended to testing compounds with VHL as the E3 ligase ligand. Interestingly, the VHL-based compounds were inactive with $IC_{50} > 30$ µM suggesting VHL is not optimal for the design of napabucasin-based PROTACs (Table III-2).

In conclusion, CRBN E3 ligases were more effective in the design of PROTACs compared to VHL. Thalidomide and lenalidomide-based compounds were less cytotoxic than pomalidomide-based conjugates suggesting that pomalidomide provides a more stable complex with napabucasin and CRBN.

Table III-1. Cytotoxicity of CRBN-based PROTACs in pancreatic cancer cell lines.

Pomalidomide: X=CO, R=NH$_2$
Thalidomide: X=CO, R=H
Lenalidomide: X= CH$_2$, R=NH$_2$
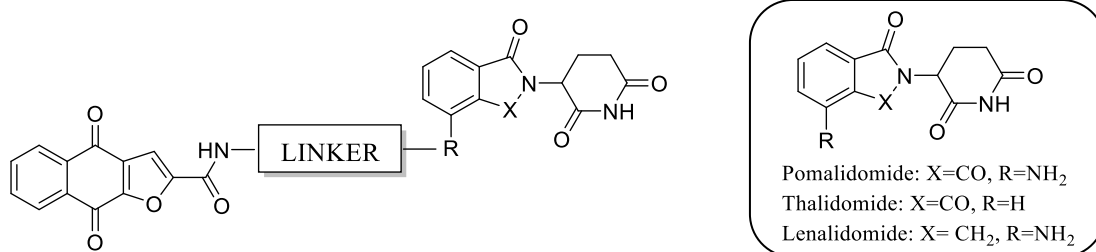
Pomalidomide-based PROTACs

ID	Linker	MW	cLogP	IC$_{50}$ (µM)	
				MIA PaCa-2	BxPC-3
NP[a]		240.21	2.19	1.2 ± 0.8	1.4 ± 0.3
2-5a		540.49	2.29	4.0 ± 0.9	1.7 ± 0.7
2-5b		554.52	2.65	2.7 ± 0.4	3.5 ± 0.6
2-5c		567.54	2.61	1.60 ± 0.3	4.1 ± 1.1
2-5d		582.57	3.14	1.8 ± 0.7	3.2 ± 1.3

ID	Linker	MW	cLogP	MIA PaCa-2	BxPC-3
2-5e		596.60	3.67	3.0 ± 0.4	4.2 ± 1.4
2-5f		584.54	2.36	2.6 ± 0.9	4.6 ± 1.2
2-5g, XD97		628.59	2.18	1.3 ± 0.5	4.3 ± 1.1
2-5h		672.65	2.01	2.1 ± 0.8	4.5 ± 0.9
2-5i		716.70	1.83	4.4 ± 0.7	10.1 ± 3.5
2-5j		804.29	1.48	5.0 ± 1.0	7.5 ± 0.4
3-6a		652.66	1.80	18.1 ± 11.4	25.6 ± 2.0
3-6b		651.68	3.55	1.1 ± 0.3	1.1 ± 0.5
3-6c		665.70	4.08	0.6 ± 0.3	0.6 ± 0.1
3-6d, XD2-149		693.76	5.14	1.0 ± 0.1	0.8 ± 0.2

[a]Napabucasin

Thalidomide-based PROTACs

ID	Linker	MW	cLogP	IC$_{50}$ (µM)	
				MIA PaCa-2	BxPC-3
4-5		563.52	2.83	2.1 ± 1.0	5.3 ± 0.8
5-5a		569.53	2.78	2.0 ± 0.3	4.2 ± 0.7
5-5b		629.58	2.24	3.8 ± 1.0	8.2 ± 4.1
6-6a		686.63	1.55	16.7 ± 3.8	20.4 ± 7.4
6-6b		730.68	1.38	3.7 ± 1.1	6.0 ± 5.5
6-6c		626.58	1.55	10.5 ± 3.0	23.8 ± 3.9

Lenalidomide-based PROTACs

ID	Linker	MW	cLogP	IC$_{50}$ (µM)	
				MIA PaCa-2	BxPC-3
7-4		614.62	1.96	13.7 ± 1.0	10.5 ± 4.5
8-1		553.57	3.37	6.4 ± 3.4	13.8 ± 7.7

Table III-2. Cytotoxicity of VHL-based PROTACs in pancreatic cancer cell lines.
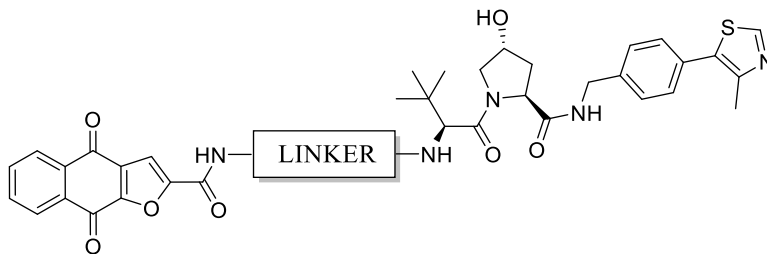
ID	Linker	MW	cLogP	IC$_{50}$ (μM)	
				MIA PaCa-2	BxPC-3
9-4a		799.90	3.82	14.5 ± 7.1	>30
9-4b		755.84	3.99	15.8 ± 4.6	>30

XD2-149 (3-6d) is cytotoxic in pancreatic cancer cell lines

Previous studies on napabucasin have proven its activity against pancreatic cancer for which it was approved as an orphan drug.[6] BxPC-3 cells have high protein levels of STAT3 and pSTAT3.[37] We tested our compounds for their ability to inhibit cell growth in MIA PaCa-2 and BxPC-3 cell lines using MTT assay (Tables III-1/2, Appendix Table III-5). Compound **XD2-149** was among the most active compounds in both cell lines with an IC$_{50}$ ~ 1 μM. We synthesized **11-7 (XD2-162)** as a negative control by replacing the NH of the glutarimide ring in pomalidomide with an N-methyl group (Figure III-4A). The N-methylated pomalidomide lacks the key H-bond donor involved in an interaction with His378 of CRBN, in addition to, the steric hindrance created by the methyl in the binding pocket.[45, 46] **XD2-149** is significantly more potent than **XD2-162** in the MTT assay suggesting that the cell growth inhibition involves target degradation (Figure III-4A/B). The colony formation assay (CFA), a cell survival assay that assesses the ability of the cells to survive and form colonies was also used to test the cytotoxicity of the compounds. **XD2-149** inhibits colony formation in different pancreatic cancer cells lines and displays a greater inhibitory activity than napabucasin in BxPC-3 cell line (Figure III-4C/D).
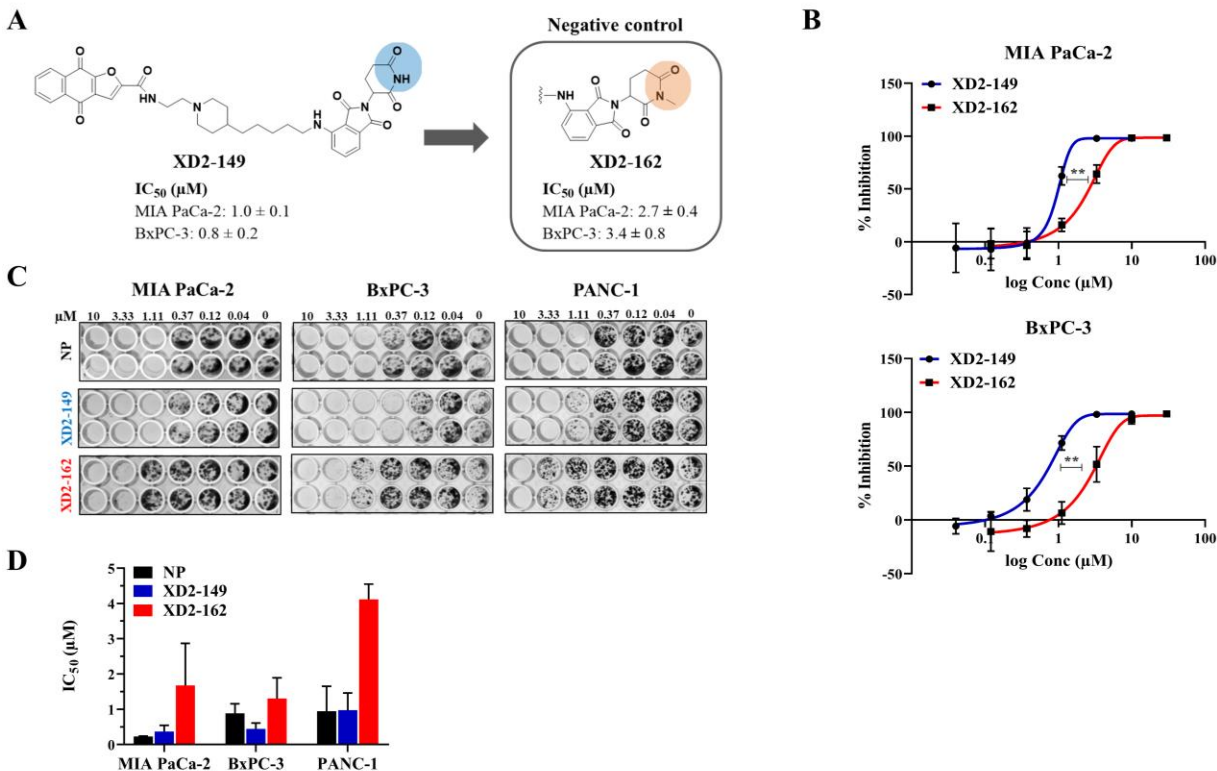
Figure III-4. **XD2-149** inhibits cell proliferation and colony formation in pancreatic cancer cell lines. (A) Design of **XD2-162**, the negative control for the PROTAC **XD2-149**. IC$_{50}$ values correspond to the cytotoxicity of the compounds in the MTT assay. (B) Dose-response curves of the cytotoxicity of **XD2-149** and **XD2-162** in the MTT assay after 72 h. (C) Colony formation assay for napabucasin (NP), **XD2-149** and **XD2-162** in pancreatic cancer cell lines. Cells were treated for 7-10 days. (D) Quantification for the colony formation assay was done by dissolving the colonies using Sorensen's buffer and reading the absorbance at 570 nm. All data presented were generated from three biological replicates and are presented as mean ± SD. ** denotes $p \leq 0.01$.

XD2-149 inhibits IL6-dependent STAT3 signaling

To determine whether our compounds have an effect on the transcriptional activity of STAT3, we screened the compounds at 2 and 10 µM in the STAT3 luciferase assay using HEK-293 cell line. The luciferase reporter assay is commonly used in the discovery and evaluation of STAT3 inhibitors.[28, 47] Following IL6-induced STAT3 activation, the cells were treated with the compounds for 24 h. The majority of the compounds resulted in a reduced signal indicating inhibition of STAT3-driven transcription (Appendix Figure III-3). All compounds were more potent in the luciferase assay than a 24 h MTT assay, indicating the signal loss was not due to cytotoxicity and cell death. Among the tested compounds, **XD2-149** was the most efficient in the

inhibition of STAT3-driven transcription with an $IC_{50} \sim 1$ µM which is almost 7-fold greater than its activity in the MTT assay (Figure III-5).

A

A. *Activation*
(IL6)

C

B

ID	IC_{50} (µM)	
	LUC	MTT
NP	3.2 ± 0.6	10.4 ± 0.6
XD2-149	0.9 ± 0.1	8.7 ± 2.2
XD2-162	1.7 ± 1.0	>30
2-5i	2.7 ± 0.9	>10
12-5	3.4 ± 0.8	>10
5-5a	5.7 ± 3.8	>10
4-5	4.2 ± 1.0	18.6 ± 4.1
2-5j	2.5 ± 0.7	10.8 ± 2.0
2-5d	4.6 ± 2.0	>10
7-4	10.9 ± 2.1	>30
6-6c	10.3 ± 0.5	>30
9-4a	11.4, 9.9	>30
9-4b	>30	>30
2-5h	2.6 ± 1.6	11.2 ± 2.9
2-5a	15.3 ± 8.6	>30
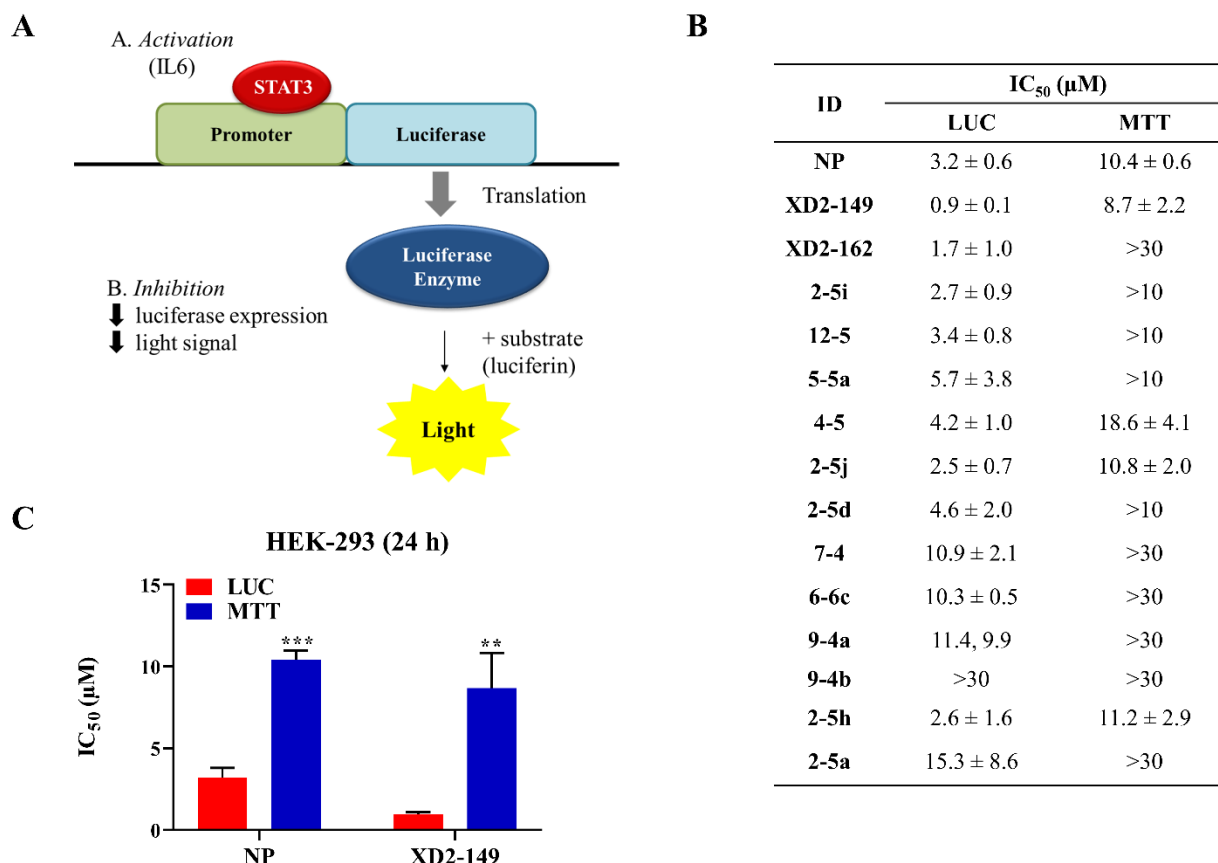
Figure III-5. **XD2-149** inhibits STAT3-driven gene transcription. (A) Diagram representing the principal of the STAT3 luciferase reporter assay. Transfected HEK-293 cells line that express renilla luciferase reporter under the transcriptional control of STAT3 were used. (B) IC_{50} values of the tested compounds in the luciferase assay after treatment for 24 h compared to their IC_{50} in the MTT assay at the same treatment time-point. For the luciferase assay, cells were pretreated with 100 ng/ml of IL6 for 24 h followed by treatment with the compounds for 24 h. The luciferin substrate was then added and the luminescence signal was measured. (C) IC_{50} values of napabucasin (NP) and **XD2-149** in MTT and luciferase (LUC) assays after a 24 h-treatment. Data were generated from three biological replicates and are presented as mean ± SD. ** denotes $p \leq 0.01$, *** denotes $p \leq 0.001$.

XD2-149 reduces STAT3 and NQO1 proteins' expression independent of the proteasome

To evaluate the ability of **XD2-149** to degrade STAT3, we treated MIA PaCa-2 and BxPC-3 cells with the compound at a range of concentrations up to 5 µM ($\sim$ 5X IC_{50}). In BxPC-3, after a 16 h-treatment, we observed a decrease in the STAT3 protein expression at 5 µM while a significant decrease in the pSTAT3 level was achieved at 1 µM (Figure III-6A). In contrast, **XD2-162** did not have any effect on STAT3 expression but resulted in a decrease in pSTAT3 expression

at 5 µM (Figure III-6A). This offset in concentration-dependent protein downregulation correlates well with the differences in MTT IC_{50} values. Interestingly, napabucasin alone was able to reduce the total STAT3 protein levels in addition to decreasing pSTAT3. The fact that the mechanism of action of the parent inhibitor involves reduction of STAT3 protein expression makes it challenging to study napabucasin PROTACs. The small-molecule analog of napabucasin **1-6** was also tested for its structural similarity to our compounds. Compound **1-6** did not have any effect on STAT3 expression at 0.5 µM (5X IC_{50}) with a reduced pSTAT3 expression at the same concentration. As previously discussed, napabucasin is reported as a substrate of NQO1. Therefore, we tested the effect of **XD2-149** on NQO1 as another possible target for degradation. We observed similar results to STAT3 which suggests that the activity of the compounds is not selective to STAT3 and the possibility of NQO1 degradation by the PROTAC given that napabucasin is a substrate of the enzyme. A reduction in STAT3 activation can result from increased ROS levels generated from NQO1-induced bioactivation of napabucasin.[22]

We repeated the experiment in MIA PaCa-2 cells, however, we observed less prominent effects on the proteins' expression than in BxPC-3 (Figure III-6A). Notably, **XD2-149** was less effective in inhibiting the phosphorylation of STAT3 in MIA PaCa-2 with no effect on the NQO1 level. It is worth noting that in MIA PaCa-2 cells, we were able to test napabucasin and **XD2-149** only up to 1 µM due to their high cytotoxicity. Napabucasin did not have a significant effect on the STAT3 protein expression but completely depleted the pSTAT3 levels at 1 µM (Figure III-6A).

Among the tested cell lines, BxPC-3 displayed the best activity for **XD2-149** in terms of cell growth inhibition and reduced STAT3 expression and activation. Therefore, further experiments were conducted in BxPC-3. To determine whether the reduction of STAT3 expression

is due to proteasome-dependent degradation, we treated the cells with **XD2-149** in the presence of the proteasome inhibitor MG132. Proteasome inhibition did not block the **XD2-149**-induced decrease in STAT3 protein (Figure III-6B). In contrast, we observed an enhanced reduction in NQO1 expression with **XD2-149** treatment in the presence of MG132 (Figure III-6B).

To determine if these effects occur at the translational level, we tested the effect of **XD2-149** on STAT3 and NQO1 in the presence of the protein synthesis inhibitor, cycloheximide. We observed an enhanced cycloheximide-mediated protein synthesis inhibition of STAT3 (Figure III-6C). Similar results were previously reported on napabucasin in osteosarcoma cells where the study demonstrated the inhibitory effect of napabucasin on protein synthesis as a result of STAT3 inhibition.[24] On the other hand, the reduced NQO1 expression caused by **XD2-149** was blocked in the presence of cycloheximide suggesting that the compound-induced downregulation of NQO1 is dependent on the *de novo* protein synthesis. Moreover, we sought to determine whether napabucasin engages its downregulated proteins by performing cellular thermal shift assay (CETSA). We tested the effect of napabucasin on the thermal stability of STAT3, NQO1 and an irrelevant protein (protein disulfide isomerase (PDI)) and observed a slight shift in the melting curve with all tested proteins except for the control protein GAPDH (Appendix Figure III-4).

Collectively, even though **XD2-149** displayed pronounced cytotoxicity in various cell lines compared to the negative control, it proved to not degrade the STAT3 protein through the proteasome machinery. It interferes with the protein synthesis of NQO1 resulting in reduced NQO1 levels, which was restored in the presence of a protein synthesis inhibitor.
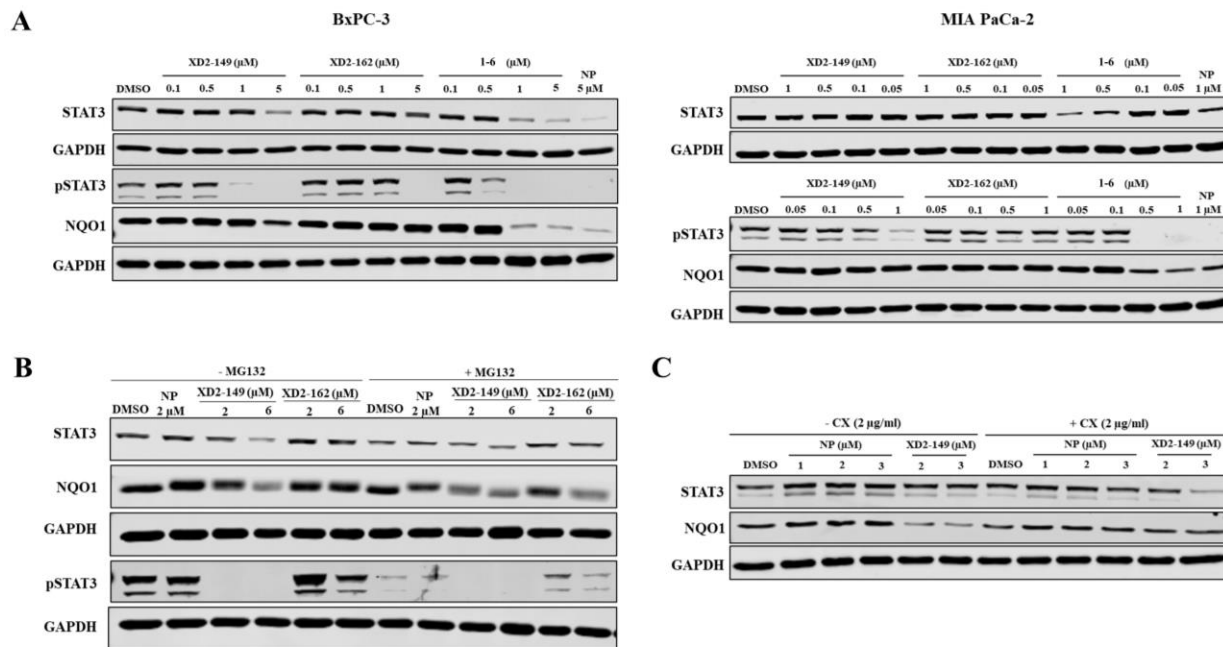
Figure III-6. **XD2-149** reduces the expression of STAT3 and NQO1 in a proteasome-independent manner. (A) **XD2-149** reduces the expression of STAT3, pSTAT3 and NQO1 proteins while **XD2-162** showed effect only on pSTAT3. The small molecules **1-6** and napabucasin (NP) displayed similar effects to **XD2-149**. BxPC-3 and MIA PaCa-2 cells were treated with **XD2-149**, **XD2-162**, **1-6** or NP at the indicated concentrations for 16 h. (B) The effect of **XD2-149** on STAT3/pSTAT3 and NQO1 expression is independent of the proteasome. BxPC-3 cells were pretreated with 10 µM MG132 for 2 h then with **XD2-149**, **XD2-162** or NP for 12 h. (C) **XD2-149** is possibly interfering with the protein synthesis of STAT3 and NQO1. BxPC-3 cells were pretreated with cycloheximide (CX) for 1 h followed by NP or **XD2-149** for 16 h. Data presented are from a single experiment.

XD2-149 is a *bona fide* degrader of ZFP91

To further study the effect of **XD2-149** at the protein level and determine proteins selectively altered upon treatment, we performed proteomics analysis in BxPC-3. We evaluated proteome changes after 16 h treatment with either **XD2-149**, napabucasin, or **XD2-162**. The negative control was included in the study for comparison and elimination of nonspecific proteins or proteins whose expression is affected as a result of the inhibitor only or other transcriptional changes. A total of 136 proteins were deregulated (> 1.5 fold-change (FC), $p \leq 0.05$) by **XD2-149** out of which 84 proteins were downregulated (Figure III-7A). The top 25 upregulated and downregulated proteins for each treatment are presented in Appendix Tables III-6-11. Comparative analysis with napabucasin and **XD2-162** showed 40 proteins that were exclusively downregulated by **XD2-149** (Figure III-7B, Tables III-3/4). Interestingly, STAT3 was among the

proteins exclusive for **XD2-149** with a $\log_2FC$ of -0.69. This downregulation was consistent with our Western blot results.

Among the downregulated proteins is the E3 ubiquitin-protein ligase ZFP91 that has been reported as a neo-substrate that can be recruited by CRBN-based PROTACs independent of the target protein.[46] Previous studies show that the nonspecific recruitment of ZFP91 was observed with CRBN ligase but not VHL possibly due to differences in the protein surface that allows CRBN to create high-affinity binding interfaces.[46] A pSILAC mass spectrometric study was performed for target identification of small molecules that can induce protein degradation.[48] The study identified ZFP91 as a substrate of lenalidomide-induced CRBN exploring the possibility of IMiD-induced repurposing of CRBN to target new proteins for degradation. The structural basis and mechanism for lenalidomide-induced CRBN-mediated degradation of proteins were reported to prove that protein recruitment is dependent on the presence of the IMiD that remodels the CRBN surface for binding of these proteins.[49] This intrigued us to test for the degradation of ZFP91 especially that **XD2-149** did not result in proteasome-dependent degradation of STAT3; the intended target protein. We performed Western blot experiments treating BxPC-3 cells with **XD2-149** and napabucasin for 16 h. Interestingly, ZFP91 protein was significantly downregulated by **XD2-149** at 1 µM while we observed no effect with napabucasin up to 3 µM (Figure III-8A). To determine whether this effect occurs at an earlier time point, we tested the effect of **XD2-149** after 4, 16 and 24 h. A significant decrease in the expression of ZFP91 was observed at a comparable DC_{50} for the 16 and 24 h treatments while the earlier time point showed no effect (Figure III-8B). Next, we repeated the experiment in the presence of the proteasome inhibitor carfilzomib to determine if the downregulation is a result of proteasome-dependent degradation. Gratifyingly, the results showed a restoration in the ZFP91 protein levels due to the blockade of the **XD2-149-**

induced degradation (Figure III-8C). We obtained similar results in MIA PaCa-2 cells (Appendix Figure III-5). This confirms that our PROTAC results in proteasome-dependent degradation of ZFP91 and provides a possible explanation for the lack of degradation effect on the STAT3 protein. Combining napabucasin with **XD2-149** did not affect the activity of the PROTAC suggesting it does not compete with napabucasin for its binding site (Figure III-8D).

Pomalidomide has been reported to induce the degradation of CRBN neo-substrates like ZFP91.[48] We sought to test its effect on ZFP91 in BxPC-3 cells to better understand the activity of our PROTAC. Pomalidomide displayed a DC_{50} of 0.42 µM, which is 5-fold less potent than the PROTAC (Figure III-8E). This result shows that although the pomalidomide moiety contributes to ZFP91-induced degradation, the PROTAC might be involved in a more stable ternary complex that results in more effective degradation. Moreover, pomalidomide does not show any cytotoxicity in the MTT assay up to 30 µM (Appendix Table III-4). We also tested for other targets like GSPT1 that might be recruited for proteasome-dependent degradation. However, **XD2-149** did not degrade GSPT, excluding the possibility that our PROTAC is non-selectively targeting CRBN neo-substrates (Figure III-8F). Other proteins that have also been reported as CRBN neo-substrates including IKZF1 and IKZF3,[50, 51] CK1α,[49] and ZBTB16[52] were not found among the proteins exclusively downregulated with **XD2-149** treatment.

ZFP91 is involved in various biological processes and among its oncogenic properties is the regulation of NF-κB signaling pathway and HIF-1α promoting tumorigenesis.[53, 54] It is also reported to play a role in ubiquitination and destabilization of FOXA1 to promote cancer cell survival.[55] In-depth understanding of the exact role of ZFP91 is lacking. However, the published data so far suggests that its inhibition or degradation could be beneficial as an anti-cancer strategy.

Consistent with the napabucasin reported mechanism of action, proteomics results for **XD2-149** show differential expression of proteins involved in cancer stemness and STAT3 signaling including downregulation of WNT16, DDR1, DSP, CST3, PLK1, DTX3L and CCNB1 (Table III-3) and upregulation of JUN, IL1RL1, RND3, ECM1, RHOB, EPHB3, UCUG and AKR1C2 (Table III-4). As previously discussed, **XD2-149** inhibits STAT3-driven transcription in the luciferase assay indicating that it acts through inhibition of the IL6-STAT3 pathway. Altered proteins in common between napabucasin, **XD2-149** and **XD2-162** include 10 downregulated proteins and 14 upregulated proteins presented in Appendix Tables III-12/13.

We performed gene set enrichment analysis (GSEA) to gain insight into the signaling pathways involved in the mechanism of action of **XD2-149** (Appendix Table III-21-28). Enriched gene sets for napabucsain and **XD2-162** are presented in Appendix Tables III-14-20 and III-29-36, respectively. GSEA analysis for **XD2-149** displayed nine upregulated and five downregulated enriched Hallmark gene sets (Figure III-7C/D). Comparison with napabucasin and **XD2-162** revealed enrichment of eight common upregulated Hallmark gene sets including TNFA signaling *via* NF-κB, hypoxia, IL2/STAT5 signaling, KRAS signaling, unfolded protein response, inflammatory response, apoptosis and coagulation (Appendix Figure III-6). These pathways are commonly altered with STAT3 inhibition suggesting napabucasin and its PROTAC work through inhibition of STAT3 signaling. The altered pathways are also possibly cumulative as a result of multiple actions. We mentioned earlier that ZFP91 is involved in regulation of NF-κB and HIF-1α pathways and our GSEA data shows upregulation of both pathways suggesting that these effects can be secondary to degradation of ZFP91. On the other hand, there are seven downregulated gene sets in common including E2F targets, DNA replication, mismatch repair, and telomere maintenance *via* semiconservative replication (Appendix Figure III-6). STAT3 plays a role in

regulation of cell cycle through activation of E2F targets including Cyclin D1, Cyclin B1 and Cdc2.[15, 56] This explains the observed downregulation in E2F targets that can result from STAT3 downregulation caused by napabucasin and **XD2-149** treatment. STAT3 is known to play an important role in cell proliferation through mechanisms that include suppression of ATR and modulation of DNA repair.[57] **XD2-149** was also found to downregulate the Hallmark interferon-alpha response gene set (Figure III-7D). IFN-α engages with its receptor and triggers the activation of STAT3. Studies have shown that STAT3 itself plays a role in regulating the IFN-mediated response.[58] This data is in accord with the reported experiments that STAT3 signaling is a major target pathway in the mechanism of action of napabucasin.
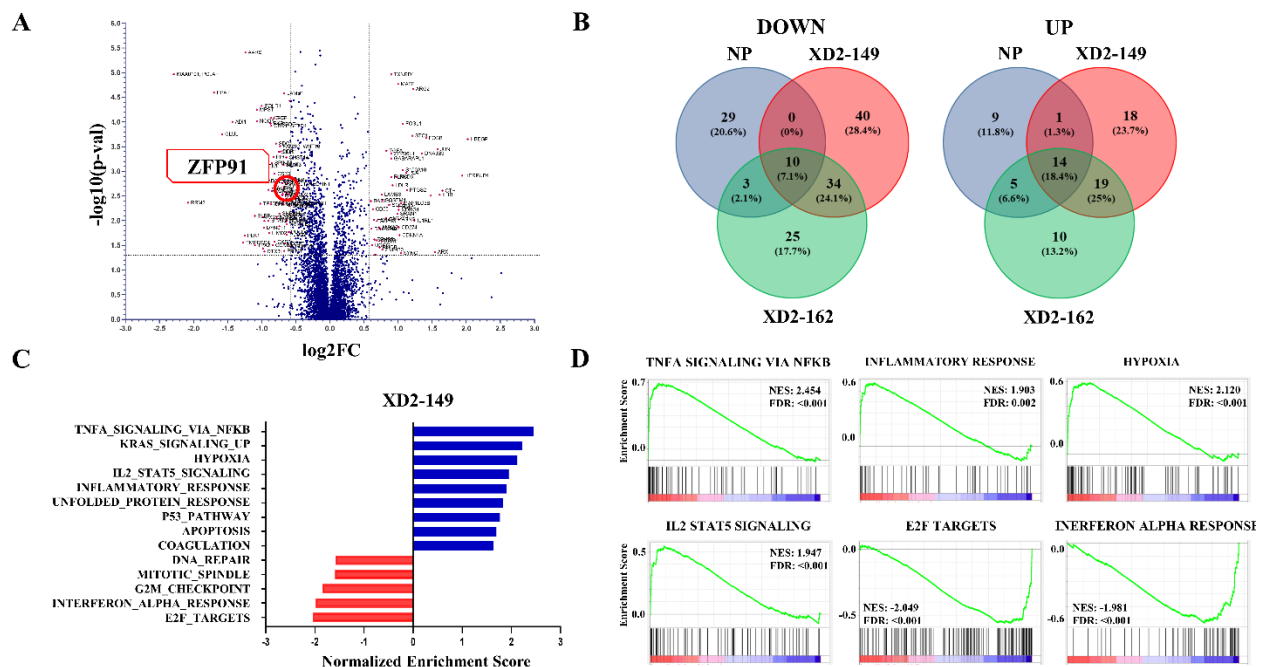
Figure III-7. Transcriptomic profile of **XD2-149** shows the exclusive downregulation of ZFP91 compared to napabucasin and the negative control in BxPC-3 cells with the enriched Hallmark gene sets presented. BxPC-3 cells were treated with **XD2-149** (2 µM), napabucain (2 µM) and **XD2-162** (4 µM) for 16 h. (A) Volcano plot for **XD2-149** proteins. The significant upregulated and downregulated proteins are colored in pink. (FC > 1.5 and *p*-value ≤ 0.05). (B) Venn diagram showing the overlap of common proteins between the three treatments and the exclusive proteins for each. Significant proteins > 1.5 FC and *p*-value ≤ 0.05 were used to generate the diagram. (C) Upregulated and downregulated enriched Hallmark gene sets from GSEA analysis of **XD2-149**. (D) Select enrichment plots for the top upregulated and downregulated enriched gene sets from GSEA analysis of **XD2-149.**
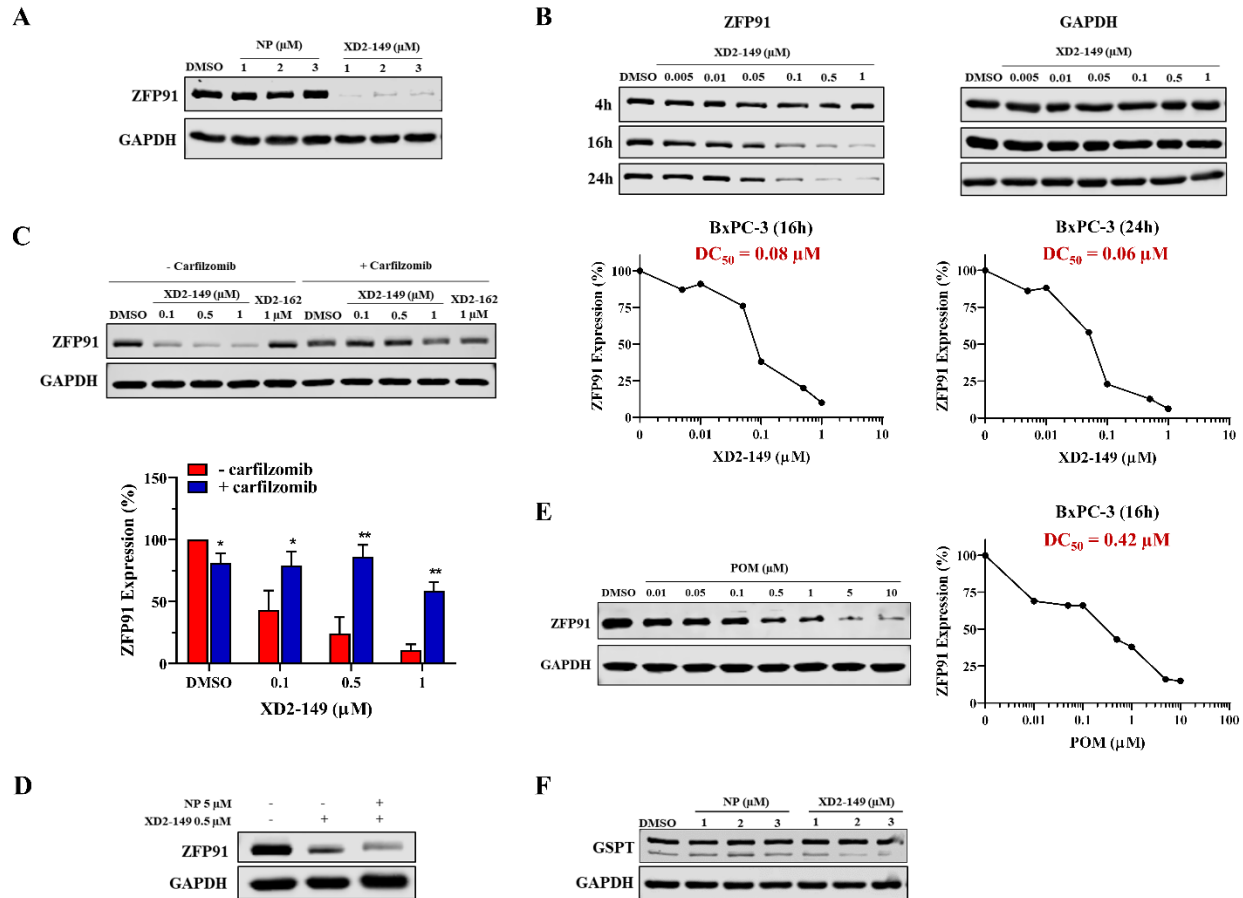
Figure III-8. **XD2-149** degrades ZFP91 protein in a proteasome-dependent manner. (A) **XD2-149** reduces ZFP91 expression while napabucasin (NP) has no effect. BxPC-3 cells were treated with NP or **XD2-149** at the indicated concentrations for 16 h. (B) **XD2-149** degrades ZFP91 at 16 and 24 h with no effect at 4 h. Dose-response curves of ZFP91 degradation by **XD2-149** are presented for the 16 and 24 h time-points. (C) The effect of **XD2-149** on ZFP91 is proteasome-dependent. BxPC-3 cells were pretreated with 1 µM of the proteasome inhibitor carfilzomib for 1 h followed by **XD2-149** or **XD2-162** treatment for 16 h. Data were generated from three biological replicates and are presented as mean ± SD. (D) NP does not abolish the effect of **XD2-149**. BxPC-3 cells were treated with **XD2-149** in presence or absence of NP for 16 h. (E) Pomalidomide (POM) induces ZFP91 degradation after 16 h. (F) **XD2-149** have no effect on the expression of GSPT. BxPC-3 cells were treated with NP or **XD2-149** for 16 h. Immunoblots were quantified using ImageJ and the DC_{50} values were calculated using GraphPad Prism 8. Data from panels A, B, D, and E are from a single experiment. * denotes $p \leq 0.05$, ** denotes $p \leq 0.01$, *** denotes $p \leq 0.001$.

Table III-3. Downregulated proteins exclusive to **XD2-149** treatment in BxPC-3 cells.

No	Gene Symbol	Name	Log_2FC^a	p-value[b]
1	TMPRSS4	Transmembrane protease serine 4	-1.27	0.028
2	PLK1	Serine/threonine-protein kinase PLK1	-1.25	0.020
3	TP53BP2	Apoptosis-stimulating of p53 protein 2	-1.02	0.005
4	DYNLT1	Dynein light chain Tctex-type 1	-0.97	0.014
5	DTX3L	E3 ubiquitin-protein ligase DTX3L	-0.96	0.042
6	MAGED1	Melanoma-associated antigen D1	-0.9	0.002
7	STAT2	Signal transducer and activator of transcription 2	-0.9	0.010
8	CBR1; SETD4	Carbonyl reductase [NADPH] 1	-0.86	<0.001
9	SPINT1	Kunitz-type protease inhibitor 1	-0.85	0.001
10	CCNB1	G2/mitotic-specific cyclin-B1	-0.84	0.031

11	EDF1	Endothelial differentiation-related factor 1	-0.82	<0.001
12	CST3	Cystatin-C	-0.81	0.001
13	NABP2	SOSS complex subunit B1	-0.78	0.008
14	WDFY4	WD repeat- and FYVE domain-containing protein 4	-0.78	0.009
15	CSDE1	Cold shock domain-containing protein E1	-0.75	<0.001
16	SHPRH	E3 ubiquitin-protein ligase SHPRH	-0.74	0.007
17	FAM3C; WNT16	Protein FAM3C	-0.73	<0.001
18	DDR1	Epithelial discoidin domain-containing receptor 1	-0.73	<0.001
19	DSP	Desmoplakin	-0.70	0.002
20	GPR56; ADGRG1	Adhesion G-protein coupled receptor G1	-0.69	0.004
21	STAT3	Signal transducer and activator of transcription 3	-0.69	0.001
22	LTV1	Protein LTV1 homolog	-0.69	0.003
23	AGRN	Agrin	-0.68	0.001
24	SDF4	45 kDa calcium-binding protein	-0.67	0.002
25	LAMB1	Laminin subunit beta-1	-0.67	<0.001
26	UBE2T	Ubiquitin-conjugating enzyme E2 T	-0.66	0.029
27	PHLDB1	Pleckstrin homology-like domain family B member 1	-0.64	0.009
28	CHST14	Carbohydrate sulfotransferase 14	-0.64	0.001
29	PLOD2	Procollagen-lysine,2-oxoglutarate 5-dioxygenase 2	-0.63	0.019
30	PVRL1; NECTIN1	Nectin-1	-0.63	0.002
31	PRRC2B	Protein PRRC2B	-0.63	0.003
32	MGMT	Methylated-DNA--protein-cysteine methyltransferase	-0.63	0.004
33	NSMCE2	E3 SUMO-protein ligase NSE2	-0.63	0.012
34	ZFP91	E3 ubiquitin-protein ligase ZFP91	-0.62	0.002
35	SERF2	Small EDRK-rich factor 2	-0.61	0.002
36	POLD4	DNA polymerase delta subunit 4	-0.61	0.017
37	PRDM16	Histone-lysine N-methyltransferase PRDM16	-0.6	0.033
38	CIAPIN1	Anamorsin	-0.59	<0.001
39	CCNDBP1	Cyclin-D1-binding protein 1	-0.59	0.005
40	USP8	Ubiquitin carboxyl-terminal hydrolase 8	-0.59	0.008

[a]FC > 1.5
[b]p-value ≤ 0.05

Table III-4. Upregulated proteins exclusive to **XD2-149** treatment in BxPC-3 cells.

No	Gene Symbol	Name	Log_2FC[a]	p-value[b]
1	JUN	Transcription factor AP-1	1.58	<0.001
2	ARX	Homeobox protein ARX	1.54	0.043
3	DNAJB9	DnaJ homolog subfamily B member 9	1.35	<0.001
4	IL1RL1	Interleukin-1 receptor-like 1	1.24	0.010
5	SYNC	Syncoilin	1.04	0.045
6	RND3	Rho-related GTP-binding protein RhoE	0.98	0.001
7	HMGCR	3-hydroxy-3-methylglutaryl-coenzyme A reductase	0.83	0.009
8	ZNF430	Zinc finger protein 430	0.77	0.039
9	ECM1	Extracellular matrix protein 1	0.76	0.026
10	RHOB	Rho-related GTP-binding protein RhoB	0.73	0.035
11	GDF15	Growth/differentiation factor 15	0.69	0.010
12	ABCB6	ATP-binding cassette sub-family B member 6, mitochondrial	0.68	0.025
13	AFF1	AF4/FMR2 family member 1	0.67	0.049
14	MPV17	Protein Mpv17	0.66	0.049
15	EPHB3	Ephrin type-B receptor 3	0.65	0.024
16	UGCG	Ceramide glucosyltransferase	0.62	0.032
17	AKR1C2	Aldo-keto reductase family 1 member C2	0.6	0.004

| 18 | BACH1 | Transcription regulator protein BACH1 | 0.6 | 0.004 |

[a]FC > 1.5
[b]p-value $\leq$ 0.05

XD2-149 cytotoxicity is partially dependent on ZFP91

Until now, there are no reported ZFP91-targeted anticancer therapies. A previous study on the kinase inhibitor foretinib demonstrated that GSPT1 and ZFP91 proteins are neo-substrates for the CRBN-based PROTAC but did not investigate their contribution to its anticancer activity.[46] ZFP91 regulates different pathways that are involved in tumorigenesis and its targeting will present a novel class of anti-cancer agents.[54, 55] ZFP91 is highly expressed in pancreatic cancer cells and is associated with lower overall survival (Figure III-9A).[59] Knockdown studies of ZFP91 in pancreatic cancer cells demonstrated reduced cell growth.[60] To determine whether the cytotoxicity of **XD2-149** is dependent on ZFP91, we knocked down the protein in BxPC-3 using siRNA (Figure III-9B). This resulted in a significant reduction ($p < 0.01$) in the cytotoxicity of **XD2-149** after a 48-h treatment in MTT providing evidence to the importance of ZFP91 for its anti-cancer activity (Figure III-9C).

ID	scrRNA	siZFP91
NP	1.3 ± 0.2	1.8 ± 1.1
XD2-149	1.2 ± 0.1	2.1 ± 0.3
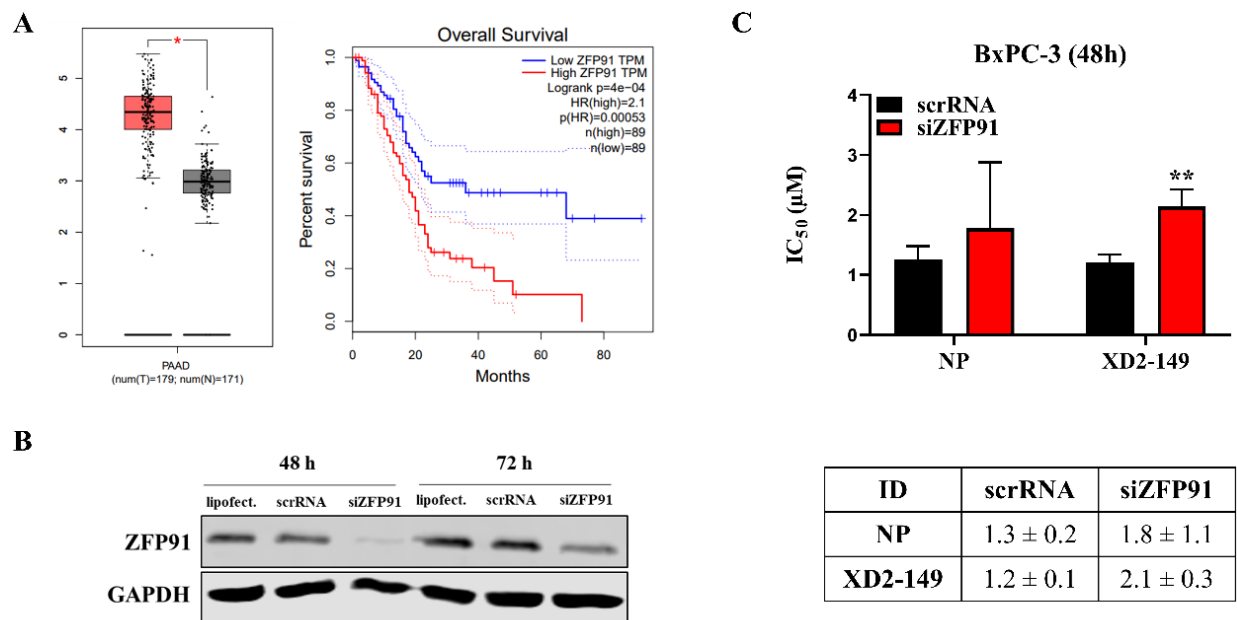
Figure III-9. Cytotoxicity of **XD2-149** is partially dependent on ZFP91. (A) Expression levels of ZFP91 in normal (grey) and pancreatic adenocarcinoma (PAAD) (red) tissues and the overall survival with low vs high ZFP91 expression in PAAD. The data

were obtained from the GEPIA2 web server that is based on TCGA and GTEx databases. (B) siRNA knockdown of ZFP91 in BxPC-3 cells after 48 and 72 h. (C) IC$_{50}$ values of **XD2-149** show significant reduction in its cytotoxicity with ZFP91 knockdown compared to the siRNA control cells (scrRNA). BxPC-3 cells were treated with siZFP91 and NP or **XD2-149** for 48 h in the MTT assay. Data were generated from three biological replicates and are presented as mean ± SD. ** denotes $p \leq 0.01$.

NQO1-mediated cytotoxicity of XD2-149 is independent of ZFP91

To further study the cell death mechanisms that contribute to the cytotoxicity of **XD2-149**, we examined the mechanism induced by napabucasin to determine if they kill the cells similarly. As previously mentioned, NQO1 activates napabucasin to induce ROS and subsequently kill the cancer cells.[22] In the presence of the NQO1 inhibitor, dicoumarol (DIC), napabucasin and **XD2-149** displayed reduced colony formation in BxPC-3 and MIA PaCa-2 cells (Figure III-10A). These results suggest that the cell death mechanism of **XD2-149** is similar to napabucsain and is dependent on NQO1. To determine whether the NQO1-induced cytotoxicity is associated with ZFP91, we tested for the ZFP91 levels when treated with the PROTAC in the presence of DIC. The presence of DIC did not alter the ZFP91 levels suggesting a ZFP91-independent cell death mechanism (Figure III-10B).
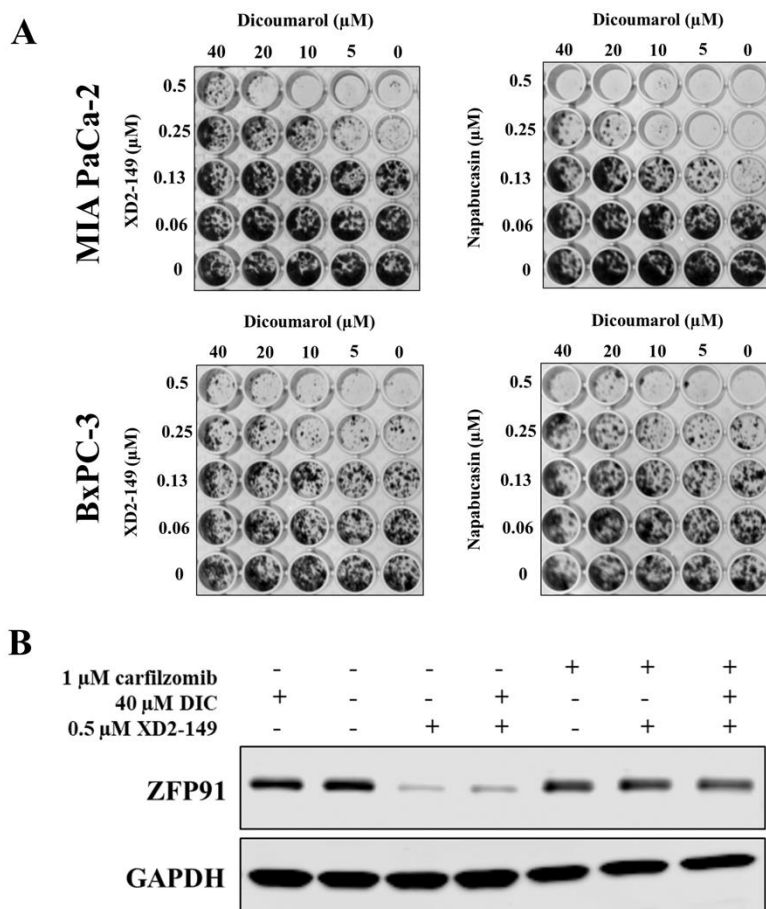
Figure III-10. NQO1-induced cytotoxicity of **XD2-149** is independent of ZFP91. (A) Dicoumarol partially rescues the cell death caused by **XD2-149** in CFA. BxPC-3 and MIA PaCa-2 cells were treated with **XD2-149** or napabucsain for 7-10 days. (B) Dicoumarol (DIC) effect is independent of ZFP91. BxPC-3 cells were treated with **XD2-149** in absence or presence of DIC for 16 h. The proteasome inhibitor carfilzomib was added 1 hr prior to the treatments. Data presented are from a single experiment.

Conclusions

We synthesized and tested a series of napabucasin-based PROTACs for targeting STAT3. We optimized the linker and the E3 ligase ligand to produce the lead compound **XD2-149** that showed significant cytotoxicity in several cancer cell lines. Although **XD2-149** resulted in inhibition of IL6/STAT3 pathway signaling, its effect was independent of the proteasome-mediated STAT3 degradation. GSEA of the proteomics data revealed several gene sets that indicated the STAT3 and other signaling pathways were targeted. Proteomics and Western blot analyses identified and validated a proteasome-dependent degradation of ZFP91 by **XD2-149**. The PROTAC was more effective in degrading ZFP91 than the IMiD pomalidomide. Furthermore, we

132

confirmed that the cytotoxicity of **XD2-149** is partially dependent on ZFP91. We also demonstrated that NQO1 contributes to the cytotoxicity of **XD2-149** independent of ZFP91 which suggests that the PROTAC kills the cancer cells *via* multiple cell death mechanisms. ZFP91 is an oncogenic protein that has been studied for its potential as an anticancer target and further optimization may lead to the development of potent degraders of ZFP91 for anticancer therapy.

Experimental Section

General methods. Reagents and anhydrous solvents were purchased from commercial sources and used without further purification. Reaction progress was monitored by UV absorbance using thin-layer chromatography (TLC) on aluminum-backed precoated silica plates from Silicycle (SiliaPlate, 200 μm thickness, F254). Glassware for reactions were oven-dried in preparation, and reactions were performed using nitrogen or argon atmosphere using standard inert conditions. ^{1}H NMR spectra were obtained using a Bruker (300 or 400 MHz) instrument. Purifications using flash chromatography were performed using a Biotage Isolera chromatography system (25 μM spherical silica). Column chromatography was performed on silica gel (200−300 mesh), and preparative TLC was performed on UV 254 (0.5 mm thickness, Sigma-Aldrich). A Shimadzu LCMS 20-20 system was utilized for generating HPLC traces, obtaining mass spectrometry data, and evaluating purity. The system is equipped with a PDA UV detector and Kinetex 2.6 μm, XB-C18 100 Å, 75 mm × 4.6 mm column, which was used at room temperature. HPLC gradient method utilized a 1% to 90% MeCN in H_2O with 0.01% formic acid over 15 min with a 0.50 mL/min flow rate. Purity of the final compounds is ≥95% and was assessed at 254 nm using the described column and method.

Cell culture. Cell lines were maintained in RPMI-1640 or DMEM supplemented with 10% fetal bovine serum (FBS) (ThermoFisher Scientific). The cells were grown as monolayer cultures at 37

°C in a humidified atmosphere of 5% CO_2 and tested for *Mycoplasma* contamination with the *Mycoplasma* detection kit, PlasmaTest (InvivoGen). BxPC-3 cell line was authenticated with STR DNS profiling (University of Michigan Sequencing Core) and matched to reference profiles from the ATCC database. The STAT3-knockout cell lines were generated in our laboratory using CRISPR Cas9.[38]

Cytotoxicity assays. For MTT assay, the experiments were carried out in 96-well plates where cells (3000-6000 cells/well) were seeded in the medium and incubated overnight. The compounds or the vehicle (DMSO) were added to the cells the following day and incubated for 3 days. MTT solution (0.3 mg/ml) was added to the wells and plates were incubated for 3h at 37 °C after which MTT was discarded and cells were dissolved in DMSO. The absorbance of the formazan crystals was read by a microplate reader (Molecular Devices) at 570 nm and the data were analyzed using GraphPad Prism 8 software. For colony formation assays, the cells (200-500 cells/well) were seeded in 96-well plates overnight and then treated with DMSO or the compound for 7-10 days until 80% confluency. After colony formation, the medium was removed and the cells were stained with 0.05% crystal violet, washed with water and imaged with iBright™ imaging system (Invitrogen). The colonies were dissolved in Sorensen buffer (0.1 M sodium citrate, pH 4.2) for colorimetric quantification.

Western blot analysis. Cells were seeded (OVCAR-3: 500 x 10^3, MIA PaCa-2: 200 x 10^3, BxPC-3: 500 x 10^3 cells/well) in 6-well plates. Following treatment, cells were lysed at 4 °C by sonication with lysis buffer (25 mM tris(hydroxymethyl)aminomethane, 150 mM NaCl, 17 mM Triton X-100, 3.5 mM SDS, pH 7.4) supplemented with protease inhibitor and phosphatase inhibitor. The cells were then spun at 12,000 rpm at 4 °C for 10 min and collected for determining the protein concentration with the BCA assay (ThermoFischer Scientific, Waltham, MO). Samples were then

prepared and loaded onto 10 or 12 % acrylamide (BioRad, Hercules, CA) gels followed by the transfer of the proteins onto PVDF membranes (EMD Millipore, La Jolla, CA). The membranes were blocked for 1 h prior to incubation with the primary antibodies using Odyssey blocking buffer (LI-COR Biosciences). Membranes were then probed for STAT3/pSTAT3/STAT1/NQO1 (Cell Signaling, Danvers, MA, 1:1000), GAPDH (Cell Signaling, Danvers, MA, 1:4000), GSPT (Cell signaling, 1:1000), ZFP91 (Bethyl, 1:1000). Following overnight incubation with the primary antibodies at 4 °C, the membranes were incubated with the secondary antibodies (anti-rabbit, Cell Signaling, 1:7500 or anti-mouse, Cell Signaling, 1:5000) for 1 h and imaged with the Odyssey imaging system (LI-COR Biosciences).

STAT3 luciferase reporter assay. The GloResponse[TM] SIE-*luc2P* HEK-293 cells (10,000 cells/well) were seeded in a 96-well plate (white, opaque bottom) and incubated overnight. On day 2, IL6 (100 ng/ml) was added to the cells for 24 h to induce activation of the STAT3 pathway. The compounds were then added for 24 h after which the Bio-Glo[TM] luciferase assay reagent (Promega # G7940) was added to each well. The luminescence was measured after 5 min using a plate reader. An MTT assay in HEK-293 was performed in parallel treating the cells with the compounds for 24 h.

Protein identification and relative quantitation by TMT labeling and LC-Tandem MS. BxPC-3 cells were treated with DMSO (control), napabucasin (2 µM), **XD2-149** (2 µM) or **XD2-162** (4 µM) for 16 h then collected and lysed in RIPA buffer (Pierce, #89900) at 4 °C. The control and **XD2-149** treatments were carried out in triplicate while napabucasin and **XD2-162** were carried out in duplicate. Protein samples were then collected and the concentrations were determined using the BCA assay (ThermoFisher Scientific). Samples were prepared in a concentration of 75 µg and submitted to the Proteomics Core in the Department of Pathology at

University of Michigan. Tandem mass tag (TMT) labeling was performed using the TMT 10plex™ isobaric labeling kit (ThermoFisher Scientific, #90110) according to the manufacturer's protocol with minor modifications. This involves reduction of the samples with DTT (1 h, 55 ℃) followed by alkylation with 2-chloroacetamide (30 min, RT). Proteins were precipitated using cold acetone overnight. Next, the proteins were pelleted and resuspended in TEAB to which trypsin (Promega, V5113) was added for digestion (overnight, 37 ℃). TMT reagents were reconstituted in anhydrous acetonitrile and the digested peptides were transferred to TMT reagent vials and incubated at RT for 1 h. The reaction was quenched with 5% hydroxylamine for 15 min then samples were combined and dried. Prior to MS analysis, two-dimensional separation of the sample was performed. For the first dimension, an offline fractionation of an aliquot of each sample into 10 fractions was performed following the manufacturer's protocol (Pierce, #84868). Fractions were then dried and reconstituted in loading buffer (0.1% formic acid and 2% acetonitrile). For quantitation, the MultiNotch-MS3 method was employed[61]. MS was performed on the Orbitrap Fusion Tribrid with ETD (ThermoFisher Scientific) equipped with nano-LC system (Dionex RSLC-nano). Proteome discoverer (v2.1, ThermoFisher Scientific) was used for data analysis. MS2 spectra were searched against SwissProt human protein database. The abundance ratio data sets were transformed to $\log_2 FC$ values and the whole protein list was used for GSEA analysis (GSEA 4.0.3). For ranking, the proteins were filtered applying a FC cut-off of 1.5 and p-val ≤ 0.05. All proteins have experimental q-val of < 0.1.

siRNA knockdown of ZFP91. ZFP91 siRNA (hs.Ri.ZFP91.13.1, Integrated DNA Technologies) or scrambled negative control siRNA (#51-01-19-09, Integrated DNA Technologies) with Lipofectamine RNAiMAX transfection reagent (ThermoFisher Scientific) was added to BxPC-3 cells in Opti-MEM medium (ThermoFisher Scientific) for 48 and 72 h after which the cells were

harvested for immunoblotting. The siRNA transfection reagent complex was prepared following the manufacturer's instructions. Briefly, 30 pmol of siRNA in 150 µl of Opti-MEM medium were added to 9 µl of the lipofectamine reagent in 150 µl of Opti-MEM medium. After 5 min incubation at room temperature, the siRNA transfection complex was added to each well in a 6-well plate. For MTT assay, 5 pmol of siRNA in 25 µl of Opti-MEM medium were added to 1.5 µl of the lipofectamine reagent in 25 µl of Opti-MEM medium. After 5 min incubation at room temperature, 10 µl of the siRNA transfection complex was added to each well in a 96-well plate. **XD2-149** or napabucasin was added to the cells simultaneously with the siRNA transfection reagent complex for 48 h to determine their cytotoxicity.

Cellular Thermal Shift Assay (CETSA). Cells were seeded in 10 cm cell culture dish. After overnight attachment, cells were trypsinized, washed with DPBS, and suspended in DPBS with protease inhibitor for cell lysis. Samples were subject to freeze/thaw cycles three times and spun at 13000 rpm for 10 min. The cell lysate was incubated with DMSO (control) or napabucasin (100 µM) for 1 h at room temperature. Following treatment, each sample was split into 50 µL aliquots, heated at indicated temperatures for 3 min in a Veriti Thermal Cycler (Applied Biosystems), and incubated for 3 min at room temperature. The samples were then centrifuged at 13000 rpm for 20 min and the supernatants were collected for western blotting following the previously mentioned procedure.

Statistical analysis. Significance levels for assays and immunoblots were calculated using unpaired Student's *t*-test in GraphPad Prism. Results are shown as mean ± standard deviation from three independent experiments.

Appendix
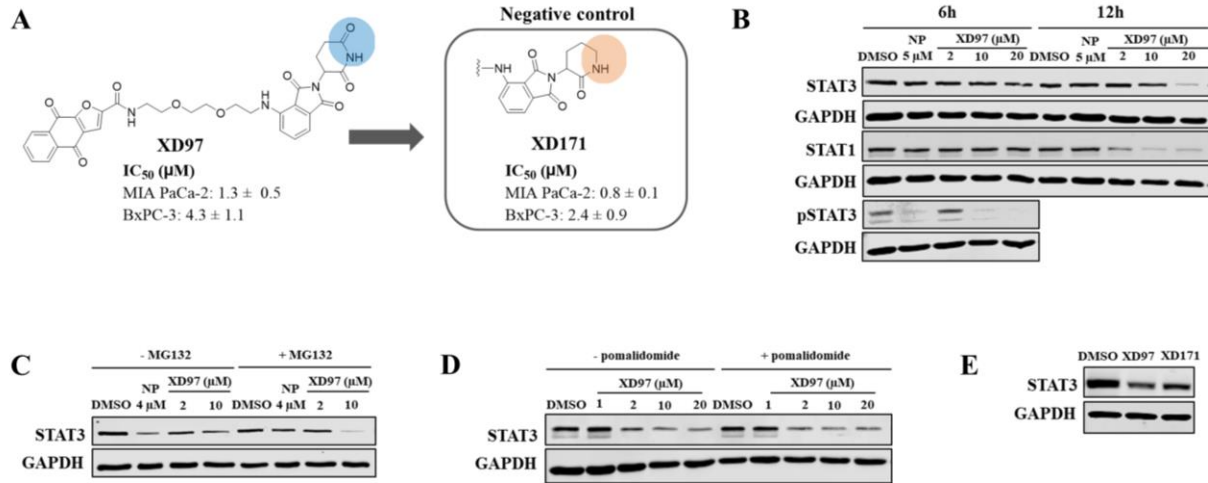
Appendix Figure III-1. **XD97** non-selectively reduces STAT3 expression in OVCAR-3 cells in a proteasome-independent manner. (A) Design of the negative control **XD171**. IC$_{50}$ values correspond to the cytotoxicity of the compounds in MTT assay. (B) **XD97** dose-dependently decreases STAT1 expression at 12 h with no effect at 6 h, similar to STAT3. (C) Effect of **XD97** on STAT3 is proteasome-independent. Cells were pretreated with or without 20 µM of the proteasome inhibitor MG132 for 1 h followed by **XD97** or NP for 24 h. (D) The CRBN ligand pomalidomide does not compete with **XD97** for its effect on STAT3. Cells were pretreated with or without 10 µM pomalidomide for 1 h followed by **XD97** for 12 h. (E) **XD97** and the negative control **XD171** reduce STAT3 expression at 12 h. Cells were treated with 10 µM of **XD97** or **XD171** for 12 h. Data presented are from a single experiment.
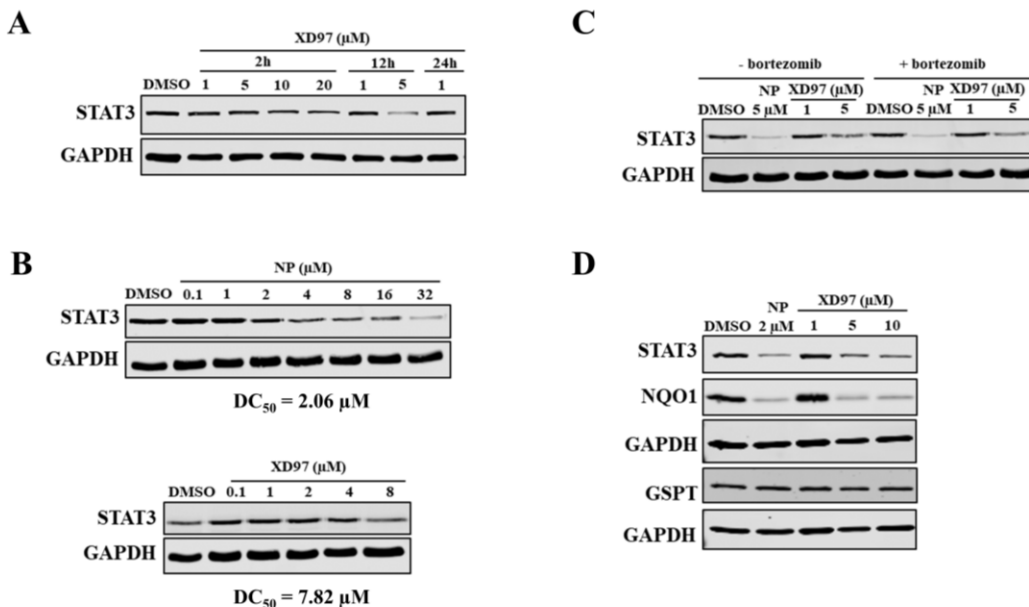
Appendix Figure III-2. **XD97** non-selectively reduces STAT3 expression in BxPC-3 cells in a proteasome-independent manner. (A) **XD97** reduces STAT3 expression in a dose-dependent manner at different time-points. Cells were treated with **XD97** at the indicated concentrations and time-points. (B) Napabucasin (NP) and **XD97** result in dose-dependent decrease in STAT3 expression at 12 h. Immunoblots were quantified using ImageJ and DC$_{50}$ was calculated using GraphPad Prism 8. (C) Effect of **XD97** on STAT3 is proteasome-independent. Cells were pretreated with or without 1 µM of the proteasome inhibitor bortezomib for 2 h then

XD97 or NP for 12 h. (D) NP and **XD97** reduce NQO1 expression with no effect on GSPT. Cells were treated with NP or **XD97** at the indicated concentrations for 16 h. Data presented are from a single experiment.
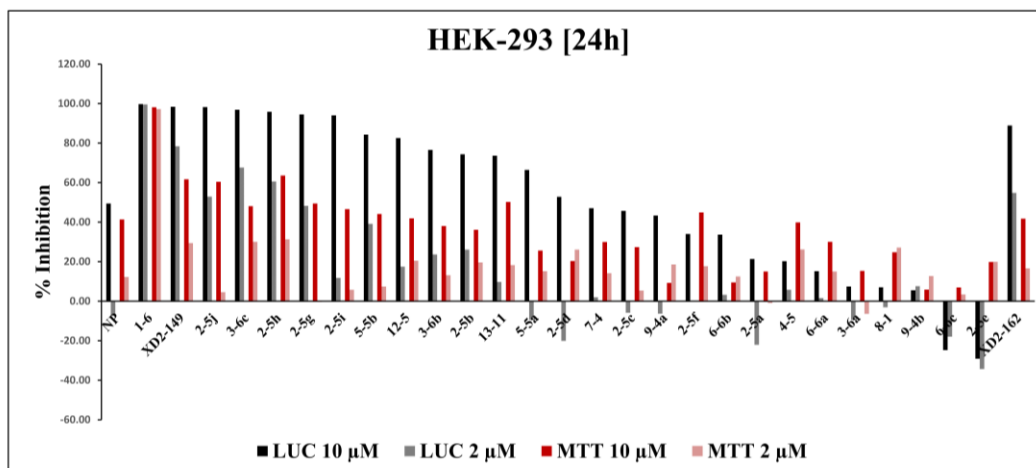
Appendix Figure III-3. Synthesized compounds inhibit IL6-dependent STAT3 pathway. The STAT3 luciferase assay (LUC) was carried out where HEK-293 cells were pretreated with 100 ng/ml of IL6 for 24 h followed by 2 or 10 µM of each compound for 24 h. The luciferin substrate was then added and the luminescence was measured to detect STAT3 pathway activation. Cytotoxicity of the compounds was determined in HEK-293 cells at the same time-point (24 h) using an MTT assay. Data presented are from a single experiment.
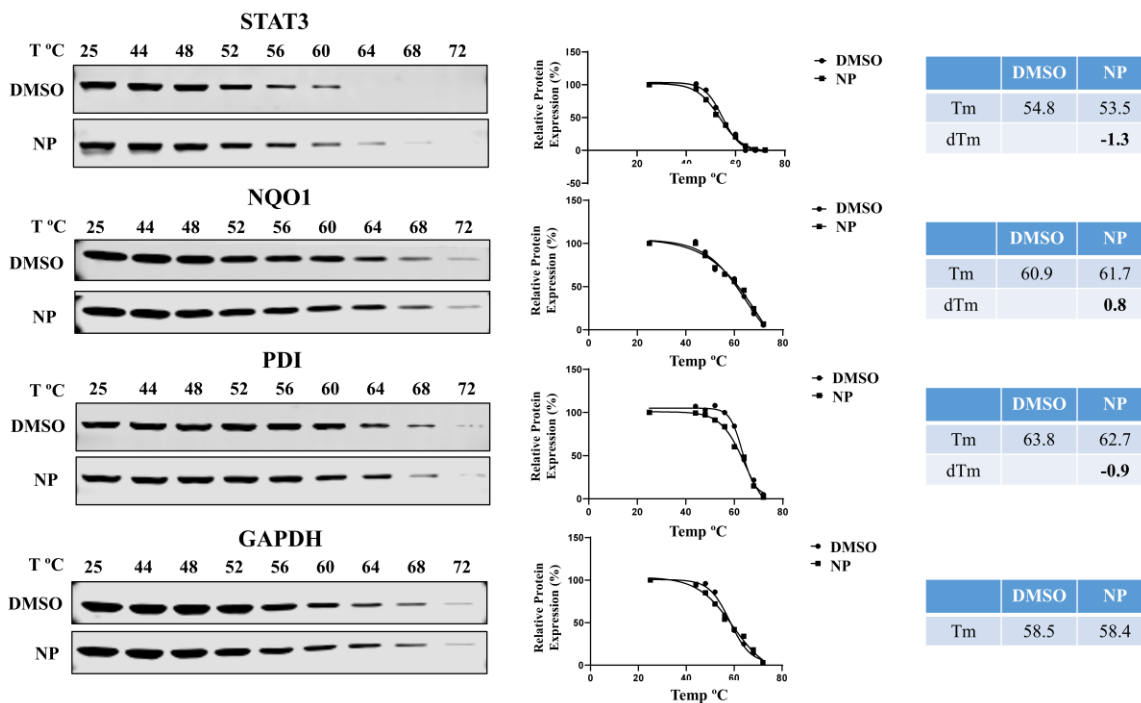
Appendix Figure III-4. Napabucasin alters the thermal stability of STAT3, NQO1 and PDI. The cell lysate of BxPC-3 cells was treated with DMSO (control) or napabucasin (NP, 100 µM) for 1 h. A slight shift was observed with all proteins except GAPDH. Data presented are from a single experiment.
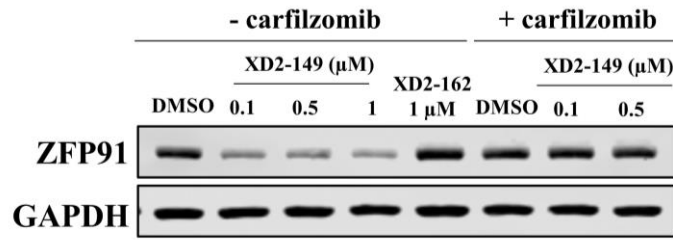
Appendix Figure III-5. **XD2-149** results in proteasome-dependent degradation of ZFP91 in MIA PaCa-2 cells. Cells were pretreated with carfilzomib (1 µM) for 1h followed by compound treatment for 16 h. Data presented are from a single experiment.

A
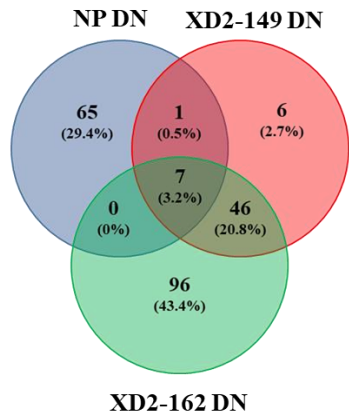
No	Set
1	GO_4_IRON_4_SULFUR_CLUSTER_BINDING
2	GO_METAL_CLUSTER_BINDING
3	KEGG_DNA_REPLICATION
4	GO_TELOMERE_MAINTENANCE_VIA_SEMI_CONSERVATIVE_REPLICATION
5	GO_NUCLEAR_DNA_REPLICATION
6	KEGG_MISMATCH_REPAIR
7	HALLMARK_E2F_TARGETS

B
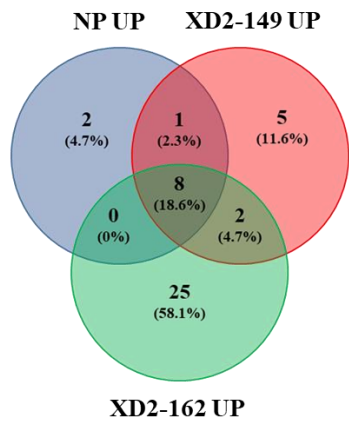
No	Set
1	HALLMARK_TNFA_SIGNALING_VIA_NFKB
2	HALLMARK_UNFOLDED_PROTEIN_RESPONSE
3	HALLMARK_KRAS_SIGNALING_UP
4	HALLMARK_IL2_STAT5_SIGNALING
5	HALLMARK_HYPOXIA
6	HALLMARK_INFLAMMATORY_RESPONSE
7	HALLMARK_COAGULATION
8	HALLMARK_APOPTOSIS

Appendix Figure III-6. Upregulated and downregulated gene sets in common between napabucasin (NP), **XD2-149** and **XD2-162**.

Appendix Table III-1. Summary of cancer clinical trials reported on napabucasin.

No	Study	Clinical phase	Cancer type	Outcome	Year
1	NCT02024607 Combination FOLFIRI +/- bevacizumab	Ib/II	Colorectal cancer (metastatic)	Safe combination and encouraging signs of efficacy[62]	2017
2	NCT02315534 Combination with temolomide	Ib/II	Glioblastoma (recurrent)	Safe combination and encouraging antitumor activity[63]	2017
3	NCT01776307 Combination with panitumumab	Ib/II	Colorectal cancer (metastatic)	Safe combination and encouraging antitumor activity[64]	2017
4	NCT01775423 Monotherapy	I	Solid tumors (advanced)	Signs of anticancer activity[65]	2017
5	NCT01830621 (with best supportive care)	III	Colorectal cancer (pretreated advanced)	No difference in overall survival[66]	2018
6	NCT02231723 Combination + nab-paclitaxel and gemcitabine]	Ib/II	Pancreatic cancer (metastatic)	Well tolerated with encouraging signs of activity[8]	2018
7	NCT02178956 Combination with paclitaxel "The BRIGHTER trial"	III	Gastric and gastroesophageal cancer (pretreated advanced)	No improvement in overall survival/progression-free survival[67]	2018
8	NCT01325441 Combination with paclitaxel	Ib	Thymoma and thymic carcinoma (advanced)	Clinical activity and reasonable clinical safety[68]	2018
9	NCT02851004 Combination with pembrolizumab	I/II	Colorectal cancer (metastatic)	Preliminary efficacy and acceptable toxicity[69]	2018
10	NCT02993731 Combination + nab-paclitaxel with gemcitabine	III	Pancreatic cancer (metastatic)	Announced to be discontinued due to futility[9]	2019
11	JapicCTI-142420 Combination with paclitaxel	I	Gastric cancer (pretreated unresectable or recurrent)	Well tolerated[70]	2019

Appendix Table III-2. Cytotoxicity of compounds in a panel of cancer cell lines.

ID	IC$_{50}$ (µM)

	HCT116	MCF-7	HepG2	U-87	A549	OVCAR-8
NP[a]	0.4	0.4, 0.5	1.1	0.7	3.4	2.0
6-6b	10.4	2.5, 5.3	>30	16.1	9.3	10.2
2-5b	3.9	2.4, 2.3	4.0	1.6	8.9	6.9
2-5c	2.0	1.7, 1.7	1.6	0.9	8.2	4.9
2-5d	3.0	1.6, 2.1	1.6	0.8	5.8	6.7
2-5g, XD97	1.9	1.5, 0.1	3.4	1.5	8.5	3.2
6-6a	22.7	15.4, 17.8	>30	11.5	>30	>30
6-6c	19.3	9.4, 11.1	19.8	3.5	>30	22.1
2-5e	2.9	2.3, 3.1	1.8	1.5	4.7	8.50
2-5h	2.2	2.2, 0.9	4.5	1.1	10.2	5.1
5-5a	3.1	2.0, 3.0	3.2	1.1	5.4	7.7
2-5f	2.8	2.2, 1.2	3.4	1.3	14.1	4.8
5-5b	3.7	3.4	11.8	2.1	25.2	NT[b]
2-5a	2.5	1.8	2.6	0.7	5.4	NT
2-5i	3.4	1.8	7.1	1.2	9.3	NT
12-5	4.1	3.7	7.7	4.2	15.1	NT

[a]Napabucasin
[b]NT: Not tested
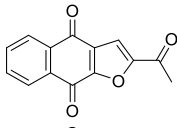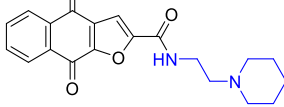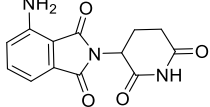
Appendix Table III-3. Cytotoxicity of compounds in STAT3 WT and KO cell lines.

ID	IC$_{50}$ (µM)			
	OVCAR-3	OVCAR-3 STAT3 KO	SK-OV-3	SK-OV-3 STAT3 KO
NP[a]	0.7, 0.5	1.2, 0.9	2.0	3.0
6-6b	2.7, 2.0	12.2, 10.9	7.7	10.7
2-5b	1.6, 1.3	4.1, 4.4	6.0	9.8
2-5c	1.2, 0.5	4.0, 3.1	4.8	7.7
2-5d	1.3, 1.0	2.9, 3.3	3.5	5.4
2-5g, XD97	0.1, 0.3	2.2, 2.1	4.0	5.3
6-6a	17.3, 19.0	22.9, 21.1	>30	>30
6-6c	8.7, 8.4	17.8, 18.0	>30	>30
2-5e	1.5	4.6	NT[b]	NT
2-5h	0.5	2.2	NT	NT
5-5a	1.1	3.5	NT	NT
2-5f	0.6	3.4	NT	NT
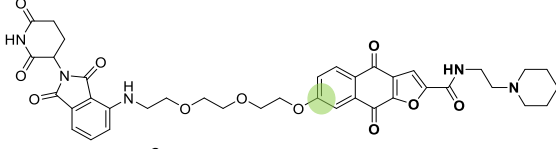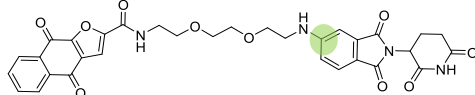
[a]Napabucasin

Appendix Table III-4. Cytotoxicity of small molecules in pancreatic cancer cell lines.

ID	Structure	MW	cLogP	IC$_{50}$ (µM)	
				MIA PaCa-2	BxPC-3
NP[a]		240.21	2.19	1.2 ± 0.8	1.4 ± 0.3
1-6		352.39	3.28	0.1 ± 0.0	0.1 ± 0.1
POM[b]		273.25	-0.19	>30	>30

[a]Napabucasin
[b]Pomalidomide

Appendix Table III-5. Cytotoxicity for CRBN-based PROTACs displaying different linker attachment positions in pancreatic cancer cell lines – positions highlighted in green.

ID	Structure	MW	cLogP	IC$_{50}$ (µM)	
				MIA PaCa-2	BxPC-3
13-11		755.78	3.44	3.9 ± 1.1	4.2 ± 0.6
12-5		628.59	2.18	3.1 ± 0.4	7.9 ± 1.9

Appendix Table III-6. Top 25 upregulated proteins for napabucasin treatment in BxPC-3 cells.

No	Symbol	Protein name	Log$_2$FC[a]	p-value[b]
1	LHX6	LIM/homeobox protein Lhx6	2.69	0.010
2	ASNS	Asparagine synthetase [glutamine-hydrolyzing]	2.57	<0.001
3	CTH	Cystathionine gamma-lyase	2.37	0.007
4	PSAT1	Phosphoserine aminotransferase	2.30	<0.001
5	UCHL1	Ubiquitin carboxyl-terminal hydrolase isozyme L1	2.24	0.014
6	RBM4B	RNA-binding protein 4B	2.02	0.014
7	FHOD1	FH1/FH2 domain-containing protein 1	1.82	0.019
8	AKAP12	A-kinase anchor protein 12	1.81	0.029
9	PRSS3	Trypsin-3	1.74	0.050
10	FOSB	Protein fosB	1.67	0.004
11	TMSB10	Thymosin beta-10	1.54	0.009
12	HIST2H2AC	Histone H2A type 2-C	1.54	0.005
13	S100A10	Protein S100-A10	1.45	0.004
14	HBEGF	Proheparin-binding EGF-like growth factor	1.43	0.049
15	ANXA2	Annexin A2	1.29	0.025
16	LAMB3	Laminin subunit beta-3	1.23	0.009
17	MAFF	Transcription factor MafF	1.19	<0.001

No	Symbol	Protein name	Log$_2$FC^a	p-value^b
18	ARG2	Arginase-2, mitochondrial	1.18	0.001
19	FLNC	Filamin-C	1.17	0.009
20	TMSB4X	Thymosin beta-4	1.06	0.042
21	FOSL1	Fos-related antigen 1	1.06	0.003
22	MAP1LC3B	Microtubule-associated proteins 1A/1B light chain 3B	1.03	0.032
23	SARS	Serine--tRNA ligase, cytoplasmic	0.99	<0.001
24	RIOK3	Serine/threonine-protein kinase RIO3	0.99	0.017
25	FAM174B	Membrane protein FAM174B	0.98	0.002

^{a}FC > 1.5.
^{b}p-value ≤ 0.05.

Appendix Table III-7. Top 25 downregulated proteins for napabucasin treatment in BxPC-3 cells.

No	Symbol	Protein name	Log$_2$FC^a	p-value^b
1	MNF1; UQCC2	Ubiquinol-cytochrome-c reductase complex assembly factor 2	-1.21	0.044
2	MRPS12	28S ribosomal protein S12, mitochondrial	-1.00	0.012
3	ERAL1	GTPase Era, mitochondrial	-0.99	<0.001
4	KIAA0101; PCLAF	PCNA-associated factor	-0.98	0.003
5	MSR1	Macrophage scavenger receptor types I and II	-0.97	0.023
6	GLUL	Glutamine synthetase	-0.94	0.004
7	AARSD1; PTGES3L-AARSD1	Alanyl-tRNA editing protein Aarsd1	-0.93	0.005
8	ADI1	1,2-dihydroxy-3-keto-5-methylthiopentene dioxygenase	-0.92	0.002
9	FXYD3	FXYD domain-containing ion transport regulator 3	-0.87	0.019
10	CKB	Creatine kinase B-type	-0.85	0.016
11	TSPAN15	Tetraspanin-15	-0.85	0.037
12	MRPS11	28S ribosomal protein S11, mitochondrial	-0.84	0.005
13	DDX28	Probable ATP-dependent RNA helicase DDX28	-0.82	0.003
14	DAG1	Dystroglycan	-0.79	<0.001
15	GFM2	Ribosome-releasing factor 2, mitochondrial	-0.79	0.002
16	MRPS23	28S ribosomal protein S23, mitochondrial	-0.78	0.001
17	PIR	Pirin	-0.76	0.003
18	SESTD1	SEC14 domain and spectrin repeat-containing protein 1	-0.76	0.010
19	CECR5; HDHD5	Haloacid dehalogenase-like hydrolase domain-containing 5	-0.75	0.008
20	CTNNBIP1	Beta-catenin-interacting protein 1	-0.74	0.018
21	MRPS18B	28S ribosomal protein S18b, mitochondrial	-0.73	<0.001
22	APPL2	DCC-interacting protein 13-beta	-0.72	0.040
23	ATAD2	ATPase family AAA domain-containing protein 2	-0.71	0.019
24	YARS2	Tyrosine-tRNA ligase, mitochondrial	-0.70	<0.001
25	XPNPEP3	Xaa-Pro aminopeptidase 3	-0.69	0.006

Appendix Table III-8. Top 25 upregulated proteins for **XD2-149** treatment in BxPC-3 cells.

No	Symbol	Protein name	Log$_2$FC^a	p-value^b
1	HBEGF	Proheparin-binding EGF-like growth factor	2.02	<0.001

No	Symbol	Protein name	Log₂FC	p-value
2	HERPUD1	Homocysteine-responsive endoplasmic reticulum-resident ubiquitin-like domain member 1 protein	1.94	0.001
3	CTH	Cystathionine gamma-lyase	1.65	0.002
4	IL1B	Interleukin-1 beta	1.61	0.003
5	JUN	Transcription factor AP-1	1.58	<0.001
6	AKAP12	A-kinase anchor protein 12	1.48	0.003
7	FOSB	Protein fosB	1.41	<0.001
8	DNAJB9	DnaJ homolog subfamily B member 9	1.35	<0.001
9	ARG2	Arginase-2, mitochondrial	1.22	<0.001
10	STC1	Stanniocalcin-1	1.21	<0.001
11	PTGS2	Prostaglandin G/H synthase 2	1.13	0.002
12	PLAT	Tissue-type plasminogen activator	1.12	0.001
13	FOSL1	Fos-related antigen 1	1.07	<0.001
14	S100A10	Protein S100-A10	1.07	0.001
15	MAP1LC3B	Microtubule-associated proteins 1A/1B light chain 3B	1.04	0.005
16	MAFF	Transcription factor MafF	1.00	<0.001
17	RND3	Rho-related GTP-binding protein RhoE	0.98	0.001
18	LDLR	Low-density lipoprotein receptor	0.92	0.002
19	TXNRD1	Thioredoxin reductase 1, cytoplasmic	0.90	<0.001
20	GABARAPL1	Gamma-aminobutyric acid receptor-associated protein-like 1	0.90	0.001
21	ZFP36L1	mRNA decay activator protein ZFP36L1	0.90	<0.001
22	FLNC	Filamin-C	0.90	0.001
23	SQLE	Squalene monooxygenase	0.87	0.005
24	TGFA	Protransforming growth factor alpha	0.83	<0.001
25	SQSTM1	Sequestosome-1	0.77	0.004

Appendix Table III-9. Top 25 downregulated proteins for **XD2-149** treatment in BxPC-3 cells.

No	Symbol	Protein name	Log₂FC[a]	p-value[b]
1	KIAA0101; PCLAF	PCNA-associated factor	-2.29	<0.001
2	RRM2	Ribonucleoside-diphosphate reductase subunit M2	-2.08	0.004
3	NDC80	Kinetochore protein NDC80 homolog	-1.72	0.001
4	PPAT	Amidophosphoribosyltransferase	-1.70	<0.001
5	GLUL	Glutamine synthetase	-1.58	<0.001
6	ID1	DNA-binding protein inhibitor ID-1	-1.57	0.001
7	CDC20	Cell division cycle protein 20 homolog	-1.44	0.001
8	ADI1	1,2-dihydroxy-3-keto-5-methylthiopentene dioxygenase	-1.43	<0.001
9	AARS	Alanine--tRNA ligase, cytoplasmic	-1.24	<0.001
10	TRIM26	Tripartite motif-containing protein 26	-1.23	0.001
11	AARSD1; PTGES3L-AARSD1	Alanyl-tRNA editing protein Aarsd1	-1.21	0.001
12	NQO1	NAD(P)H dehydrogenase [quinone] 1	-1.07	<0.001
13	MPST	3-mercaptopyruvate sulfurtransferase	-1.07	<0.001
14	CHEK1	Serine/threonine-protein kinase Chk1	-1.05	0.001
15	ATAD2	ATPase family AAA domain-containing protein 2	-1.05	0.001
16	TP53BP2	Apoptosis-stimulating of p53 protein 2	-1.02	0.004
17	POLD1	DNA polymerase delta catalytic subunit	-1.00	<0.001
18	MAGED1	Melanoma-associated antigen D1	-0.90	0.002
19	PKP1	Plakophilin-1	-0.87	<0.001
20	DAG1	Dystroglycan	-0.86	<0.001
21	CBR1; SETD4	Carbonyl reductase [NADPH] 1	-0.86	<0.001
22	DHFR; DHFRP1	Dihydrofolate reductase	-0.86	0.005

No	Symbol	Protein name	Log$_2$FC[a]	p-value[b]
23	CDK2AP1	Cyclin-dependent kinase 2-associated protein 1	-0.85	0.002
24	SPINT1	Kunitz-type protease inhibitor 1	-0.85	0.001
25	PIR	Pirin	-0.83	0.001

[a]FC > 1.5.
[b]p-value ≤ 0.05.

Appendix Table III-10. Top 25 upregulated proteins for **XD2-162** treatment in BxPC-3 cells.

No	Symbol	Protein name	Log$_2$FC[a]	p-value[b]
1	LHX6	LIM/homeobox protein Lhx6	2.18	0.027
2	AKAP12	A-kinase anchor protein 12	1.72	0.002
3	IL1B	Interleukin-1 beta	1.62	0.005
4	CDKN1A	Cyclin-dependent kinase inhibitor 1	1.51	0.010
5	HBEGF	Proheparin-binding EGF-like growth factor	1.37	0.004
6	IGKC	Immunoglobulin kappa constant	1.36	0.048
7	ASNS	Asparagine synthetase [glutamine-hydrolyzing]	1.16	0.004
8	HERPUD1	Homocysteine-responsive endoplasmic reticulum-resident ubiquitin-like domain member 1 protein	1.09	0.043
9	MAP1LC3B	Microtubule-associated proteins 1A/1B light chain 3B	1.01	0.005
10	PLAU	Urokinase-type plasminogen activator	1.00	0.004
11	LDLR	Low-density lipoprotein receptor	1.00	0.004
12	CTH	Cystathionine gamma-lyase	1.00	0.036
13	FOSL1	Fos-related antigen 1	1.00	<0.001
14	MMP1	Interstitial collagenase	0.96	0.010
15	SQSTM1	Sequestosome-1	0.95	0.002
16	TGFA	Protransforming growth factor alpha	0.91	0.001
17	CD274	Programmed cell death 1 ligand 1	0.87	0.031
18	UCHL1	Ubiquitin carboxyl-terminal hydrolase isozyme L1	0.85	0.049
19	PTGS2	Prostaglandin G/H synthase 2	0.84	0.018
20	TMSB10	Thymosin beta-10	0.83	0.014
21	SRXN1	Sulfiredoxin-1	0.82	0.013
22	S100A10	Protein S100-A10	0.82	0.005
23	MAFF	Transcription factor MafF	0.79	<0.001
24	TNFRSF10B	Tumor necrosis factor receptor superfamily member 10B	0.79	0.010
25	LAMB3	Laminin subunit beta-3	0.79	0.005

[a]FC > 1.5.
[b]p-value ≤ 0.05.

Appendix Table III-11. Top 25 downregulated proteins for **XD2-162** treatment in BxPC-3 cells.

No	Symbol	Protein name	Log$_2$FC[a]	p-value[b]
1	RRM2	Ribonucleoside-diphosphate reductase subunit M2	-1.84	0.015
2	SLBP	Histone RNA hairpin-binding protein	-1.79	0.001
3	KIAA0101; PCLAF	PCNA-associated factor	-1.72	<0.001
4	PPAT	Amidophosphoribosyltransferase	-1.39	<0.001
5	NDC80	Kinetochore protein NDC80 homolog	-1.39	0.006
6	CDC20	Cell division cycle protein 20 homolog	-1.31	0.004
7	GLUL	Glutamine synthetase	-1.29	0.001
8	MOCS3	Adenylyltransferase and sulfurtransferase MOCS3	-1.19	0.026
9	UBE2C	Ubiquitin-conjugating enzyme E2 C	-1.20	0.029
10	FSBP; RAD54B	Fibrinogen silencer-binding protein	-1.18	0.005
11	TPX2	Targeting protein for Xklp2	-1.16	0.042
12	ATAD2	ATPase family AAA domain-containing protein 2	-1.10	0.002
13	KIF23	Kinesin-like protein KIF23	-1.08	0.014
14	ECT2	Protein ECT2	-1.00	0.039

No	Gene Symbol	Name	Log$_2$FC	p-value
15	DAG1	Dystroglycan	-1.00	<0.001
16	POLD1	DNA polymerase delta catalytic subunit	-0.98	<0.001
17	CHEK1	Serine/threonine-protein kinase Chk1	-0.95	0.002
18	DHFR; DHFRP1	Dihydrofolate reductase	-0.93	0.006
19	SORT1	Sortilin	-0.92	0.002
20	CKS2	Cyclin-dependent kinases regulatory subunit 2	-0.85	0.040
21	PIR	Pirin	-0.85	0.001
22	MCM7	DNA replication licensing factor MCM7	-0.83	<0.001
23	TK1	Thymidine kinase, cytosolic	-0.82	0.035
24	LIMD2	LIM domain-containing protein 2	-0.82	0.048
25	MCM6	DNA replication licensing factor MCM6	-0.81	0.002

[a]FC > 1.5.
[b]p-value ≤ 0.05.

Appendix Table III-12. Downregulated proteins in common between napabucasin, **XD2-149** and **XD2-162**.

No	Gene Symbol	Name	Log$_2$FC[a]	p-value[b]
1	KIAA0101; PCLAF	PCNA-associated factor	-2.29	<0.001
2	PPAT	Amidophosphoribosyltransferase	-1.70	<0.001
3	GLUL	Glutamine synthetase	-1.58	<0.001
4	ADI1	1,2-dihydroxy-3-keto-5-methylthiopentene dioxygenase	-1.43	<0.001
5	AARSD1; PTGES3L-AARSD1	Alanyl-tRNA editing protein Aarsd1	-1.21	0.001
6	ATAD2	ATPase family AAA domain-containing protein 2	-1.05	0.002
7	FXYD3	FXYD domain-containing ion transport regulator 3	-0.98	0.009
8	DAG1	Dystroglycan	-0.86	<0.001
9	PIR	Pirin	-0.83	0.001
10	BCL2L12	Bcl-2-like protein 12	-0.63	0.010

[a]FC > 1.5, values listed correspond to protein expression in **XD2-149** treatment.
[b]p-value ≤ 0.05, values listed correspond to protein expression in **XD2-149** treatment.

Appendix Table III-13. Upregulated proteins in common between napabucasin, **XD2-149** and **XD2-162**.

No	Gene Symbol	Name	Log$_2$FC[a]	p-value[b]
1	HBEGF	Proheparin-binding EGF-like growth factor	2.02	<0.001
2	CTH	Cystathionine gamma-lyase	1.65	0.002
3	AKAP12	A-kinase anchor protein 12	1.48	0.003
4	ARG2	Arginase-2, mitochondrial	1.22	<0.001
5	PLAT	Tissue-type plasminogen activator	1.12	0.001
6	FOSL1	Fos-related antigen 1	1.07	<0.001
7	S100A10	Protein S100-A10	1.07	0.001
8	MAP1LC3B	Microtubule-associated proteins 1A/1B light chain 3B	1.04	0.004
9	ASNS	Asparagine synthetase [glutamine-hydrolyzing]	1.01	0.009
10	MAFF	Transcription factor MafF	1.00	<0.001
11	FLNC	Filamin-C	0.90	0.001
12	LAMB3	Laminin subunit beta-3	0.76	0.003
13	ANXA2	Annexin A2	0.72	0.014

| 14 | DNAJC18 | DnaJ homolog subfamily C member 18 | 0.61 | 0.015 |

Appendix Table III-14. Upregulated Hallmark gene sets from GSEA analysis of napabucasin.

No	Gene set	Size	NES	NOM p-value	FDR q-val
1	HALLMARK_TNFA_SIGNALING_VIA_NFKB	67	2.327	<0.001	<0.001
2	HALLMARK_UNFOLDED_PROTEIN_RESPONSE	85	1.913	<0.001	0.006
3	HALLMARK_KRAS_SIGNALING_UP	54	1.901	<0.001	0.004
4	HALLMARK_IL2_STAT5_SIGNALING	72	1.890	<0.001	0.003
5	HALLMARK_HYPOXIA	81	1.741	0.002	0.016
6	HALLMARK_INFLAMMATORY_RESPONSE	48	1.704	0.008	0.018
7	HALLMARK_COAGULATION	45	1.615	0.013	0.033
8	HALLMARK_APOPTOSIS	80	1.586	0.009	0.036

Appendix Table III-15. Downregulated Hallmark gene sets from GSEA analysis of napabucasin.

No	Gene set	Size	NES	NOM p-value	FDR q-val
1	HALLMARK_OXIDATIVE_PHOSPHORYLATION	173	-2.187	<0.001	<0.001
2	HALLMARK_FATTY_ACID_METABOLISM	99	-2.018	<0.001	<0.001
3	HALLMARK_CHOLESTEROL_HOMEOSTASIS	45	-1.711	0.005	0.013
4	HALLMARK_E2F_TARGETS	136	-1.608	<0.001	0.036
5	HALLMARK_ADIPOGENESIS	120	-1.565	0.002	0.043

Appendix Table III-16. Upregulated KEGG gene sets from GSEA analysis of napabucasin.

No	Gene set	Size	NES	NOM p-value	FDR q-val
1	KEGG_SYSTEMIC_LUPUS_ERYTHEMATOSUS	22	1.859	<0.001	0.046

Appendix Table III-17. Downregulated KEGG gene sets from GSEA analysis of napabucasin.

No	Gene set	Size	NES	NOM p-value	FDR q-val
1	KEGG_VALINE_LEUCINE_AND_ISOLEUCINE_DEGRADATION	33	-2.252	<0.001	<0.001
2	KEGG_BUTANOATE_METABOLISM	22	-2.202	<0.001	<0.001
3	KEGG_CITRATE_CYCLE_TCA_CYCLE	27	-1.993	<0.001	0.001
4	KEGG_DNA_REPLICATION	29	-1.957	<0.001	0.002
5	KEGG_PROPANOATE_METABOLISM	21	-1.937	<0.001	0.003
6	KEGG_FATTY_ACID_METABOLISM	26	-1.875	<0.001	0.006
7	KEGG_LYSINE_DEGRADATION	20	-1.829	0.002	0.010
8	KEGG_ARGININE_AND_PROLINE_METABOLISM	26	-1.730	0.015	0.032
9	KEGG_MISMATCH_REPAIR	19	-1.688	0.006	0.045

Appendix Table III-18. Upregulated GO gene sets from GSEA analysis of napabucasin.

No	Gene set	Size	NES	NOM p-value	FDR q-val
1	GO_CELLULAR_RESPONSE_TO_STARVATION	61	2.075	<0.001	0.047

Appendix Table III-19. Top 20 downregulated GO gene sets from GSEA analysis of napabucasin.

No	Gene set	Size	NES	NOM *p*-value	FDR *q*-val
1	GO_MITOCHONDRIAL_GENE_EXPRESSION	117	-3.019	<0.001	<0.001
2	GO_MITOCHONDRIAL_TRANSLATION	104	-2.975	<0.001	<0.001
3	GO_MITOCHONDRIAL_TRANSLATIONAL_TERMINATION	75	-2.955	<0.001	<0.001
4	GO_TRANSLATIONAL_TERMINATION	84	-2.951	<0.001	<0.001
5	GO_ORGANELLAR_RIBOSOME	72	-2.904	<0.001	<0.001
6	GO_MITOCHONDRIAL_MATRIX	300	-2.855	<0.001	<0.001
7	GO_CELLULAR_PROTEIN_COMPLEX_DISASSEMBLY	139	-2.814	<0.001	<0.001
8	GO_TRANSLATIONAL_ELONGATION	99	-2.724	<0.001	<0.001
9	GO_ORGANELLAR_LARGE_RIBOSOMAL_SUBUNIT	46	-2.653	<0.001	<0.001
10	GO_RIBOSOME	186	-2.628	<0.001	<0.001
11	GO_RIBOSOMAL_SUBUNIT	161	-2.621	<0.001	<0.001
12	GO_STRUCTURAL_CONSTITUENT_OF_RIBOSOME	134	-2.615	<0.001	<0.001
13	GO_ORGANELLAR_SMALL_RIBOSOMAL_SUBUNIT	25	-2.613	<0.001	<0.001
14	GO_MITOCHONDRIAL_PROTEIN_COMPLEX	201	-2.610	<0.001	<0.001
15	GO_ORGANELLE_INNER_MEMBRANE	307	-2.583	<0.001	<0.001
16	GO_PROTEIN_CONTAINING_COMPLEX_DISASSEMBLY	202	-2.539	<0.001	<0.001
17	GO_SMALL_RIBOSOMAL_SUBUNIT	65	-2.518	<0.001	<0.001
18	GO_LARGE_RIBOSOMAL_SUBUNIT	98	-2.436	<0.001	<0.001
19	GO_MITOCHONDRIAL_ENVELOPE	408	-2.266	<0.001	<0.001
20	GO_IRON_ION_BINDING	34	-2.191	<0.001	<0.001

Appendix Table III-20. Upregulated TFT gene sets from GSEA analysis of napabucasin.

No	Gene set	Size	NES	NOM *p*-value	FDR *q*-val
1	MSX1_01	45	2.014	0.002	0.040

Appendix Table III-21. Upregulated Hallmark gene sets from GSEA analysis of **XD2-149**.

No	Gene set	Size	NES	NOM *p*-value	FDR *q*-val
1	HALLMARK_TNFA_SIGNALING_VIA_NFKB	67	2.454	<0.001	<0.001
2	HALLMARK_KRAS_SIGNALING_UP	54	2.220	<0.001	<0.001
3	HALLMARK_HYPOXIA	81	2.120	<0.001	<0.001
4	HALLMARK_IL2_STAT5_SIGNALING	72	1.947	<0.001	0.001
5	HALLMARK_INFLAMMATORY_RESPONSE	48	1.903	<0.001	0.002
6	HALLMARK_UNFOLDED_PROTEIN_RESPONSE	85	1.832	<0.001	0.004
7	HALLMARK_P53_PATHWAY	94	1.768	<0.001	0.007
8	HALLMARK_APOPTOSIS	80	1.695	<0.001	0.014
9	HALLMARK_COAGULATION	45	1.636	0.011	0.021

Appendix Table III-22. Downregulated Hallmark gene sets from GSEA analysis of **XD2-149**.

No	Gene set	Size	NES	NOM *p*-value	FDR *q*-val
1	HALLMARK_E2F_TARGETS	136	-2.049	<0.001	<0.001
2	HALLMARK_INTERFERON_ALPHA_RESPONSE	53	-1.981	<0.001	<0.001
3	HALLMARK_G2M_CHECKPOINT	123	-1.851	<0.001	0.001
4	HALLMARK_MITOTIC_SPINDLE	123	-1.589	<0.001	0.031
5	HALLMARK_DNA_REPAIR	97	-1.581	0.006	0.028

Appendix Table III-23. Upregulated GO gene sets from GSEA analysis of **XD2-149**.

No	Gene set	Size	NES	NOM p-value	FDR q-val
1	GO_NEGATIVE_REGULATION_OF_SECRETION	56	2.124	<0.001	0.026
2	GO_STEROL_HOMEOSTASIS	24	2.114	<0.001	0.020
3	GO_REGULATION_OF_WOUND_HEALING	51	2.072	<0.001	0.037

Appendix Table III-24. Top 20 downregulated GO gene sets from GSEA analysis of **XD2-149**.

No	Gene set	Size	NES	NOM p-value	FDR q-val
1	GO_NEGATIVE_REGULATION_OF_NUCLEAR_DIVISION	25	-2.135	<0.001	0.002
2	GO_SISTER_CHROMATID_SEGREGATION	100	-2.119	<0.001	0.002
3	GO_METAPHASE_ANAPHASE_TRANSITION_OF_CELL_CYCLE	30	-2.103	0.002	0.001
4	GO_MITOTIC_SISTER_CHROMATID_SEGREGATION	87	-2.090	<0.001	0.001
5	GO_NEGATIVE_REGULATION_OF_METAPHASE_ANAPHASE_TRANSITION_OF_CELL_CYCLE	19	-2.072	<0.001	0.002
6	GO_NEGATIVE_REGULATION_OF_CHROMOSOME_SEGREGATION	22	-2.067	<0.001	0.002
7	GO_REGULATION_OF_CHROMOSOME_SEPARATION	34	-2.030	<0.001	0.003
8	GO_NUCLEAR_DNA_REPLICATION	29	-2.014	<0.001	0.004
9	GO_REGULATION_OF_CHROMOSOME_SEGREGATION	56	-1.998	<0.001	0.005
10	GO_REGULATION_OF_SISTER_CHROMATID_SEGREGATION	43	-1.990	<0.001	0.005
11	GO_MITOTIC_SPINDLE_ASSEMBLY	37	-1.990	<0.001	0.005
12	GO_CELL_CYCLE_DNA_REPLICATION	35	-1.986	<0.001	0.005
13	GO_ATTACHMENT_OF_SPINDLE_MICROTUBULES_TO_KINETOCHORE	19	-1.984	<0.001	0.005
14	GO_SPINDLE	157	-1.984	<0.001	0.004
15	GO_MICROTUBULE_CYTOSKELETON_ORGANIZATION_INVOLVED_IN_MITOSIS	75	-1.934	<0.001	0.009
16	GO_SPINDLE_ASSEMBLY	54	-1.914	<0.001	0.012
17	GO_NUCLEAR_CHROMOSOME_SEGREGATION	121	-1.913	<0.001	0.012
18	GO_IRON_ION_BINDING	34	-1.907	<0.001	0.013
19	GO_TELOMERE_MAINTENANCE_VIA_SEMI_CONSERVATIVE_REPLICATION	21	-1.906	<0.001	0.012
20	GO_MITOTIC_SPINDLE_ORGANIZATION	68	-1.896	<0.001	0.014

Appendix Table III-25. Upregulated KEGG gene sets from GSEA analysis of **XD2-149**.

No	Gene set	Size	NES	NOM p-value	FDR q-val
1	KEGG_SYSTEMIC_LUPUS_ERYTHEMATOSUS	22	2.116	<0.001	0.004
2	KEGG_ERBB_SIGNALING_PATHWAY	42	1.960	<0.001	0.015

Appendix Table III-26. Downregulated KEGG gene sets from GSEA analysis of **XD2-149**.

No	Gene set	Size	NES	NOM p-value	FDR q-val
1	KEGG_DNA_REPLICATION	29	-2.053	<0.001	<0.001
2	KEGG_CELL_CYCLE	61	-2.008	<0.001	<0.001

No	Gene set	Size	NES	NOM p-value	FDR q-val
3	KEGG_PROGESTERONE_MEDIATED_OOCYTE_MATURATION	33	-1.968	<0.001	0.002
4	KEGG_PURINE_METABOLISM	70	-1.941	<0.001	0.003
5	KEGG_MISMATCH_REPAIR	19	-1.864	0.002	0.007
6	KEGG_UBIQUITIN_MEDIATED_PROTEOLYSIS	72	-1.776	<0.001	0.021
7	KEGG_PYRIMIDINE_METABOLISM	55	-1.775	0.003	0.018
8	KEGG_RNA_POLYMERASE	17	-1.756	0.002	0.021
9	KEGG_OOCYTE_MEIOSIS	54	-1.739	0.002	0.022

Appendix Table III-27. Upregulated TFT gene sets from GSEA analysis of **XD2-149**.

No	Gene set	Size	NES	NOM p-value	FDR q-val
1	AP1_Q2_01	95	2.045	<0.001	0.020
2	CEBPDELTA_Q6	78	2.038	<0.001	0.010

Appendix Table III-28. Downregulated TFT gene sets from GSEA analysis of **XD2-149**.

No	Gene set	Size	NES	NOM p-value	FDR q-val
1	STTTCRNTTT_IRF_Q6	70	-1.817	<0.001	0.047

Appendix Table III-29. Upregulated Hallmark gene sets from GSEA analysis of **XD2-162**.

No	Gene set	Size	NES	NOM p-value	FDR q-val
1	HALLMARK_TNFA_SIGNALING_VIA_NFKB	67	2.622	<0.001	<0.001
2	HALLMARK_KRAS_SIGNALING_UP	54	2.303	<0.001	<0.001
3	HALLMARK_INFLAMMATORY_RESPONSE	48	2.266	<0.001	<0.001
4	HALLMARK_HYPOXIA	81	2.183	<0.001	0.001
5	HALLMARK_COAGULATION	45	2.031	<0.001	0.001
6	HALLMARK_EPITHELIAL_MESENCHYMAL_TRANSITION	65	1.987	<0.001	0.001
7	HALLMARK_UNFOLDED_PROTEIN_RESPONSE	85	1.883	<0.001	0.003
8	HALLMARK_COMPLEMENT	86	1.863	<0.001	0.004
9	HALLMARK_IL2_STAT5_SIGNALING	72	1.797	<0.001	0.009
10	HALLMARK_APOPTOSIS	80	1.747	<0.001	0.012
11	HALLMARK_IL6_JAK_STAT3_SIGNALING	25	1.724	0.009	0.012
12	HALLMARK_MTORC1_SIGNALING	149	1.575	<0.001	0.039

Appendix Table III-30. Downregulated Hallmark gene sets from GSEA analysis of **XD2-162**.

No	Gene set	Size	NES	NOM p-value	FDR q-val
1	HALLMARK_G2M_CHECKPOINT	123	-2.286	<0.001	<0.001
2	HALLMARK_E2F_TARGETS	136	-2.207	<0.001	<0.001
3	HALLMARK_MITOTIC_SPINDLE	123	-1.784	<0.001	0.001
4	HALLMARK_DNA_REPAIR	97	-1.677	<0.001	0.008

Appendix Table III-31. Upregulated GO gene sets from GSEA analysis of **XD2-162**.

No	Gene set	Size	NES	NOM p-value	FDR q-val
1	GO_EXTRACELLULAR_MATRIX	110	2.436	<0.001	<0.001

2	GO_COLLAGEN_CONTAINING_EXTRACELLULAR_M ATRIX	102	2.365	<0.001	<0.001
3	GO_NEGATIVE_REGULATION_OF_COAGULATION	19	2.295	<0.001	<0.001
4	GO_REGULATION_OF_WOUND_HEALING	51	2.274	<0.001	<0.001
5	GO_REGULATION_OF_COAGULATION	29	2.273	<0.001	0.001
6	GO_BLOOD_MICROPARTICLE	43	2.272	<0.001	<0.001
7	GO_RECEPTOR_REGULATOR_ACTIVITY	44	2.272	<0.001	<0.001
8	GO_GROWTH_FACTOR_ACTIVITY	20	2.174	<0.001	0.005
9	GO_REGULATION_OF_RESPONSE_TO_WOUNDING	58	2.160	<0.001	0.007
10	GO_NEGATIVE_REGULATION_OF_RESPONSE_TO_W OUNDING	31	2.144	<0.001	0.008
11	GO_GROWTH_FACTOR_RECEPTOR_BINDING	43	2.127	<0.001	0.011
12	GO_EXTRACELLULAR_MATRIX_STRUCTURAL_CON STITUENT	25	2.114	<0.001	0.012
13	GO_ENDOPLASMIC_RETICULUM_UNFOLDED_PROTE IN_RESPONSE	60	2.076	<0.001	0.019
14	GO_POSITIVE_REGULATION_OF_LIPID_METABOLIC_ PROCESS	33	2.065	<0.001	0.019
15	GO_REGULATION_OF_SIGNALING_RECEPTOR_ACTI VITY	71	2.062	<0.001	0.019
16	GO_REGULATION_OF_NIK_NF_KAPPAB_SIGNALING	35	2.012	0.003	0.034
17	GO_WATER_HOMEOSTASIS	25	2.009	<0.001	0.033
18	GO_POSITIVE_REGULATION_OF_LIPID_BIOSYNTHET IC_PROCESS	19	1.997	<0.001	0.035
19	GO_ENDOCHONDRAL_BONE_MORPHOGENESIS	19	1.980	<0.001	0.042
20	GO_CARTILAGE_DEVELOPMENT	35	1.979	<0.001	0.040
21	GO_SMOOTH_ENDOPLASMIC_RETICULUM	18	1.971	<0.001	0.043

Appendix Table III-32. Top 20 downregulated GO gene sets from GSEA analysis of **XD2-162**.

No	Gene set	Size	NES	NOM p-value	FDR q-val
1	GO_DNA_REPLICATION	135	-2.377	<0.001	<0.001
2	GO_MITOTIC_SISTER_CHROMATID_SEGREGATION	87	-2.317	<0.001	<0.001
3	GO_NUCLEAR_CHROMOSOME_SEGREGATION	121	-2.299	<0.001	<0.001
4	GO_NUCLEAR_DNA_REPLICATION	29	-2.290	<0.001	<0.001
5	GO_SISTER_CHROMATID_SEGREGATION	100	-2.277	<0.001	<0.001
6	GO_DNA_DEPENDENT_DNA_REPLICATION	78	-2.256	<0.001	<0.001
7	GO_CHROMOSOME_SEPARATION	46	-2.252	<0.001	<0.001
8	GO_CELL_CYCLE_DNA_REPLICATION	35	-2.219	<0.001	<0.001
9	GO_MICROTUBULE_CYTOSKELETON_ORGANIZATIO N_INVOLVED_IN_MITOSIS	75	-2.195	<0.001	<0.001
10	GO_REGULATION_OF_CHROMOSOME_SEGREGATION	56	-2.193	<0.001	<0.001
11	GO_CHROMOSOME_SEGREGATION	148	-2.190	<0.001	<0.001
12	GO_TELOMERE_MAINTENANCE_VIA_SEMI_CONSERV ATIVE_REPLICATION	21	-2.186	<0.001	<0.001
13	GO_NEGATIVE_REGULATION_OF_CHROMOSOME_OR GANIZATION	73	-2.158	<0.001	<0.001
14	GO_REGULATION_OF_CHROMOSOME_SEPARATION	34	-2.147	<0.001	<0.001
15	GO_MITOTIC_SPINDLE_ASSEMBLY	37	-2.144	<0.001	<0.001
16	GO_NEGATIVE_REGULATION_OF_NUCLEAR_DIVISIO N	25	-2.138	<0.001	<0.001
17	GO_REGULATION_OF_SISTER_CHROMATID_SEGREG ATION	43	-2.136	<0.001	<0.001
18	GO_REPLICATION_FORK	45	-2.135	<0.001	<0.001
19	GO_ORGANELLE_FISSION	185	-2.134	<0.001	<0.001

20	GO_DNA_REPLICATION		19	-2.124	<0.001	<0.001

Appendix Table III-33. Upregulated KEGG gene sets from GSEA analysis of **XD2-162**.

No	Gene set	Size	NES	NOM *p*-value	FDR *q*-val
1	KEGG_CYTOKINE_CYTOKINE_RECEPTOR_INTERACTION	19	1.957	<0.001	0.041

Appendix Table III-34. Downregulated KEGG gene sets from GSEA analysis of **XD2-162**.

No	Gene set	Size	NES	NOM *p*-value	FDR *q*-val
1	KEGG_DNA_REPLICATION	29	-2.391	<0.001	<0.001
2	KEGG_MISMATCH_REPAIR	19	-2.130	<0.001	<0.001
3	KEGG_PROGESTERONE_MEDIATED_OOCYTE_MATURATION	33	-2.099	<0.001	<0.001
4	KEGG_CELL_CYCLE	61	-2.001	<0.001	<0.001
5	KEGG_NUCLEOTIDE_EXCISION_REPAIR	33	-1.939	<0.001	0.002
6	KEGG_UBIQUITIN_MEDIATED_PROTEOLYSIS	72	-1.767	<0.001	0.024
7	KEGG_OOCYTE_MEIOSIS	54	-1.738	<0.001	0.029
8	KEGG_PYRIMIDINE_METABOLISM	55	-1.734	<0.001	0.026

Appendix Table III-35. Upregulated TFT gene sets from GSEA analysis of **XD2-162**.

No	Gene set	Size	NES	NOM *p*-value	FDR *q*-val
1	AP1_Q2_01	95	1.969	<0.001	0.034

Appendix Table III-36. Downregulated TFT gene sets from GSEA analysis of **XD2-162**.

No	Gene set	Size	NES	NOM *p*-value	FDR *q*-val
1	E2F1DP1RB_01	104	-1.981	<0.001	0.004
2	SGCGSSAAA_E2F1DP2_01	76	-1.928	<0.001	0.007
3	E2F1_Q6	114	-1.899	<0.001	0.007
4	E2F1_Q3	110	-1.898	<0.001	0.005
5	E2F_Q6	112	-1.889	<0.001	0.005
6	E2F_Q4	114	-1.867	<0.001	0.006
7	E2F4DP1_01	109	-1.866	<0.001	0.005
8	E2F1DP2_01	106	-1.856	<0.001	0.006
9	E2F1DP1_01	106	-1.839	<0.001	0.007
10	E2F4DP2_01	106	-1.838	<0.001	0.006
11	E2F_02	107	-1.827	<0.001	0.007
12	E2F1_Q6_01	114	-1.786	<0.001	0.012
13	E2F_01	32	-1.764	0.002	0.015
14	E2F_03	116	-1.730	<0.001	0.023
15	E2F_Q4_01	103	-1.721	<0.001	0.024
16	E2F1_Q4_01	97	-1.706	<0.001	0.027
17	ALPHACP1_01	85	-1.701	0.003	0.027
18	E2F_Q3	100	-1.678	0.001	0.034
19	E2F_Q3_01	100	-1.664	0.001	0.040

Notes

Hanafi, M.; Chen, X.; Neamati, N., Discovery of a Napabucasin PROTAC as an Effective Degrader of the E3 Ligase ZFP91. *J Med Chem* **2021,** *64* (3), 1626-1648.

References

1. Rao, M. M.; Kingston, D. G., Plant anticancer agents. XII. Isolation and structure elucidation of new cytotoxic quinones from Tabebuia cassinoides. *J Nat Prod* **1982,** *45* (5), 600-604.

2. Nagata, K.; Hirai, K. I.; Koyama, J.; Wada, Y.; Tamura, T., Antimicrobial activity of novel furanonaphthoquinone analogs. *Antimicrob Agents Chemother* **1998,** *42.3*, 700-702.

3. Li, Y.; Rogoff, H. A.; Keates, S.; Gao, Y.; Murikipudi, S.; Mikule, K.; Leggett, D.; Li, W.; Pardee, A. B.; Li, C. J., Suppression of cancer relapse and metastasis by inhibiting cancer stemness. *Proc Natl Acad Sci U S A* **2015,** *112* (6), 1839-1844.

4. Jiang, Z. L., Chiang, J., ; Li, W. ; Leggett, D. Novel STAT3 Pathway Inhibitors and Cancer Stem Cell Inhibitors. WO 2009036059A3, July 2, 2009.

5. Karandish, F.; Mamnoon, B.; Feng, L.; Haldar, M. K.; Xia, L.; Gange, K. N.; You, S.; Choi, Y.; Sarkar, K.; Mallik, S., Nucleus-targeted, echogenic polymersomes for delivering a cancer stemness inhibitor to pancreatic cancer cells. *Biomacromolecules* **2018,** *19* (10), 4122-4132.

6. https://www.accessdata.fda.gov/scripts/opdlisting/oopd/listResult.cfm. (accessed October 10, 2020).

7. Neoptolemos, J. P.; Kleeff, J.; Michl, P.; Costello, E.; Greenhalf, W.; Palmer, D. H., Therapeutic developments in pancreatic cancer: current and future perspectives. *Nat Rev Gastroenterol Hepatol* **2018,** *15* (6), 332-347.

8. Bekaii-Saab, T. S.; Starodub, A.; El-Rayes, B. F.; Shahda, S.; O'Neil, B. H.; Noonan, A. M., Phase 1b/2 trial of cancer stemness inhibitor napabucasin (NAPA) plus nab-paclitaxel (nPTX) and gemcitabine (Gem) in metastatic pancreatic adenocarcinoma (mPDAC). *J Clin Oncol* **2018,** *36* (15), 4110.

9. Sonbol, M. B.; Ahn, D. H.; Goldstein, D.; Okusaka, T.; Tabernero, J.; Macarulla, T.; Reni, M.; Li, C. P.; O'Neil, B.; Van Cutsem, E.; Bekaii-Saab, T., CanStem111P trial: a Phase III study of napabucasin plus nab-paclitaxel with gemcitabine. *Future Oncol* **2019,** *15* (12), 1295-1302.

10. https://www.bostonbiomedical.com/news-and-media/20190701_boston-biomedical-inc-announces-update-canstem111p-study-following-interim-analysis/. (accessed August 1, 2019).

11. Li, C.; Chen, C.; An, Q.; Yang, T.; Sang, Z.; Yang, Y.; Ju, Y.; Tong, A.; Luo, Y., A novel series of napabucasin derivatives as orally active inhibitors of signal transducer and activator of transcription 3 (STAT3). *Eur J Med Chem* **2019,** *162*, 543-554.

12. Zhou, Q. F.; Peng, C.; Du, F. Y.; Zhou, L. B.; Shi, Y. J.; Du, Y.; Liu, D. D.; Sun, W. J.; Zhang, M. X.; Chen, G. L., Design, synthesis and activity of BBI608 derivatives targeting on stem cells. *Eur J Med Chem* **2018,** *151*, 39-50.

13.   Frank, D. A., STAT3 as a central mediator of neoplastic cellular transformation. *Cancer Lett* **2007,** *251* (2), 199-210.

14.   Turkson, J.; Jove, R., STAT proteins: novel molecular targets for cancer drug discovery. *Oncogene* **2000,** *19* (56), 6613-6626.

15.   Bromberg, J. F.; Wrzeszczynska, M. H.; Devgan, G.; Zhao, Y. X.; Pestell, R. G.; Albanese, C.; Darnell, J. E., Stat3 as an oncogene. *Cell* **1999,** *98* (3), 295-303.

16.   Ogura, M.; Uchida, T.; Terui, Y.; Hayakawa, F.; Kobayashi, Y.; Taniwaki, M.; Takamatsu, Y.; Naoe, T.; Tobinai, K.; Munakata, W.; Yamauchi, T.; Kageyama, A.; Yuasa, M.; Motoyama, M.; Tsunoda, T.; Hatake, K., Phase I study of OPB-51602, an oral inhibitor of signal transducer and activator of transcription 3, in patients with relapsed/refractory hematological malignancies. *Cancer Sci.* **2015,** *106* (7), 896-901.

17.   Bendell, J. C.; Hong, D. S.; Burris, H. A.; Naing, A.; Jones, S. F.; Falchook, G.; Bricmont, P.; Elekes, A.; Rock, E. P.; Kurzrock, R., Phase 1, open-label, dose-escalation, and pharmacokinetic study of STAT3 inhibitor OPB-31121 in subjects with advanced solid tumors. *Cancer Chemoth. Pharm.* **2014,** *74* (1), 125-130.

18.   Locken, H.; Clamor, C.; Muller, K., Napabucasin and related heterocycle-fused naphthoquinones as STAT3 inhibitors with antiproliferative activity against cancer cells. *J Nat Prod* **2018,** *81* (7), 1636-1644.

19.   Zhan, T.; Rindtorff, N.; Boutros, M., Wnt signaling in cancer. *Oncogene* **2017,** *36* (11), 1461-1473.

20.   Chang, A. Y.; Hsu, E.; Patel, J.; Li, Y. Q.; Zhang, M. J.; Iguchi, H.; Rogoff, H. A., Evaluation of tumor cell-tumor microenvironment component interactions as potential predictors of patient response to napabucasin. *Mol Cancer Res* **2019,** *17* (7), 1429-1434.

21.   Parkinson, E. I.; Hergenrother, P. J., Deoxynyboquinones as NQO1-activated cancer therapeutics. *Acc Chem Res* **2015,** *48* (10), 2715-2723.

22.   Froeling, F. E. M.; Swamynathan, M. M.; Deschenes, A.; Chio, I. I. C.; Brosnan, E.; Yao, M. A.; Alagesan, P.; Lucito, M.; Li, J. Y.; Chang, A. Y.; Trotman, L. C.; Belleau, P.; Park, Y.; Rogoff, H. A.; Watson, J. D.; Tuveson, D. A., Bioactivation of napabucasin triggers reactive oxygen species-mediated cancer cell death. *Clin Cancer Res* **2019,** *25* (23), 7162-7174.

23.   Hu, S.; Sechi, M.; Singh, P. K.; Dai, L.; McCann, S.; Sun, D.; Ljungman, M.; Neamati, N., A novel redox modulator induces a GPX4-mediated cell death that is dependent on iron and reactive oxygen species. *J Med Chem* **2020,** *63* (17), 9838-9855.

24.   Zuo, D. Q.; Shogren, K. L.; Zang, J.; Jewison, D. E.; Waletzki, B. E.; Miller, A. L.; Okuno, S. H.; Cai, Z. D.; Yaszemski, M. J.; Maran, A., Inhibition of STAT3 blocks protein synthesis and tumor metastasis in osteosarcoma cells. *J Exp Clin Cancer Res* **2018,** *37*, 1-11.

25.   Gadd, M. S.; Testa, A.; Lucas, X.; Chan, K. H.; Chen, W.; Lamont, D. J.; Zengerle, M.; Ciulli, A., Structural basis of PROTAC cooperative recognition for selective protein degradation. *Nat Chem Biol* **2017,** *13* (5), 514-521.

26.   Buckley, D. L.; Crews, C. M., Small-molecule control of intracellular protein levels through modulation of the ubiquitin proteasome system. *Angew Chem Int Ed Engl* **2014,** *53* (9), 2312-2330.

27.   Cromm, P. M.; Crews, C. M., Targeted protein degradation: From chemical biology to drug discovery. *Cell Chem Biol* **2017,** *24* (9), 1181-1190.

28.   Bai, L. C.; Zhou, H. B.; Xu, R. Q.; Zhao, Y. J.; Chinnaswamy, K.; McEachern, D.; Chen, J. Y.; Yang, C. Y.; Liu, Z. M.; Wang, M.; Liu, L.; Jiang, H.; Wen, B.; Kumar, P.; Meagher, J. L.; Sun, D. X.; Stuckey, J. A.; Wang, S. M., A potent and selective small-molecule degrader of STAT3 achieves complete tumor regression in vivo. *Cancer Cell* **2019,** *36* (5), 498-511.

29.   Zhou, H. B.; Bai, L. C.; Xu, R. Q.; Zhao, Y. J.; Chen, J. Y.; McEachern, D.; Chinnaswamy, K.; Wen, B.; Dai, L. P.; Kumar, P.; Yang, C. Y.; Liu, Z. M.; Wang, M.; Liu, L.; Meagher, J. L.; Yi, H.; Sun, D. X.; Stuckey, J. A.; Wang, S. M., Structure-based discovery of SD-36 as a potent, selective, and efficacious PROTAC degrader of STAT3 rotein. *J. Med. Chem.* **2019,** *62* (24), 11280-11300.

30.   Salami, J.; Alabi, S.; Willard, R. R.; Vitale, N. J.; Wang, J.; Dong, H. Q.; Jin, M. Z.; McDonnell, D. P.; Crew, A. P.; Neklesa, T. K.; Crews, C. M., Androgen receptor degradation by the proteolysis-targeting chimera ARCC-4 outperforms enzalutamide in cellular models of prostate cancer drug resistance. *Commun Biol* **2018,** *1* (1), 1-9.

31.   Li, Y. B.; Yang, J. L.; Aguilar, A.; McEachern, D.; Przybranowski, S.; Liu, L.; Yang, C. Y.; Wang, M.; Han, X.; Wang, S. M., Discovery of MD-224 as a first-in-class, highly potent, and efficacious proteolysis targeting chimera murine double minute 2 degrader capable of achieving complete and durable tumor regression. *J Med Chem* **2019,** *62* (2), 448-466.

32.   Wang, Z. Q.; He, N. Z.; Guo, Z. W.; Niu, C. L.; Song, T.; Guo, Y. F.; Cao, K. K.; Wang, A. H.; Zhu, J. J.; Zhang, X. D.; Zhang, Z. C., Proteolysis targeting chimeras for the selective degradation of Mcl-1/Bcl-2 derived from nonselective target binding ligands. *J Med Chem* **2019,** *62* (17), 8152-8163.

33.   Raina, K.; Lu, J.; Qian, Y. M.; Altieri, M.; Gordon, D.; Rossi, A. M. K.; Wang, J.; Chen, X.; Dong, H. Q.; Siu, K.; Winkler, J. D.; Crew, A. P.; Crews, C. M.; Coleman, K. G., PROTAC-induced BET protein degradation as a therapy for castration-resistant prostate cancer. *Proc Natl Acad Sci U S A* **2016,** *113* (26), 7124-7129.

34.   Chamberlain, P. P.; Cathers, B. E., Cereblon modulators: Low molecular weight inducers of protein degradation. *Drug Discov Today Technol* **2019,** *31*, 29-34.

35.   Girardini, M.; Maniaci, C.; Hughes, S. J.; Testa, A.; Ciulli, A., Cereblon versus VHL: Hijacking E3 ligases against each other using PROTACs. *Bioorg Med Chem* **2019,** *27* (12), 2466-2479.

36.   Shahbazi, S.; Peer, C. J.; Polizzotto, M. N.; Uldrick, T. S.; Roth, J.; Wyvill, K. M.; Aleman, K.; Zeldis, J. B.; Yarchoan, R.; Figg, W. D., A sensitive and robust HPLC assay with fluorescence detection for the quantification of pomalidomide in human plasma for pharmacokinetic analyses. *J Pharm Biomed Anal* **2014,** *92*, 63-68.

37.   Debnath, B.; Xu, S. L.; Neamati, N., Small molecule inhibitors of signal transducer and activator of transcription 3 (Stat3) protein. *J Med Chem* **2012,** *55* (15), 6645-6668.

38.   Lu, T.; Bankhead, A.; Ljungman, M.; Neamati, N., Multi-omics profiling reveals key signaling pathways in ovarian cancer controlled by STAT3. *Theranostics* **2019,** *9* (19), 5478-5496.

39.   Huang, H. T.; Dobrovolsky, D.; Paulk, J.; Yang, G.; Weisberg, E. L.; Doctor, Z. M.; Buckley, D. L.; Cho, J. H.; Ko, E.; Jang, J.; Shi, K.; Choi, H. G.; Griffin, J. D.; Li, Y.; Treon, S. P.; Fischer, E. S.; Bradner, J. E.; Tan, L.; Gray, N. S., A chemoproteomic approach to query the degradable kinome using a multi-kinase degrader. *Cell Chem. Biol.* **2018,** *25* (1), 88-99.

40.   Lin, J.; Buettner, R.; Yuan, Y. C.; Yip, R.; Horne, D.; Jove, R.; Vaidehi, N., Molecular dynamics simulations of the conformational changes in signal transducers and activators of transcription, Stat1 and Stat3. *J Mol Graph Model* **2009,** *28* (4), 347-356.

41.   Ishoey, M.; Chorn, S.; Singh, N.; Jaeger, M. G.; Brand, M.; Paulk, J.; Bauer, S.; Erb, M. A.; Parapatics, K.; Muller, A. C.; Bennett, K. L.; Ecker, G. F.; Bradner, J. E.; Winter, G. E., Translation termination factor GSPT1 Is a phenotypically relevant off-target of heterobifunctional phthalimide degraders. *ACS Chem Biol* **2018,** *13* (3), 553-560.

42.   Matyskiela, M. E.; Lu, G.; Ito, T.; Pagarigan, B.; Lu, C.-C.; Miller, K.; Fang, W.; Wang, N.-Y.; Nguyen, D.; Houston, J. J. N., A novel cereblon modulator recruits GSPT1 to the CRL4 CRBN ubiquitin ligase. *Nature* **2016,** *535* (7611), 252-257.

43.   Yang, J.; Li, Y.; Aguilar, A.; Liu, Z.; Yang, C. Y.; Wang, S., Simple structural modifications converting a bona fide MDM2 PROTAC degrader into a molecular glue molecule: A cautionary tale in the design of PROTAC degraders. *J Med Chem* **2019,** *62* (21), 9471-9487.

44.   Han, X.; Wang, C.; Qin, C.; Xiang, W.; Fernandez-Salas, E.; Yang, C. Y.; Wang, M.; Zhao, L.; Xu, T.; Chinnaswamy, K.; Delproposto, J.; Stuckey, J.; Wang, S., Discovery of ARD-69 as a highly potent proteolysis targeting chimera (PROTAC) degrader of androgen receptor (AR) for the treatment of prostate cancer. *J Med Chem* **2019,** *62* (2), 941-964.

45.   Akuffo, A. A.; Alontaga, A. Y.; Metcalf, R.; Beatty, M. S.; Becker, A.; McDaniel, J. M.; Hesterberg, R. S.; Goodheart, W. E.; Gunawan, S.; Ayaz, M.; Yang, Y.; Karim, M. R.; Orobello, M. E.; Daniel, K.; Guida, W.; Yoder, J. A.; Rajadhyaksha, A. M.; Schonbrunn, E.; Lawrence, H. R.; Lawrence, N. J.; Epling-Burnette, P. K., Ligand-mediated protein degradation reveals functional conservation among sequence variants of the CUL4-type E3 ligase substrate receptor cereblon. *J Biol Chem* **2018,** *293* (16), 6187-6200.

46.   Bondeson, D. P.; Smith, B. E.; Burslem, G. M.; Buhimschi, A. D.; Hines, J.; Jaime-Figueroa, S.; Wang, J.; Hamman, B. D.; Ishchenko, A.; Crews, C. M., Lessons in PROTAC design from selective degradation with a promiscuous warhead. *Cell Chem Biol* **2018,** *25* (1), 78-87.

47.   Chau, M. N.; Banerjee, P. P., Development of a STAT3 reporter prostate cancer cell line for high throughput screening of STAT3 activators and inhibitors. *Biochem Biophys Res Commun* **2008,** *377* (2), 627-631.

48.   An, J.; Ponthier, C. M.; Sack, R.; Seebacher, J.; Stadler, M. B.; Donovan, K. A.; Fischer, E. S., pSILAC mass spectrometry reveals ZFP91 as IMiD-dependent substrate of the CRL4(CRBN) ubiquitin ligase. *Nat Commun* **2017,** *8* (1), 1-11.

49.   Petzold, G.; Fischer, E. S.; Thomä, N. H., Structural basis of lenalidomide-induced CK1α degradation by the CRL4(CRBN) ubiquitin ligase. *Nature* **2016,** *532* (7597), 127-30.

50.   Kronke, J.; Udeshi, N. D.; Narla, A.; Grauman, P.; Hurst, S. N.; McConkey, M.; Svinkina, T.; Heckl, D.; Comer, E.; Li, X.; Ciarlo, C.; Hartman, E.; Munshi, N.; Schenone, M.; Schreiber, S. L.; Carr, S. A.; Ebert, B. L., Lenalidomide causes selective degradation of IKZF1 and IKZF3 in multiple myeloma cells. *Science* **2014,** *343* (6168), 301-305.

51.   Gandhi, A. K.; Kang, J.; Havens, C. G.; Conklin, T.; Ning, Y.; Wu, L.; Ito, T.; Ando, H.; Waldman, M. F.; Thakurta, A.; Klippel, A.; Handa, H.; Daniel, T. O.; Schafer, P. H.; Chopra, R., Immunomodulatory agents lenalidomide and pomalidomide co-stimulate T cells by inducing degradation of T cell repressors Ikaros and Aiolos via modulation of the E3 ubiquitin ligase complex CRL4(CRBN.). *Br. J. Haematol.* **2014,** *164* (6), 811-821.

52.   Matyskiela, M. E.; Zhu, J.; Baughman, J. M.; Clayton, T.; Slade, M.; Wong, H. K.; Danga, K.; Zheng, X.; Labow, M.; LeBrun, L.; Lu, G.; Chamberlain, P. P.; Thompson, J. W., Cereblon Modulators Target ZBTB16 and Its Oncogenic Fusion Partners for Degradation via Distinct Structural Degrons. *ACS Chem Biol* **2020**, 3149-3158.

53.   Jin, X.; Jin, H. R.; Jung, H. S.; Lee, S. J.; Lee, J. H.; Lee, J. J., An atypical E3 ligase zinc finger protein 91 stabilizes and activates NF-kappaB-inducing kinase via Lys63-linked ubiquitination. *J Biol Chem* **2010,** *285* (40), 30539-30547.

54.   Ma, J.; Mi, C. L.; Wang, K. S.; Lee, J. J.; Jin, X. J., Zinc finger protein 91 (ZFP91) activates HIF-1 alpha via NF-kappa B/p65 to promote proliferation and tumorigenesis of colon cancer. *Oncotarget* **2016,** *7* (24), 36551-36562.

55.   Tang, D. E.; Dai, Y.; Xu, Y.; Lin, L. W.; Liu, D. Z.; Hong, X. P.; Ou, M. L.; Jiang, H. W.; Xu, S. H., The ubiquitinase ZFP91 promotes tumor cell survival and confers chemoresistance through FOXA1 destabilization. *Carcinogenesis* **2020,** *41* (1), 56-66.

56.   Sun, J. J.; Du, Y. P.; Song, Q. L.; Nan, J.; Guan, P. Z.; Guo, J. H.; Wang, X.; Yang, J. B.; Zhao, C. Y., E2F is required for STAT3-mediated upregulation of cyclin B1 and Cdc2 expressions and contributes to G2-M phase transition. *Acta Biochim Biophys Sin* **2019,** *51* (3), 313-322.

57.   Koganti, S.; Hui-Yuen, J.; McAllister, S.; Gardner, B.; Grasser, F.; Palendira, U.; Tangye, S. G.; Freeman, A. F.; Bhaduri-McIntosh, S., STAT3 interrupts ATR-Chk1 signaling to allow oncovirus-mediated cell proliferation. *Proc Natl Acad Sci U S A* **2014,** *111* (13), 4946-4951.

58.   Wang, W. B.; Deng, H. K.; Levy, D. E.; Lee, C. K., STAT3 negatively regulates antiviral responses through suppression of TLR and type I IFN-mediated responses. *Cytokine* **2009,** *48* (1-2), 126-126.

59.   Tang, Z.; Kang, B.; Li, C.; Chen, T.; Zhang, Z., GEPIA2: an enhanced web server for large-scale expression profiling and interactive analysis. *Nucleic Acids Res* **2019,** *47* (W1), W556-W560.

60.   Huang, W.; Li, N.; Hu, J.; Wang, L., Inhibitory effect of RNA-mediated knockdown of zinc finger protein 91 pseudogene on pancreatic cancer cell growth and invasion. *Oncol Lett* **2016,** *12* (2), 1343-1348.

61.   McAlister, G. C.; Nusinow, D. P.; Jedrychowski, M. P.; Wuhr, M.; Huttlin, E. L.; Erickson, B. K.; Rad, R.; Haas, W.; Gygi, S. P., MultiNotch MS3 enables accurate, sensitive, and multiplexed detection of differential expression across cancer cell line proteomes. *Anal Chem* **2014,** *86* (14), 7150-7158.

62.   Bendell, J. C.; Hubbard, J. M.; O'Neil, B. H.; Jonker, D. J.; Starodub, A.; Peyton, J. D.; Pitot, H. C.; Halfdanarson, T. R.; Nadeau, B. R.; Zubkus, J. D.; Adesunloye, B.; Edenfield, W. J.; Li, Y.; Li, W.; Grothey, A.; Borodyansky, L.; Li, C., Phase 1b/II study of cancer stemness inhibitor napabucasin (BBI-608) in combination with FOLFIRI +/- bevacizumab (bev) in metastatic colorectal cancer (mCRC) patients (pts). *J Clin Oncol* **2017,** *35* (15_suppl), 3529-3529.

63.   Mason, W. P.; de Robles, P.; Borodyansky, L.; Hitron, M.; Ortuzar, W. F.; Khan, W.; Xu, B.; Li, W.; Li, Y. Z.; Li, C. J., BBI608-201GBM: A phase Ib/II clinical study of napabucasin (BBI608) in combination with temozolomide (TMZ) for adult patients with recurrent glioblastoma (GBM). *J Clin Oncol* **2017,** *35*, e13525-e13525.

64.   Larson, T.; Ortuzar, W. F.; Bekaii-Saab, T. S.; Becerra, C.; Ciombor, K. K.; Hubbard, J. M.; Edenfield, W. J.; Shao, S. H.; Grothey, A.; Borodyansky, L.; Xu, B.; Li, W.; Li, Y. Z.; Li, C.; Khan, W., BBI608-224: A phase Ib/II study of cancer stemness inhibitor napabucasin (BBI-608) administered with panitumumab in KRAS wild-type patients with metastatic colorectal cancer. *J Clin Oncol* **2017,** *35* (4), 677.

65.   Jonker, D. J.; Stephenson, J.; Edenfield, W. J.; Supko, J. G.; Li, Y. Z.; Li, W.; Hitron, M.; Leggett, D.; Kerstein, D.; Li, C., A phase I extension study of BBI608, a first-in-class cancer stein cell (CSC) inhibitor, in patients with advanced solid tumors. *J Clin Oncol* **2014,** *32* (15), 2546.

66.   Jonker, D. J.; Nott, L.; Yoshino, T.; Gill, S.; Shapiro, J.; Ohtsu, A.; Zalcberg, J.; Vickers, M. M.; Wei, A. C.; Gao, Y.; Tebbutt, N. C.; Markman, B.; Price, T.; Esaki, T.; Koski, S.; Hitron, M.; Li, W.; Li, Y.; Magoski, N. M.; Li, C. J.; Simes, J.; Tu, D.; O'Callaghan, C. J., Napabucasin versus placebo in refractory advanced colorectal cancer: a randomised phase 3 trial. *Lancet Gastroenterol Hepatol* **2018,** *3* (4), 263-270.

67.   Shah, M. A.; Shitara, K.; Lordick, F.; Bang, Y. J.; Tebbutt, N. C.; Metges, J. P., The BRIGHTER trial: A phase 3 randomized double-blind study of napabucasin (NAPA) plus paclitaxel (PTX) versus placebo (PBO) plus PTX in patients (pts) with pretreated advanced gastric and gastroesophageal junction (GEJ) adenocarcinoma. *J Clin Oncol* **2018,** *36* (15), 4010.

68.   Kalra, M.; Cote, G. M.; Heist, R. S.; Spittler, A. J.; Yu, S.; Hitron, M., A phase 1b study of napabucasin (NAPA) plus weekly paclitaxel (PTX) in patients (pts) with advanced thymoma and thymic carcinoma. *J Clin Oncol* **2018,** *36* (15), e20578.

69.   Shinozaki, E.; Kawazoe, A.; Kuboki, Y.; Komatsu, Y.; Nishina, T.; Hara, H.; Yuki, S.; Shitara, K.; Bando, H.; Kotani, D.; Takahashi, K.; Mikamoto, Y.; Hasegawa, H.; Hirano, N.; Nomura, S.; Togashi, Y.; Nishikawa, H.; Sato, A.; Ohtsu, A.; Yoshino, T., Multicenter phase I/II trial of BBI608 and pembrolizumab combination in patients with metastatic colorectal cancer (SCOOP Study): EPOC1503. *J Clin Oncol* **2018,** *36* (15_suppl), 3530.

70.   Shitara, K.; Yodo, Y.; Iino, S., A phase I study of napabucasin plus paclitaxel for japanese patients With advanced/recurrent gastric cancer. *In Vivo* **2019,** *33* (3), 933-937.

CHAPTER IV

Significance and Future Directions[2]

Challenges in the Treatment of Pancreatic Cancer

Pancreatic cancer is a lethal disease that has been investigated for many years with a limited number of treatment options. Early diagnosis of pancreatic cancer remains challenging owing to its rapid progression and insidious symptoms.[1] Despite the curative potential of surgery, metastasis is a major hurdle that precludes surgical resection in most patients.[1] Conventional therapies including gemcitabine and FOLFIRINOX have a limited efficacy due to systemic toxicity and chemoresistance.[2-4] Targeted treatments present a more favorable therapeutic approach due to the reduced side effects that lessen the burden of chemotherapy on patients. However, critical targets including KRAS that is the most common mutated oncogenes in pancreatic cancer failed to present an effective therapeutic approach due to the lack of well-defined pockets, alternative signaling pathways, and developed resistance.[5-7] Erlotinib, an inhibitor of the upstream epidermal growth factor receptor (EGFR), given with gemcitabine is the only FDA-approved targeted therapy for the treatment of pancreatic cancer.[8, 9] Unfortunately, although the combination demonstrated statistically significant improved patient survival, the clinical benefit was modest questioning its cost-effectiveness.[8-10] Importantly, pancreatic cancer is characterized by a complex microenvironment that contributes to the progression of the disease, reduced therapeutic efficacy, and chemoresistance.[11] The pancreatic tumor microenvironment includes regulatory T-cells

---

[2] Sigma-2 receptor and TMEM97 are interchangeable terms.

(Treg), tumor-associated macrophages (TAM), myeloid-derived suppressor cells (MDSC), and pancreatic stellate cells.[11] The pancreatic stellate cells can possibly form a stem cell niche that resist treatment and contributes to cancer recurrence.[12] In addition, Treg, TAM, and MSDC produce an immunosuppressive microenvironment that results in immune escape.[13] Overall, the success of therapeutic strategies for pancreatic cancer is limited by metastasis, relapse, systemic toxicity, and chemoresistance. Thus, there is an unmet medical need for effective anticancer agents and combination strategies that target essential pathways implicated in pancreatic cancer and can overcome the previously addressed challenges. Our work investigates the therapeutic potential of two targets that play a role in pancreatic cancer cell growth: sigma-2 receptor (S2R) and ZFP91. S2R plays a role in cholesterol uptake on which pancreatic cancer cells are dependent for their growth.[14] Sigma-2 ligands (S2Ls) and low-density lipoprotein receptor (LDLR) silencing enhanced the tumor reduction in murine models of pancreatic cancer compared to gemcitabine only presenting S2R as a promising target.[14-16] Importantly, cholesterol and oxysterols are enriched in the tumor microenvironment and play a role in tumor progression.[17, 18] Thus, interfering with the cholesterol availability will not only alter the cancer cell metabolism but can also have an impact on the tumor microenvironment. Little is known about the second target; ZFP91, however, it plays a role in the pancreatic cancer cell growth and its overexpression correlates with poor prognosis.[19, 20] In conclusion, S2R and ZFP91 are proteins implicated in pancreatic cancer that we sought to target in an attempt to identify novel anticancer agents.

Significance of the Study

The major focus of this dissertation is on the development of inhibitors/degraders of (S2R) and ZFP91 for the treatment of pancreatic cancer. Currently, there are no clinically available S2R- or ZFP91-targeted anticancer therapeutics. S2R is overexpressed in select cancers and plays a

163

critical role in cholesterol homeostasis. TMEM97 silencing inhibits the cell proliferation in various cancers and its overexpression correlates with poor prognosis. Thus, developing small molecules that can inhibit TMEM97 by interfering with the cancer cell's cholesterol metabolism represents a promising therapeutic strategy. With the use of transcriptomics, proteomics, and extensive mechanistic studies, we identified a highly selective and potent S2L that is cytotoxic to pancreatic cancer cells. In the second project, we describe the discovery of a napabucasin-based PROTAC that degrades ZFP91. ZFP91 is a potential oncogenic protein that is overexpressed in pancreatic cancer. Collectively, this dissertation provides further evidence for S2R and ZFP91 as targets in pancreatic cancer and rationalizes the pursuit of their targeted agents as well as S2L combinations with FDA-approved drugs in preclinical models.

Future Directions

Chapter II

ROS detection

Although we were able to demonstrate the involvement of reactive oxygen species (ROS) through the increase in the heme oxygenase 1 (HMOX1) protein level and the rescued cell death in presence of NAC, we were not able to consistently detect ROS using the CM-H_2DCFDA (5-(and-6)-chloromethyl-2',7'-dichlorodihydrofluorescein diacetate, acetyl ester)) assay as previously described.[21] I propose detecting ROS using a different assay (e.g. ROS-Glo™ H_2O_2 luminescent assay) or optimizing for the experimental conditions.

Detection of cholesterol and calcium levels

Since previous studies demonstrated the role of S2R in cholesterol and calcium metabolism, investigating the effect of **JR235** in this context will further support its mechanism

of action. The effect of **JR235** on the calcium levels will be indicative of its S2R-mediated cellular effects. We observed downregulation of calcium signaling genes with our treatment. With the unclear function of S2R in calcium homeostasis, investigating these genes (e.g. Neurotensin Receptor 1, NTSR1) can provide findings that better elucidate its role. The expression of S2R increases under cholesterol-deprived conditions.[22, 23] Testing the activity of **JR235** under these conditions will be informative of its dependence on the S2R. Monitoring the rate of cholesterol uptake can be used to identify TMEM97 inhibitors that interfere with its binding to the LDLR and reduce the LDL uptake.

Further optimization for more selective analogs

Since the cytotoxicity of **JR235** was only partially dependent on S2R suggesting its multi-targeted mechanism, further optimization might identify a more selective analog with reduced off-target binding. Testing other analogs for their S2R binding is undergoing.

Obtaining a crystal structure of S2R is important for identification of the active site and for structure-based drug design. A co-crystal structure of **JR235** will be informative of its binding mode and mechanism of inhibition. This will guide future studies for optimizing for more selective inhibitors. We can also test whether **JR235** fits the reported S2R pharmacophore model to identify the structural features that can be further optimized.

Combination studies

In our work, we demonstrated *in vitro* synergistic cytotoxicity when combining **JR235** with cholesterol and lipid biosynthesis inhibitors including HMCR and SCD inhibitors, respectively. Although not well-established yet, the recently unveiled identity of S2R suggests that TMEM97 inhibitors will interfere with the LDL uptake and cholesterol availability in the cells.[24] Inhibiting both the cholesterol/lipid uptake and biosynthesis will block two important sources by

which the cells acquire their nutrients and will lead to starvation and cancer cell death. It is worth pursuing these combinations in *in vivo* models. The VEGF pathway plays a role in cancer progression.[25] It activates mTOR through the PI3K/AKT pathway to promote angiogenesis.[26, 27] Cholesterol regulates VEGFR expression and signaling.[28, 29] The mTOR activates the SREBP-induced transcription of the genes involved in the cholesterol synthesis (Figure IV-1). Hence, VEGFR and mTOR inhibitors may result in synergistic cell death when combined with S2Ls. Importantly, previous literature demonstrated synergistic cell death with combinations of cholesterol biosynthesis inhibitors and mTOR/VEGFR inhibitors.[30, 31] I propose combining the previously discussed inhibitors with **JR235** and other known S2Ls. This may introduce novel and promising anticancer combination therapies for the treatment of pancreatic cancer (Figure IV-1).

Combination therapies of S2L with the standard-of-care treatments including gemcitabine have demonstrated enhanced tumor reduction in murine models of pancreatic cancer compared to gemcitabine alone.[16, 32] Testing **JR235** in combination with gemcitabine is worth investigating.
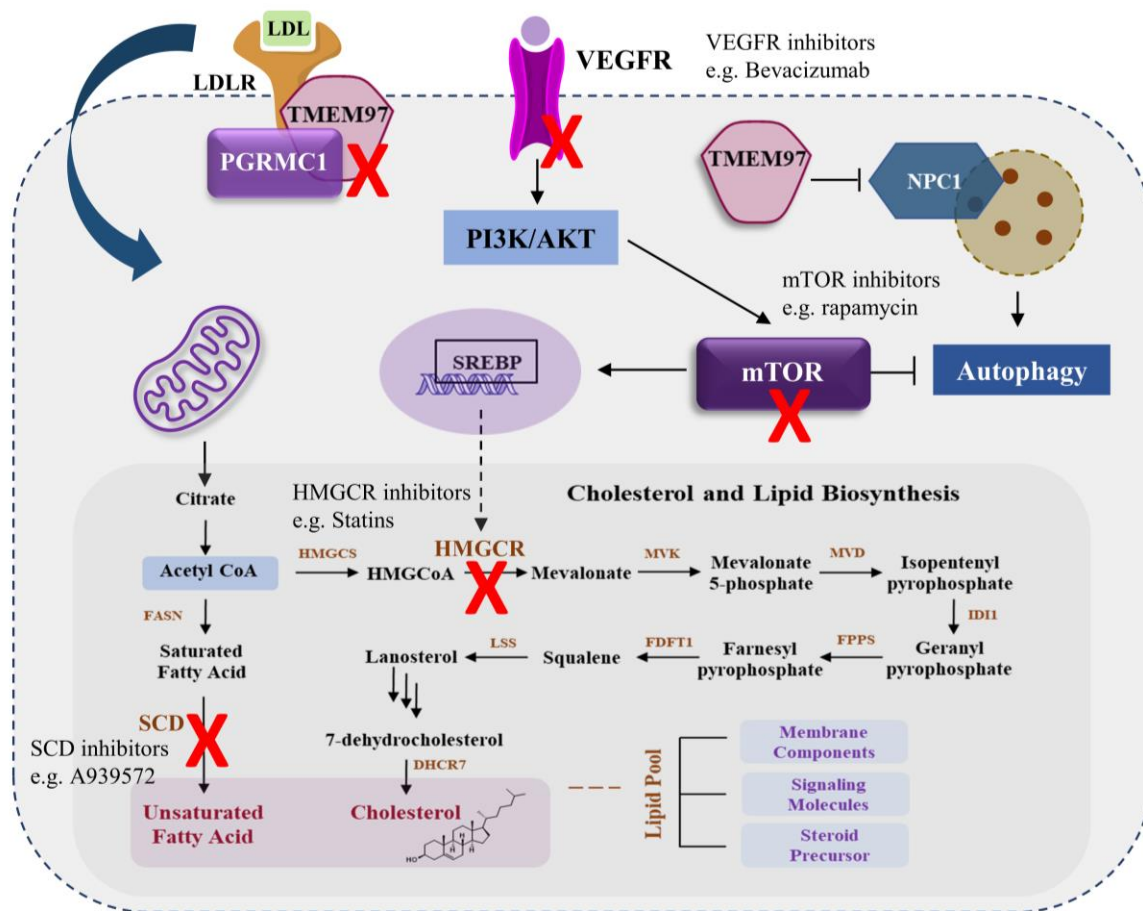
Figure IV-1. Potential sites of inhibition for synergistic cell death. LDLR: low-density lipoprotein receptor; NPC1: Niemann–Pick C1 protein; VEGFR: vascular endothelial growth factor receptor; PI3K: phosphatidylinositol 3-kinase; AKT: protein kinase B; mTOR: mammalian target of rapamycin; SREBP: sterol regulatory element binding protein; HMGCS: 3-hydroxy-3-methylglutaryl-CoA synthase; HMGCR: 3-hydroxy-3-methylglutaryl-CoA reductase; MVK: mevalonate kinase; MVD: diphosphomevalonate decarboxylase; IDI1: isopentenyl pyrophosphate isomerase 1; FPPS: farnesyl pyrophosphate synthase; FDFT: farnesyl-diphosphate farnesyltransferase 1; LSS: lanosterol synthase; DHCR7: 7-dehydrocholesterol reductase; FASN: fatty acid synthase; SCD: stearoyl-CoA desaturase; TCA: tricarboxylic acid cycle.

Validation of GUK1

Our work is the first to use bioinformatics analysis to study the mechanistic signature of S2Ls like **JR235**. Protein-protein interaction analysis of the top 100 upregulated genes was conducted using STRING[33] that revealed a correlation between TMEM97 and guanylate kinase (GUK1, $\log_2$FC = 0.90) (Figure IV-2).[34] GUK1 is an essential protein that is required for guanidine diphosphate (GDP) production and cyclic GMP (cGMP) metabolism.[35] GUK1 plays an important role in tumorigenesis where altered metabolism in cancer cells is associated with upregulated nucleotide biosynthesis.[35] There are no studies investigating the role of TMEM97 with respect to

167

GUK1 thus, it is worth pursuing understanding this relationship further. Importantly, GUK1 has been reported as a survival kinase in pancreatic cancer cells.[36] Moreover, cGMP activation results in increased levels of intracellular calcium,[37] a mechanism associated with S2Ls that is not well-understood. Validation of this gene and investigating its role with respect to TMEM97 might identify a novel gene/pathway and assist in elucidating TMEM97's function and its role in cancer.
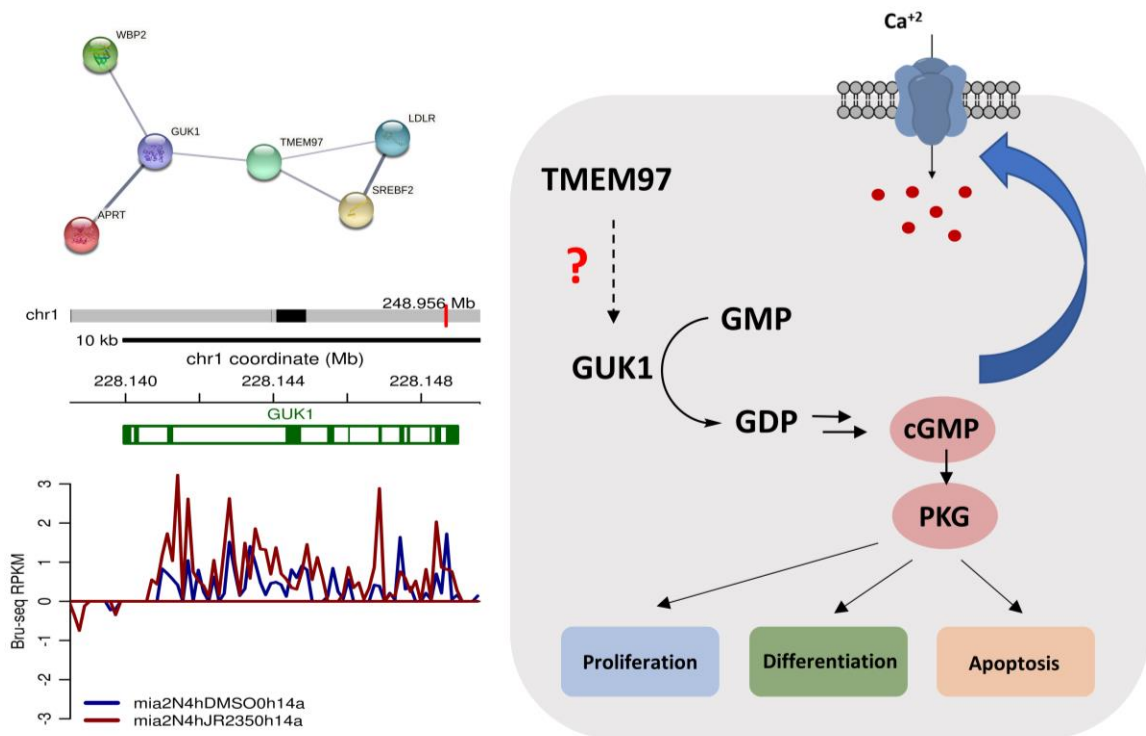

Figure IV-2. Investigation of the relationship between GUK1 and TMEM97. STRING analysis reveals a correlation between TMEM97 with GUK1 that is upregulated with **JR235** treatment as presented in the trace diagram. The diagram on the right highlights the role of GUK1. PKG: protein kinase G.

TMEM97 silencing studies in various cancer cell lines

TMEM97's implication in cancer has been investigated using knockdown studies in breast, gastric and brain cancers but not pancreatic cancer.[38-40] We only tested the cytotoxicity of **JR235** in TMEM97-silenced MIA PaCa-2 cells. Knocking down TMEM97 in various pancreatic cancer cell lines and cell lines with low, medium, and high S2R expression is important to determine 1) The dependency of pancreatic cancer cells on TMEM97 for survival. 2) The correlation between **JR235**'s cytotoxicity and TMEM97 expression. The breast cancer cell line MCF-7 and the

neuroblastoma cell line SK-N-SH are considered powerful research tools in S2R studies for their high S2R expression and low affinity-state or no S1R expression. It will be beneficial to use these cell lines as a control.

Pharmacokinetics and *in vivo* studies

Assessment of the pharmacokinetic properties and the *in vivo* efficacy of our compounds in murine models of pancreatic cancer is undergoing. This will allow determining the success of this class of compounds in preclinical studies and their potential as clinical candidates.
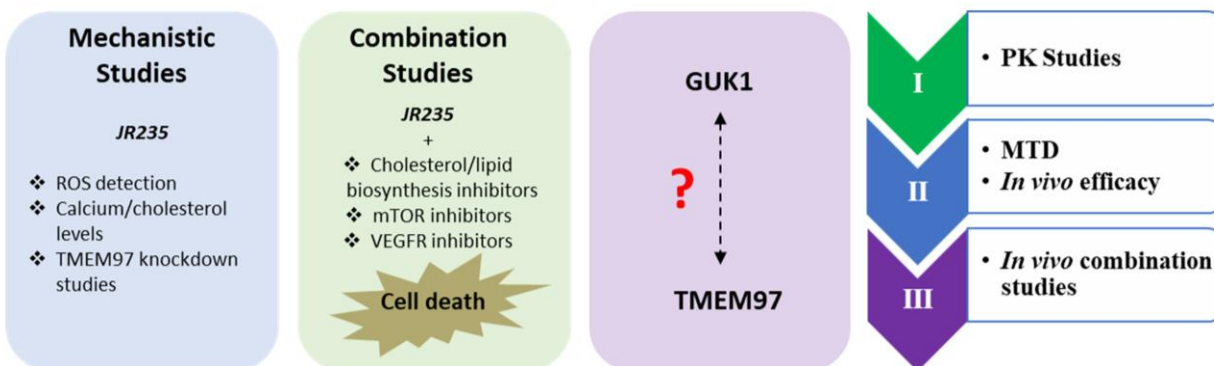

Figure IV-3. Future directions for Chapter II.

Chapter III

Validation of other proteins as potential targets

XD2-149 exhibits its antitumor activity partially through ZFP91 degradation. ZFP91 has been reported as a degradable target for CRBN-based PROTACs and IMiDs such as pomalidomide suggesting ZFP91 targeting is independent of napabucasin.[41, 42] Validation of other downregulated proteins might lead to the identification of proteins whose degradation is driven by napabucasin binding and/or contribute to the cytotoxicity of **XD2-149**. We found that many of the **XD2-149** top downregulated proteins are linked to STAT3 including the transmembrane protease serine 4 (TMPRSS4) ($\log_2$FC = -1.27), a protein that can play a role in STAT3 activation.[43, 44] Although

previous studies reported the binding of napabucasin to STAT3, it is still unclear whether napabucasin's effect on STAT3 is direct or is mediated by other proteins and signaling pathways.[45, 46] Therefore, further investigation of this protein is worth pursuing to determine if it's a degradable target of **XD2-149** (Figure IV-4). If proven, this will identify a novel target of napabucasin and elucidate its mechanism of action with respect to STAT3. It is worth noting that previous studies demonstrated that simple structural modifications could lead to repurposing of the PROTAC to proteins other than the intended target.[47, 48] Further optimization of the PROTAC might be required for the degradation of napabucasin's target.
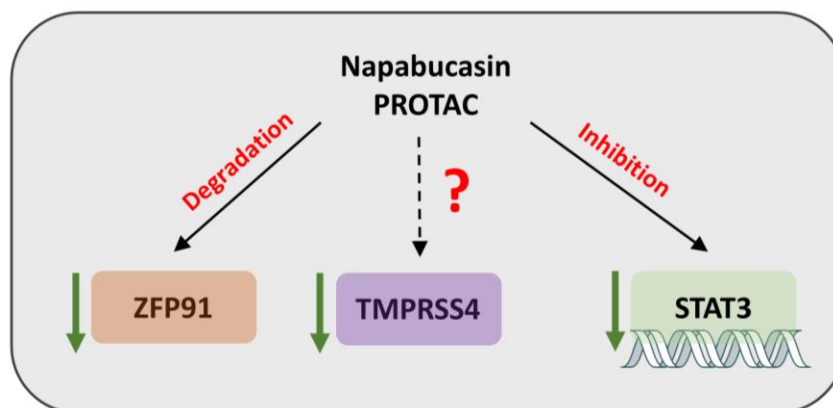

Figure IV-4. Investigation of the effect of **XD2-149** on TMPRSS4.

Testing ZFP91 degradation in different cancer cell lines

Although we focused in our work on pancreatic cancer and we proved ZFP91 degradation in two different pancreatic cancer cell lines, it is worth examining ZFP91 degradation in various cancer cell lines to assess **XD2-149**'s specificity, potency, and potential use against other cancers.

Assessment of the P-gp substrate potential and permeability

Our PROTACs displayed variations in the cytotoxicity across different cancer cell lines. Assessing the P-glycoprotein (P-gp) substrate potential will determine whether the compound is a substrate of P-gp that can be differentially expressed in various cell lines, hence, contribute to the

differences in the cytotoxicity. Determining the compound permeability will also be beneficial in making more solid conclusions on the cellular activity.

Pharmacokinetics and preclinical evaluation of XD2-149

Napabucasin showed success in early clinical trials demonstrating its safety and tolerability and was designated orphan drug status for treatment of pancreatic cancer.[49, 50] This data in conjunction with the *in vitro* cytotoxicity displayed by our napabucasin-PROTAC **XD2-149** is promising for further assessment of its metabolic stability, pharmacokinetics, and *in vivo* efficacy. ZFP91 silencing studies demonstrated reduced tumor growth, however, its exact role in cancer is yet to be established.[51] *In vivo* studies on **XD2-149** will provide insight to the efficacy of a new class of anticancer agents and will provide a rationale for the targeting of ZFP91.
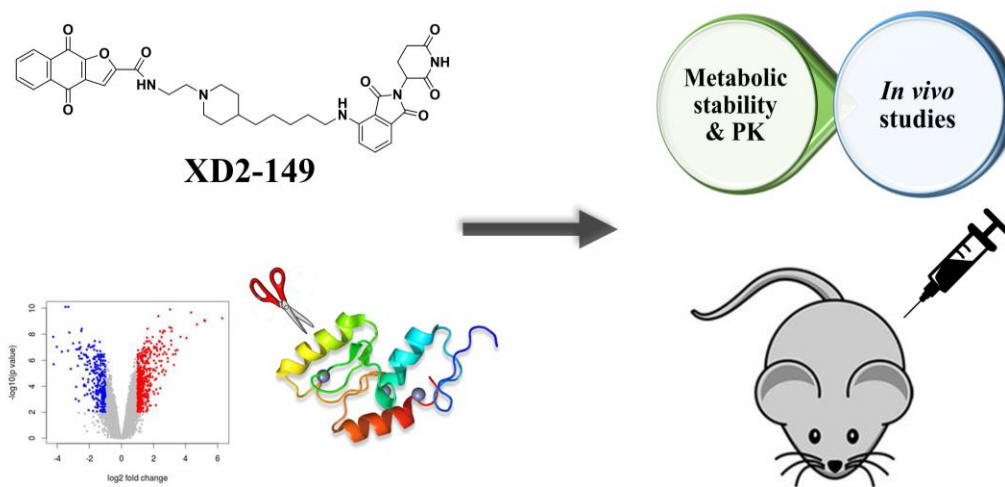

Figure IV-5. Future directions for Chapter III.

171

References

1.   Kleeff, J.; Korc, M.; Apte, M.; La Vecchia, C.; Johnson, C. D.; Biankin, A. V.; Neale, R. E.; Tempero, M.; Tuveson, D. A.; Hruban, R. H.; Neoptolemos, J. P., Pancreatic cancer. *Nat Rev Dis Primers* **2016,** *2*, 16022.

2.   Andersson, R.; Aho, U.; Nilsson, B. I.; Peters, G. J.; Pastor-Anglada, M.; Rasch, W.; Sandvold, M. L., Gemcitabine chemoresistance in pancreatic cancer: molecular mechanisms and potential solutions. *Scand J Gastroenterol* **2009,** *44* (7), 782-786.

3.   Conroy, T.; Desseigne, F.; Ychou, M.; Bouche, O.; Guimbaud, R.; Becouarn, Y.; Adenis, A.; Raoul, J. L.; Gourgou-Bourgade, S.; de la Fouchardiere, C.; Bennouna, J.; Bachet, J. B.; Khemissa-Akouz, F.; Pere-Verge, D.; Delbaldo, C.; Assenat, E.; Chauffert, B.; Michel, P.; Montoto-Grillot, C.; Ducreux, M.; Groupe Tumeurs Digestives of, U.; Intergroup, P., FOLFIRINOX versus gemcitabine for metastatic pancreatic cancer. *N Engl J Med* **2011,** *364* (19), 1817-1825.

4.   Gourgou-Bourgade, S.; Bascoul-Mollevi, C.; Desseigne, F.; Ychou, M.; Bouche, O.; Guimbaud, R.; Becouarn, Y.; Adenis, A.; Raoul, J. L.; Boige, V.; Berille, J.; Conroy, T., Impact of FOLFIRINOX compared with gemcitabine on quality of life in patients with metastatic pancreatic cancer: results from the PRODIGE 4/ACCORD 11 randomized trial. *J Clin Oncol* **2013,** *31* (1), 23-29.

5.   Qian, Y.; Gong, Y.; Fan, Z.; Luo, G.; Huang, Q.; Deng, S.; Cheng, H.; Jin, K.; Ni, Q.; Yu, X.; Liu, C., Molecular alterations and targeted therapy in pancreatic ductal adenocarcinoma. *J Hematol Oncol* **2020,** *13* (1), 130.

6.   Kapoor, A.; Yao, W.; Ying, H.; Hua, S.; Liewen, A.; Wang, Q.; Zhong, Y.; Wu, C. J.; Sadanandam, A.; Hu, B.; Chang, Q.; Chu, G. C.; Al-Khalil, R.; Jiang, S.; Xia, H.; Fletcher-Sananikone, E.; Lim, C.; Horwitz, G. I.; Viale, A.; Pettazzoni, P.; Sanchez, N.; Wang, H.; Protopopov, A.; Zhang, J.; Heffernan, T.; Johnson, R. L.; Chin, L.; Wang, Y. A.; Draetta, G.; DePinho, R. A., Yap1 activation enables bypass of oncogenic Kras addiction in pancreatic cancer. *Cell* **2014,** *158* (1), 185-197.

7.   Zeitouni, D.; Pylayeva-Gupta, Y.; Der, C. J.; Bryant, K. L., KRAS mutant pancreatic cancer: No lone path to an effective treatment. *Cancers* **2016,** *8* (4), 45.

8.   Moore, M. J.; Goldstein, D.; Hamm, J.; Figer, A.; Hecht, J. R.; Gallinger, S.; Au, H. J.; Murawa, P.; Walde, D.; Wolff, R. A.; Campos, D.; Lim, R.; Ding, K.; Clark, G.; Voskoglou-Nomikos, T.; Ptasynski, M.; Parulekar, W.; National Cancer Institute of Canada Clinical Trials, G., Erlotinib plus gemcitabine compared with gemcitabine alone in patients with advanced pancreatic cancer: a phase III trial of the National Cancer Institute of Canada Clinical Trials Group. *J Clin Oncol* **2007,** *25* (15), 1960-1966.

9.   Danovi, S. A.; Wong, H. H.; Lemoine, N. R., Targeted therapies for pancreatic cancer. *Br Med Bull* **2008,** *87*, 97-130.

10.   Grubbs, S. S.; Grusenmeyer, P. A.; Petrelli, N. J.; Gralla, R. J., Is it cost-effective to add erlotinib to gemcitabine in advanced pancreatic cancer? *J Clin Oncol* **2006,** *24* (18), 313s.

11.   Wang, S.; Li, Y.; Xing, C.; Ding, C.; Zhang, H.; Chen, L.; You, L.; Dai, M.; Zhao, Y., Tumor microenvironment in chemoresistance, metastasis and immunotherapy of pancreatic cancer. *Am J Cancer Res* **2020,** *10* (7), 1937-1953.

12.   Apte, M. V.; Xu, Z.; Pothula, S.; Goldstein, D.; Pirola, R. C.; Wilson, J. S., Pancreatic cancer: The microenvironment needs attention too! *Pancreatology* **2015,** *15* (4), S32-S38.

13.   Huang, X.; Ding, L.; Liu, X.; Tong, R.; Ding, J.; Qian, Z.; Cai, L.; Zhang, P.; Li, D., Regulation of tumor microenvironment for pancreatic cancer therapy. *Biomaterials* **2021,** *270*, 120680.

14.   Guillaumond, F.; Bidaut, G.; Ouaissi, M.; Servais, S.; Gouirand, V.; Olivares, O.; Lac, S.; Borge, L.; Roques, J.; Gayet, O.; Pinault, M.; Guimaraes, C.; Nigri, J.; Loncle, C.; Lavaut, M. N.; Garcia, S.; Tailleux, A.; Staels, B.; Calvo, E.; Tomasini, R.; Iovanna, J. L.; Vasseur, S., Cholesterol uptake disruption, in association with chemotherapy, is a promising combined metabolic therapy for pancreatic adenocarcinoma. *Proc Natl Acad Sci U S A* **2015,** *112* (8), 2473-2478.

15.   Hornick, J. R.; Xu, J.; Vangveravong, S.; Tu, Z.; Mitchem, J. B.; Spitzer, D.; Goedegebuure, P.; Mach, R. H.; Hawkins, W. G., The novel sigma-2 receptor ligand SW43 stabilizes pancreas cancer progression in combination with gemcitabine. *Mol Cancer* **2010,** *9* (1), 1-11.

16.   Kashiwagi, H.; McDunn, J. E.; Simon, P. O., Jr.; Goedegebuure, P. S.; Vangveravong, S.; Chang, K.; Hotchkiss, R. S.; Mach, R. H.; Hawkins, W. G., Sigma-2 receptor ligands potentiate conventional chemotherapies and improve survival in models of pancreatic adenocarcinoma. *J Transl Med* **2009,** *7* (1), 1-8.

17.   Ma, X. Z.; Bi, E. G.; Lu, Y.; Su, P.; Huang, C. J.; Liu, L. T.; Wang, Q.; Yang, M. J.; Kalady, M. F.; Qian, J. F.; Zhang, A. J.; Gupte, A. A.; Hamilton, D. J.; Zheng, C. Y.; Yi, Q., Cholesterol induces CD8(+) T cell exhaustion in the tumor microenvironment. *Cell Metab* **2019,** *30* (1), 143-156.

18.   Huang, B. L.; Song, B. L.; Xu, C. Q., Cholesterol metabolism in cancer: mechanisms and therapeutic opportunities. *Nat Metab* **2020,** *2* (2), 132-141.

19.   Tang, Z.; Kang, B.; Li, C.; Chen, T.; Zhang, Z., GEPIA2: an enhanced web server for large-scale expression profiling and interactive analysis. *Nucleic Acids Res* **2019,** *47* (W1), W556-W560.

20.   Huang, W.; Li, N.; Hu, J.; Wang, L., Inhibitory effect of RNA-mediated knockdown of zinc finger protein 91 pseudogene on pancreatic cancer cell growth and invasion. *Oncol Lett* **2016,** *12* (2), 1343-1348.

21.   Hu, S.; Sechi, M.; Singh, P. K.; Dai, L.; McCann, S.; Sun, D.; Ljungman, M.; Neamati, N., A novel redox modulator induces a GPX4-mediated cell death that is dependent on iron and reactive oxygen species. *J Med Chem* **2020,** *63* (17), 9838-9855.

22.   Shen, H.; Li, J.; Xie, X.; Yang, H.; Zhang, M.; Wang, B.; Kent, K. C.; Plutzky, J.; Guo, L. W., BRD2 regulation of sigma-2 receptor upon cholesterol deprivation. *Life Sci Alliance* **2021,** *4* (1).

23.   Bartz, F.; Kern, L.; Erz, D.; Zhu, M. G.; Gilbert, D.; Meinhof, T.; Wirkner, U.; Erfle, H.; Muckenthaler, M.; Pepperkok, R.; Runz, H., Identification of cholesterol-regulating genes by targeted RNAi screening. *Cell Metab* **2009,** *10* (1), 63-75.

24.   Riad, A.; Zeng, C. B.; Weng, C. C.; Winters, H.; Xu, K. Y.; Makvandi, M.; Metz, T.; Carlin, S.; Mach, R. H., Sigma-2 Receptor/TMEM97 and PGRMC-1 increase the rate of internalization of LDL by LDL receptor through the formation of a ternary complex. *Sci Rep* **2018,** *8* (1), 1-12.

25.   Korc, M., Pathways for aberrant angiogenesis in pancreatic cancer. *Mol Cancer* **2003,** *2*, 8.

26.   Katayama, Y.; Uchino, J.; Chihara, Y.; Tamiya, N.; Kaneko, Y.; Yamada, T.; Takayama, K., Tumor neovascularization and developments in therapeutics. *Cancers (Basel)* **2019,** *11* (3).

27.   Apte, R. S.; Chen, D. S.; Ferrara, N., VEGF in signaling and disease: Beyond discovery and development. *Cell* **2019,** *176* (6), 1248-1264.

28.   Casalou, C.; Costa, A.; Carvalho, T.; Gomes, A. L.; Zhu, Z.; Wu, Y.; Dias, S., Cholesterol regulates VEGFR-1 (FLT-1) expression and signaling in acute leukemia cells. *Mol Cancer Res* **2011,** *9* (2), 215-24.

29.   Trape, J.; Morales, C.; Molina, R.; Filella, X.; Marcos, J. M.; Salinas, R.; Franquesa, J., Vascular endothelial growth factor serum concentrations in hypercholesterolemic patients. *Scand J Clin Lab Invest* **2006,** *66* (3), 261-267.

30.   Calabro, A.; Tai, J.; Allen, S. L.; Budman, D. R., In-vitro synergism of m-TOR inhibitors, statins, and classical chemotherapy: potential implications in acute leukemia. *Anticancer Drugs* **2008,** *19* (7), 705-712.

31.   Zhao, T. T.; Trinh, D.; Addison, C. L.; Dimitroulakos, J., Lovastatin inhibits VEGFR and AKT activation: synergistic cytotoxicity in combination with VEGFR inhibitors. *PLoS One* **2010,** *5* (9), e12563.

32.   Hornick, J. R.; Xu, J. B.; Vangveravong, S.; Tu, Z. D.; Mitchem, J. B.; Spitzer, D.; Goedegebuure, P.; Mach, R. H.; Hawkins, W. G., The novel sigma-2 receptor ligand SW43 stabilizes pancreas cancer progression in combination with gemcitabine. *Mol Cancer* **2010,** *9*.

33.   Szklarczyk, D.; Gable, A. L.; Lyon, D.; Junge, A.; Wyder, S.; Huerta-Cepas, J.; Simonovic, M.; Doncheva, N. T.; Morris, J. H.; Bork, P.; Jensen, L. J.; Mering, C. V., STRING

v11: protein-protein association networks with increased coverage, supporting functional discovery in genome-wide experimental datasets. *Nucleic Acids Res* **2019,** *47* (D1), D607-D613.

34.   Huttlin, E. L.; Bruckner, R. J.; Paulo, J. A.; Cannon, J. R.; Ting, L.; Baltier, K.; Colby, G.; Gebreab, F.; Gygi, M. P.; Parzen, H.; Szpyt, J.; Tam, S.; Zarraga, G.; Pontano-Vaites, L.; Swarup, S.; White, A. E.; Schweppe, D. K.; Rad, R.; Erickson, B. K.; Obar, R. A.; Guruharsha, K. G.; Li, K.; Artavanis-Tsakonas, S.; Gygi, S. P.; Harper, J. W., Architecture of the human interactome defines protein communities and disease networks. *Nature* **2017,** *545* (7655), 505-509.

35.   Khan, N.; Shah, P. P.; Ban, D.; Trigo-Mourino, P.; Carneiro, M. G.; DeLeeuw, L.; Dean, W. L.; Trent, J. O.; Beverly, L. J.; Konrad, M.; Lee, D.; Sabo, T. M., Solution structure and functional investigation of human guanylate kinase reveals allosteric networking and a crucial role for the enzyme in cancer. *J Biol Chem* **2019,** *294* (31), 11920-11933.

36.   Giroux, V.; Iovanna, J.; Dagorn, J. C., Probing the human kinome for kinases involved in pancreatic cancer cell survival and gemcitabine resistance. *FASEB J* **2006,** *20* (12), 1982-91.

37.   Pfeifer, A.; Kilic, A.; Hoffmann, L. S., Regulation of metabolism by cGMP. *Pharmacol Ther* **2013,** *140* (1), 81-91.

38.   Qu, T.; Zhao, Y.; Chen, Y.; Jin, S.; Fang, Y.; Jin, X.; Sun, L.; Ma, Y., Down-regulated MAC30 expression inhibits breast cancer cell invasion and EMT by suppressing Wnt/beta-catenin and PI3K/Akt signaling pathways. *Int J Clin Exp Pathol* **2019,** *12* (5), 1888-1896.

39.   Qiu, G.; Sun, W.; Zou, Y.; Cai, Z.; Wang, P.; Lin, X.; Huang, J.; Jiang, L.; Ding, X.; Hu, G., RNA interference against TMEM97 inhibits cell proliferation, migration, and invasion in glioma cells. *Tumour Biol* **2015,** *36* (10), 8231-8238.

40.   Xu, X. Y.; Zhang, L. J.; Yu, Y. Q.; Zhang, X. T.; Huang, W. J.; Nie, X. C.; Song, G. Q., Down-regulated MAC30 expression inhibits proliferation and mobility of human gastric cancer cells. *Cell Physiol Biochem* **2014,** *33* (5), 1359-1368.

41.   Bondeson, D. P.; Smith, B. E.; Burslem, G. M.; Buhimschi, A. D.; Hines, J.; Jaime-Figueroa, S.; Wang, J.; Hamman, B. D.; Ishchenko, A.; Crews, C. M., Lessons in PROTAC design from selective degradation with a promiscuous warhead. *Cell Chem Biol* **2018,** *25* (1), 78-87.

42.   An, J.; Ponthier, C. M.; Sack, R.; Seebacher, J.; Stadler, M. B.; Donovan, K. A.; Fischer, E. S., pSILAC mass spectrometry reveals ZFP91 as IMiD-dependent substrate of the CRL4(CRBN) ubiquitin ligase. *Nat Commun* **2017,** *8* (1), 1-11.

43.   Zhang, J. W.; Li, Q.; Xu, Q. Q.; Wang, T. E.; Wang, Q. W., TMPRSS4 upregulates TWIST1 expression through STAT3 activation to induce prostate cancer cell migration. *Pathol Oncol Res* **2018,** *24* (2), 251-257.

44.   Min, H. J.; Lee, Y.; Zhao, X. F.; Park, Y. K.; Lee, M. K.; Lee, J. W.; Kim, S., TMPRSS4 upregulates uPA gene expression through JNK signaling activation to induce cancer cell invasion. *Cell Signal* **2014,** *26* (2), 398-408.

45.   Li, C.; Chen, C.; An, Q.; Yang, T.; Sang, Z.; Yang, Y.; Ju, Y.; Tong, A.; Luo, Y., A novel series of napabucasin derivatives as orally active inhibitors of signal transducer and activator of transcription 3 (STAT3). *Eur J Med Chem* **2019,** *162*, 543-554.

46.   Locken, H.; Clamor, C.; Muller, K., Napabucasin and related heterocycle-fused naphthoquinones as STAT3 inhibitors with antiproliferative activity against cancer cells. *J Nat Prod* **2018,** *81* (7), 1636-1644.

47.   Yang, J.; Li, Y.; Aguilar, A.; Liu, Z.; Yang, C. Y.; Wang, S., Simple structural modifications converting a bona fide MDM2 PROTAC degrader into a molecular glue molecule: A cautionary tale in the design of PROTAC degraders. *J Med Chem* **2019,** *62* (21), 9471-9487.

48.   Ishoey, M.; Chorn, S.; Singh, N.; Jaeger, M. G.; Brand, M.; Paulk, J.; Bauer, S.; Erb, M. A.; Parapatics, K.; Muller, A. C.; Bennett, K. L.; Ecker, G. F.; Bradner, J. E.; Winter, G. E., Translation termination factor GSPT1 Is a phenotypically relevant off-target of heterobifunctional phthalimide degraders. *ACS Chem Biol* **2018,** *13* (3), 553-560.

49.   https://www.accessdata.fda.gov/scripts/opdlisting/oopd/listResult.cfm. (accessed October 10, 2020).

50.   Bekaii-Saab, T. S.; Starodub, A.; El-Rayes, B. F.; Shahda, S.; O'Neil, B. H.; Noonan, A. M., Phase 1b/2 trial of cancer stemness inhibitor napabucasin (NAPA) plus nab-paclitaxel (nPTX) and gemcitabine (Gem) in metastatic pancreatic adenocarcinoma (mPDAC). *J Clin Oncol* **2018,** *36* (15), 4110.

51.   Tang, D. E.; Dai, Y.; Xu, Y.; Lin, L. W.; Liu, D. Z.; Hong, X. P.; Ou, M. L.; Jiang, H. W.; Xu, S. H., The ubiquitinase ZFP91 promotes tumor cell survival and confers chemoresistance through FOXA1 destabilization. *Carcinogenesis* **2020,** *41* (1), 56-66.